UNIVERSITY OF THE
WITWATERSRAND,
JOHANNESBURG

Techno-economic evaluation of membrane system for CO_2 capture from a coal-fired power plant

Thesis by

Natsayi Chiwaye

545382

A thesis submitted to the faculty of Engineering and the Built Environment, University of the Witwatersrand, Johannesburg, South Africa, for the degree of Doctor of Philosophy.

Supervisors: Professor. M.O. Daramola

Professor. T. Majozi

Candidate's Declaration

I declare that this dissertation is my own unaided work. It is being submitted for the degree of Doctor of Philosophy to the Faculty of Engineering and Built Environment at the University of the Witwatersrand, Johannesburg, South Africa. It has not been submitted for any degree or examination to any other university.

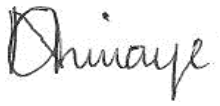
.....

Natsayi Chiwaye

On this……18……day of……October…..2021 at…..Johannesburg

Abstract

The need to mitigate climate change by reducing the emission of greenhouse gases such as CO_2 has never been more urgent. The increase in CO_2 emissions is driven mainly by the combustion of fossil fuels for electricity generation. Capturing it from point emitters such as power plants would ensure the continued exploration of fossil fuels such as coal. Recent efforts continue to focus on reducing the cost associated with CO_2 capture.

Membranes as a tool for CO_2 separation from flue gas have been investigated through experimental work and modelling. The main challenge to the large scale implementation of membranes for CO_2 capture from coal plants is the low driving force because of the low CO_2 composition in the flue gas. This necessitates the use of compressors for driving force generation and large membrane area, which results in high operational and capital cost. Simulation and optimisation studies continue to assess the feasibility of membrane application for CO_2 capture. Optimisation models have been based on constant CO_2 permeance values. However, the CO_2 permeance in facilitated transport membranes such as fixed-site carrier membranes varies with the partial pressure, which is proportional to the pressure and concentration of the target gas. The membrane also requires humid conditions for optimal permeance to be realised. In this work, superstructure based multistage membrane optimisation of the CO_2 capture process by a facilitated transport membrane from power plants has been carried out. A mixed-integer nonlinear program model (MINLP) is developed that has a variable CO_2 permeation model for a fixed site carrier (FSC) membrane is developed. The superstructure embeds numerous potential process routes and involves the treatment of a multicomponent humidified flue gas for CO_2 capture by membranes. The superstructure involves the option of vacuum only operation and sweep gas operation on the permeate side. The model simultaneously optimises the feed humidity, the energy consumption of the compressors, the membrane area required, the flowrate and gives the optimum process flowsheet. The objective of the model is to minimise the annualised cost of CO_2 capture. The benefits of the optimisation model are explored by analysing the results of different scenarios. Next, a sensitivity analysis of the CO_2 capture process is carried out. High separation targets of up to 100% recovery are also studied.

The results show that the multistage optimisation leads to a decrease in the membrane area of 39% and reduces the annual specific cost of capture by 14% compared to a predetermined two stage membrane process flowsheet. The lower cost of capture is attributed to the smaller membrane area at relatively unchanged power consumption. The use of combining vacuum only and sweep driven stages can further reduce the cost of capture by 3%.

The model is also applied to a South African context. The simulation of the supercritical boiler power plant takes into account the high average atmospheric temperature (32.3 °C) of the location and low pressure (0.81 bar) values of Limpopo as well as air cooling, which is peculiar to the power plant. The type of coal specific to the area and the coal characteristics are also taken into account. The capture process would reduce the power output of the plant from 727.3 MW to 515.9 MW which is an efficiency penalty of 10.6%. The Carbon Capture and Storage (CCS) system would contribute 40% of the total annual cost of the power plant.

The utilisation of an N_2 selective membrane together with a CO_2 selective membrane in an integrated process system is also studied. An optimisation model is developed based on a superstructure that allows both the retentate and permeate streams to become the residue and product streams. The choice of operating either an N_2 selective or CO_2 selective membrane is an added degree of freedom. At the conventional separation targets of recovery of 90% and purity, 95% the optimised the N_2 -CO_2 hybrid process system results in 14% savings in the cost of capture compared to the CO_2 selective membrane process.

Dedication

To my parents Kudakwashe. S. Mutamba and Laiza Mutamba *nee* Masvora *(Baba na Mai Meso/ Mbuya na Sekuru va Kuu)* for life and love.

Acknowledgements

I would like to express my heartfelt gratitude to my thesis advisors, Professor M. O. Daramola and Professor T. Majozi, for their guidance and support throughout this research. I especially appreciate their honest feedback and hard truth approach to training which has positively moulded me as a researcher.

My deepest appreciation to Christie Bazolana-Mutunda my dear colleague. Thanks for taking the time to discuss the work with me. I will forever be grateful to you. You are a wonderful and intelligent soul. I also acknowledge Phumlile Kunene and Morongwa Mapaya for reading and asking a lot of important questions that got me thinking and helped me give a better discussion. To the rest of my colleagues in the SPE and SEERU research groups, thank you.

I am also grateful to Dr Phylis Makurunje and Nyasha Machakaire-Jakata, my dear friends at WITS and co-heirs, for hot, home-cooked meals, good conversation and for the countless tips on how to tackle the various difficulties I encountered along the way. My friends, Zvanaka Mazhandu, Tatenda Motsi, Zviemurwi Chihambakwe and Dr Fortunate Farirai, for always checking on my progress, encouragement and the many laughs. My former colleagues and friends from the WITS CATOMMAT research group who inspired, cheered, consoled, visited and encouraged me to stay the course when I felt otherwise; Dr Manoko Maubane-Nkadimeng, Dr Zikhona Tetana-Cabunda, Dr Sibongile Dube-Manikai, Dr Thobeka Kente, and Dr Myriam Motchelaho.

Heartfelt appreciation to my mom-in-law, Zvinaiye, for always availing herself to help with the child whenever requested. I am also grateful for her love and care at the times I was not feeling well. I love you, mommy. You always have the right words to comfort and encourage. Indeed, the depth of my gratitude can only be comprehended by my heart, as the Shona proverb says '*kutenda kwa kitsi kuri mumoyo'.* Acknowledgements to the rest of my family, Chiwaye and Mutamba, you are precious.

Many thanks to Henry, my husband and companion, for his unwavering support on this long research journey. You supported me in every way humanly possible. You became all things to our small family and me so that by all means, I could get to this point. I love you HTC, what more can I ask for (*wozodei)?*! I thank YHWH, the Almighty God, who brought all these people into my life. Out of His abundance, I received grace upon grace on this research journey. Glory, honour and praise to Him, King Eternal, my Lord and my God, and to the Soon Coming King!

Publications and Presentations

Publications

Chiwaye. N., Majozi. T., Daramola. M.O., Optimization of post-combustion carbon dioxide capture by use of a fixed site carrier membrane. *International Journal for Greenhouse Gas Control.* 104 (2021) 103182, doi.org/10.1016/j.ijggc.2020.103182. (Chapter 3)

Chiwaye. N., Majozi. T., Daramola. M.O., On optimisation of N_2 and CO_2-selective hybrid membrane process systems for post-combustion CO_2 capture from coal-fired power plants. *Journal of Membrane Science 638 (2021)* doi.org/10.1016/j.memsci.2021.119691 (Chapter 5)

Conference Presentations

Chiwaye. N., Majozi. T., Daramola. M.O., Optimisation of post-combustion carbon dioxide capture by use of a carrier facilitated transport membrane. Trondheim Carbon Capture and Storage conference, Trondheim, Norway, 2019. **Oral presentation.**

Chiwaye. N., Majozi. T., Daramola. M.O., Techno-economic Evaluation of Membrane System for CO_2 Capture from Coal Fired Power Plant. South Africa Carbon Capture and Storage conference, Durban, South Africa, 2017. **Poster presentation.**

Prepared Manuscripts for Submission to Journals

Chiwaye. N., Majozi. T., Daramola. M.O., Techno-economic evaluation of membrane-based carbon capture and storage from a coal-fired power plant in South Africa. (Chapter 4)

Chiwaye. N., Majozi. T., Daramola. M.O., An assessment of the various strategies used in modelling, optimisation and techno-economic evaluation of membrane based CO_2 capture. (Chapter 6)

Table of contents

Candidate's Declaration i

Abstract ii

Dedication iv

Acknowledgements v

Publications and Presentations vi

Table of contents vii

List of Figures xiii

List of Tables xvii

Abbreviations xix

1 Chapter 1 – Introduction 1

1.1 Introduction 1

1.1.1 South African Context 4

1.2 Background and motivation 5

1.3 Problem statement and scope of the study 7

1.4 Research objectives 10

1.4.1 Contributions 10

1.5 Outline of the thesis 11

2 Chapter 2 - Literature review 13

2.1 Introduction 13

2.2 Introduction to membrane technology 13

2.3 Gas separation by membranes 14

2.4 Types of membranes for CO_2 capture 18

2.4.1 CO_2 selective membranes 18

2.4.2 N_2 selective membranes for the separation of CO_2/N_2 gas mixtures 23

2.5 Mechanism of gas permeation in polymer membranes 25

2.5.1 Polymer permeation models 25
2.5.2 Facilitated transport models 28
2.6 Facilitation of CO_2 through a membrane 32
2.7 Design considerations for CO_2 capture 34
2.7.1 Flow patterns 34
2.7.2 Module configurations 35
2.7.3 Parameters of interest in membrane separation 39
2.8 Economic indicators for CO_2 capture 42
2.8.1 Levelised cost of capture 42
2.8.2 Cost of CO_2 avoided 44
2.8.3 Specific cost of capture 44
2.9 Review of techno-economic feasibility studies for CO_2 capture by membranes 45
2.9.1 Two stage dry gases 47
2.9.2 Wet Flue gas 48
2.9.3 Whole plant design for CO_2 capture from coal power plants 52
2.9.4 Use of N_2 selective membranes 54
2.9.5 Cost models adopted in literature 55
2.9.6 Solving optimisation models for gas membrane networks 55
2.10 Review of optimisation of multistage membrane systems for CO_2 capture 56
2.10.1 Early work on membrane gas separation optimisation 57
2.10.2 Optimisation of other membrane gas processes 59
2.10.3 Optimisation of multistage CO_2/N_2 separation by membranes 61
2.11 Pilot studies of membrane CO_2 capture processes 65
2.12 Concluding remark 67
3 Chapter 3 – Optimisation of post-combustion carbon dioxide capture by use of a fixed site carrier membrane 69

3.1 Introduction 69
3.2 Problem statement 70
3.3 Model description 70
3.3.1 Superstructure description 71
3.3.2 Permeation model 75
3.3.3 Material balances 78
3.3.4 Inequality constraints 84
3.3.5 Logic constraints 85
3.3.6 Compressors 85
3.3.7 CO_2 permeance and relative humidity 87
3.3.8 Water condensation 88
3.3.9 The objective function 90
3.4 Illustrative example 92
3.5 Results and discussion 94
3.5.1 Case 1: Vacuum only driven process 95
3.5.2 Case 2: Consideration for water vapour sweep 99
3.5.3 Relative humidity profiles 103
3.5.4 In-depth analysis of the FSC membrane application for CO_2 capture from coal plant flue gas 105
3.6 Concluding remark 120
3.7 Nomenclature 121
4 Chapter 4 - Techno-economic evaluation of membrane-based carbon capture and storage from a coal power plant in South Africa 127
4.1 Introduction 127
4.2 Method 129
4.2.1 Coal power plant modelling 130
4.2.2 Membrane based CO_2 capture system model description 135

4.3 Results and discussion 139
4.4 Concluding remark 147
4.5 Nomenclature 148
5 Chapter 5 – On Optimisation of N_2 and CO_2 selective membrane hybrid process system for CO_2 capture from coal power plants flue gas 149
5.1 Introduction 149
5.2 Problem statement 149
5.3 Model description 150
5.3.1 Superstructure description 150
5.3.2 Membrane permeation model 153
5.3.3 Material balance constraints 155
5.3.4 Compressors 163
5.3.5 Cooling 164
5.3.6 Separation targets 164
5.3.7 Cost Model 165
5.3.8 Objective function 166
5.4 Illustrative example 167
5.5 Results and discussion 170
5.5.1 Case 1: Recovery 90% and purity 80% 170
5.5.2 Case 2: Recovery 90% and purity 95% 179
5.5.3 Sensitivity to N_2 permeance on the hybrid process 184
5.5.4 Sensitivity to N_2/CO_2 selectivity on the hybrid process 187
5.6 Concluding remark 190
5.7 Nomenclature 191
6 Chapter 6 – An assessment of the various strategies used in modelling, optimisation and techno-economic evaluation of membrane based CO_2 capture 195
6.1 Introduction 195

6.2 Problem statement 197
6.3 Model description 197
6.3.1 Superstructure description 198
6.3.2 Membrane permeation models 201
6.3.3 Material balance constraints 206
6.3.4 Objective function 210
6.3.5 Cost Models 211
6.4 Illustrative example 214
6.5 Results and discussion 216
6.5.1 Effect of increased recovery and purity and assessment of the cost associated with zero CO_2 emission 216
6.5.2 Assessment of the strategies used in modelling and techno-economic evaluation of membrane based CO_2 capture 222
6.6 Concluding remark 238
6.7 Nomenclature 239
7 Chapter 7 - General conclusions and recommendations 244
7.1 General Conclusions 244
7.1.1 Optimisation of post-combustion carbon dioxide capture by use of a fixed site carrier membrane 244
7.1.2 Techno-economic evaluation of membrane-based carbon capture and storage from a coal power plant in South Africa 245
7.1.3 On Optimisation of N_2 and CO_2 selective membrane hybrid process system for CO_2 capture from coal power plants flue gas 246
7.1.4 An assessment of the various strategies used in modelling, optimisation and techno-economic evaluation of membrane based CO_2 capture 246
7.2 Limitation of study 247
7.3 Recommendation for future work 248

References 250

Appendix A. Membrane model validation 280

Appendix B. Partial pressure profiles along the membrane profiles of different flow configurations of FSC membrane 281

Appendix C. Copies of Journal articles published 283

Appendix D. Turnitin plagiarism report 284

Appendix E. Copyright permission for use of own published work in this thesis 286

Appendix F. Copyright Permission for Figures reproduced (Table and certificates) 287

Appendix G. GAMS Files 295

List of Figures

Figure 1.1. The volume contribution of CO_2 to the total greenhouse gases (IPCC, 2018).....3
Figure 1.2. Figure showing sources of anthropogenic CO_2 from fossil fuels (adapted from (IPCC, 2018).....4
Figure 2.1. Scheme of membrane separation cast onto a membrane support (Baker, 2004; Perry and Green, 1997).....14
Figure 2.2. Robeson plot (Reproduced from (Robeson, 2008) with permission from Elsevier). 18
Figure 2.3. Scheme of a CO_2 molecule showing the double bonds between carbon and oxygen atoms.....32
Figure 2.4. CO_2 transport in a high pH, FSC PVAm/Psf membrane (T.-J. Kim et al., 2013; Yu et al., 2011) 34
Figure 2.5. Common flow patterns employed in gas separation by membranes (Pan, 1983) .35
Figure 2.6. Hollow fibre membrane modules (Reproduced from (Harlacher and Wessling, 2015), figure reprinted with permission from Elsevier) 36
Figure 2.7. Spiral wound membrane modules ((Harlacher and Wessling, 2015) figure reprinted with permission from Elsevier).....37
Figure 2.8. Driving force enhancement strategies (Zhao et al., 2010) 40
Figure 2.9. Two-stage membrane configurations showing recycle and reuse streams (Hao et al., 2008; Zhao et al., 2010) 41
Figure 2.10. Whole power plant design for membrane based carbon capture from power plants ((Merkel et al., 2010) reused with permission from Elsevier).....53
Figure 2.11. The superstructure presented by Qi and Henson (1998),(reused with permission from Elsevier) 58
Figure 2.12.Cascading superstructure presented by Aliaga-vicente et al. (2017,)(resused with permission from Wiley).....60
Figure 3.1.Superstructure representation of the process.....73
Figure 3.2. Water vapour sweep system 74
Figure 3.3. Schematic representation of a typical membrane module.....75
Figure 3.4. Mass balance around the flue gas condenser and the flue gas splitter. 78

Figure 3.5. Material balance around flue gas permeate mixer, feed mixer and retentate splitter, residue mixer.....80
Figure 3.6 Material balance around the permeate condenser, permeate splitter, product mixer and product condenser 82
Figure 3.7. Scenario 1 process flowsheet, 2 stage membrane process operating at uniform operating pressure. 97
Figure 3.8. Process flowsheet of scenario 3 which is a 3 stage vacuum driven with non-uniform operating pressure. 97
Figure 3.9. Scenario 6 Optimum process flowsheet for 3-stage, combined sweep and vacuum with non-uniform operating pressure. 102
Figure 3.10. Humidity profiles along the membrane 104
Figure 3.11. Figure showing the annual cost, CAPEX and OPEX of the three flow patterns 107
Figure 3.12.Showing optimum membrane area and optimum power consumption for the different flow patterns 109
Figure 3.13 Annual cost for uniform operation versus non-uniform operation. 111
Figure 3.14.Membrane area (a) and power consumption (b) of two and three stage processes with uniform pressure values vs non-uniform pressure values 112
Figure 3.15. Variation of specific cost with increased recovery and purity 114
Figure 3.16. Effect of increasing the cost of membrane on the membrane area and power consumption 115
Figure 3.17. Effect of increasing the cost of membrane on the OPEX, CAPEX and TAC…116
Figure 3.18. Effect of increasing the cost of electricity on the membrane area and power consumption. 117
Figure 3.19. Effect of increasing the cost of electricity on OPEX, CAPEX and TAC. 118
Figure 3.20. Effect of the membrane area and power consumption. 119
Figure 3.21. Effect of increased water permeance on OPEX, CAPEX and TAC. 119
Figure 4.1.Methodology for assessing membrane based CCS (Riboldi et al., 2014) 131
Figure 4.2. Superstructure for the membrane flue gas separation process 136
Figure 4.3.Optimum membrane process flowsheet 142
Figure 4.4. Cost-share of the aspects of CCS. 144
Figure 4.5. Cost-share of the total annual cost (PC + FGD + CCS) 145

Figure 5.1. Superstructure for the N_2/CO_2 hybrid membrane system.....152
Figure 5.2.Countercurrent flow in a membrane module (without a sweep gas).....153
Figure 5.3. Balance around flue gas condenser and flue gas splitter.....155
Figure 5.4. Balance around the flue gas-permeate recycle and feed mixer.....156
Figure 5.5. The process design of the streams from the stream that leaves the retentate side 158
Figure 5.6. Streams on the permeate side 160
Figure 5.7. Streams that make up the product that is sent for sequestration.....161
Figure 5.8. Streams that make up the final residue released into the atmosphere 162
Figure 5.9. Optimum membrane network for N_2-selective membrane system, CO_2 recovery 90% and purity 80%. The balance of the composition is O_2 173
Figure 5.10. Optimum membrane network for N_2/CO_2-selective hybrid membrane system, CO_2 recovery 90% and purity 80%.The balance of the composition is O_2 178
Figure 5.11. Optimum membrane network for N_2/CO_2 selective hybrid membrane system, CO_2 recovery 90% and purity 95%.....183
Figure 5.12. Effect of increased N_2 permeance in the N_2 selective membrane on the membrane area and power consumption of the N_2-CO_2 hybrid system 186
Figure 5.13. Impact of N_2 permeance in the N_2 selective membrane on the total annual cost of the N_2-CO_2 hybrid system.....187
Figure 5.14. Effect of N_2/CO_2 selectivity in the N_2 selective membrane on the membrane area and power consumption of the N_2-CO_2 hybrid system.....188
Figure 5.15. Impact of N_2/CO_2 selectivity in the N_2 selective membrane on the annual cost of the N_2-CO_2 hybrid system.....189
Figure 6.1. Superstructure representation of the membrane process system for CO_2 capture 200
Figure 6.2. Flow of components through the membrane for countercurrent set.....202
Figure 6.3. Countercurrent mode of flow in a membrane module.....205
Figure 6.4. Optimum membrane network for CO_2 recovery of 90% and target purity of 95%. 217
Figure 6.5. Optimum membrane network for CO_2 recovery of 100% and target purity 95%. 218

Figure 6.6. Optimum membrane network for CO_2 recovery of 100% and target purity 99%. 218
Figure 6.7. Effect of the recovery on the membrane area for purity 95% and 99%. 220
Figure 6.8. Effect of recovery on the net power consumption for purity 95% and 99%. 221
Figure 6.9. Effect of recovery on total annual cost for purity 95% and 99%. 222
Figure 6.10. Effect of CO_2 recovery on membrane area for 2 stage and 3 stage optimisation at different CO_2 recovery. 223
Figure 6.11. Net power consumption for two stage and three stage optimisations at different CO_2 capture targets 224
Figure 6.12. Annualised cost capture for two stage and three stage optimisations at different CO_2 capture targets 225
Figure 6.13. Graph showing the capital and operating cost at different maximum membrane areas for CO_2 recovery 98% and purity 99% 229
Figure 6.14. CAPEX, OPEX and TAC for the various cost models 231
Figure 6.15. Comparison of optimum results for varying cost models 232
Figure 6.16. Graph showing variation in power consumed for different permeation models for CO_2 recovery 90% and purity 95% 233
Figure 6.17. Effect of permeation model and flue gas components on the cost of CO_2 capture for recovery 90% and purity 95% 235
Figure 6.18. Graph showing variation of the power consumption as the recovery is increased with set lower bound of permeate side pressure 236
Figure 6.19. Graph showing variation power consumed with set lower bound of permeate side pressure 237
Figure 6.20. Graph showing the variation of annual cost with set lower bound of the permeate side pressure. 238

List of Tables

Table 2.1: Membranes for CO_2 capture[ ]adapted from Sreenivasulu et al. (2015) 19
Table 2.2: Examples of facilitated transport membranes for CO_2 capture 22
Table 2.3: Membranes used in modelling post-combustion CO_2 capture 23
Table 2.4: Permeance and selectivity of N_2 selective membranes 24
Table 2.5: Kinetic diameters (Robeson, 1991; Zhao et al., 2017) 27
Table 2.6:The solubility of different gases in a polymer (Baker, 2004; Wang et al., 2016) ... 27
Table 3.1: PVAm/Psf membrane parameters used in simulation 93
Table 3.2: Economic data for the case study 93
Table 3.3: Computational results of scenario 1, 2 and 3. 95
Table 3.4: Optimum pressure values 98
Table 3.5: Comparative study on overall plant energy consumption 98
Table 3.6: Comparison with other studies 99
Table 3.7: Results for Case 2 100
Table 3.8: Optimum pressure values 102
Table 3.9: Comparative model statistics for different scenarios- Case 1 105
Table 3.10: Comparative model statistics for different scenarios- Case 2 105
Table 4.1: Power plant and cost specifications 132
Table 4.2: Coal composition 133
Table 4.3: Correction factors applied to USA cost values (EPRI, 2015) 134
Table 4.4: South Africa emission restrictions (DEA SA, 2010). 134
Table 4.5. Membrane Cost parameters 138
Table 4.6 Power Consumption of different sub-modules of the power plant 140
Table 4.7: Flue gas emissions without carbon capture 141
Table 4.8: Optimum design values for variables for the membrane process with storage 143
Table 4.9: Plant performance 146
Table 4.10: Table showing the effect of adding carbon tax at the gazetted price 147
Table 5.1: Flue gas composition 167
Table 5.2: Gas permeance through the different membranes 168
Table 5.3: Economic data 168

Table 5.4: Results obtained for the N_2-selective membrane recovery 90% and purity 80%.171
Table 5.5: Results obtained for the CO_2- selective membrane recovery 90% and purity 80% 174
Table 5.6: Results for the CO_2 /N_2 hybrid process; recovery 90% and purity 80% 176
Table 5.7: Optimum pressure values for recovery 90% and purity 80%.....177
Table 5.8: Results obtained for the CO_2-selective membrane, recovery 90% and purity 95% 179
Table 5.9: Results for the CO_2 /N_2 hybrid process; recovery 90% and purity 95% 180
Table 5.10: Optimum pressure values for recovery 90% and purity 95%.....182
Table 5.11: Statistics for Case 1 – Recovery 90% and purity 80 % 184
Table 5.12: Statistics for Case 2 – Recovery 90% and purity 95 % 184
Table 5.13 Permeance of N_2 in the different N_2-selective membranes simulated # 185
Table 5.14: Selectivity of N_2/CO_2 in the different N_2 selective membranes# 188
Table 6.1: Flue gas and membrane specifications 215
Table 6.2: Cost Model A economic data 215
Table 6.3: Comparison of optimum results for 100% recovery at different purities.....219
Table 6.4: Comparison of optimum results for varying maximum membrane area.....227
Table 6.5: Comparison of optimum results for different maximum membrane areas.....228
Table 6.6: Comparison of optimum results for varying cost models.....230
Table 6.7: Results for permeation models, binary and multicomponent flue gas for recovery 90% and purity 95%.....235

Abbreviations

ANTIGONE	Algorithms for coNTinuous / Integer Global Optimization
BARON	Branch-and-Reduce Optimization Navigator
BFD	Backward Finite Difference
CAPEX	Capital Expenditure
CC	Carbon Capture
CCS	Carbon Capture Storage
CESAR	Carbon Enhanced Storage and Recovery
CFD	Central Finite Difference
CNT	Carbon nanotubes
CO_2	Carbon Dioxide
COE	Cost of Electricity
COM	Operational and Maintenance Cost
CPU	Central Processing Unit
DOE	Department of Energy
DP	Desired purity
DR	Desired recovery
EOR	Enhanced Oil Recovery
EPRI	Electric Power Research Institute
ESKOM	Electricity Power Commission
FGD	Flue Gas Desulphurisation
FOM	Annual fixed operating and maintenance cost
FSC	Fixed Site Carrier
GAMS	General Algebraic Modelling Systems
GPU	Gas Permeance Unit
HHV	High Heating Value
IECM	Integrated Environmental Control Model
KJ	Kilojoule
KW	Kilowatt
LBPP	Lower bound of the permeate side pressure
LCOE	Levelised Cost of Electricity
LHV	Low Heat Value
MEA	Mono ethyl amine
MINLP	Mixed-integer nonlinear program model
MIP	Mixed Integer Program
MJ	Mega Joule
MW	Megawatt
MWNT	Multiwalled carbon nanotubes
NLP	Non Linear Program

OCTAVIUS	Optimisation of CO_2 Capture Technology Allowing Verification and Implementation at Utility Scale
OM	Operational and maintenance
OPEX	Operational expenditure
PVAm	Polyvinylamine
PCC	Post-combustion capture
SA	South Africa
SACCCS	South Africa Centre for Carbon Capture and Storage
SANEDI	South African National Energy Development Institute
SARS	South Africa Revenue Services
TAC	Total Annual Cost
TCC	Total Cost of Capture
TR	Thermally rearranged
UN	United Nations
US	United States
USA	United States of America
VOM	Variable operating and maintenance
ZAR	South Africa Rand

Chapter 1 – Introduction

1.1 Introduction

Global warming occurs when greenhouse gases trap the sun's rays (mainly infrared) and prevent them from returning to space. The net difference between the energy returned to space and the insolation absorbed by the earth due to external agents such as greenhouse gases is termed radiative forcing. An increase in the amount of the greenhouse gases present in the atmosphere translates to more infra-red rays being radiated back to earth and less returning to space thus an increase in radiative forcing (Haigh, 2002). This increases the average ambient temperature on earth over time as the concentration of greenhouse gases increases. Carbon dioxide (CO_2), hydrofluorocarbons (HFC), water vapour, Ozone (O_3) and methane (CH_4), perfluorinated compounds (PFC) are the commonly known greenhouse gases. The role these gases play in warming the earth is referred to as the greenhouse effect, and the increase in the average temperature on earth is global warming.

The world average temperature has increased by 0.8 °C from the pre-20th Century to the year 2015 (IPCC, 2018). Global warming by this margin has already resulted in the melting of ice in Antarctica which causes an increase in the sea level, causes floods, droughts, heatwaves and extreme winters in various parts of the world. Floods and droughts have an impact on food security. The increase in temperature allows more CO_2 to be absorbed by the water in oceans, increasing its acidity (IPCC, 2018, 2005). This, in turn, has negative effects on aquamarine species. Heatwaves cause spontaneous fires and wildfires, resulting in further deforestation and the death of wildlife animals (Hoegh-Guldberg et al., 2018). If unabated, the temperature rise is projected to reach 1.5 °C by the year 2052. This will only further the severity of global warming on climate change. The Paris agreement of 2015 put a road map to restrain further global temperature increase to only 1.5 °C above pre-industrial levels (UN, 2015). The solution is to curb and reduce the emission of greenhouse gases, including CO_2 emission, by finding alternative methods that are more environmentally friendly. CO_2 emissions caused by human activities should be reduced by 45 % by 2030 from its 2010 level and reach net zero emission by 2050 (Hoegh-Guldberg et al., 2018).

This goal of reducing CO_2 emission can be achieved via several pathways. These include the use of renewable energy sources such as solar, hydropower and wind. The capture of CO_2 from large point sources and isolation from the atmosphere, and also increased reforestation would assist in reducing CO_2. Improving efficiency and enhancing energy-saving systems and the use of alternatives sources of fuels that emit less carbon, such as natural gas and hydrogen, would reduce CO_2 emissions. Innovative ways to reduce CO_2 are being sought, such as the reduction of demand for goods like steel and cement that are produced by CO_2 emitting technologies. Direct capture is a method where attempts are being made to reduce the CO_2 already in the atmosphere by directly capturing it from the air (Leung et al., 2014). Direct air CO_2 capture offers the opportunity to not only achieve net-zero emission but return to pre-industrial era CO_2 levels if successfully deployed (Quintella et al., 2011).

Greenhouse concentration in the atmosphere has increased due to increased industrial activities. Of these, CO_2 plays the most critical role in warming the earth's surface. According to the magazine; Greenhouse Gas Bulletin, 'CO_2 is the most significant anthropogenic greenhouse gas as it contributes about 65%, to radiative forcing by the Total Long-Lived Greenhouse Gas' (LLGHGs) (GAW, 2014). Methane contributes 17% and NO_x gases 6%. Methane is produced from biological waste and landfills and is also naturally occurring, whilst NO_x is mainly produced in fertilizer and power plants (Tan, 2014). LLGHGs are the gases that exist in the atmosphere for long periods without their destruction. CO_2 is the longest LLGHG of all greenhouse gases (Masson-Delmotte et al., 2018).

Radiative forcing has been steadily increasing in the last century, and CO_2 alone has contributed 84% of that increase in the past decade. CO_2 concentration in the atmosphere has almost doubled from 280 ppm to 400 ppm in the year 2000 (Farmer and Cook, 2013). The demand for energy led to the extensive use of fossil fuel which became a major source of CO_2 emissions. Figure 1.1 shows that of the total GHGs produced in 2018, 76% was CO_2.

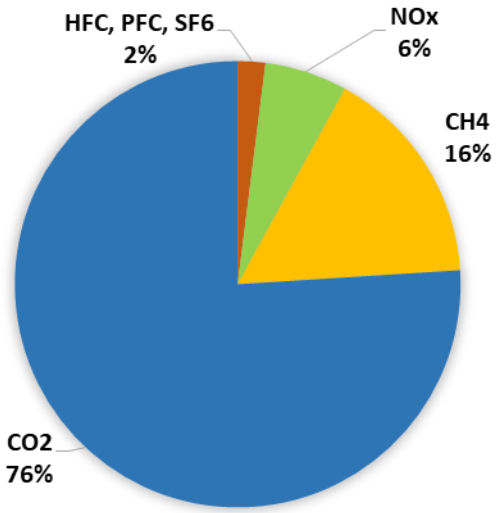

Figure 1.1. The volume contribution of CO_2 to the total greenhouse gases (IPCC, 2018)

CO_2 is produced by various industries, transport vehicles, electricity generation, cement and steel manufacture. The forecast shows that CO_2 production is likely to increase if intervention strategies are not put in place to reduce the anthropogenic production of CO_2. 2013 saw the World Meteorological Organisation and Global Atmosphere Watch record the highest increase of CO_2 emissions (Seyboth et al., 2011).

More CO_2 is produced during heat and electricity generation than by any other activity such as exhaust from vehicles (IEA, 2011). Figure 1.2 shows that 72 % of the total CO_2 is produced in produced from the energy sector, 31% is generated during electricity and heat production. Coal combustion is the biggest contributor to CO_2 emissions, producing the highest CO_2/KJ of energy compared to the other fossil fuel sources such as CH_4. Coal is the most used source of fuel for electricity and heat generation because it is a cheap source of energy. About 41% of the electricity generation power plants worldwide are coal-based (IEA, 2018)

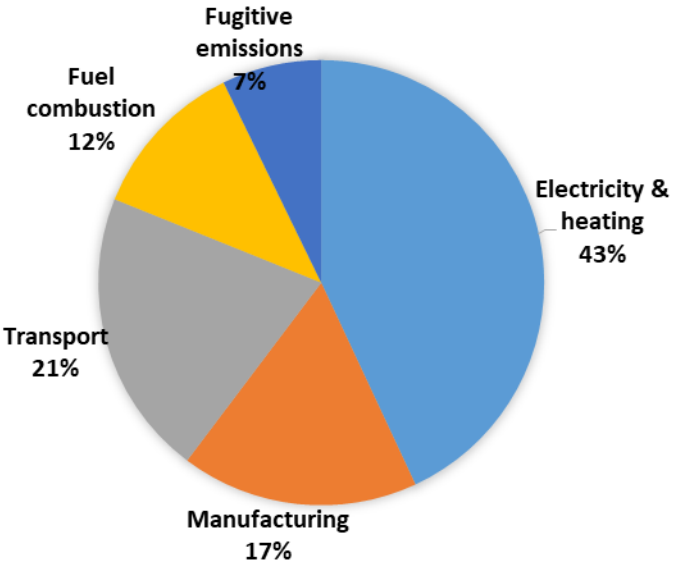

Figure 1.2. Figure showing sources of anthropogenic CO_2 from fossil fuels (adapted from (IPCC, 2018)

1.1.1 South African Context

South Africa is one of the leading coal-producing countries in the world. In the year 2017, it was number 7th in terms of total metric tonnes, the lead producer being China since 1985. 21% of the total coal produced in South Africa is exported (Masson-Delmotte et al., 2018).

Of all the coal utilised in South Africa, 61 % is used for electricity, and 23% is used by the petrochemical industries (mainly Sasol) for coal to gas and coal to liquid technology generation (Mineral Resources & Energy Department SA, 2020). The bulk of electricity is produced, and the national electricity grid is managed by the Electricity Commission (ESKOM). ESKOM is ranked 7th in terms of electricity-producing companies in the world, and Sasol is the top Coal to Petrochemicals Company in the world. Coal is relatively cheap in South Africa compared to the rest of the world since South Africa's coal is found in shallow seams, which makes the cost of mining low. Therefore coal plays an important role in the South African economy. The higher quality coal is exported whilst, the lower grade coal with higher ash content, and lower calorific value is used for electricity generation by ESKOM. This results in more coal being required to produce a specific unit of electricity, and this leads to more CO_2/MW being produced relative to the rest of the plants in other parts of the world where high-grade coal is used for power generation.

95% of the electricity produced in South Africa comes from coal power plants. According to the Mineral Resources Department, there are more than 50-year reserves of coal (Mineral Resources & Energy Department SA, 2020). The South Africa Energy plan has reiterated that coal will continue to be part of the energy mix up to 2050 as more renewable sources increase their contribution to power generation. The plan also highlights the need for CO_2 emission mitigation such as carbon capture and storage and other less carbon emitter technologies (clean coal technologies) such as Fluidised Coal and the Integrated Gasification Combined Cycle (IGCC) power plant to ensure sustainable continued use of coal (DOE SA, 2019).

'Greener' options such as increasing renewable sources such as solar, nuclear, hydro for power generation are alternatives to reduce CO_2 emissions from electricity production. Capturing the CO_2 produced from large emitting point sources and storing away from the atmosphere or utilising it is another alternative that will allow continued use of fossil fuels such as coal in a sustainable way. These technologies also include carbon capture and storage (CCS), carbon capture and utilisation (CCU) and carbon mineralisation. CCS is a "process consisting of the separation of CO_2 from industrial and energy-related sources, transport to a storage location and long-term isolation from the atmosphere" (IPCC, 2005).

CCS has been successfully demonstrated in enhanced oil recovery (EOR) projects in the United States, where millions of tonnes of CO_2 have been stored in depleted oil wells (IEAGHG, 2012) since 1970. CO_2 separated from extracted methane is injected back into the well to assist in oil recovery and then eventually left there when the oil is depleted. This demonstrated that CO_2 could be stored in geological formations safely.

1.2 Background and motivation

In view of the significant amount of CO_2 produced by the electricity sector and especially by coal power plants, it is then imperative that mitigation strategies are implemented. Carbon capture from power plants can be implemented by various configurations. These have been proposed as pre-combustion, oxy-combustion and post-combustion. In pre-combustion capture, as the term suggests, the CO_2 is separated before the combustion chamber. Pre-combustion has been applied to IGCC technology, where the air and the fuel are mixed, and partial oxidation occurs (reformation) in the presence of steam to form a mixture of CO_2 and H_2 gas that is separated to produce H_2 before the combustion chamber. Subsequent combustion

of air and the H_2 produces pure N_2 gas and water (H_2O). Oxy-fuel combustion is also applied to coal power plants where cryogenic air separation is the pre-step to produce pure O_2, which is then fed to the boiler. The flue gas from the boiler is pure CO_2 which can be sequestered (Ji and Zhao, 2017). In post-combustion, air and fuel are supplied to the boiler where combustion occurs, and flue gas is produced, which comprises CO_2, N_2, O_2 and H_2O. Post-combustion then involves the separation of CO_2 and mainly N_2, which is the major constituent in the flue gas produced.

Post-combustion capture can be implemented immediately by retrofitting to already existing power plants with fewer modifications to the existing plant and also will not affect the power produced, unlike pre-combustion (Kanniche et al., 2010). However, adequate land for the capture unit should be available on-site, else the flue gas can be transported, and separation can be carried out at the storage site. The motivation for CO_2 capture is purely for sustainability in most cases. Retrofitting CO_2 capture to existing power plants results in less power being supplied to the grid as the capture unit will use the energy produced by the power plant. Post-combustion capture in power plants lowers the efficiency by a further 7-11% (Budinis et al., 2018; Sai Prasad and Raghavan, 2012). The design of efficient capture processes is therefore crucial to make CO_2 capture economically feasible for commercial implementation.

Post-combustion capture is a gas separation problem (Zhao et al., 2013). The most effective method is the ability to produce high throughput whilst achieving high purity of the CO_2 captured stream at lower energy requirements to achieve capture at the lowest cost possible.

The most mature and conventional method is the separation of the flue gas by chemical absorption. Absorbents such as amines and ammonia have been studied (Lawal et al., 2009; Shakerian et al., 2015). The Absorption method is a two-step process that involves firstly, absorption of CO_2 in an absorption column, where the CO_2 reacts and is absorbed by the absorbent at a temperature of 40-50 °C. The products are fed to a desorption column for absorbent regeneration. The desorber operating temperature is higher at 100-140 °C. This second step makes use of some of the steam produced in the boiler, which lowers the amount of steam that goes into driving the turbines for electricity generation (Afkhamipour and Mofarahi, 2014; Biliyok et al., 2012; Lawal et al., 2012). Absorption is now considered an established technology, with several plants being erected around the world. The first

commercial mono-ethylamine based CCS plant for power plant went online on the 1st of October 2014 in Canada at the Boundary Dam power plant (Goldenberg, 2014).

As mentioned, chemical absorption has disadvantages, such as being energy-intensive. Solvent degradation also occurs in the presence of common flue gas pollutants like NO_x and SO_2 (Roussanaly et al., 2019; Zhao et al., 2011). One outstanding disadvantage is that the potential for retrofitting to existing power plants is low, as considerable modifications would need to be made on the steam cycle. Carbon capture by solvent absorption also considerably increases the water requirements of the whole coal power plant by up to 60% (Magneschi et al., 2017; Zhai and Rubin, 2011). This makes absorption less feasible for regions where water is scarce, like South Africa, where dry cooling is already in use because of water shortages (ESKOM, 2013).

In light of these drawbacks, more efficient and cheaper alternatives ways for CO_2 capture in power plants are being explored. Adsorption and membrane gas separation are being investigated (Belaissaoui et al., 2012a; Lee and Park, 2015; Merkel et al., 2008; White et al., 2017). Adsorption faces a similar challenge of the need for adsorbent regeneration which is also energy-intensive.

Membrane gas separation technology can be easily retrofitted to an existing power plant with minimum modifications. The technology is a great separation tool that is usually less energy-intensive. Membrane gas separation has the advantage of compactness and simplicity of operation as there are no moving parts (Czyperek et al., 2010; Sreedhar et al., 2017). It is also relatively more environmentally friendly than chemical absorption (Lin et al., 2014).

1.3 Problem statement and scope of the study

The implementation of CCS at a large scale has been derailed by the energy penalty associated with it, which can be as high as 10%. The cost of CO_2 capture is about 60% of the total plant energy penalty. The cost of compression as a preparation stage for transport and storage account for 30% of the total plant energy loss (Rubin, 2012). Carbon capture by membrane gas separation technology, therefore, will only become competent for large scale deployment when these cost has been reduced.

The implementation of post-combustion capture by membranes faces a huge challenge because the driving force is low. Flue gas from power plants are CO_2 dilute, with CO_2 composition less than 15% and is produced at atmospheric pressure from the power plant (Ramasubramanian and Ho, 2011). This necessitates the compression of the huge flue gas volumes and/or the use of vacuum conditions on the permeate side to increase the driving force and limit the membrane area requirement. Electricity produced by the plant goes into driving the compressors and vacuum pumps which penalises the energy efficiency and the power output of the plant. Early studies on a single membrane stage process indicated membrane technology to be less competitive when compared to absorption at the current level of CO_2 concentration. It was established from techno-economic studies that a CO_2 concentration of 20% and selectivity greater than 40 would make the technology competent (Zhao et al., 2008). Research efforts continue to find ways to incorporate membranes in post-combustion capture. Hybrid solutions such as membrane–adsorption and membrane-absorption have been proposed (Ramasubramanian and Ho, 2011). Moreover, improved membrane process system designs have been proposed from a single-stage membrane process to complex multistage membranes (Belaissaoui et al., 2012b; Roussanaly and Anantharaman, 2017; Zhang et al., 2014).

Membranes that show high permeability and selectivity have been reported. Among the most promising ones are the Polaris^{TM} which is a commercial brand and the Fixed Site Carrier (FSC) membrane. These are both polymer-based membranes (T.-J. Kim et al., 2013; White et al., 2017). At laboratory scale, FSC membranes have shown high permeance of up to 2000 and high selectivity of up to 500 compared to 50 that is exhibited by the Polaris.

Most laboratory studies are based on small membrane samples and make use of pure gases, usually, N_2/CO_2 mixtures leading to ideal permeance and selectivity data (Deng et al., 2009; He, 2018a). This may not hold in real-life large scale applications. The feasibility of implementing the membranes at a large scale is carried out through modelling and simulation (Ferrari et al., 2016; Hussain and Hägg, 2010; Murad Chowdhury et al., 2005; Zhai and Rubin, 2013).

This is mostly true for FSC membranes where the CO_2 permeance varies with varying concentration and pressure on both the feed side and permeate side of the membrane profile by the carrier saturation phenomena. The permeance is also dependent on the feed humidity level. The actual representation of CO_2 concentration along the membrane module cannot be

observed during experimental work but can be understood in detail by modelling. Integrated design and optimisation of variables and operating conditions can lead to overall cost reduction of the capture process.

Techno-economic studies for the application of membrane systems for CO_2 capture from power plants have been carried out and reported in the literature by some research groups. Synthesis, design and optimisation of membrane processes have been carried out based on the different polymeric membranes. The optimisation studies are based on the ideal N_2/CO_2 mixture and do not take into account water vapour which usually accounts for more than 10% of the flue gas. In addition, only a few techno-economic studies that evaluated the potential application of fixed-site carrier (FSC) membranes for post-combustion CO_2 capture have been reported though the membrane exhibited exceptionally high CO_2 permeance and high CO_2/N_2 selectivity at laboratory scale (Han et al., 2020; He and Hägg, 2014). To the best of the research on reported literature carried out, none has optimised the CO_2 capture process by use of facilitated transport membranes such as the FSC membrane.

Process design for the industrial application of the FSC membrane is complicated by the need for humid conditions for maximum possible CO_2 permeance and CO_2/N_2 selectivity to be realised. Whilst a high operating pressure would normally result in increased driving force and overall flux, for an FSC membrane, CO_2 permeance is highest at lower pressure for the capture region most analysed for CO_2 capture (1 to 5 bar). Therefore there is a trade-off between the driving force and the permeance as they are dependent on the operating pressure and hence the need for optimising the feed side operating pressure. The relative humidity of a gas stream is directly proportional to the mole fraction of water in the stream and the pressure at a given temperature. However, a high water composition in the membrane feed may dilute the permeate since water is also highly permeable in the membrane. This may lead to additional membrane stages being required to achieve the desired purity of the product stream. Additional separation units require a larger membrane area and more compression and vacuum pumps and thus may lead to an increase in cost. It is evident that several variables are at play. It is therefore important to optimise the process taking into account these operating requirements for optimum application of the FSC membrane for the CO_2 capture operation.

The use of an FSC membrane offers the opportunity for the implementation of water vapour as a sweep gas since the presence of water enhances CO_2 transport across the membrane rather than damage the membrane.

In this study, an optimisation approach that employs modelling and simulation methods will be used to understand the techno-economic feasibility of applying this membrane for post-combustion CO_2 capture in coal-fired power plants. Availability of such information could be instrumental in making decisions on the adoption of CO_2 capture technology to reduce the carbon footprint in South Africa.

1.4 Research objectives

The following are the specific objectives:

- To develop a superstructure based optimisation model for the capture of CO_2 by an FSC from multicomponent saturated flue gas from a coal power plant
- To carry out an in-depth analysis of the FSC membrane based CO_2 capture process, the technical requirements and their economic implications.
- To assess the feasibility of membrane-based carbon capture from a South African coal power plant.
- To develop an optimisation model for the CO_2 capture from a multicomponent coal plant flue gas by use of an N_2 selective membrane. To optimise the N_2- and CO_2-selective hybrid membrane process for the CO_2 capture process from a coal power plant.
- To assess the possibility of achieving zero CO_2 emissions by membrane-based CO_2 capture. To assess the various strategies employed in the optimisation of the CO_2 capture by membranes from power plants.

1.4.1 Contributions

Listed below are the contributions that this thesis made.

- An optimisation model for gas separation by facilitated transport (FSC) membrane that includes variable permeability of CO_2 for carbon capture.
- An optimisation model for gas separation by membranes that includes the choice for vacuum only and water sweep on the permeate side.
- An optimisation model that includes a comprehensive design for CO_2 separation from a multicomponent humidified flue gas.
- Evaluation of membrane-based CO_2 carbon capture application in South Africa.
- Optimisation of membrane-based CO_2 capture from flue gas based on the use of a process that combines N_2 selective membrane and CO_2 selective membrane.
- An optimised membrane process design that achieves 100% CO_2 recovery (zero emission) and 99% pure CO_2 stream.

1.5 Outline of the thesis

Chapter 1 gives the background of the study, the problem statement and the research objectives of the study. **Chapter 2** is a review of the literature concerning membrane permeation principles and mechanism, membrane modelling, membrane optimisation, methods for carbon capture technical and economic evaluation. It reviews the techno-economic studies for post-combustion CO_2 capture and optimisation studies of the same to date.

Chapter 3 presents the optimisation model for the FSC membrane based CO_2 capture from a power plant and applies it to a power plant case study found in literature. **Chapter 3** also provides an in-depth analysis of the influence of parameters on the feasibility of CO_2 capture. **Chapter 4** applies the optimisation model for FSC membrane based capture to a South Africa power plant to assess the feasibility of membrane-based capture in South Africa, taking into account local conditions.

Chapter 5 provides the synthesis, design and optimisation of an N_2 and N_2-CO_2 selective hybrid membrane process for CO_2 capture. Its feasibility and benefits of applying an N_2 selective membrane are highlighted.

Chapter 6 analyses in detail the various strategies used in simulation and optimisation of carbon capture by membranes from flue gas and investigates the cost of achieving zero CO_2 emission from coal power plants by use of membrane technology.

Chapter 7 gives the final discussion, conclusion, recommendation and outlook of future study.

Chapter 2 - Literature review

2.1 Introduction

This chapter provides the progress that has been made in the development of membranes as a separation technology applicable to carbon capture. It is structured by firstly introducing the principles of membrane separation and giving the types of membranes suitable for CO_2 capture. The mechanism of CO_2 permeation through membranes is then discussed. The models that represent facilitated transport of gas components through membranes are reviewed. Next, a thorough review of the literature on techno-economic studies and optimisation of membrane-based CO_2 capture is carried out. A brief discussion is then given on the field test studies carried out to date as an indicator of the progression of membrane gas separation for CO_2 capture from power plants.

2.2 Introduction to membrane technology

Membrane technology is a separation technique. According to Ulbricht, (2006), " A membrane is an interphase between two adjacent phases acting as a selective barrier, regulating the transport of substances between the two compartments " (Ulbricht, 2006). The main advantages of membrane technology are compactness and simplicity of operation. The first and most important application of membrane use is the lifesaving process of dialysis and allows organ transplant through membrane blood oxygenator (Blagg, 2007; Murphy et al., 2015). Membranes also find use in drug delivery (Zylberberg and Matosevic, 2016).Membranes also have found use in processes such as water purification (Liu, 2014). A lot of success has been in water treatment where reverse osmosis, microfiltration, nano-filtration and electro dialysis is used (Ying et al., 2017).

Industrial application of membranes for gas separation commenced in the 1980s. The application was for separating Hydrogen (H_2) from ammonia (NH_3) (Baker, 2004). Since then, a number of gas separation processes have been carried out by membranes, such as the purification of natural gas by separating CO_2 from CH_4 and the separation of N_2 from air (Buzek et al., 1999; Falbo et al., 2016). Membrane separation technology has expanded into pervaporation, catalytic membranes and membrane distillation, to name a few. (Fontalvo, 2006;

Oke et al., 2018; Wang et al., 2005). Research continues in an attempt to apply membranes in other separation problems such as CO_2 separation from power plant flue gas (Mat and Lipscomb, 2017)

2.3 Gas separation by membranes

Gas separation by a membrane occurs when molecules of a gas component in a mixture selectively pass through a membrane with much ease than the other gas component in the mixture. Table 2.1 shows the separation of a gas mixture by membranes. This is enabled by the differences in molecular diameter, which in turn determine its intrinsic diffusivity and chemical potential, which determines its absorption, adsorption and its ability to dissolve in a material (membrane) (Baker, 2004). The molecules diffuse through spaces between atoms in the membrane structure. The spaces are called free volume, and the extent of the spaces in a particular membrane is the free volume fraction (Harms et al., 2012).

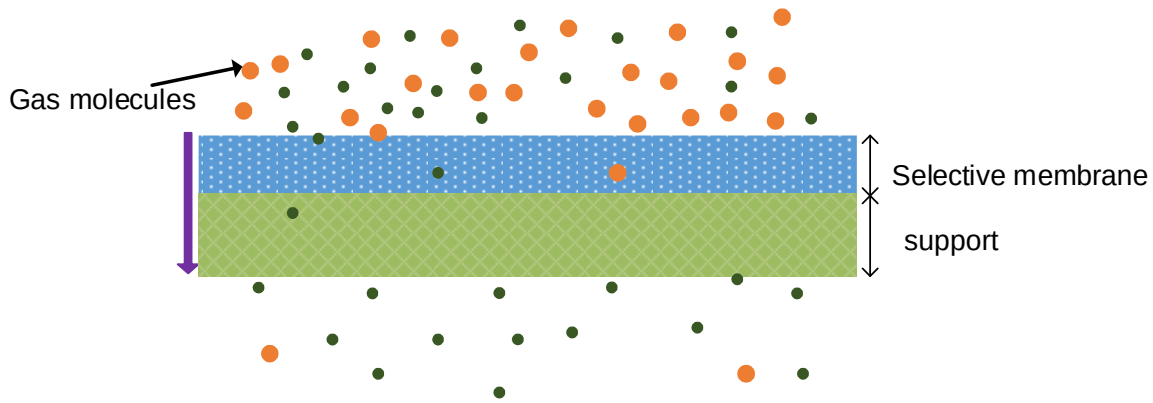

Figure 2.1. Scheme of membrane separation cast onto a membrane support (Baker, 2004; Perry and Green, 1997)

The membranes for gas separation are usually supported on a porous substance that offers negligible resistance to permeate transport (Pan, 1986). The support may be inert materials that do not enhance mass transfer; however, some supports aid the transport of gases through them (Harlacher and Wessling, 2015).

There are certain characteristics a membrane should possess for it to be considered suitable for a specific application. A suitable membrane should be resistant to fouling and should require cleaning at long intervals to minimise downtime and related complications (Jaffrin, 2015; Perry and Green, 1997). The membrane should be thermally stable at the operating temperature it is applied. It should also be mechanically and chemically stable under the transmembrane pressure and in the presence of chemical impurities, respectively (Rodrigues et al., 2018; Scholes et al., 2009). The membrane should also be stable, and permeability and selectivity must be stable at the operating temperature (Han et al., 2019b). The need for driving force may dictate high transmembrane pressure, and this should not physically destroy the membrane (Harms et al., 2012). Other engineering requirements are that the membrane should be easy and affordable to manufacture (Alshehri et al., 2013).

Different materials have been investigated for membrane gas separation. These include inorganic materials such as Zeolites, Silicas and Carbon, metals, metal-organic frameworks and polymers. Zeolites are desirable for their micro sieving abilities, whilst polymers are preferred as they are easy to fabricate and scale up at a relatively cheaper cost (Iulianelli and Drioli, 2020). Polymer membranes such as cellulose acetate have been commercialised and used in natural gas purification (Abanades et al., 2015). Polymer membranes are also a base for mixed matrix membranes and hybrid membranes (Ansaloni et al., 2015; Dai et al., 2019). Since polymer and polymer based membranes are the most commonly used for gas separation by membranes, reference will be made to them from now on.

The separation factor is the indicator of the extent of preference of one gas component to pass through the membrane compared to another component in the gas mixture to be separated. The Equation (2.1) shows the separation factor is the ratio of the molar fractions of components *A* and *j* on the feed side (y^{rt}) and the permeate side (y^{pm}).

$$\alpha_{Aj} = \frac{y_A^{pm} / y_j^{pm}}{y_A^{rt} / y_j^{rt}} \tag{2.1}$$

In most cases, the pressure on the permeate side is very small in comparison to the feed pressure and the ratio of the permeability of the ideal gases is used as the separation factor; and in this case, the term selectivity is used as shown by Equation (2.2) (Baker, 2004). The selectivity is

always reported in terms of the more permeable gas and is, therefore, always greater than one (> 1) (Perry and Green, 1997).

$$\alpha_{Aj} = \frac{P_A}{P_j} \tag{2.2}$$

Polymers can be classified as glassy polymers or rubbery polymers, depending on whether the membrane temperature is above or below the glass transition temperature. Glassy polymers are structurally rigid chain-linked and thus exhibit high selectivity as the rigid structure means only a certain molecular structure and size can pass through. (Han and Ho, 2018). Glassy polymers have the advantage of being mechanically and chemically stable (Mazinani et al., 2018). A common membrane, Polysulphone and Matrimid, are examples of glassy polymers that are available commercially (Huang and Paul, 2007). Rubbery polymers have flexible mobile chains and therefore exhibit high permeability since molecules can find a passage through such a structure easier. Rubbery polymers, therefore, have a drawback of low selectivity (Wang et al., 2016). Polymers can also suffer problems of plasticisation and aging.

Plasticisation of membranes results in the deformation of the polymer structure. Molecules of the penetrants dissolve and get lodged in the polymer structure and this causes swelling of the structure (Suleman et al., 2016). This leads to increased free volume and allows many components to pass through which compromises selectivity. Condensable gases such as heavy hydrocarbons, CO_2 are some of the causing penetrants that result in plasticisation in natural gas separation. Plasticisation is more prevalent in high pressure operations such as natural gas purification where feed pressure can be over 30 bar. In this case, a plasticised membrane can become mechanically weak to the point of collapsing (Kentish, 2011).

The aging of polymer membranes is more pronounced in glassy polymers (Harms et al., 2012; Swaidan et al., 2015). Over time the membrane structure loses fractional free volume as the chains become more packed and dense, and this is termed volume relaxation (Müller et al., 2016). This consequently results in a decrease in permeability as pore channels are constricted (Lau et al., 2014).

The methods of creating aging resisting polymer membranes include crosslinking or physical blending to introduce molecules that can keep the structure open to unrestricted diffusion. However, this process may also make the chain more fixed, rigid or open the structure too much and reduce the selectivity. Hence a balance is needed when the modifications are effected (Müller et al., 2016; Smith et al., 2020). Similarly, the extent of plasticisation may be reduced by crosslinking, thermal treatment and thermal rearrangement. Polymer blending and polymer grafting are the other techniques that can be used so that the membrane can resist plasticisation and increase mechanical strength at high pressure operation (Kentish, 2011; Suleman et al., 2016).

The temperature of operation also affects the permeability and selectivity of polymer membranes. At high temperature, the diffusivity and solubility of components within the membrane increases, which increases the permeability. However, this happens to all the components, and as a result, the selectivity decreases (Harlacher and Wessling, 2015).

Robeson, (1991) showed that there is a correlation between the separation factor and the permeability of gases in polymer membranes. A plot of the log of the separation factor against the log of the permeability (Barrer) of a pair of gases showed that there exists a boundary for the hundreds of results analysed. Some of the gas pairs presented were O_2/N_2, CO_2/CH_4, H_2/CH_4, H_2/N_2. The gradient of the boundary line was proved to be equal to the difference in the diameter of the molecules. This indicates that diffusion contributed significantly to the performance of the membrane for the gases being separated. Robeson, (2008) revised the upper bounds presented previously for the several pair of gases and noted a slight shift of the boundary. New gas pairs that had generated research interests and led to several publications such as CO_2/N_2 were also plotted, and the upper bound determined. Figure 2.2 shows the plot for the CO_2/N_2 separation which is used to determine the potential of membranes for post-combustion CO_2 capture from flue gas.

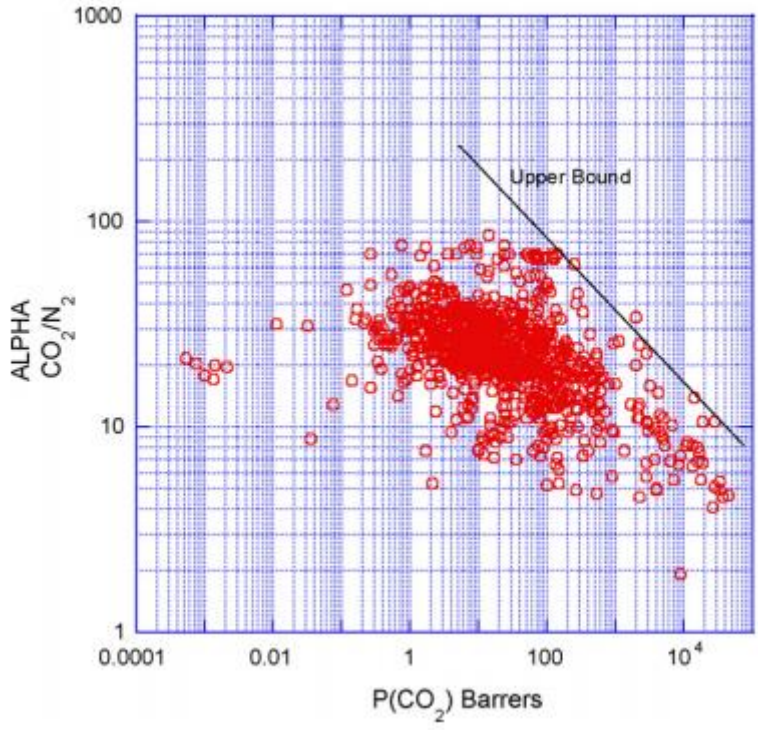

Figure 2.2. Robeson plot (Reproduced from (Robeson, 2008) with permission from Elsevier).

2.4 Types of membranes for CO_2 capture

The flue gas from power plants have CO_2 composition of 10-15%, and N_2 makes up over 60% (James et al., 2019). CO_2 selective membranes have been extensively synthesised and investigated for CO_2 capture and to a lesser extent N_2 selective membranes have also been investigated for CO_2 capture.

2.4.1 CO_2 selective membranes

Post-combustion flue gas consists of high N_2 content, and thus CO_2 capture consists of mainly separating CO_2 from N_2. Therefore, a suitable membrane for post-combustion CO_2 capture should have high CO_2 permeability and selectivity. The favourable material should be mechanically strong to withstand pressure differences across the membrane as compressors, and vacuum pumps are usually installed at the opposite sides of the membrane (Favre, 2011). The membrane must also be able to maintain its permeability and selectivity ability in the presence of minor elements such as SO_2, NO_x and traces of fly ash that can be present in the flue gas (Deng et al., 2006; Lasseuguette et al., 2016).

Table 2.1 shows the different types of membranes which have been investigated for CO_2 capture. Inorganic materials such as zeolites, alumina, silica, and carbon were investigated, and results indicated poor selectivity though the permeability was encouraging (Sreedhar et al., 2017).

Table 2.1: Membranes for CO_2 capture‘‘adapted from Sreenivasulu et al. (2015)

	Permeability	**Selectivity**	**Material**	**Examples**
Inorganic	High	Low		Zeolites, silicas, Perovskite, carbon
Polymers	Low	High	Pure polymers	Rubbery polymer Glassy polymers
Mixed matrix	high	Low	Polymer+ molecular sieves	
Hybrid	high	High	Polymers + ceramics	
Facilitated transport	High	High	Polymer + carrier agent	Fixed carrier Mobile carrier Immobilised liquid membranes

Polymer materials have already been industrialised for other applications (Harlacher and Wessling, 2015). Therefore, this motivated numerous studies to be conducted to investigate their applicability to CO_2 capture.

Polar groups have been introduced to increase CO_2 permeability. For instance, Poly(ethyne) oxide-based membranes utilise the ether group to make CO_2 more soluble in the membrane structure since ethers have a high affinity for CO_2. Methods such as co-polymerisation, physical blending and crosslinking are used to synthesise polyethene oxide based membranes. The resulting polymer membranes are rubbery and have higher CO_2 permeability. Several commercial membranes for CO_2 separation, such as the Pebax and Polaris, are based on this technique.

Thermally rearranged (TR) membranes are fabricated by heat treatment of the synthesis materials at temperature higher to open up the structure and create a high free volume which

increases the permeability. The synthesis process can also involve crosslinking agents that make the structure rigid and further opens up the structure, and increases the selectivity (Xiao and Chung, 2011). The TR membranes are characterised by high permeances and examples include polybenzimidazole (PBI) and polybenzothiazole (PBT). These membranes are thermally stable and thus applicable to high temperature operations.

Polymers of intrinsic microporosity (PIMs), known as 'PIMs' refer to those membranes that have fixed but twisted polymer chains. The bent shape makes up microcavities that enhance gas sieving and thus give high CO_2 permeability (Wang et al., 2016). The angle of distortion can be tuned to increase the free volume and increase permeation rates, and like other polymer membranes crosslinking with other groups can enhance the selectivity (McDonald et al., 2015).

In facilitated transport, membranes transport CO_2 across the membrane by carrier agents through chemical reactions in addition to the physical interaction of CO_2 with the material of the membrane. The carriers are involved in reversible reactions with the CO_2 within the membrane. Facilitated transport membranes have improved CO_2 flux and selectivity because of a carrier agent incorporated into the membrane (Huang et al., 2008). The facilitation of transport overcomes the permeability and selectivity trade-off as the carriers are targeted to facilitate the transport of only CO_2. This simultaneously aids the permeability and increases the selectivity multi-fold (Tong and Ho, 2017). Facilitated transport membranes come in two types; mobile and fixed-site carrier membranes. Various amines are used as carriers as these are good CO_2 absorbers (Kim et al., 2013; Qiao et al., 2013). The kinetics of the reversible reaction is important. The forward reaction represents the absorption of CO_2, and the backward reaction determines the rate of regeneration of the carriers.

Mobile carrier facilitated transport membranes can be liquid membranes or ion exchange membranes (Tomé et al., 2013). In liquid membranes, pores of a polymer material are filled with a liquid which acts as a CO_2 absorbent which allows the movement of the CO_2 from the feed side to the permeate side where CO_2 desorbs and leaves the membrane (Sai Prasad and Raghavan, 2012). These are also called supported liquid membranes. Ion-exchange membranes are also a type of mobile carrier membranes. Mobile carrier facilitated transport membranes suffer some drawbacks, which includes solution degradation and solution depletion (Zhao et

al., 2012). This can be overcome by developing more viscous liquids and less volatile solvents. Because of these challenges, FSC membranes appear more suitable.

In fixed site carrier (FSC) membranes, polymers are the backbone of the membrane, and they are functionalised using carriers to selectively transport CO_2 (Ansaloni et al., 2015). The carrier groups are attached to their locations and do not move. Table 2.2 presents selected FSC membranes investigated for CO_2 capture. Examples of fixed-site carrier membranes studied for CO_2 capture are polyvinylamine (PVAm), polyvinyl alcohol (PVA), Pollyallymine(PAAm) and a blend of these membranes. A PVAm supported on Polysulfone showed very high gas permeance of 1827GPU and selectivity above CO_2/N_2 500 (T.-J. Kim et al., 2013). The major drawback of using PVAm for CO_2 separation is that plasticisation occurs, which reduces the selectivity. Crosslinking with other carriers such as peperazine was investigated to make a PVAm –PIP/Psf resistant to plasticisation with much success as the CO_2 permeance increased to 6500 GPU and a modesty selectivity CO_2/N_2 of 277 was realised (Qiao et al., 2013).

Membranes that have both mobile and fixed carriers have been synthesised and tested for CO_2 capture. Zou and Ho, (2006) synthesised a PVA membrane crosslinked with formaldehyde to enhance the membrane stability at temperatures higher than 100 °C. Han et al. (2018) incorporated multi-walled carbon nanotubes (MWNT) into the polyvinylpyrrolidone (PVP)-matrix to produce co-polymer wrapped (MWNT) membranes. These were functionalised to produce a membrane with amino groups as fixed carriers and an aminoacid salt as mobile carriers for CO_2/N_2 separation. The incorporation of the MWNT was to strengthen the membrane and prevent the facilitated membrane from collapsing under a large transmembrane pressure difference as a result of vacuum pulling on the permeate side. The nanotube-reinforced membrane was able to withstand the large pressure difference and resist compaction at high feed pressure up to 7bar with no loss of permeability or selectivity. Subsequent work with a different mobile carrier amino salt 2-(1-piperazinyl)ethylamine also showed high permeance of 1451 GPU and CO_2/N_2 selectivity of 167 at a temperature of 67 °C in the presence of trace SO_2 and 7% O_2 (Han et al., 2019b).

Table 2.2: Examples of facilitated transport membranes for CO_2 capture

Material	Support	Process	Reference
PAAm/PVA blend	Polysulfone	CO_2/N_2	(Zou and Ho, 2006)
PVAm	Polysulfone	CO_2/N_2	(Kim et al., 2013)
CNT-reinforced PVAm/PVA	Polysulfone	CO_2/N_2	(Han et al., 2018)
PVA/PVAm blend	-	CO_2/N_2	(Deng et al., 2006)

The trade-off between selectivity and permeability is addressed by introducing fillers that aid either selectivity or permeability. The modification of polymer membranes in order to fine-tune the properties result in composite membranes such as mixed matrix membranes and metal-organic framework. A mixed matrix membrane is polymer-based membranes whose matrix is doped with another material (filler) of usually nano-scale size to form a mixed matrix (Wang et al., 2017). Traditionally the fillers have been inorganic, such as various zeolite-based material, carbon silica, metal-organic framework material. Graphene oxides and carbon nanotubes are some of the materials that have been incorporated into the polymeric structures to form mixed matrix membranes (He et al., 2014; Quan et al., 2017; Zhou et al., 2019). However, the problem of adhesions of the polymer and the inorganic filler which reduces the free volume, needs to be further addressed (He, 2018b). Sarfraz and Ba-Shammakh, (2018) synthesised an Ultrason® polymer doped with ZIF-300 nanocrystals MMM for CO_2 capture from humidified flue gas. The CO_2 permeance increased by four times compared to the undoped polymer membrane, and the selectivity remained unchanged. Organic fillers include polyaniline, poly(N-isopropylacrylamide) nanohydrogels and crosslinked polystyrene (Wang et al., 2017).

Experimental work on the development of membranes for CO_2 capture involves synthesis, characterisation and testing. These laboratory studies are carried out to determine the permeability of a gas through a membrane and also to assess the ability of one gas to permeate the membrane over the other, which is the selectivity of the membrane with respect to one gas over the other. Selectivity is determined from the different permeability of the studied gases. These indicate the potential of the material for CO_2 capture. Experiments for carbon capture

are usually carried out using binary gases, CO_2/N_2 and CO_2/CH_4, since N_2 and CH_4 are usually the gases with a major composition in post-combustion capture.

Simulation and optimisation for techno-economic studies are based on the results from these laboratory experiments and at times on virtual membranes with the permeability and selectivity arbitrarily selected. Listed in Table 2.3 are some of the studies these membranes have been used in modelling membrane based CO_2 capture. The Polaris is a commercial polymeric membrane that has also been investigated for flue gas separation and has been tested on real flue gas in pilot studies (Merkel et al., 2010; White et al., 2015).

Table 2.3: Membranes used in modelling post-combustion CO_2 capture

	CO_2 Permeance (GPU)	**Selectivity CO_2/N_2**	**References**
Polaris1	1000	50	(Merkel et al., 2010)
Polaris 2	2200	50	(Merkel et al., 2013)
FSC	2000	500	(Kim et al., 2013)
Polyactive	1850	60	(Yave et al., 2010)

2.4.2 N_2 selective membranes for the separation of CO_2/N_2 gas mixtures

For the CO_2/N_2 mixture which is representative of post-combustion capture, most research has focused on developing CO_2 selective membranes. However, a few reports have been published on the CO_2 /N_2 separation by use of N_2 selective membranes since N_2 makes a major composition of the flue gas. Table 2.4 shows the performance of some of the N_2 selective membranes.

Table 2.4: Permeance and selectivity of N_2 selective membranes

Membrane	Permeance (GPU)	Selectivity N_2/CO_2	Reference
PEI/MCM-48	27	3	(Kumar et al., 2008)
HAS	12.3	6.8	(Kim et al., 2015)
CA/Si-CL	1866	22.3	(Hussain et al., 2015)
Vanadium	1.05×10^{-5}	$>10^5$	(Liguori et al., 2019)

Kumar et al. (2008) synthesised a PEI/MCM-48 composite membrane which comprised of MCM-48 as the matrix. The matrix was stabilised and functionalised by a polyethyleneimine (PEI) which added amines to the membranes. In the presence of water vapour of 2.6% by volume at 20 °C temperature, the N_2/CO_2 selectivity was 3. It would be expected that the amine groups would increase the CO_2 permeance, however in this case, the PE-CO_2 absorption bonds are too strong and reduce the CO_2 mass transfer rate resulting in this unexpected result. (Ghosal et al., 1996; Kumar et al., 2008). Following the work of Kumar et al., Kim et al. observed that a mesoporous silica polymer membrane functionalised with Aziridine produced branched Aminosilica (HAS) composite membrane. The membrane was CO_2 selective in the separation of humidified CO_2/N_2 gas, whilst the membrane was N_2 selective when the dry CO_2/N_2 gas mixture was separated. In the absence of water, CO_2 strongly adsorb onto the amino sites, which slows the CO_2 diffusion. One mole of CO_2 adsorps onto two moles of RNH_2 which causes extensive crossing within the structure and reduces the free volume. In contrast, in humidified gas, the ratio is one mole of CO_2 to one mole of RNH_2, which results in less crosslinking (Kim et al., 2015).

Hussain et al. (2015) reported the synthesis of an N_2 selective membrane that showed high N_2 permeance. A cellulose acetate (CA) membrane matrix was modified by introducing silica (Si) and p-tert-butylcalix[4]arene-immobilisedsilica (CL−Si) as fillers. The resulting membrane was a cellulose acetate silica p-tert-butylcalix[4]arene-immobilisedsilica (CA/CL-Si) membrane. N_2 has a higher permeability than CO_2 in the CA/CL-Si membrane despite having

a larger kinetic diameter. CO_2 gets trapped on the surface of the membrane by the cavities present in the CL structure (Hussain et al., 2015; Tsue et al., 2012).

Metallic membranes have been explored as N_2 selective membranes because of they exhibited high selectivity in the H_2/CO_2 separation, first by Yuan et al. and recently by Liguori et al. (Liguori et al., 2019; Yuan et al., 2014). The metallic membranes, i.e. vanadium, niobium and tantalum, all showed almost ideal N_2/CO_2 selectivity with values above 10^5. However, the major drawback of the metallic membranes for CO_2/N_2 separation is the very low N_2 permeability. Another challenge is the high operating temperature (>400 °C) which would mean high energy consumption at industrial-scale application.

2.5 Mechanism of gas permeation in polymer membranes

Permeation of gases through polymers have been shown to follow the 'solution diffusion' mechanism, which is usually assumed for most flue gas membrane separation (Shao et al., 2013; Sreenivasulu et al., 2015). The facilitated transport involves the movement of molecules by the polymer and also facilitated by the carriers.

2.5.1 Polymer permeation models

The transport of gas molecules through a polymer membrane barrier is commonly described by the 'solution- diffusion'. Firstly the molecules are absorbed onto the surface of the membrane at the feed side. The second step is the diffusion of the molecule through the bulk of the membrane structure. The molecules finally have to desorb from the other side of the membrane. The steps mentioned describe the 'permeation' of a gas in a membrane (Baker, 2004).

Fick's law states that the molar flux of a diffusing molecule is proportional to the concentration gradient and is assumed to be the basis of molecule transport through the membrane. Fick's Law of diffusion describes the diffusion of a molecule, and at a steady state, the molar flowrate *(F)* of a gas component *($_A$)* that passes through an area *(A_{mem})* of the polymer is proportional to the concentration gradient of the component *(dc/dx)*. The Equation (2.3) describes the flowrate component through the polymer membranes. The flowrate per unit area (F/A_{mem}) is the flux. The diffusion coefficient *(D)* is the constant of proportionality. The diffusion coefficient

depends on the temperature, structure of the polymer and concentration of the gas molecules dissolved within the polymer. The expression *(dc/dx)* represents the chemical potential which is also the driving force. Equation (2.4) shows the change in concentration from the feed side (C_A^{rt}) of the membrane to the permeate side (C_A^{pm}) of thickness *(l)*.

$$F_A = -D_A A_{mem} \frac{dc}{dx} \tag{2.3}$$

$$\frac{dF_A}{dA_{mem}} = -D_A \frac{C_A^{rt} - C_A^{pm}}{l} \tag{2.4}$$

The solubility of the gas in a polymer is low, and therefore Henry's law of solubility holds. It states that the concentration is equal to the solubility constant/coefficient multiplied by the partial pressure *(p)* of the gas molecule *($_A$)* at a point as given by Equation (2.5). *S* is the solubility coefficient for the gas/solvent system, which in this case is the polymer material and the gas molecule travelling through it. Substitution of the concentration *(C)* in Equation (2.4) results in Equation (2.6) and further rearranging gives Equation (2.7).

$$C_A = p_A S_A \tag{2.5}$$

$$\frac{dF_A}{dA_{mem}} = -D_A \frac{p_A^{rt} S_A - p_A^{pm} S_A}{l} \tag{2.6}$$

$$\frac{dF_A}{dA_{mem}} = -\frac{D_A S_A}{l} (p_A^{rt} - p_A^{pm}) \tag{2.7}$$

$D_A S_A$ is the permeability coefficient of a gas component through a specific polymer membrane. Thus the permeability is directly proportional to the diffusivity of the gas components and the solubility of the component in the polymer. Molecules of lower kinetic diameter have higher diffusivity coefficients and thus more permeable than molecules of larger kinetic diameter. Table 2.5 gives the kinetic diameters of some of the gases that are separated by polymeric membranes. CO_2 has a lower kinetic diameter than the other gases found in flue

gas like O_2 and N_2, and therefore, CO_2 will likely be more permeable than other gases in the mixture based on its diffusivity (Joseph et al., 2018).

Table 2.5: Kinetic diameters (Robeson, 1991; Zhao et al., 2017)

Gas	Kinetic diameter (Å)
N_2	3.64
O_2	3.46
CH_4	3.8
H_2	2.89
CO_2	3.3

Table 2.6 shows that CO_2 has a higher solubility in a polymer than the other gases. The molecules that can absorb onto the surface of the membrane can then diffuse through the membrane. Combining the high CO_2 solubility and higher diffusivity gives CO_2 a greater permeability in polymer films than the other gases and therefore enables gas separation and CO_2 capture by membranes. The product of the diffusivity coefficient and solubility of a gas molecule determines the more permeable membrane.

Table 2.6:The solubility of different gases in a polymer (Baker, 2004; Wang et al., 2016)

Gas	Critical temperature °C	Ideal solubility in a polymer [10^{-3} cm^3 (STP)/$cm^3 \cdot$ cmHg]	Reaction with carriers
N_2	-147	2.6	No
O_2	-118	4.8	Yes
CH_4	-82	18.4	No
CO_2	31	29.5	No

The term $D_A S_A / l$ presented in Equation (2.7) is the permeance (φ). It can be seen that a very thin film membrane will result in high permeance and hence high flux. Hence fabrication of defect-free thin-film membranes is an area of research interest (Liang et al., 2019). The Equation (2.7) can be rewritten as for a particular membrane in terms of known thickness and in terms of permeance as shown by Equation (2.8).

$$-\frac{dF_A}{dA_{mem}} = \varphi_A (p_A^{rt} - p_A^{pm}) \tag{2.8}$$

The Equation (2.8) gives the two important parameters that influence the large scale design of membrane based gas separation: the membrane area and the partial pressure difference. The flowrate of the target component that permeates is directly proportional to the membrane area and the difference in the partial pressure. The partial pressure of a gas is equal to the product of pressure and mole fraction.

2.5.2 Facilitated transport models

CO_2 permeation by fixed facilitators is described as the sum of the solution diffusion and chemical facilitated transport (reversible reactions). The target gas component to permeate the membrane is termed the solute *(A)* and reacts with the facilitator which is also called the carrier *(C)* to form a complex *(AC)* as shown by Equation (2.9) (Stern and Walawender, 1969).

$$A + C \rightleftharpoons AC \tag{2.9}$$

The complex *AC* then breaks down on the opposite end of the membrane, releasing the target component *A* and freeing the carrier *C* to facilitate the transport of more *A,* which in this case is CO_2. The other components simply travel by the 'solution diffusion' mechanism through the membrane (Rea et al., 2019). The flux is, therefore a sum of the solution-diffusion mechanism and the gas transported by facilitated transport. The carrier is usually assumed to be much bigger than the solute, such that the size of the complex is taken to be equal to the size of the carrier. So the total concentration of the carrier present can be described as a sum of the complex and free carrier at a time (Kemena et al., 1983).

Goddard et al. (1974) mentioned that even if the flux was sensitive to the permeate concentration, it would be difficult to show. The theoretical predictions cannot be verified with any experimental setup. Whilst pressure can be controlled, the concentration on the permeate side cannot be controlled or predicted because of stirring effects. The permeate concentration on the boundary layer and the bulk phase maybe different due to insufficient stirring. The net flux also depends strongly on the permeate concentration. Unstirred boundary layer maybe at play in real life. True facilitated transport would be displayed for negligible boundary –layer which did not show any flux resistance (Goddard et al., 1974).

Siegel et al. (1992) presented a mathematical model for fixed site facilitated transport that proved that the distance between the carrier sites did not have an impact on the facilitation of the solute transport through the polymeric membrane. The solute could still hop from one site to another. The models, however, assumed the presence of excess carriers (Noble, 1992).

The flow of a solute through a membrane in the presence of fixed carriers was likened to the flow of electricity through a resistor capacity circuit by (Kang et al., 1996). It is considered that gas transport through a framework membrane without carriers is similar to the flow of electrons in a circuit with a resistor only. The membrane with FSC is then likened to a resistor circuit that also has a capacitor resistor capacity circuit. The FSC facilitated transport model was developed from the analogy of a parallel resistor capacity. When voltage is applied, the total flux of electrons is a sum of the contribution of the resistor in the circuit as well as the contribution of the capacitor. The resistor is likened to the polymer matrix where gas flows due to Fickian diffusion and the capacitor is likened to the solute- carrier complex in the membrane. The voltage and conductivity is analogous to the pressure gradient (driving force) and permeability, respectively. With this regard, therefore, the facilitated factor is analogous to the ratio of conductivity of an RC circuit to that of a resistor only based circuit. The model was verified by the permeation of O_2 through poly(dimethyl siloxane), poly(butylmethacrylate) and poly(methyl methacrylate) with metallo-porphyrin. The model could capture the carrier saturation phenomenon with better accuracy than previously presented models such as the dual sorption (Hong et al., 1996; Rea et al., 2019).

Zhang et al. (2013) presented a more practical and applicable model which showed the relationship between the permeability of a gas component with partial pressure across the

membrane. The parameters in the permeance model can be easily determined, and the model can be implemented in simulation and optimisation studies. The reaction equilibrium at the feed side and the concentration of the carrier is assumed to be the sum of the un-complexed carrier and the complexed carrier. The partial pressure of a solute is directly proportional to its concentration in solutions if it is a dilute solution according to Henry‘s Law. The permeability model indicates that low partial pressure on both the retentate and permeate side could increase the permeance rate of a gas across the membrane, however, a high partial pressure difference is still the driving force. The permeation model was applied to both mobile carrier facilitated membranes and fixed site carrier facilitated membranes as a verification step. The model results for the mobile carriers fitted more excellently than that of the fixed site carriers. The difference between the experimental trend line and model results was attributed to the diffusivity of the carrier solute complex which had been largely guessed (Zhang et al., 2013). This challenge was also highlighted in another report. Ebadi Amooghin et al. (2018) stated that ‘the challenge to modelling facilitated transport in membrane include the lack of kinetic data such as diffusivity’.

The model showed that the permeance decreases with an increase in both the feed and permeate partial pressure. It follows that an increase in the concentration of the target component on the permeate side results in a decrease in the permeance. The permeance also decreased significantly for a thicker membrane than a thinner membrane. The results from their simulation studies showed that increasing the carrier load would significantly increase the permeance. The model reiterated Shultz’s observation that the impact of variables on the effective gas transport cannot be investigated experimentally as the concentration of the solute cannot be measured within the membrane (Goddard et al., 1974). Zhang et al. (2013) also noted that experiments are usually carried out with sweep gas on the permeate which is of high concentration and significantly dilute the target component making the permeate partial pressure of the solute negligible (Zhang et al., 2013). Practical application of the fixed site carrier may not include a sweep gas and the flowrate of the sweep gas may not be large enough to significantly dilute the target component to the extent of experimental runs.

Zarca et al. (2017) synthesised the PVDF-HFP/AgBF4 membranes for the separation of propane /propylene gas mixtures. A model was determined from Arrhenius law to describe the contribution of the fixed site carrier to propylene transport across the membrane. The mechanism proposed for propylene was a combination of the ‘solution diffusion’, and FSC

facilitated transport. The ‘hopping’ theory suggested by Noble was adopted but simplified (Noble, 1991). The model assumed that the resultant permeance was predominantly due to facilitated transport, and therefore, the solution diffusion could be neglected. It is noteworthy that the permeability is expressed in terms of the concentration of the carrier concentration and the equilibrium constant. This is advantageous since the concentration of the carrier is a known parameter. This model can be implemented in simulation and optimisation models and can be solved easier. Experimentally determined parameter such as the activation energy, dictates that an experimental study be carried out first for a particular membrane to be simulated (Zarca et al., 2017a).

The work was further extended to include the contribution of mobile carriers. Zarca et al., (2017b) developed an advanced model for olefin flux through a polymer ionic liquid membrane which is a mobile-fixed site hybrid model. Three mechanisms were at play in the membrane, which is solution diffusion, fixed-site carrier and mobile carrier transport. In the model, the flux was described in terms of all these three mechanisms, which was a first for polymer/ionic membranes. Similar to the previous model, the permeability coefficient of the liquid/mobile carrier solute is the product of the diffusivity and solubility of the complex within the liquid. Both the solubility and diffusivity of the solute (propylene) in the membrane are temperature dependant, and therefore, their thermal dependency was captured in the model by Arrhenius relation. Both these models by Zarca et al. fitted well with experimental data (Zarca et al., 2017a, 2017b). The results showed that the permeance of propylene increases with an increase in pressure following a log function. The inclusion of a thermal parameter can facilitate simultaneous optimisation of pressure, carrier concentration and membrane operating temperature. A similar permeation model for dual facilitated membranes was presented recently; however, it was assumed that the permeate partial pressure was negligible in order to reduce the complexity of the model (Han and Ho, 2020a).

Zarca et al. developed models that could enable temperature and concentration to be variables that can be optimised as these influence the permeance of components (Zarca et al., 2017a, 2017b). The drawback of the developed models is that experimental work needs to be carried out to determine parameters such as the activation energy. The model developed by Zhang et al. can be recommended for use in techno-economic feasibility studies of FSC membrane processes. The model presented by Zhang et al. does not pose the mentioned challenge as it is

easier to implement in modelling work since all the parameters in the model can be determined without prior experimental work (Zhang et al., 2013).

2.6 Facilitation of CO_2 through a membrane

The CO_2 molecule contains two electronegative oxygen molecules, as depicted by Figure 2.3. The CO_2 molecule is, therefore acidic and reacts with bases.

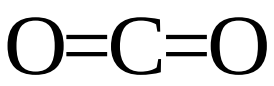

Figure 2.3. Scheme of a CO_2 molecule showing the double bonds between carbon and oxygen atoms

The polymer membranes with amine groups are naturally the functional groups used in FSC membranes since CO_2 scrubbing with amines has a long history of success. The Equation (2.10) and (2.11) shows the formation of a zwitterion ($NH_2^+COO^-$) from CO_2 and non-sterically hindered amine (Danckwerts, 1979). The zwitterion loses a proton to another amine to form a carbamate ion ($NHCOO^-$) (Danckwerts, 1979; Kortunov et al., 2016). The Equation (2.12) is the overall resultant equation showing that it takes 2 moles of the amine to facilitate the movement of 1 mole of CO_2. The backward reaction of Equation (2.12) occurs on the permeate side of the membrane and the CO_2 is released and the amine is regenerated.

$$CO_2 + RNH_2 \rightleftharpoons RNH_2^+COO^- \quad (2.10)$$

$$RNH_2^+COO^- + RNH_2 \rightleftharpoons RNHCOO^- + RNH_3^+ \quad (2.11)$$

$$CO_2 + 2RNH_2 \rightleftharpoons RNHCOO^- + RNH_3^+ \quad (2.12)$$

However, sterically hindered amines exhibit superior permeability and selectivity for CO_2 transport since they require only 1 mole of amine to facilitate 1 mole of CO_2. Equations (2.13) -(2.15) shows the role water plays in facilitating CO_2 movement in the membrane. In this case, the carbamate ion is unstable and reacts with water to form a bicarbonate ion (HNO_3^-). The CO_2 is transported in the form of the bicarbonate ion. The formation of the bicarbonate ion is

therefore catalysed by the amines present in the membranes (Han and Ho, 2020b; Tong and Ho, 2017).

$$CO_2 + R_1NHR_2 \rightleftharpoons R_1R_2NH^+COO^- \leftrightharpoons R_1R_2NCOOH \quad (2.13)$$

$$R_1R_2NCOOH + R_1NHR_2 \leftrightharpoons R_1R_2NCOO^- + R_1R_2NH_2^+ \quad (2.14)$$

$$R_1R_2NCOO^- + H_2O \leftrightharpoons R_1NHR_2 + HCO_3^- \quad (2.15)$$

In the case of membranes with tertiary amines as functional groups, water reacts with CO_2 to form carbonic acid (H_2CO_3) as depicted by Equation (2.16) . The H_2CO_3 formed then reacts with the tertiary amine to form a bicarbonate ion as shown in Equation (2.17) (Han and Ho, 2020b).

$$H_2O + CO_2 \leftrightharpoons H_2CO_3 \quad (2.16)$$

$$H_2CO_3 + R_1R_2NR_3 \leftrightharpoons HCO_3^- + R_1R_2NH^+R_3 \quad (2.17)$$

Depicted in Figure 2.4 is a schematic diagram that elaborates on the FSC facilitated transport of CO_2 through a PVAm membrane. It shows the role of water within the membrane in facilitating the movement of CO_2. The figure also shows that other components that make up power plant flue gas such as N_2 and O_2 pass through via non facilitated transport and this results in a much enhanced CO_2/N_2 and CO_2/O_2 selectivity (Kim et al., 2013).

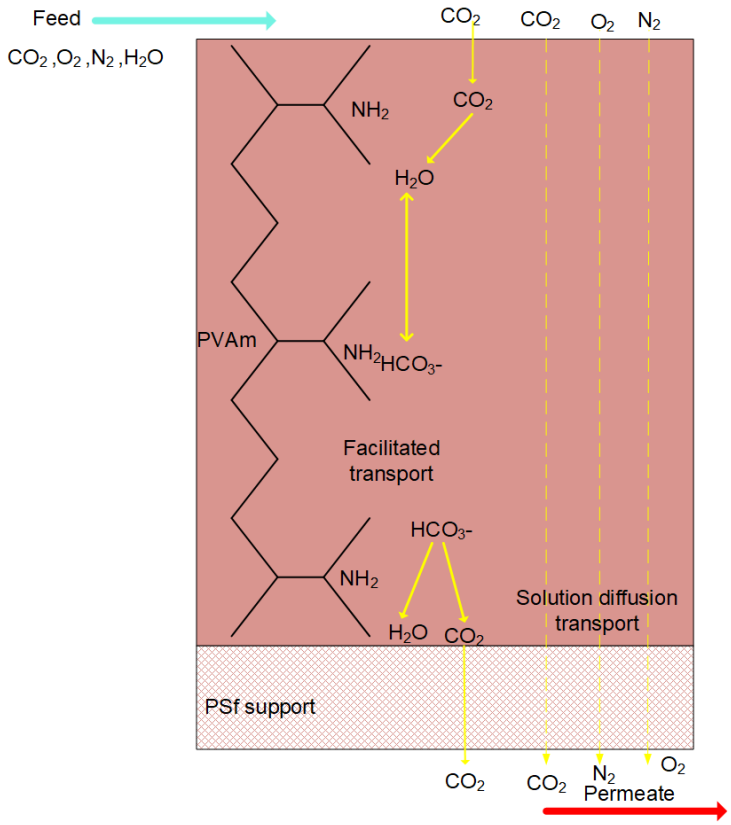

Figure 2.4. CO_2 transport in a high pH, FSC PVAm/Psf membrane (Kim et al., 2013; Yu et al., 2011)

2.7 Design considerations for CO_2 capture

The factors that affect the design of gas membranes are the composition of the target component in the mixture to be separated, the driving force generation strategy and the flow pattern and membrane module chosen for a specific operation which are described in this section.

2.7.1 Flow patterns

The flow pattern can be cocurrent, crossflow or countercurrent illustrated in Figure 2.5 are the common flow patterns commonly modelled in literature (Rautenbach and Dahm, 1985). A sweep gas can also be introduced to dilute the permeate and thus increase the potential and

driving force across the membrane. The sweep gas should be separated easily from the target component (CO_2) to achieve the desired CO_2 purity.

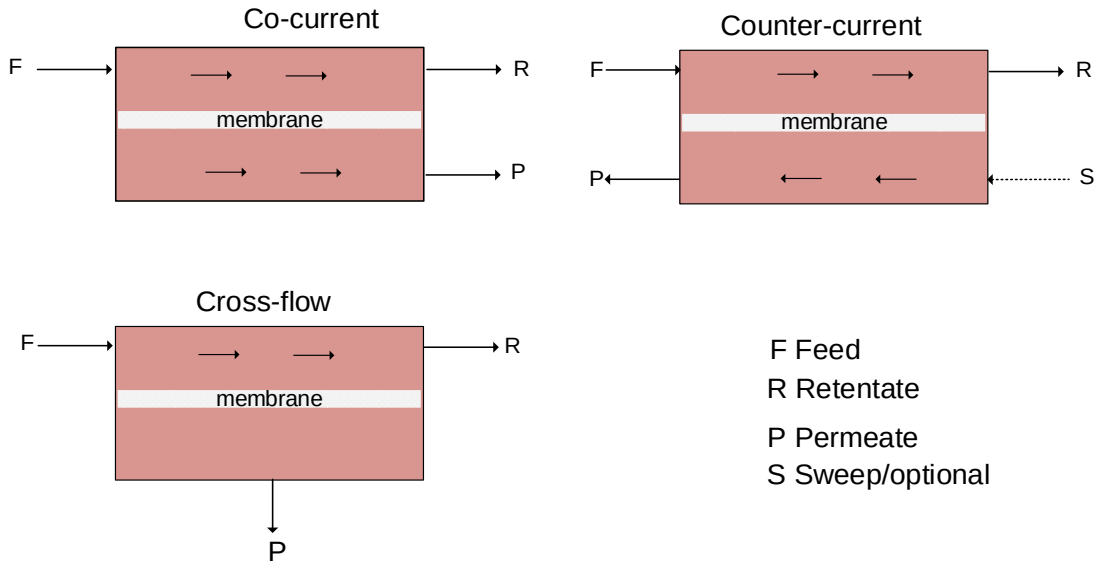

Figure 2.5. Common flow patterns employed in gas separation by membranes (Pan, 1983)

CO_2 stripped flue gas may be used as sweep, this greatly improves the flux, thereby reducing membrane area required significantly (Merkel et al., 2010). Combustion air has also been used as a sweeping gas before being fed to the boiler to generate flue gas of higher CO_2 composition (Ramasubramanian et al., 2012; Scholes et al., 2013).

2.7.2 Module configurations

Hollow fibres have been commonly modelled and proposed for CO_2 capture. Generally, they are cheap to produce and have the advantage of high packing density that can be as high as $10000 m^2/m^3$. As depicted in Figure 2.6, the fibres are packed in a tube and configured as shell and tube. The major drawback is the huge pressure drop that can be realised. Polysulfone and Polymide are examples of commercial membranes available in hollow fibre modules (Harlacher and Wessling, 2015).

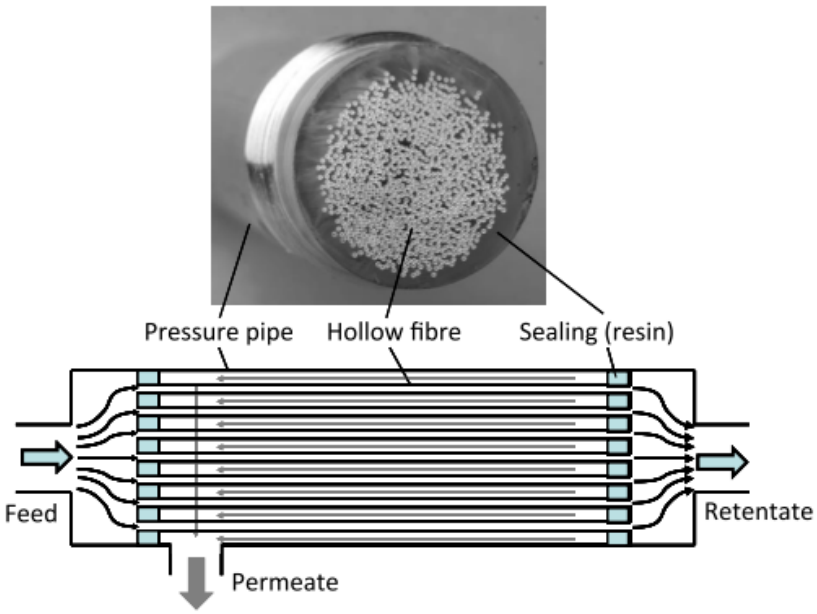

Figure 2.6. Hollow fibre membrane modules (Reproduced from (Harlacher and Wessling, 2015), figure reprinted with permission from Elsevier)

Figure 2.7 shows the spiral wound module. It offers a good balance between the cost of fabrication and resistance to fouling and less pressure drop. However, the packing density is low at 200m^2/m^3 and thus may have a larger footprint. Cellulose acetate membrane is available as spiral wound membrane modules for purchase. It is a crossflow pattern configuration by design (Harlacher and Wessling, 2015; Perry and Green, 1997).

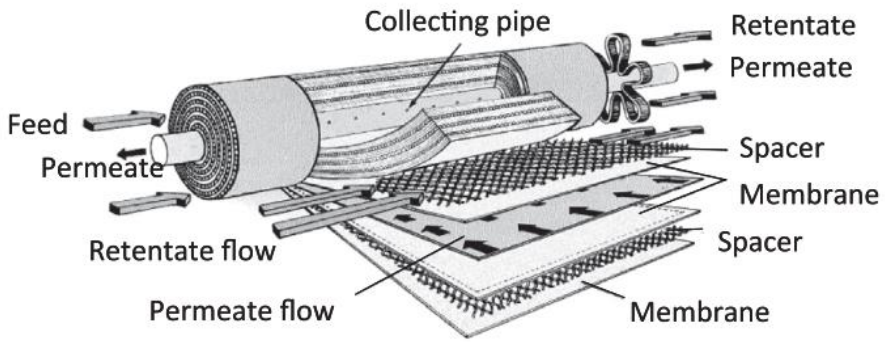

Figure 2.7. Spiral wound membrane modules ((Harlacher and Wessling, 2015) figure reprinted with permission from Elsevier)

The plate and frame membrane modules are made up of a flat sheet of membrane with membrane spacers that are the plates. The flow is directed by the feed distribution plate. Plate and frame modules have the least packing density and, therefore are less applied in gas separation by membranes since huge flowrates are processed (Balster 2013).

The permeation models previously discussed in section 2.5, combined with the material balances around the membrane make up the membrane model. Solving these models can be a challenge because of the unknowns at the boundaries. The easiest to solve is the cocurrent as the boundary conditions on the inlet points of both the retentate and permeate are known (Stern and Wang, 1978). The solving of the countercurrent flow pattern is complex as the inlet boundaries, which are the known ones, are at the opposite ends and also the unknown composition of the permeate and retentate are at the opposite end. The countercurrent flow gives a larger permeate compared to the cocurrent flow pattern (Stern and Wang, 1978). Pan, (1986) presented a crossflow model for multicomponent permeation through the hollow fibre membrane module that considered pressure drop as an improvement of the previous models. The resulting model was a system of nonlinear differential equations that were difficult to solve as estimates of the pressure profile and area had to be provided. Coker et al. (1998) decided to linearize and use the first-order finite difference method. Chowdhury et al. (2005) suggested the use of an initial value algorithm which was written in FORTRAN, which invoked different solvers. The membrane model included accounts of pressure drop in hollow fibre membranes. This subroutine was integrated with Aspen to make up a flowsheet for CO_2 capture from flue gas. Further efforts resulted in a model that looked at non-isothermal conditions within the membrane of the countercurrent configuration of a hollow fibre module was presented by Coker et al. (1999). The model included heat transfer models across the membrane from retentate to the permeate side in addition to mass transfer models. Heat balances were carried out also for the feed to the retentate exit as well as on the permeate side. For CO_2/CH_4 the temperature could drop by 40 °C. Scholz et al. (2013) presented a more detailed model that took into account real gas effects, pressure drop on both the retentate and permeate side, non-isothermal operation and concentration polarisation. The model could easily be integrated into a simulator unlike previous models (Scholz et al., 2013). The results confirmed that the Joule

Thompson effect was at play for CO_2/CH_4 and non-ideal effects should be taken into account in modelling permeation for such a process (Coker et al., 1999; Scholz et al., 2013). However, for CO_2/N_2 membrane separation, negligible joule Thompson effects due to gas expansion were noted (Mat, 2016).

In simulation and optimisation of membrane gas separation, the membrane module can be specified or modelled as a generic area profile. Qi and Henson, (1998) used a simplified algebraic model for the spiral wound modules in the optimisation of membrane based gas separation process for the separation of CO_2/CH_4 gas. Qi and Henson, (2000) then extended the work to the optimisation of membrane process that treated a multicomponent gas based on an approximate nonlinear-algebraic spiral wound model. Zarca et al. (2018) imbedded the hollow fibre permeation model in the optimisation model for the upcycling of post-combustion gas into syngas or hydrogen. The one-dimensional differential equations developed were parameterised by considering implicit Runge-Kutta methods and solved in an algebraic based environment. Lee et al. (2018) also assumed a hollow fibre module in countercurrent configuration for the automated synthesis and optimisation of membrane based CO_2 capture from flue gas. The solution strategy involves taking the tube profile as a system of tanks in series. On the other hand, approximate models that do not specify the membrane module have been implemented in simulation and optimisation of membrane gas separation (Arias et al., 2016). Uppaluri et al. (2004) regarded the membrane profile as system of compartments and the retentate and permeate sides as different 'states'. The method could be easily adopted for cocurrent, crossflow and countercurrent flow patterns. This was later adopted in subsequent works (Hasan et al., 2012; Uppaluri et al., 2006).

For feasibility studies, generic approximate models such as those used by Arias et al. and Mores et al. in the respective optimisation studies are sufficient to give reasonable estimates (Arias et al., 2016; Mores et al., 2019). The approximate models also have the benefit of making the models relatively easier to solve as they reduce the complexity of the model. This gives the chance to finding reasonable feasible solutions. At pre-feasibility and feasibility stage the decision on the type of module configuration may not have been made and the initial indicative cost would determine if further development steps can be taken thus models such as these that are not based on module configuration are useful. After the feasibility stage, if the project progress, models that are module specific can be be used for the detailed design and analysis.

2.7.3 Parameters of interest in membrane separation

The Equation (2.8) which describes the transport of gas through a membrane is rewritten here in terms of a specific component *(A)* in Equation (2.18). The Equation (2.18) gives the generalised equation for gas permeation through a polymer membrane and fixed site membrane and φ is the permeance due to solution diffusion and also facilitated transport as previously given by Equations (2.8). The driving force in the membrane separation process of flue gas is the difference in the partial pressure of the component in the feed side and on the permeate side (Perry and Green, 1997; Wang et al., 2016). A partial pressure gradient must exist for the movement of components from the retentate side to the permeate side as shown by the inequality presented by Equation (2.19). Rearranging this inequality gives Equation (2.20).

$$-\frac{dF_A}{dA_{mem}} = \varphi_A \left(y_A^{rt} P^{rt} - y_A^{pm} P^{pm} \right) \tag{2.18}$$

$$y_A^{rt} P^{rt} > y_A^{pm} P^{pm} \tag{2.19}$$

$$\frac{y_A^{rt} P^{rt}}{P^{pm}} > y_A^{pm} \tag{2.20}$$

Equation (2.20) highlights the importance of the pressure ratio (P^{rt}/P^{pm}) and the initial composition of the target component in the feed in achieving set purity targets (y^{pm}) of the permeate. There is a limit to the feed pressure that can be applied on both the feed and permeate side. Besides, there is also a maximum transmembrane pressure difference the membrane can withstand. Pulverised coal power plants produce large quantities of flue gas which need to be treated to meet environmental laws. For membrane based CO_2 capture, systems energy is mostly consumed in handling the high rates of flue gas by either compressors or vacuum pumps as these are needed to create the necessary partial pressure difference to drive the separation process (Favre, 2011).

As previously mentioned, the difference in the partial pressures of gas in the retentate side and permeate side is the driving force. Compressors are employed at the feed side to increase the pressure of the flue gas whilst vacuum pumps are deployed at the permeate side to create sub-

ambient operating pressure (Perry and Green, 1997). The use of sweep gas on the permeate sides dilutes and reduces the concentration of the CO_2 on the permeate side thereby lowering its partial pressure. The energy required to run the compressors are a significant operational cost and contributes significantly to the operational expenditure (OPEX). In the case of a power plant, electricity which is a high-quality source of energy is used to drive the compressors and this results in an energy penalty on the overall energy output of the plant (Belaissaoui et al., 2012b; Giordano et al., 2017) . Figure 2.8 presents four options for driving force generation on the countercurrent flow patterns. In Figure 2.8, (a) involves the use of feed compression only, and (b) involves the use of vacuum operation on the permeate side only, (c) is a combination of both the vacuum and feed compression, (d) is a combination of feed compression, and also a sweep and (e) is a combination of feed compression, vacuum and also a sweep to enhance the driving force (Favre, 2011; Sreedhar et al., 2017; Vallieres and Favre, 2004).

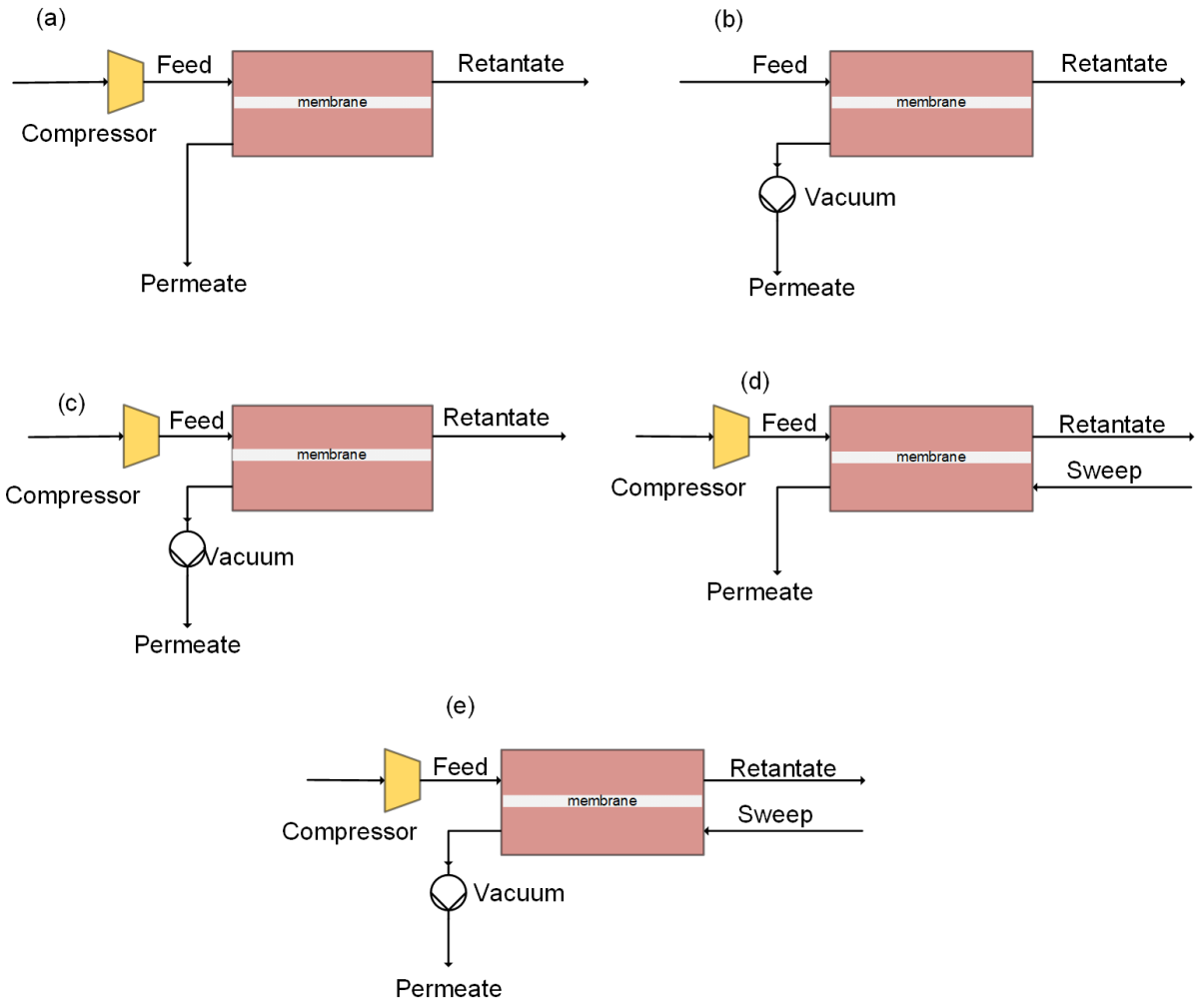

Figure 2.8. Driving force enhancement strategies (Zhao et al., 2010)

When the concentration of the target component in the feed is low as in the case of CO_2 in post-combustion flue gas, there is the possibility that the desired purity and flux will not be achieved by a single-stage membrane separation step as described by the limitations presented in Equation (2.20). This necessitates the deployment of multi-stage membrane systems arranged either in series or parallel with the retentate being fed back to achieve higher overall separation and desired purity. Some of the two stage configurations that have been analysed are shown in Figure 2.9. Recycle streams enhance the concentration of the feed to be fed into the membrane.

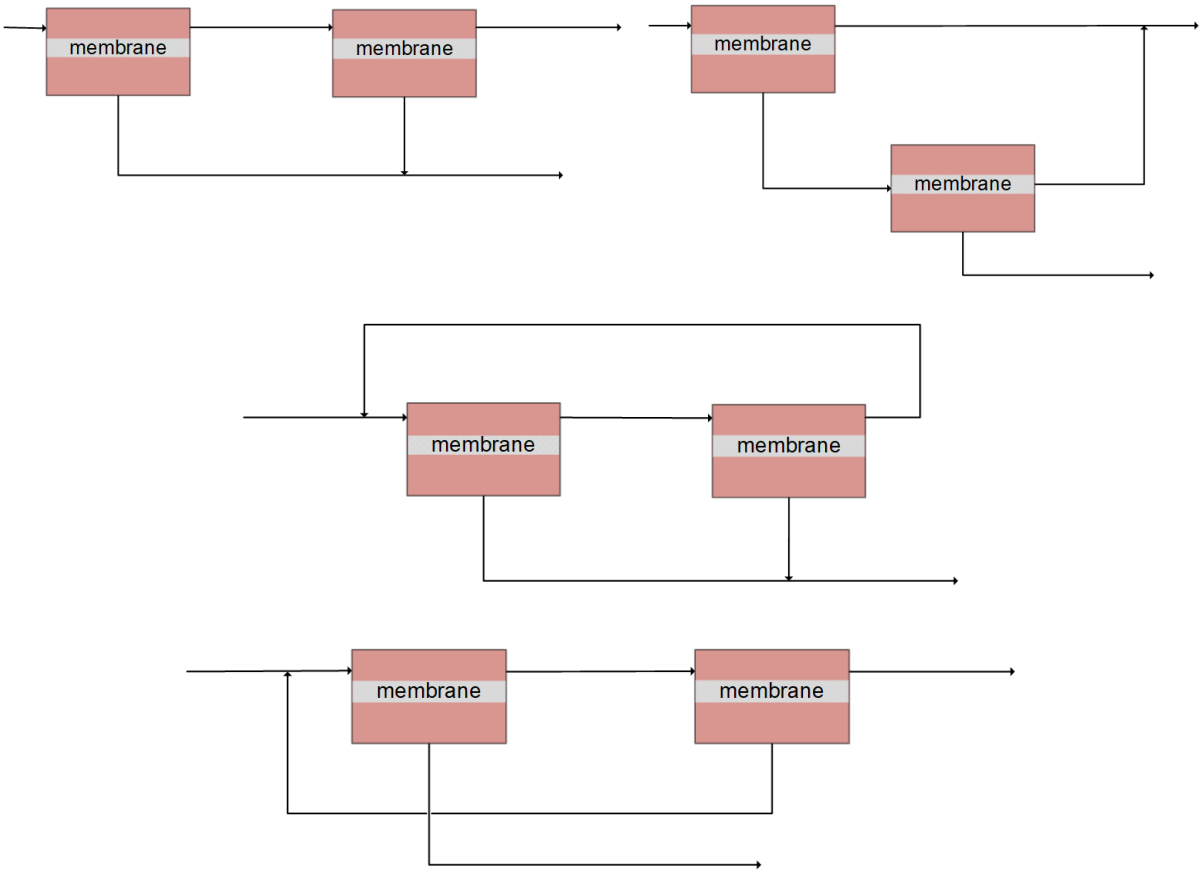

Figure 2.9. Two-stage membrane configurations showing recycle and reuse streams (Hao et al., 2008; Zhao et al., 2010)

From Equation (2.18) it is also apparent that a membrane of high permeance can achieve high recovery of the target species. Having a large membrane area can also increase the flowrate of the permeate. A membrane that has high permeance of the target component can reduce the membrane area required to achieve set recovery targets. A large membrane area required translates to high capital costs (CAPEX). For post-combustion CO_2, a large membrane area has to be employed as well as relatively high pressure has to be applied due to the high volumes of

the flue gas to be processed as well as the low driving force due to low CO_2 concentration (Alshehri et al., 2013).

For flue gas carbon capture, other important parameters are flue gas composition, temperature and flowrate (Favre, 2011). The department of energy of the USA has set a target of 90 % recovery and 95% purity as a requirement for worthwhile carbon capture in power plants (DOE, 2005). Several research groups have used these set parameters for the design, modelling and simulation studies of carbon capture systems (He and Hägg, 2011b; Hussain and Hägg, 2010; Lee et al., 2018; Ramasubramanian et al., 2012).

2.8 Economic indicators for CO_2 capture

An economic evaluation of power plants with CO_2 capture is reported in various ways, which is levelised cost of electricity, cost of electricity, cost of CO_2 avoided and the specific cost of capture (E. S. Rubin et al., 2013a; Rubin, 2012).

2.8.1 Levelised cost of capture

The levelised cost of electricity (LCOE, *$/MW*) is the most comprehensive indicator. It is the cost at which electricity should be sold to recoup all expenses and get the expected return as well. It considers the total cost associated with the generation of electricity for the lifetime *(T*) of the plant and takes into account the interest and insurance. This total cost is divided by the total electricity the plant produces during the lifetime of the plant.

The present value of the income is given in Equation (2.21). It includes the total cost incurred in producing electricity in the year *t*. The discount rate *(r)*, sometimes called the interest rate which is sufficient to cover debt, is determined beforehand. In other works, the fuel cost is lumped as an operating cost (Viebahn et al., 2015). In others, the cost of the fuel is deemed significant, so it is highlighted separately (Rubin, 2012).

$$Present\ value = \sum_t \frac{Electricity \times P}{(1+r)^t} = \sum_t \frac{total\ capital\ cost\ +\ operating\ \&mantainence\ costs + Fuel}{(1+r)^t} \tag{2.21}$$

The levelised cost of electricity *($/MWh)* is given as presented by Equation (2.22). It gives the 'real dollar' as it accounts for the fluctuations in net electricity produced as well as the changes in the fuel and operating costs for the different years *(t)* of the lifetime of the plant.

$$LCOE = \sum_t \left[\frac{\left(\frac{(total\ capital\ costs + operating\ \&\ maintainance\ costs + Fuel)_t}{(1+r)^t} \right)}{\sum_t \frac{(Electricitysold) \times t}{(1+r)^t}} \right] \tag{2.22}$$

A fixed charge factor (*fcf)* is determined as given by Equation (2.23). It is the annuity factor that levelises the capital-related expenses to annual capital expenses.

$$fcf = \frac{r(1+r)^T}{(1+r)^T - 1} \tag{2.23}$$

The Equation (2.22) can be reduced to Equation (2.24) when it is assumed that maintenance costs and fuel cost, and the net electricity produced is constant each year (*8766 hrs*) for the entire lifetime of the power plant. These assumptions are usually made in techno-economic feasibility studies, and 'constant dollars' are reported. The LCOE presented in Equation (2.24) is also commonly reported as the cost of electricity (COE, *US$/MW*).

$$LCOE = \frac{(fcf \cdot TCR) + FOM}{cf \cdot MW \cdot 8766} + VOM + HR \cdot FC \tag{2.24}$$

Fcf = fixed charge factor

cf = plant capacity factor

TCR = total capital related costs ($)

MW_{net} *= total power produced by the plant for sale*

HR = heating rate, MJ/MWh

FC = fuel cost $/MJ

FOM =annual fixed operating and maintenance cost, $

VOM = *variable operating and maintenance cost, $/MW*

Introducing the carbon capture and storage process into a power plant results in decreased power output as some power goes into the capture process hence the extra cost of capture. This makes the cost of electricity (COE) of a power plant with CCS to be higher than that without (Huang et al., 2013).

2.8.2 Cost of CO_2 avoided

The cost of CO_2 avoided *($/ton)* gives the price of preventing the emission of a unit of CO_2 into the atmosphere whilst a unit of electricity is produced. The Equation (2.25) shows that the cost of CO_2 avoided makes a comparison of a plant without CCS and a plant with CCS and takes into account the energy loss resulting from CO_2 capture. It is inclusive of the cost of capture, transport and storage of the CO_2 captured. If a carbon tax is to be introduced to make CO_2 capture economically sensible, the tax *($/ton)* should be at least equal to the cost of CO_2 avoided (Rubin, 2012).

The reference plant and the plant with the CCS are assumed to be producing the same equal amount of CO_2 (E. S. Rubin et al., 2013a; Rubin, 2012).

$$C_{avoided} = \frac{LCOE_{ccs} - LCOE_{woccs}}{E(ton/MWh)_{woccs} - E(ton/MWh)_{ccs}} \tag{2.25}$$

2.8.3 Specific cost of capture

The cost of CO_2 captured *($/ton)* gives the cost associated only with the capture process and does not include the cost of transport nor storage (Merkel et al., 2010). It is also reported as a specific cost of capture or the levelised cost of capture (TLC). It is equal to the total annual cost divided by the mass of the CO_2 captured as given by Equation (2.26). The annualised cost of capture is reported especially in superstructure optimisation studies of CO_2 capture by membranes since many studies have focused on membrane process network as a standalone (Arias et al., 2016; Mores et al., 2019).

$$TLC = \frac{Annualised\ cost\ of\ capture\ (\$)}{Mass\ of\ CO_2\ captured\ per\ annum\ (ton)} = \frac{(fcf \cdot TCR + O\&M)_{CO_2 capture}}{M_{co_2}} \quad (2.26)$$

O&M= annual operating and maintenance cost= sum of FOM and VOM, $

2.9 Review of techno-economic feasibility studies for CO_2 capture by membranes

Techno-economic studies have been carried out based on different promising membranes to determine their feasibility for large scale CO_2 capture (Cao et al., 2013; He et al., 2015; Singh and Rao, 2016; Zhao et al., 2013). Most of the studies targeted to recover 90% CO_2 and to achieve product stream purity of 95% as guidelines set by the US DOE (He and Hägg, 2014). Equations (2.27) describes the stage cut that can be achieved by each membrane stage. Equations (2.28)-(2.30) define the recovery, capture ratio and product purity as indicators of the carbon capture process.

$$Stage\ cut = \frac{total\ material\ flowarate\ collected\ from\ the\ permeate\ side}{Total\ material\ fed\ to\ the\ membrane\ for\ separation} \quad (2.27)$$

$$Recovery_A = \frac{moles\ of\ target\ component\ A\ in\ product\ stream}{moles\ of\ target\ component\ A\ in\ feed\ gas\ to\ be\ separated} \quad (2.28)$$

$$Capture\ ratio_A = \frac{fraction\ of\ target\ component\ A\ in\ feed\ gas}{fraction\ of\ target\ component\ A\ in\ product\ steam} \quad (2.29)$$

$$Product\ purity_A = \frac{flowrate\ of\ target\ component\ A\ in\ product\ stream}{total\ flowrate\ of\ all\ components\ in\ the\ product\ stream} \quad (2.30)$$

A majority of the membrane based techno-economic post-combustion capture studies are based on the dry binary gas CO_2/N_2 since the main component in the flue gas is N_2 (65-75%) and few optimisation studies are based on multicomponent gases (Arias et al., 2016; He and Hägg, 2014; Lee et al., 2018; Mores et al., 2019; Roussanaly and Anantharaman, 2017). The major goal of the studies is to determine the cost of CO_2 capture and how the cost is distributed between the CAPEX and the OPEX as influenced by the size of membrane area utilised and energy consumption, respectively. The studies sought to investigate the impact of various

variables on the cost of CO_2, such as the effect of the CO_2 composition in the feed, the effect of an increase in the membrane cost and the strategy that generates the driving force, i.e. the compression/vacuum configuration that makes most economic sense. The studies also sought to determine the membrane selectivity and CO_2 permeance that would make CO_2 capture by membranes more competitive with the chemical absorption method. Some authors reported the cost of CO_2 avoided and the specific cost of capture (Ho et al., 2008; Zhai and Rubin, 2013). In comparison, many of the optimisation studies reported the specific capture cost only (Lee et al., 2018; Mores et al., 2019; Roussanaly and Anantharaman, 2017).

Van Der Sluijs et al. (1992) assessed the feasibility and cost of capture from a power plant by a membrane. A single stage and a two stage membrane process with retentate recycle were studied. The simulation was carried out based on the binary gas mixture CO_2/N_2. The single stage process could not achieve higher permeate purity. However, for CO_2 purity of less than 70%, the single stage process was more economical. When the purity target increased to 80% the two stage process proved to have a lower cost of CO_2 capture and CO_2 avoided. It was suggested in the study that for the membrane technology to compete with solvent absorption for CO_2 capture, the membranes needed to have CO_2/N_2 selectivity greater than 200. This was disputed later as it was shown that a membrane of higher permeance with moderate CO_2/N_2 selectivity (40) could compete with solvent absorption for CO_2 capture from power plants (Merkel et al., 2008).

Zhao et al. (2008) assessed the effect of parameters such as membrane permeability, selectivity, CO_2 flue gas composition and membrane area on the separation of CO_2/N_2 gas. The study showed that a large membrane area gives an opportunity for N_2 permeance and results in less pure CO_2 permeate. It was also concluded that feed compression could achieve similar purity targets as vacuum operation by a much smaller membrane area. The relatively higher energy consumed by the feed compressor would be offset by an expander on the retentate side which would also process large flowrates. The limitations of a single stage process were also reiterated and two stage operation was recommended.

In a review study, Zhao et al. revealed that the implementation of a retrofit CO_2 capture system would cost the power plant about 20% of the energy it produces (Zhao et al., 2013). The cost of capture for a multi-stage gas membrane was found to be 30% less than amine absorption by

(Bocciardo et al., 2013). 'The term ''efficiency penalty'' refers to the power generation loss by installing CCS on a power plant, and is generally considered the difference in thermodynamic performance between plants with and without CCS ' (Goto et al., 2013).

The comparison of the energy efficiency of the different capture technologies is not straightforward. The energy consumption of CO_2 capture based on solvent absorption is mainly during the regeneration of the solvent steam produced in the boiler of the power plant which is thermal energy. CO_2 capture by membranes, however, utilises electricity which is a high quality energy source to drive the compressors. Some models have been proposed to accurately assess how the energy demand of membrane technology compares to that of solvent absorption.

2.9.1 Two stage dry gases

The study of Zhai and Rubin (2011) on a polymer membrane of permeance 1000GPU, using a combination of vacuum and compressor discussed the results of a two stage membrane process flowsheet. The process flowsheet could achieve recovery of 90% and 95% purity with 90% recovery. It was observed that the introduction of a sweep configuration by recycling a portion of the CO_2 separated reduced the overall cost to 32.7 from 45.6US$/ ton when compared to the two stage with vacuum operation (Zhai and Rubin, 2011). A combination of both a compressor at the feed side and a vacuum at the permeate side has been shown to be optimal strategy (Belaissaoui et al., 2012b).

Merkel et al. (2010) also presented and proposed important designs for CO_2 capture by membranes. Different process flow patterns were utilised in different membrane stages. The design involved a first crossflow membrane module, the retentate would be sent to a second cross-flow stage which is a countercurrent sweep stage. The permeate from this stage would be recycled back to be fed to the first stage whilst the retentate is emitted into the atmosphere. The permeate from the first stage that is vacuum driven is cooled and some water is separated from the product gas stream. The CO_2 enriched gas stream is compressed and further also cooled and the liquefied CO_2 is produced in a cryogenic column and then separated from the uncondensed gaseous stream. This gaseous stream is sent to a third crossflow membrane module from which the permeate is recycled and sent to the permeate compressor for CO_2 liquefaction. The retentate is fed back to the first stage for membrane separation.

Shao et al. (2013) designed a two stage membrane process for the capture of CO_2 from flue gas from a coal-fired plant. A range of pre-set feed and permeate pressures were used in different simulation runs to find the optimal conditions. From these investigations, it was ascertained that a two stage membrane process was necessary if a CO_2 purity target of 95% was to be achieved. It was also observed that the use of a membrane for CO_2 capture was more economical than the use of MEA or PSA for post-combustion CO_2 capture (Shao et al., 2013).

The feasibility for membrane based carbon capture for PCC at a coal power plant was carried out by Zhai and Rubin (2013). The duo developed a membrane gas separation system and comprehensive cost models were used these for various membrane design systems. The use of an in house developed free modelling, simulation and costing software called IECM (Integrated Environmental Control Model) was demonstrated for membrane CO_2 capture. The results indicated that multi-stages of membrane separation could achieve 90% CO_2 recovery and 95% product purity stream. It was also realised that a combination of both compressors and vacuum pumps results in a more effective driving force and therefore reduced the cost of CO_2 emission avoided. The use of this membrane resulted in a 15% less in the cost of CO_2 emission avoided compared to the MEA based chemical absorption method

Feasibility studies on facilitated transport membranes have shown less energy demand when compared to chemical adsorption (Hussain and Hägg, 2010). He and Hägg, (2014) also evaluated the CO_2 capture by FSC membranes from power plants. In the work, it was proposed that the gas stream from the compressor which is at high temperature would heat the retentate before it is sent to the expander in order to maximise energy recovery. A similar techno-economic study was carried out by He et al. (2015). The authors analysed the application of a facilitated transport membrane for CO_2 capture. An FSC membrane (polyvinyl amine) was used for the separation of CO_2/N_2 gas. Specific energy consumption of 1.02 GT and a cost of capture of $47.87/ton of CO_2 was reported. Based on these results, they reported that the process was feasible (He et al., 2015).

2.9.2 Wet Flue gas

Flue gas from other emitters such as blast furnace, steel making, and gas-fired power plants produce dry flue gas. Coal power plants, however, produce saturated flue gas. The flue gas

from coal power plant may have to be dehumidified before being fed to the membrane process and this step could increase the cost of capture. However, dehumidification also results in a lower flue gas flowrate to be handled by the equipment of the capture unit which reduces the gas processing cost. Triethylene Glycol (TEG) absorption, compression and cooling and use of membranes have been suggested for the dehydration of the flue gas (Hasan et al., 2012). Dehydration by use of membranes is expensive, whilst the TEG solution degradation leads to the production of environmentally unfriendly gases (Hasan et al., 2012; Leperi et al., 2016).

Leperi et al. (2016) reported that to reduce flue gas water composition to less than 1%, the TEG absorption is the cheaper option. However, for downstream use of greater than 1 % water, compression and cooling are cheaper than TEG (Leperi et al., 2016). The need to simultaneously optimise the water content in the stream supplied to the capture unit during the optimisation of the CO_2 capture process was therefore highlighted in the study.

Merkel et al. (2010) analysed the CO_2 capture from wet gases and based it on the inhouse Polaris membrane (1000 GPU α 50). It was reported that since water is more permeable than CO_2 it created an internal sweep for the CO_2 which aided the CO_2 driving force. This resulted in a decrease in the membrane area required by 10% and slightly higher CO_2 content in the permeate (Merkel et al., 2010).

Low et al. (2013) carried out a parametric study on the CO_2 capture from the humidified coal plant flue gas at pilot scale. The performance of common membranes reported in literature (Polaris, Polyactive and FSC membranes) was evaluated for several process designs of compression or/and vacuum operation. The results were consistent with those previously reported, that a higher stage cut resulted in less pure permeate and also a higher pressure ratio leads to a small membrane area and produces highly pure CO_2 permeate at a high energy cost. A combination of compression and vacuum was the most energy efficient. For the same pressure ratio, the vacuum mode produced highly pure CO_2 permeate but had a larger membrane size. Similar trends were observed for the dry flue gas study. In contrast to the results obtained by Merkel et al., water did not significantly affect the CO_2 permeance (Merkel et al., 2010). Slightly enhanced CO_2 permeation due to the internal sweep effect was observed.

Low et al. (2013) also reported that the water vapour effect on CO_2 permeance is membrane specific, enhancing permeability in others whilst reducing CO_2 permeability in others. For the membranes that are solution driven like PVA, and Polysulfone, the presence of water causes swelling of the polymeric membrane which aid diffusivity and can increase CO_2 permeation. Strong hydrogen bonds may result in clusters forming and increasing the mass transfer of other gases. However, in glassy polymer membranes, the water molecules can occupy sorption sites, thereby hindering other gases from absorbing onto those sites. If the membrane is not rigid, then the effect of swelling outweighs competitive sorption, and the result is increased permeance with an increase in relative humidity. Rubbery polymers are not affected by sorption hindrance and are enhanced by swelling which aids gas diffusion (Low et al., 2013; Pfister et al., 2017).

The importance of the membrane operating temperature was highlighted in the study carried out by Giordano et al. (2016). Giordano et al. (2016) analysed the effect of increasing membrane operation temperature for the separation of a humidified CO_2/N_2 gas by the Polyactive membrane. The study was based on a single stage with compression, vacuum and expander. Cooling, condensation and separation stages were part of the design in order to deal with the water present in the gas. Increasing the operating temperature increased the CO_2 permeance however, with a penalty on CO_2/N_2 selectivity as the rate of N_2 permeance was greater than that of CO_2. This increase in CO_2 permeance reduced the membrane area by 60 %. The results showed that increasing the membrane temperature without taking into account the increased N_2 permeance at the elevated temperature gave a false high CO_2 permeate purity. Accurately modelling the effects of temperature increase by an Arrhenius based model resulted in a decrease in permeate purity when the capture ratio is kept constant at 90%. A loss in the CO_2/N_2 selectivity leads to a less CO_2 pure permeate. Due to the increase in N_2 permeance, the vacuum pumps have to handle higher flowrates and this increases the power consumption. Increasing the operating temperature from 30 °C to 70°C resulted in over 50% increase in the net process power requirements. At higher temperature, less water condenses and thus higher amounts of water pass onto the membrane and permeate. The permeate CO_2 purity realised is thus lower than when the membrane operates at a lower temperature where a larger amount condenses and the gas fed to the membrane consists of lower water composition and thus a higher CO_2 permeate purity is realised. A higher membrane operating temperature also makes

for a higher water composition in the permeate which consumes extra power in the vacuum pumps, thereby increasing the energy needs of the system (Giordano et al., 2016).

Giordano et al. (2016) suggested what they termed a power recovery ratio which is the fraction of the total power that is recovered by the expander.

$$PR = \frac{P_{turbine}}{P_{compr} + P_{Vacp}} \tag{2.31}$$

The work showed the possibility of achieving 90% CO_2 purity and 90% capture ratio. For the PMI membrane, different results were observed, the permeance slightly decreased with increased temperature, and thus the membrane area required increased. Similar to the Polyactve 1500 the permeate purity decreased due to the higher water content that reports at the permeate side (Lasseuguette et al., 2016).

Pfister et al. (2017) analysed the feasibility of 'Mitrimid' a dense glassy polymer and an FSC (Polyvinylalcohol blended with amine) membrane for CO_2 capture based on a single membrane stage. The Mitrimid was used to study the effect of treating a humidified flue gas versus a dry flue gas. The simulation of CO_2 capture by a dry gas resulted in a lower membrane area and a more pure CO_2 permeate stream compared to a humidified flue gas. Simulation based on the humidified gas also resulted in a lower purity because of the competitive permeability of the water as it dilutes the permeate. Wet feed gave high specific energy consumption due to the larger volume of gas to be separated. For the FSC membrane, high feed pressure causes carrier saturation and a huge vacuum dries the membrane. Because of the high selectivity of the FSC membrane the, CO_2 purity of the permeate stream reached is higher than normal polymers like the Mitrimid for the same target CO_2 recovery (50%) value. For capture ratios below 90% the FSC showed significantly less membrane area requirement compared to a dense glassy polymer membrane, however at high recovery, the membrane area increase to greater than that of the polymer membrane (Pfister et al., 2017).

Giordano et al. (2017) studied single-stage and two-stage membrane based CO_2 capture from a five-component (CO_2, N_2, O_2, H_2O and Ar) flue gas by use of the Polyactive® 1500 membrane. Simulations were carried out at different temperatures and varying retentate and

permeate pressure. The single-stage configuration with partial permeate recycling of about 60% could achieve 90% purity and 60% capture ratio. The result reiterated previous studies that had already shown that a single-stage would not achieve 90% purity. Simulation of two stage process could achieve a higher purity of 96% (Giordano et al., 2017).

Xu et al. (2019) carried out a multistage techno-economic study of humidified flue gas from coal power plant. First single stage analysis then multistage process configuration. The profiles which showed that the specific energy consumption and specific cost initially drops as feed pressure increased from 20% recovery to 90% recovery. However, a further increase in feed pressure causes the system energy consumption to increase. This was consistent with Lee et al. it was shown that the use of a low CO_2/N_2 selective membrane in the first stage and a higher selectivity in the second stage resulted in the low membrane and low energy and consequently lower cost of capture (Lee et al., 2018).

2.9.3 Whole plant design for CO_2 capture from coal power plants

Merkel et al. (2010) suggested a more economical design for CO_2 capture from coal power plant. Figure 2.10 shows the proposed whole plant design. The flue gas from the boiler is fed to a cross-flow module which is the first membrane stage. The permeate from this first stage goes through the stages previously described. However, the retentate from this membrane stage is fed to a countercurrent flow which has air as a sweep gas on the permeate side. The air sweep combined with the permeate as it exits the permeate side of the membrane is then fed to the boiler. This air with a higher CO_2 composition is fed to the boiler. The flue gas produced from the boiler has a higher CO_2 concentration which is desirable in gas separation by membranes as it increases the driving force. Higher CO_2 reduces the energy demand of the first membrane stage and the use of the air as sweep in the second membrane stage reduces the membrane size and the energy required for the driving force. The proposed whole plant integrated design would result in a reduction of the cost of capture compared to the detached membrane process. This whole plant design reduces the membrane area from 3 million m^2 to 1.3 million m^2 and the power is also lowered from 145 MW to 97 MW. The overall effect on the cost is a saving of 41% (Merkel et al., 2010). The process design presented is available in the software IECM as an option for post-combustion membrane based CO_2 capture.

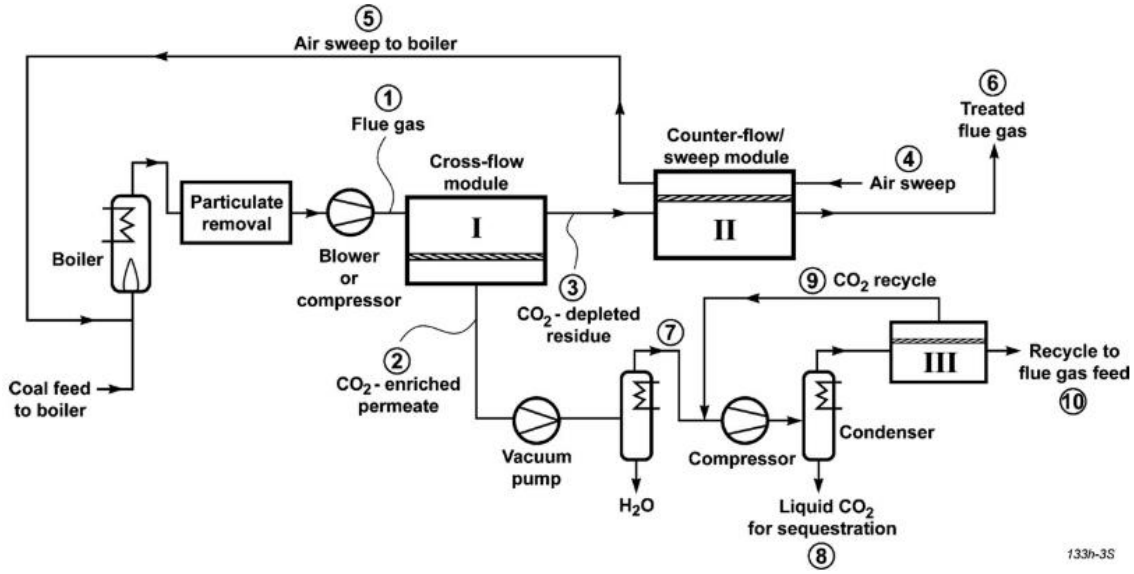

Figure 2.10. Whole power plant design for membrane based carbon capture from power plants ((Merkel et al., 2010) reused with permission from Elsevier)

It is one of the economical designs presented up to date. Follow up studies were carried out by Scholes et al. and Mat &Lipscomb (Mat and Lipscomb, 2019, 2017; Scholes et al., 2013). This was to address the problem of lowered O_2 composition that results from the use of air that has a high CO_2 concentration from the membrane based capture design. It was speculated that a low O_2 concentration in the feed air could lower the boiler efficiency and reduce the electricity produced by the power plant. Scholes et al. (2013) then proposed an additional membrane process that would separate air to get an O_2 enriched air permeate which would then be used as sweep gas in the CO_2 flue gas separation membrane process (Scholes et al., 2013). This design would still reduce the cost of CO_2 avoided from US$43 to US$32 compared to CO_2 capture by a standalone membrane process plant. Mat &Lipscomb optimised the variables involved in the design proposed by Merkel et al. (Mat and Lipscomb, 2017; Merkel et al., 2010). The results showed that the LCOE would decrease as the O_2 concentration decreased for the plant with the CCS system but 18% was the threshold minimum for the proper functioning of the boiler burner.

Giordano et al. (2017) made a whole plant cost analysis of a CCS that included transportation and storage. The cost of CO_2 avoided was found to be 65US$/ton. A comparatively high

specific power 341.6KW/h was recorded however, the plant efficiency was within membrane based range of about 10% loss. 75% of the total cost associated with the CCS was due to the membrane process and 25% was attributed to transport storage and monitoring. Recently Han and Ho did a whole plant feasibility analysis based on a dual-facilitated transport membranes they had developed (Han and Ho, 2020a).

2.9.4 Use of N_2 selective membranes

Considering the high composition of N_2 in the post-combustion flue gas from a power plant, it would be expected that an N_2 selective membrane would be economical as it already possesses a high driving force. However, not much research efforts have gone in this direction except for a few studies.

Yuan et al. (2014) carried out an optimisation study based on six pre-determined process designs based on the N_2 selective metallic membranes for the separation of CO_2/N_2. The process designs were based on only two stages of membrane. Among the process designs were hybrid designs with a CO_2 selective polymer membrane and a N_2 selective membrane. It was noted that the energy required for heating and cooling was significant (up to 76%) of the total energy requirement of the process. The metallic membranes operate at a high temperature of at least 600 °C and inter-cooling of the gas stream would be required as the polymer CO_2 selective membrane operates at 40 °C. The metallic only membrane process was also characterised by large membrane areas in the order 10^9 m^2 compared to 10^6 m^2 reported for polymer CO_2 selective membranes. This was attributed to the very low permeability of N_2 in the metallic membranes.

An investigation for the application of N_2-selective and CO_2- selective hybrid membrane process for CO_2 capture from a power plant has been reported by Ren et al. (2020). The study presented attainable regions for a fixed area of a single stage operating a N_2 selective membrane, CO_2 selective or the hybrid system as it varied with the pressure ratio. The results indicated that the N_2 selective membrane would result in less energy and lower membrane area requirement than the CO_2 polymer Polaris. When two stage processes were compared, the hybrid with an N_2 selective and a CO_2 selective in the succeeding stage resulted in the least

energy consumption and lowest membrane area requirement compared to the processes based on either the CO_2 selective membrane or the N_2 selective membrane (Ren et al., 2020).

2.9.5 Cost models adopted in literature

Differing cost models are used by different research groups for evaluating the financial implications of installing CO_2 capture from power plants. Hagg et al. adopt the CAPECOST 2012 tool as the base for the cost model (Chu and He, 2018; He et al., 2015; He and Hägg, 2014). It takes into consideration the cost of the major equipment, i.e. the compressors, vacuum pumps and the membrane area. Though the coolers are modelled, the cost of coolers is considered negligible hence the cost of the coolers is not included in the CAPEX and OPEX. Besides, a large capital charge factor (0.2) is assumed based on the interest rates of the region.

In contrast, the cost model presented by Rubin et al. in the USA considers the cost of coolers based on the surface areas and assumes a capital charge of 1.3 (Zhai and Rubin, 2013). The details of the model given and consider process contingency. This model has been adopted in simulation and optimisation by several groups around the world (Lee et al., 2018; Mores et al., 2019; Van Der Sluijs et al., 1992; Zhao et al., 2010)

Hasan considered the cost of cooling water as an operating cost in assessing CO_2 capture from power plants. The cost model of the compressors and vacuums is based on the Guthrie' s correlations and uses the Marshall Swift factor to evaluate current cost price (Hasan et al., 2012; Uppaluri et al., 2006, 2004)

2.9.6 Solving optimisation models for gas membrane networks

Various optimisation models have been presented for optimising gas membrane networks. As such different approaches have been emplemented in solving the models. Aspen Hysis has been one of the most used software for simulation studies to assess the feasibility of CO_2 capture by the use of membranes. Optimisation of variables based on predetermined designs has also been carried out in the environment. Optimisation strategies such as the iterative algorithms for the determination of global optimum have been presented (Mat and Lipscomb, 2017; Ren et al., 2020). Superstructure based optimisation models for membrane networks have been presented.

Deterministic gradient methods have been used for optimising membrane network systems by several authors (Arias et al., 2018, 2016; Hasan et al., 2012; Mores et al., 2019; Zarca et al., 2019). The formulated NLP and MINLP are complex and non -convex. The main challenge in solving MINLP and NLP problems by deterministic solvers is that of initialising the problem and finding the initial solution that is close to an optimal else, the solutions provided maybe local optima. Initialising using different values has been a strategy employed to try to ensure that the optimal solution is not missed (Qi and Henson, 2000). The computational times also can be long. The software Popularly been used to solve these programming problems is the general algebraic modelling software (GAMS).

Stochastic methods have also been utilised to solve these superstructure based models problems. Stochastic methods though more computationally expensive than gradient methods, are unlikely to be trapped in local optima (Marriott and Sørensen, 2003). Uppaluri et al. employed the simulated annealing algorithm method to membrane network superstructures (Uppaluri et al., 2002, 2006). Genetic algorithms have also been used (Marriott and Sørensen, 2003; Yuan et al., 2014). Lee et al. (2018) used a genetic algorithm available in MATLAB to solve a problem developed from a superstructure for the separation of CO_2/N_2 as post-combustion capture from coal flue gas. Yuan et al., (2014) solved a multi-objective problem for the evaluation of N_2 selective membranes for CO_2 capture.

2.10 Review of optimisation of multistage membrane systems for CO_2 capture

The optimisation of membrane processes can be limited to operating variables after designing the process beforehand through heuristic methods. This has been carried out for various membrane gas separation processes (Arias et al., 2018; Mat and Lipscomb, 2019; Ren et al., 2020; Yuan et al., 2019).

Optimisation of membrane process can also involve simultaneously optimising the process design and the process variables. Superstructures embed several possible process routes. Superstructure based optimisation has since then been adopted in many other fields such a reactive distillation, shale gas exploration, water network synthesis and heat exchanger networks (Buabeng-Baidoo and Majozi, 2015; Oke et al., 2018; Poth et al., 2003). In superstructure based gas separation by membranes, the goal is usually to simultaneously

synthesise and design the flowsheet that gives optimum operating parameters such as, optimum stream flowrates and operating pressure values of the process.

2.10.1 Early work on membrane gas separation optimisation

After developing models for binary and multi-component gas permeation through spiral wound membrane modules, Qi and Henson went on to use the models in the optimisation of membrane-based gas separations processes (Qi and Henson, 1996; R Qi and Henson, 1998). Qi and Henson, (1998) proposed 8 process flow configurations for the separation of CO_2/CH_4 based on the application of enhanced oil recovery and natural gas treatment and formulated an NLP, which was solved in the General Algebraic Modelling Systems (GAMS) environment by the solver CONOPT. The total annual process cost was minimised as the objective function. The results showed that the cost of separation was largely dominated by compression costs and to a lesser extent compared to the cost of the membrane. A higher pressure ratio led to lower energy consumption and lower cost of gas separation. The work was extended to multi-stage superstructure based simultaneous synthesis and optimisation by developing an NLP (R Qi and Henson, 1998). The superstructure is presented in Figure 2.11, and it includes recycling of retentate and permeate streams.

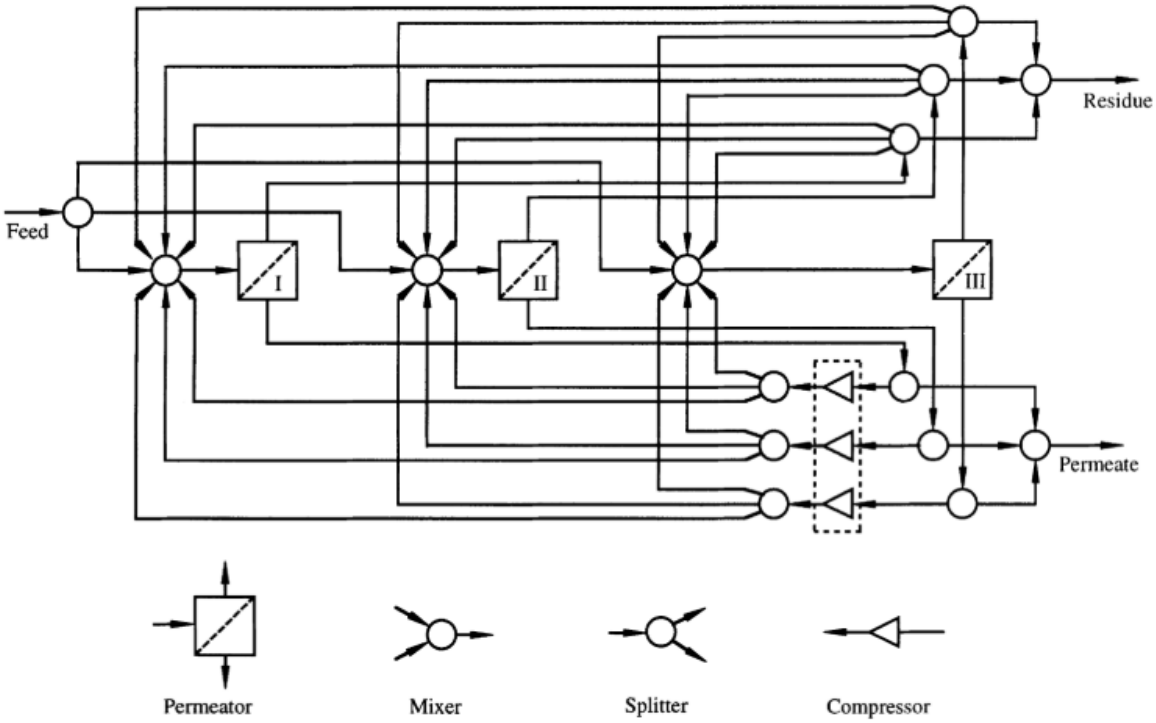

Figure 2.11. The superstructure presented by Qi and Henson (1998),(reused with permission from Elsevier)

The same superstructure was used in subsequent work where the membrane modules were modelled as discreet instead of continuous variables (Qi and Henson, 2000). A comparison of the results obtained from the NLP formulation and MINLP showed similar results. It was also concluded that the optimisation process was worthwhile for economic benefit. The authors also explored the optimisation of the membrane based gas separation by MINLP from multi-component gas mixtures with lower compositions of the target component in the feed was explored. The results showed that membrane systems could achieve stringent separation targets even from very low feed concentration (Qi and Henson, 2000).

Kookos, (2002) suggested a superstructure that had modules that had an extremely larger number of connections, including the possibility of the use of the whole or a fraction of retentate and permeate as a sweep in addition to the recycle streams previously presented in the superstructure by Qi and Henson (1998). The Robeson curve was used to determine the membrane properties that were variables in the model. The NLP model developed was applied to air separation and the production of Nitrogen enhanced air and compared to previously reported studies. Demonstrated also, was the significant cost reduction brought about by

simultaneous membrane properties optimisation with the process design and process flow as costs dropped from 0.05 $/m^2 to 0.01$/m (Kookos, 2002).

Uppaluri et al. (2004) building on the previous works presented a superstructure which involved even more process flowsheet and had novel process flowsheets embedded within. The process involved compressors and vacuum pumps for combined driving force generation, however, pressure was taken to be a fixed parameter. The developed model included the choice of membrane flow pattern, countercurrent, crossflow and cocurrent. A stochastic approach to solving optimisation problems was presented in the form of a simulated annealing algorithm to solve the model. The model was applied to air separation, H_2 –syngas, H_2/CH_4 in a refinery case. The countercurrent flow pattern was the most economic module configuration (Uppaluri et al., 2004).

Uppaluri et al. (2006) improved on the previous work to study the effect of varying feed and permeate pressure to simultaneously optimise pressure values with synthesis. As a pre-optimisation stage, the impact of various operating pressure values on the design was investigated and a suitable range could be read off from 'pressure target curves'. This range was then set as lower and upper bounds for the pressure in the optimisation process. The multistage strategy was shown to reduce the cost of gas separation when compared to the previous work. The results showed the benefits of increasing degrees of freedom by making parameters variables to increase the solution search space (Uppaluri et al., 2006).

2.10.2 Optimisation of other membrane gas processes

Ohs et al. (2016) developed a superstructure, though not in detail. For the further purification of natural gas before it is supplied to a national grid by considering the removal of N_2 from the stream. The objective was to minimise the net present value as related to the capital charge factor. Based on an MINLP model, optimisation was carried out based on a CH_4 selective and N_2 selective commercially available membrane. The optimisation, which resulted in an integrated process network, reduced the cost by 45%, the use of a combination of CH_4 selective and N_2 selective membrane further reduced the cost by 6 %. Simultaneous optimisation of the membranes material taken from the Robeson Upper bound for N_2 selective and CH_4 selective

membranes would reduce the cost by 70%. The influence of the feed flowrate was also investigated (Ohs et al., 2016).

Aliaga-vicente et al. (2017) developed an MINLP to optimise the cascading multi-stage membrane process. Different superstructures were presented, and the most complicated included a potential of 14 membrane stages. The superstructure involved a fixed first stage which received the gas to be separated from which the retentate stream would be sent to the next stripping stage or a portion would be sent to the expander before being emitted, the next retentate from the succeeding stage also is passed down to the next stage or sent for emission. The permeate from these membrane stages can be split and sent the feed side of the membrane and or can be used as a sweep gas of the next membrane and or can be sent to the product mixer. The superstructure, therefore, is a stepwise cascading order with two distinct sections for stripping and enriching as illustrated in Figure 2.12. The process makes use of compressors on the feed side to generate driving force. Uniform retentate and permeate pressure values are in operation and thus, a constant pressure ratio is used. The objective was to minimise the gas processing cost. The model was applied to separate binary gases CO_2/CH_4. Non-isothermal conditions were considered by including cooling after compressors. The result indicated small changes in temperature and the cost associated with cooling was a very small fraction of the total cost. The model was solved by SBB and CONOPT in the GAMS environment.

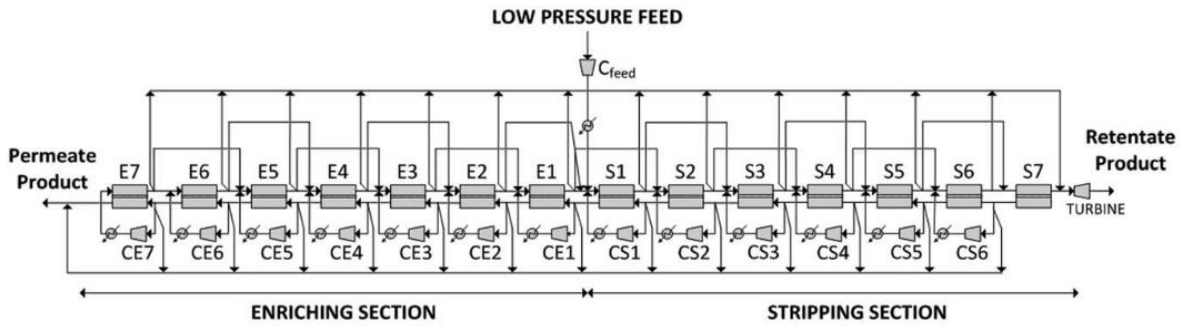

Figure 2.12.Cascading superstructure presented by Aliaga-vicente et al. (2017,)(resused with permission from Wiley)

Zarca et al. (2018) considered the separation of H_2 or Syngas (H_2+CO) from the flue gas produced in carbon black production by gas membrane separation. The work was based on a pre-determined two stage and a loop which was termed ‘half stage’. The process conditions,

such as membrane area, flowrates, and pressure, were optimised for a target recovery of H_2 from the flue gas. The objective of the NLP problem was the minimum present value which was equal to the sum of CAPEX and OPEX. With H_2 recovery targets as well as syngas targets (H_2+CO) mole fractions targets. The net present value increased by 10% when the membrane area was raised from US$50 to US$250 for a recovery of 78% and CO_2 purity and 86%. The power requirements increase with increased separation targets such as recovery and as the power requirements increase with recovery, the membrane area follows an opposite trend as the driving force increases (Zarca et al., 2018).

2.10.3 Optimisation of multistage CO_2/N_2 separation by membranes

Hasan et al. (2012) presented one of the earliest optimisation models specifically for post-combustion CO_2 capture by use of membranes (Hasan et al., 2012). In the study, optimisation of absorption by MEA and by polymer membranes was carried out, and a comparison made of the associated cost of each technology. The flue gas of varying CO_2 compositions to consider various sources for post-combustion capture was first passed through a direct contact cooler to reduce the water composition. Then the flue gas would be passed through a dehydration stage to reduce the water composition to 0.001 mol fraction before being passed onto the membrane process. A superstructure that involved membrane technology, TEG, compression and cooling are used to determine the most economical methods for dehydration of the flue gas. For both absorption and membrane technology, the TEG was the cheapest in producing a dry gas ready for further processing by CO_2 capture. The flowrate considered was however, too low and not a full power plant scale. The membrane process was represented by a cascading three stage process where the flue gas is fed into the first stage and the retentate and permeate is then fed to the next stage or is sent to the stack or to the product stream. Whilst the design allowed for independent retentate pressure, the permeate pressure was set at 1 bar for all the membrane stages as the design did not include vacuum conditions on the permeate side to increase the pressure ratio. The problem was represented by an NLP, which was represented in GAMS and solved by the solver CONOPT. The results showed that a three stage membrane was optimal. For various flue gas flowrate (0.1kmol-10kmol) the results showed that both the capital and operating cost of the membrane process was higher than that for CO_2 capture by absorption when the CO_2 composition in the flue gas is less than 20% and 40%, respectively. At CO_2 compositions greater than 20% and 40% mol, the capital and operating cost of CO_2 capture by

absorption is greater (Hasan et al., 2012). The major limitation of the study was the very low flue gas flowrate used in the simulation which are not representative of real size power plants.

Alshehri et al. (2013) presented a superstructure for the optimisation of CO_2 capture. The superstructure was a stepwise process method, where the retentate was passed to the next stage but the permeate streams recycled. The membrane model was based on a hollow fibre module and took into account the pressure drop. Multicomponent flue gas from a power plant was considered. The objective was to minimise the specific cost of capture for a recovery of 90% and a CO_2 purity stream of 90%. It was shown clearly that increasing the membrane permeance reduces the cost of capture. The results revealed that there is an optimum CO_2/N_2 selectivity value in membrane gas separation. The specific cost of CO_2 decreases with increasing selectivity and reaches an optimum after which the specific cost starts to increase again. It was, however, noted that more critical was to improve the permeance of membranes instead of focusing on improving selectivity (Alshehri et al., 2013).

Arias et al. (2016) analysed the CO_2 capture process from coal plant flue gas. The binary gas CO_2/N_2 was used in the simulation. A more comprehensive multistage membrane superstructure was presented for CO_2 than previous studies (Alshehri et al., 2013; Hasan et al., 2012). It was a four stage membrane where two of the membrane stages were fixed in the superstructure present in all scenarios. A generalised permeation model which involved finite element method to solve the permeation model was implemented. The configuration was such that the retentate operating pressure was uniform as generated by compressors that preceded each membrane stage. The permeate side operated at 1.05 bar and therefore, a vacuum pump was not present. The result was an NLP model whose objective was to minimise the total annualised cost of capture. The impact of increasing CO_2 recovery and CO_2 product purity from 90% to 98 % was investigated. The results showed that the membrane area, total power and net power consumption increased as the recovery target is increased from 90% to 98%. The CAPEX and the OPEX increased with increased recovery target and thus the minimum total annual cost also increased as the recovery target increased. According to the superstructure, the optimum membrane network involved all four membrane stages. The result was compared to previous work and the optimisation managed to reduce the specific cost of capture by $5 (Arias et al., 2016; Zhai and Rubin, 2013). The group extended their study to include independent and non-uniform retentate and permeate pressure operation based on the

same superstructure and cost model (Mores et al., 2019; Zhai and Rubin, 2013). This resulted in a cost reduction of 19.4% for similar separation targets (95% recovery and 98% purity) (Mores et al., 2019).

Mores et al. (2019) formulated an NLP and solved it with the solver CONOPT in GAMS; consistent with the previous study, the CAPEX and OPEX increased with an increase in recovery and purity. The main objective of the latest work was to determine how different variables such as the pressure ratio influenced the specific cost of capture. Unique also was the presentation of driving force profiles along the membrane length. The results indicated a general loss in the driving force, and this was due to the decrease in the partial pressure as the concentration of CO_2 increases on the permeate side along the membrane length. The results showed that when cost factors such as the capital recovery factor, the price of electricity and the cost of equipment are doubled, the total annual cost increased. However, the membrane network remained the same, with adjustments only on stream flowrates, membrane areas and pressure values. Importantly it was shown in the study that the capital recovery factor (CRF) influences the TAC more than any other parameter. A large CRF may mean that the CAPEX is always greater than the OPEX (Mores et al., 2019).

Gabrielli et al. (2017) carried out a parametric study as a first step to determine the attainable regions, and then from the results of the parametric study, determined boundaries of selected variables (Gabrielli et al., 2017). The optimisation of membrane based gas separation was formulated as a multi-objective optimisation problem where specific energy and specific membrane area were minimised. Various process configurations were set beforehand heuristically. The problem was solved by the genetic algorithm in MATLAB. The study was based on the separation of the binary gas CO_2/N_2 by a CO_2 selective membrane whose permeance and selectivity was determined from the Robeson bound curve. The paper investigated how the membrane network layout impacted the energy consumption and membrane area. The membrane material (selectivity and permeance) had a significant impact on the energy and membrane area requirements of the system. It was recommended that a different membrane with differing selectivity for each membrane stage would be ideal. The results showed that three membrane stages were optimal and gave slightly better results than two membrane stages. Further optimisation runs based on 4, 5 and 6 stages did not yield improved results. There is a trade-off between the energy saving brought by recycling streams

and the added energy consumption by compression of the recycle streams. The attainable regions indicated that when a high pressure ratio is attained, the specific energy consumption is low. A low pressure ratio, therefore, corresponds to high energy consumption and achieves a high recovery and higher purity. A large membrane area enables a higher recovery however, a permeate purity penalty is incurred. If the selectivity is very high, then the purity of the permeate would be high regardless of the size of the membrane. For the energy area plot, a horizontal asymptote could be observed, which indicated the minimum energy operation that can be achieved for the recovery and CO_2 purity targets. This minimum energy value also corresponds to the maximum area requirement the process would need. Reducing the pressure ratio was shown to reduce the power consumption, this, however, called for a larger membrane area as there exists a trade-off between membrane area and energy (Gabrielli et al., 2017).

Lee et al. (2018) introduced pressure controllers which allowed the pressure optimisation of pressure values by allowing non uniform operating pressure for the different membrane stage. A model was developed for CO_2 capture from CO_2/N_2 flue gas from a coal-fired power plant. The permeation model was based on the operation of a hollow fibre module and took into consideration the pressure drop on the permeate side. The genetic algorithm available in the MATLAB environment was utilised to solve the problem. Two stage membrane involved higher power consumption and lower membrane area compared to three stage process. The total cost of capture is lower for three stage process than two stage process which was consistent with previously reported results (Gabrielli et al., 2017). A sensitivity analysis showed that the specific cost of capture increased exponentially with an increase in recovery from 40% up to 99%. The increase was more pronounced for recovery values above 90%. The results showed that using a membrane with higher selectivity in the first stage for pre-concentration and followed by a membrane of lower selectivity in the succeeding stages would be more economical (Lee et al., 2018).

Roussanaly and Anantharaman, (2017) analysed the influence of the capture ratio on economic indicators (Roussanaly and Anantharaman, 2017). Considering CO_2 concentrations ranging from 10 to 35% which is characteristic of several flue gas sources (refineries, coal power plants, cement and steel industries. Ramírez-Santos et al. (2017) applied NLP strategy for the capture of CO_2 from the blast furnace where steel is manufactured (Ramírez-Santos et al., 2018).

Zamarripa et al. (2018) developed a MINLP model which was a first of its kind for the synthesis and design of CO_2 capture by a membrane as it included models of the entire power plant with CCS instead of optimising the membrane process as a standalone. The model developed was based on the process flow suggested previously shown in Figure 2.10. The superstructure from which the model was formulated involved six potential membrane stages and three of these were fixed in the process flowsheet. The process includes a stage which has an air sweep that carries the CO_2 permeate to the boiler to increase the CO_2 content of the flue gas that is produced, which increases the driving force of the first membrane where the flue gas is fed (Zamarripa et al., 2018). The drawback of the work is that the model loses some degrees of freedom due to some of the membrane stages that are fixed.

The superstructure developed by Lee et al. results in more possible process flow routes presented for CO_2 capture by membranes. The routes are enabled by the pressure controllers (expanders) that facilitate reuse of high pressure retentate streams to the other stages that operate at lower pressure (Lee et al., 2018). Direct comparison of the annual cost and specific cost of CO_2 capture of one study to the other is not possible because of the various assumptions and cost models that are assumed in the various reports in literature. The study carried out by Mores et al. showed significantly reduced energy consumption, however the size of the membrane stage seemed unbound and thus some stages had significantly high membrane area sizes (Mores et al., 2019).

2.11 Pilot studies of membrane CO_2 capture processes

White et al. (2015) reported the results of a pilot study that had the capacity to process flue gas containing 1 tonne CO_2 from a coal power plant. This pilot plant demonstrated the capability to capture CO_2 for periods of up to 1800 h with spiral wound Polaris membrane modules. A similar process design as proposed before and illustrated in Figure 2.10 was adopted. The membrane module was 1 m in length and 20cm wide, which is the industrial size. The effect of the membrane feed pressure and permeate pressure was investigated as well as the stability of the membrane. The CO_2 capture rate increased with an increase in membrane operating temperature, however, the purity of the permeate stream decreased with this achieved high stage cut. Large permeate rates also adversely affected the vacuum, which leads to lowered

pressure ratio. Whether the module was crossflow or countercurrent sweep also had an impact on the resultant permeate flowrate (White et al., 2015).

In a single stage analysis, a high CO_2 permeance result in high recovery, however, the purity of the permeate stream diminishes. The high permeance of CO_2 depletes CO_2 from the retentate side, lowering CO_2 composition and thus elevating N_2 partial pressure, which begins to increase the N_2 permeance, thereby diluting the permeate. Therefore a trade-off exists between purity and recovery, and to achieve both multistage systems are required. Therefore, a high stage cut results in a relatively less pure permeate (White et al., 2015). The group went on to carry out tests to show the stability and effectiveness of sweep membrane modules for CO_2 capture (White et al., 2017).

Pilot-scale trials of an FSC membrane showed resistance to the minor compounds SO_x and NO_x. in one study but posed problems in another study (Kim et al., 2011; Sandru et al., 2013). Kim et al. scaled up PVAm/PVA (polyvinyamine/polyvinylalcohol) and Sandru et al. scaled up PVAm/PSf. Both membranes showed stable performance over 500 hours online.

The FSC PVAm/PSf membrane, which showed large permeance (5.2 kmol/(m2.bar.s)) and selectivity (500) in experimental work, was tested at a large scale. CO_2 capture from flue gas produced from burning propylene had a larger membrane area ($4.2m^2$-$10m^2$) flat sheet hollow fibre membrane (He et al., 2017). Lower permeance compared to experimental values when exposed to real flue gas was observed. High water permeance and excessive membrane dehydration were also observed (He et al., 2017). An increase in pressure increased the permeate flow and continued increase showed evidence of carrier saturation. At increased pressure, high water permeation makes the feed side less humid and thus reduced the CO_2 permeance. Moderate feed pressure of 3 bar was recommended. The CO_2 permeance decreased with an increase in permeate pressure, and the permeate purity also decreased.

Han et al. (2019) demonstrated CO_2 capture by a $1.4m^2$ spiral wound membrane. Poly(N-vinyl formamide-co-vinylamine) was the FSC membrane that gave promising results and achieved a GPU of over 1400 and a selectivity up to 186 which was close to lab experiments. Concentration polarisation was also observed to be negligible and reported. CO_2 permeation dropped due to the N_2 concentration on the membrane surface. Slight carrier saturation was

observed. The module showed stability over 500 hr. The demonstration motivated for a larger size of the membrane to be manufactured and higher processing of tonnage. Consistent with laboratory experiments also was the increase in CO_2 with an increase in temperature though this led to a reduction of the CO_2/N_2 selectivity and consequently reduced permeate purity (Han et al., 2019a).

Salim et al. (2018) demonstrated the fabrication of spiral wound, shown to be leak-free and tested with actual flue gas. Concentration polarisation was observed on the feed side for flowrates as low as 1000sccm for dry flue gas but not for humidified gas. The pressure drop observed was less than 0.06 bar /m (Salim et al., 2018).

The membrane size and the flowrates of the field tests, and the techno-economic modelling results discussed in section 2.9 shows that the pilot studies are still very far from the industrial scale. The challenge of large scale fabrication of the membranes also needs to be addressed.

2.12 Concluding remark

The literature review has highlighted the state of affairs with regards to the economic evaluation of CO_2 capture from flue gas from coal power plants. Techno-economic studies based on the binary gas N_2/CO_2 gas can be misleading and not give a true representation of the actual membrane size and energy consumption which influence the OPEX and CAPEX, respectively. The flue gas is saturated with water as it exits the FGD chamber (4-13% water). The options may be to dehumidify the flue gas before sending it to the membrane or alternatively feed the humidified flue gas to the membrane capture plant.

Superstructure based optimisation studies for CO_2 capture have been based on dry flue gas. For CO_2 capture by membrane technology, optimisation of facilitated membranes capture has not been studied as far as we could ascertain. Network optimisation and analysis based on N_2 for post combustion CO_2 capture has not been presented according to the best of our search and knowledge. These were the gaps identified which this thesis sought to address. Discussed below are some of the research gaps that were also identified and recommended for future work as they were beyond the scope of this study.

Optimisation models presented for post-combustion CO_2 capture from power plants represent the membrane CO_2 capture process in isolation from the power plant with the exception of a single study (Zamarripa et al., 2018). Being able to optimise the membrane network simultaneously with the electricity generating power plant may result in more economical designs. Optimisation of membrane networks for CO_2 from power plants has not included a sweep by use of a portion of the retentate or permeate as suggested in the superstructures presented (Aliaga-vicente et al., 2017; Hasan et al., 2012). Also, experimental effort into developing more N_2 selective membranes remains largely unexplored with regards to CO_2 capture from coal power plants, with only a handful of studies published (Hussain et al., 2015; Ren et al., 2020).

Chapter 3 – Optimisation of post-combustion carbon dioxide capture by use of a fixed site carrier membrane

This study has been published (section 3.1-3.5.3)

Chiwaye, N., Majozi, T., Daramola, M.O., 2021. Optimisation of post-combustion carbon dioxide capture by use of a fixed site carrier membrane. Int. J. Greenh. Gas Control 104, 103182. https://doi.org/10.1016/j.ijggc.2020.103182

3.1 Introduction

CO_2 capture by a poly-amine FSC membrane, however, requires additional considerations such humidity which has not been included in these optimisation studies. In addition, the CO_2 permeance of the membranes studied is constant and not affected by variation in partial pressure within the pressure range studied. However, CO_2 permeance across poly-amine FSC membranes varies inversely with partial pressure (Goddard et al., 1974; Zhang et al., 2013). Experimental studies also confirm the carrier saturation phenomenon where the permeance decreases with an increase in feed pressure (Deng et al., 2009; Han et al., 2019b; Zhang et al., 2013). Therefore, the existing optimisation studies may not give a true feasibility report of an FSC membrane process. Optimisation studies of multistage membrane processes for CO_2 have also been based on ambient or vacuum pressure operation on the permeate side (Gabrielli et al., 2017; Hasan et al., 2012; Mores et al., 2019). Multistage membrane systems driven by sweep configurations have not been explored. Water vapour is suitable as a sweep gas in the operation of poly-amine FSC membranes. The presence of water enhances CO_2 permeance rather than corrupt the membrane (Hussain and Hägg, 2010). The use of a sweep can increase the driving force by increasing the partial pressure difference across the opposite sides of the membrane which can lower the costs involved in gas membrane systems. Techno economic feasibility on the use of the poly-amine FSC membrane for CO_2 capture from coal-fired plants has been carried out based on pre-determined two membrane stages at fixed CO_2 permeance and the study sets retentate and permeate operating pressure beforehand (He et al., 2015; Hussain and Hägg, 2010).

In this study, mathematical programing and superstructure approach are used for the optimisation of CO_2 capture from coal power plants by a poly-amine FSC membrane in order to develop a more economic process flowsheet. The objective of the mathematical formulation

is to minimise annual cost and therefore obtain optimal membrane area, operating pressure and flowrates of recycle streams. The superstructure based model considers requirements for the operation of poly-amine FSC membranes. The superstructure embeds other aspects which have not been explored before for poly-amine FSC membranes such as the use of more than 2 membrane stages, flue gas that can be sent to any membrane stage, operating at permeate and retentate pressure that is different in each stage and recycling of the retentate stream. The superstructure also facilitates optimisation of multistage membrane process with sweep configurations.

3.2 Problem statement

The problem statement in this work can be stated as follows.

Given;

(i) Flue gas of known flowrate, composition, temperature and pressure.
(ii) Desired product purity and the desired capture ratio.

Determine,

(i) The optimum process flow chart that results in minimum total annualised costs for the carbon capture process.
(ii) The optimum process conditions such as stream flowrate, pressure, membrane area, sweep flowrate, and compressor and vacuum pump duties.

3.3 Model description

The following assumptions are made in formulating the mathematical model:

(i) The membrane configuration is assumed to be countercurrent (Li et al., 1990).
(ii) Pressure drop along the membrane is taken to be negligible (Uppaluri et al., 2004).
(iii) Concentration polarisation is deemed negligible (Uppaluri et al., 2004).
(iv) The plug flow regime is assumed on both permeate and retentate sides (Arias et al., 2016).
(v) Membrane operation is isothermal (Bocciardo et al., 2013).

(vi) The flue gas only contains CO_2, N_2, O_2 and H_2O (Merkel et al., 2010).

(vii) The permeance of a component is independent of the other i.e pure gas permeance is assumed (Arias et al., 2016).

It is noteworthy to mention that these assumptions are mostly based on ideal conditions which may differ from the real conditions. If these assumptions were to be dropped/relaxed and a more accurate model adopted, the cost of CO_2 capture could increase as a result of an increase in membrane area and energy needed to meet the separation targets. At the same time, concentration polarisation may be significant at higher selectivity and permeance (Bhattacharya and Hwang, 1997; Mourgues and Sanchez, 2005). Also, pressure drop may be significant on the feed side and reduce the permeation rate. In spite of these demerits associated with the assumptions, they are still sufficient for the pre-design stage, but a more accurate model may need to be developed in later stages.

The model is formulated based on the superstructure presented in Figure 3.1. The superstructure is similar to that presented for membrane gas separations including expanders on each stage which facilitates for non-uniform retentate operating pressure (Lee et al., 2018; Runhong Qi and Henson, 1998). Embedded in the superstructure are the process flow routes and process conditions presented in techno-economic feasibility studies for poly-amine FSC membrane based CO_2 capture (He and Hägg, 2014; Hussain and Hägg, 2010). The model involves membrane based gas permeation constraints, mass balance, the power consumption of compressors and expanders, area of coolers and also a detailed description of the cost of the operational units involved. The aim is to achieve minimum total annualised cost (TAC) of post-combustion CO_2 capture for specified carbon capture ratio and CO_2 product stream purity.

3.3.1 Superstructure description

Presented in

Figure 3.1 is a superstructure which involves several membrane stages with the recycling of streams. The flue gas at 50 °C and 1 bar is cooled and water condensed in a cooler condenser. A splitter is responsible for adjusting the amount of flue gas that is sent to each membrane stage. The flue gas together with the permeate recycle streams are sent to a compressor where

the flue gas is compressed to membrane feed side operating pressure. The feed gas is cooled to membrane operating temperature (35 °C) and some water can condense and be removed from the feed stream. The feed gas is then mixed with retentate recycle streams if present and then passed onto the retentate side of the membrane and some of the gas permeates and is collected at the permeate side. The permeate stream is passed through cooler condenser which adjusts the water content before it is sent to a permeate splitter where the stream is split into permeate recycle streams and CO_2 product stream. The CO_2 product streams from the membrane stages are combined and compressed, cooled and water can condense to free the product stream of more water. The product is then compressed to 75 bar and further pumped to 110 bar before being sent to storage. The retentate stream that exits the membrane is split into recycle stream and residue stream which is dispensed as waste into the atmosphere. The retentate recycle streams are then made to pass through either an expander or compressor to adjust the stream pressure to the membrane stage they are destined for. The compressed retentate recycle stream is cooled to 35 °C which is membrane operating temperature for all the membrane stages. The membrane operating temperature is a parameter. The permeate pressure can be 1 bar or can be under vacuum conditions as generated by a vacuum pump. The streams are always mixed at identical pressure and temperature.

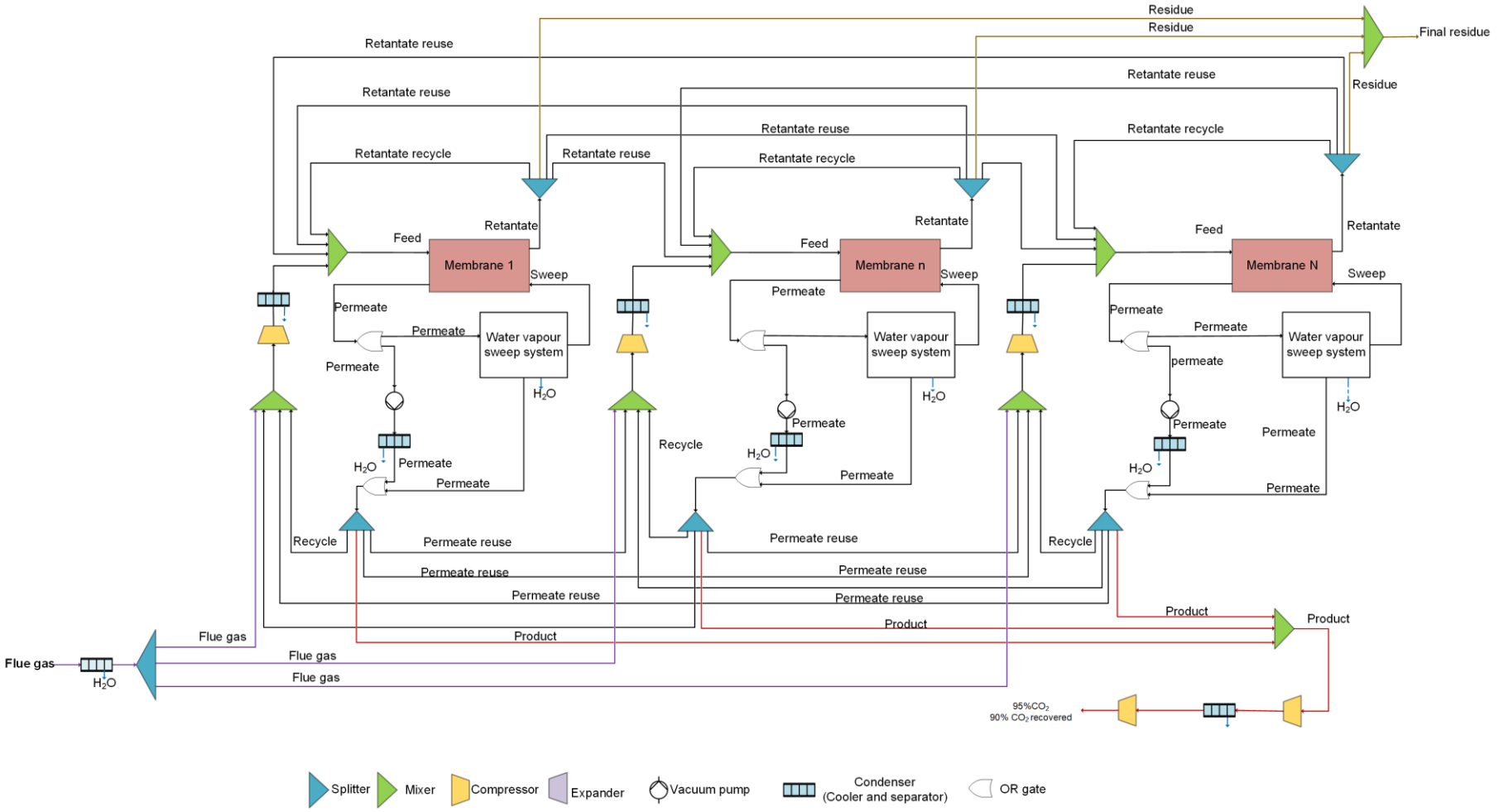

Figure 3.1.Superstructure representation of the process

Figure 3.2 shows the sweep gas system section in detail. An expander expands low pressure steam to reduce the pressure to between 0.025 bar and 0.095 bar where it can exist as a gas at the membrane operating temperature. A compressor evacuates the permeate and creates a vacuum that sucks and drives the sweep gas through the membrane. The permeate which has a high water content passes through a vacuum condenser and water vapour condenses at 25 °C. The permeate that exits the compressor which generates the vacuum is at 1 bar. The permeate is then split by the permeate splitter.

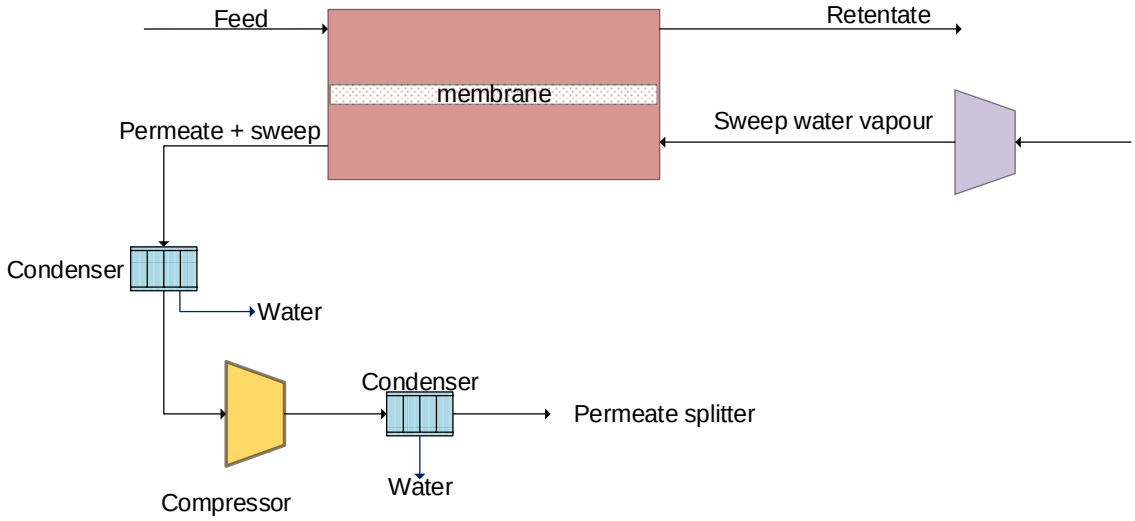

Figure 3.2. Water vapour sweep system

In the model, the flowrate is denoted by *R*, pressure by *P* and the mole fraction by *y*. The subscripts denote the sets of components *i*, membrane stages *n* and the membrane discretisation points *k*. The superscripts give the stream identity. Therefore the flowrate of component *i* in the feed stream (*fs)* to membrane stage *n* is (R_n^{fs}).

Gas permeation through the membrane is illustrated in Figure 3.3. Figure 3.3 shows a schematic representation of the membrane module being considered. A countercurrent set up is considered in this work.

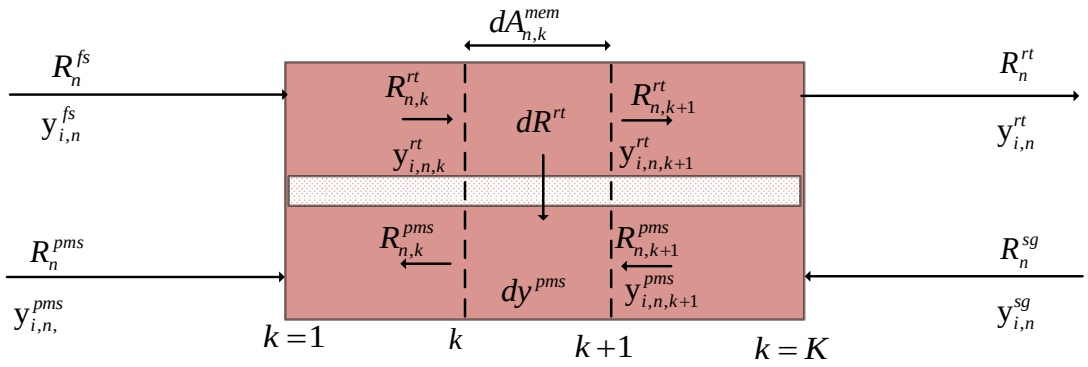

Figure 3.3. Schematic representation of a typical membrane module

3.3.2 Permeation model

Equation (3.1) gives the flux of component *i* through a membrane area (dA^{mem}) of stage *n*. Equation (3.1) states that the transport of component *i* through the membrane is equal to the difference in partial pressure on the feed side and permeate side multiplied by the permeance (φ_i). In the case of facilitated transport φ_i is a sum of the contribution of solution diffusion and facilitated transport by the carrier.

$$-\frac{d\left(R_n^{rt}\cdot y_{i,n}^{rt}\right)}{dA_n^{mem}}=\varphi_i\left(P_n{}^{rt}\cdot y_{i,n}^{rt}-P_n{}^{pms}\cdot y_{i,n}^{pms}\right)\qquad\forall i\in I,n\in N \tag{3.1}$$

In order to incorporate the differential equation into the algebraic expression based modelling software, the differential Equation (3.1) was discretised (Arias et al., 2016). A combination of central finite difference (CFD) and the backward finite difference (BFD) method of accuracy order 2 was used to discretise the differential equation. Equation (3.2) presents the general form of the central finite difference discretisation approximation for a first-order derivative differential equation approximated to the accuracy of order 2. The CFD, in this case, is used to estimate the point $k=2$ on the membrane since the value $k=1$ is unknown. The general form of the first derivative with an order of accuracy 2 of a backward finite difference approximation is given by Equation (3.3). The BFD method was implemented for $k>2$ using the values from K=2. Equations (3.4)-(3.5) show how the feed flowrate and the membrane area are related to the general form Equation (3.2). Equation (3.5) shows that the total membrane area is the product of dA^{mem} and the number of subdivisions of the area given by *K-1*.

$$f' = \frac{f(x_{k+1}) - f(x_{k-1})}{2\Delta x} \qquad ; \Delta x = h \tag{3.2}$$

$$f' = \frac{\frac{1}{2} f(x_{k-2}) - 2f(x_{k-1}) + \frac{3}{2} f(x_k)}{h} \Rightarrow f' = \frac{f(x_{k-2}) - 4f(x_{k-1}) + 3f(x_k)}{2h} \tag{3.3}$$

$$f' \Rightarrow dR_n^{rt} y_{i,n}^{rt} \quad ; h \Rightarrow dA_n^{mem} \tag{3.4}$$

$$dA_n^{mem} = \frac{A_n^{mem}}{K-1} \tag{3.5}$$

Discretising $\frac{d\left(R_n^{rt} \cdot y_{i,n}^{rt}\right)}{dA_n^{mem}}$ based on the CFD in order to estimate the flowrates at $k = 2$ yields Equation (3.6).

$$\frac{R_{n,k+1}^{rt} \cdot y_{i,n,k+1}^{rt} - R_{n,k-1}^{rt} \cdot y_{i,n,k-1}^{rt}}{2dA_n^{mem}} = \frac{(K-1)R_{n,k+1}^{rt} \cdot y_{i,n,k+1}^{rt} - R_{n,k-1}^{rt} \cdot y_{i,n,k-1}^{rt}}{2A_n^{mem}} \tag{3.6}$$

Applying BFD to discretise $\frac{d\left(R_n^{rt} \cdot y_{i,n}^{rt}\right)}{dA_n^{mem}}$ in order to compute the flowrates of the components at k >2 results in Equation (3.7).

$$\frac{R_{n,k-2}^{rt} \cdot y_{i,n,k-2}^{rt} - 4R_{n,k-1}^{rt} \cdot y_{i,n,k-1}^{rt} + 3R_{n,k}^{rt} \cdot y_{i,n,k}^{rt}}{2dA_n^{mem}} = \frac{(K-1)R_{n,k-1}^{rt} \cdot y_{i,n,k-1}^{rt} - 4R_{n,k-1}^{rt} \cdot y_{i,n,k-1}^{rt} + 3R_{n,k}^{rt} \cdot y_{i,n,k}^{rt}}{2A_n^{mem}} \tag{3.7}$$

The algebraic expressions presented in Equations (3.6) and (3.7) are substituted into Equation (1) to give Equations (3.8) and (3.9). Equations (3.8) and (3.9) therefore compute the retentate flowrates of component i at point *k* of membrane stage *n*.

$$\frac{K-1}{2A_n^{mem}}\left(-R_{n,k-1}^{rt} \cdot y_{i,n,k-1}^{rt} + R_{n,k+1}^{rt} \cdot y_{i,n,k+1}^{rt}\right) = -\varphi_i\left(P_n^{rt} \cdot y_{i,n,k}^{rt} - P_n^{pms} \cdot y_{i,n,k}^{pms}\right) \tag{3.8}$$

$$\forall i \in I, n \in N, k \in K, k = 2$$

$$\frac{K-1}{2A_n^{mem}}\left(R_{n,k-2}^{rt}y_{i,n,k-2}^{rt}-4R_{n,k-1}^{rt}y_{i,n,k-1}^{rt}+3R_{n,k}^{rt}y_{i,n,k}^{rt}\right)=-\varphi_i\left(P_n^{rt}y_{i,nk}^{rt}-P_n^{pms}y_{i,n,k}^{pm}\right) \quad \forall i\in I,n\in N,k\in K,k>2 \tag{3.9}$$

Carrying out a component mass balance around the membrane area bound by $k=k$ and $k=K$ as presented in Figure 3.3 yields Equation (3.10). Equation (3.10) states that the flowrate of component *i* in the permeate exiting point k on membrane in stage *n* is the sum of that supplied by the retentate at point *k* and sweep gas supplied to the membrane less that which exits the membrane as retentate.

$$R_{n,k}^{pms}\cdot y_{i,n,k}^{pms}=R_{n,k}^{rt}\cdot y_{i,n,k}^{rt}+R_{n,K}^{sg}\cdot y_{i,n,K}^{sg}-R_{n,K}^{rt}\cdot y_{i,n,K}^{rt} \qquad \forall k\in K,i\in I,n\in N \tag{3.10}$$

There is no sweep gas present when a vacuum pump is used on the permeate side and therefore the resultant balance is given by Equation (3.11). The overall mass balance for the total flowrate for the two scenarios are given by Equations (3.12) and (3.13).

$$R_{n,k}^{pms}\cdot y_{i,n,k}^{pms}=R_{n,k}^{rt}\cdot y_{i,n,k}^{rt}-R_{n,K}^{rt}\cdot y_{i,n,K}^{rt} \qquad \forall i\in I,n\in N,k\in K \tag{3.11}$$

$$R_{n,k}^{pms}=R_{n,k}^{rt}+R_{n,K}^{sg}-R_{n,K}^{rt} \qquad \forall n\in N,k\in K \tag{3.12}$$

$$R_{n,k}^{pms}=R_{n,k}^{rt}-R_{n,K}^{rt} \qquad \forall n\in N,k\in K \tag{3.13}$$

The boundary conditions are stated by Equations (3.14) - (3.17). Equation (3.14) states that the feed flowrate of component *i* supplied to the membrane stage *n* is equal to the retententate flow rate at point *k=1*. Therefore ($R_{i,n}^{fs}$) is the flowrate of component *i* at point *k=1*. The permeate from membrane stage *n* is given by the permeate at *k=1* since it is countercurrent configuration as given by Equation (3.15). Equation (3.16) shows that the retentate from membrane stage *n* is collected at *k=K*. Equation (3.17) states that the flowrate of the permeate stream at *k =K* is the sweep gas flowrate as supplied to the membrane. A binary variable (Z_n^{sg}) describes the existence of the sweep gas flowrate, therefore the permeate stream is zero at *k=K* when a vacuum pump is in operation.

$$R_{i,n,k}^{rt}=R_{i,n}^{fs} \qquad \forall i\in I,n\in N,k\in K,k=1 \tag{3.14}$$

$$R_{i,n,k}^{pms} = R_{i,n}^{pms} \qquad \forall i \in I, n \in N, k \in K,\ k = 1 \tag{3.15}$$

$$R_{i,n,K}^{rt} = R_{i,n}^{rt} \qquad \forall i \in I, \in N, k \in K, k = K \tag{3.16}$$

$$R_{i,n,K}^{pms} = R_{i,n}^{sg} Z_{n}^{sg} \qquad \forall i \in I, n \in N, k \in K,\ k = K \tag{3.17}$$

Equations (3.18) and (3.19) ensure that the sum of the mole fractions of the components in the gas stream can only be 1.

$$\sum_{i} y_{i,n,k}^{rt} = 1 \qquad \forall n = N, k \in K \tag{3.18}$$

$$\sum_{i} y_{i,n,k}^{pms} = 1 \qquad \forall n = N, k \in K \tag{3.19}$$

The value of *K* is determined by solving the model at different values of *K* until the solution is no longer changing in value when *K* is increased.

3.3.3 Material balances

The material balance approach described in the following section is similar to that commonly used in gas membrane network synthesis and optimisation (Arias et al., 2016; Runhong Qi and Henson, 1998; Uppaluri et al., 2004). Mass balances are carried out around the gas splitters, mixers and condensers as given in Figure 3.4, Figure 3.5 and Figure 3.6.

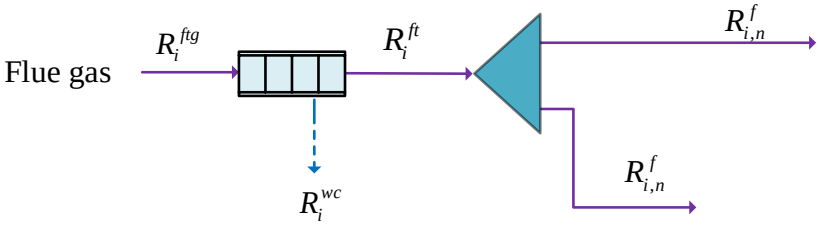

Figure 3.4. Mass balance around the flue gas condenser and the flue gas splitter.

Figure 3.4 shows the process flow of the flue gas through the condenser and the flue gas splitter. The flue gas passes through a cooler condenser to allow the water content to be adjusted to membrane requirements. Equations (3.20) and (3.21) gives the balance on flue gas condenser. Equation (3.20) gives the water balance around the condenser. The rest of the components in

the flue gas cannot be condensed under the conditions as shown by Equation (3.21) thereby ensuring that only water can be removed.

$$R_i^{ftg} = R_i^{ft} + R_i^{wc} \qquad \forall i \in I,\ i = H_2O \tag{3.20}$$

$$R_i^{ftg} = R_i^{ft} \qquad \forall i \in I,\ i \neq H_2O \tag{3.21}$$

Figure 3.5 shows the retentate stream and the residue mixture. A material balance is carried out around the flue gas splitter which is placed after the condenser. The stream can be split by split fraction (x_n^f) into multiple streams (R_n^f) and supplied to potential membrane stage *n* as illustrated by Equation (3.22) which ensures that the sum of the split fractions is 1. Equation (3.23) shows that subsequent streams from the feed splitter are a fraction of the total flue gas supplied. Equation (3.24) is the mass balance on the splitter showing that the total flowrate of component *i* of the streams from the splitter is equal to the flowrate of component *i* of the stream supplied to the splitter.

$$\sum_n x_n^f = 1 \tag{3.22}$$

$$R_{i,n}^f = x_n^f R_i^{ft} \qquad \forall i \in I \tag{3.23}$$

$$R_i^{ft} = \sum_n R_{i,n}^f \qquad \forall i \in I \tag{3.24}$$

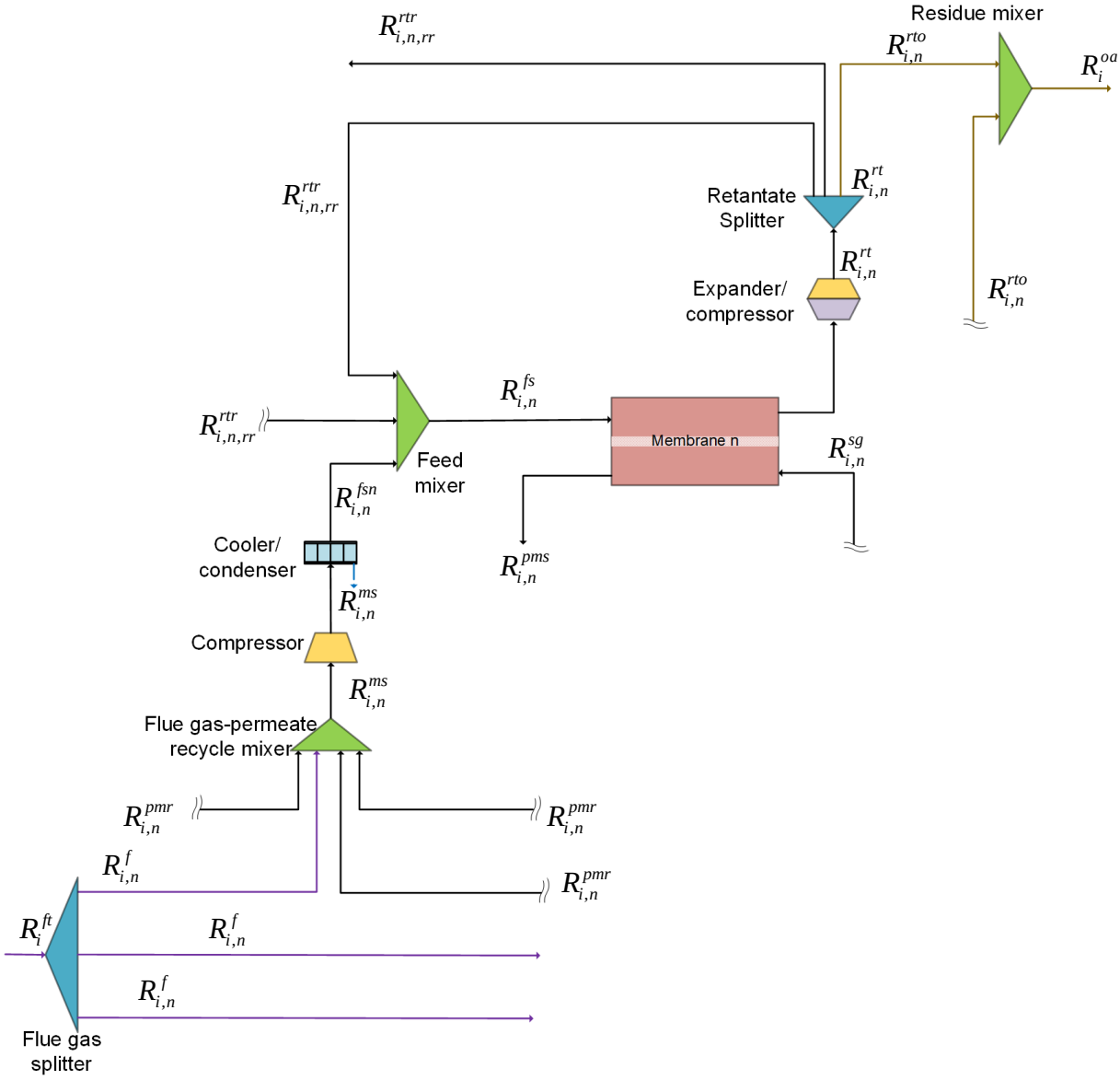

Figure 3.5. Material balance around flue gas permeate mixer, feed mixer and retentate splitter, residue mixer

A material balance on the flue gas-permeate recycle mixer is given by Equation (3.25). Equation (3.25) shows that the resultant flowrate of component *i* in the stream from the membrane feed mixer (R_n^{ms}) is a sum of the flue gas from the flue gas splitter and permeate recycle streams from membrane stages *n*.

$$R_{i,n}^{ms} = x_n^f R_i^{ft} + \sum_{pr} x_{n,pr}^{pmr} R_{i,n}^{pmr} \qquad \forall i \in I; n \in N \tag{3.25}$$

The stream that exits the flue-permeate recycle mixer is compressed to membrane pressure and cooled to 35 °C i.e. membrane operating temperature. The water that exceeds the saturation pressure at this temperature condenses out according to Equations (3.26)-(3.29). The water that is swept with the non-condensables is determined by Equation (3.28)

$$R_{i,n}^{ms} = R_{i,n}^{fms} - R_{i,n}^{wf} \qquad \forall i \in I, i = H_2O \tag{3.26}$$

$$R_{i,n}^{ms} = R_{i,n}^{fms} \qquad \forall i \in I, i \neq H_2O \tag{3.27}$$

The existence of a condenser is denoted by the binary variable (Z^{wf}) and the flowrate of the water is within a range for a condenser to be in effect as shown by Equation (3.28).

$$R^L Z_n^{wf} \leq R_{i,n}^{wf} \leq R^U Z_n^{wf} = 0 \qquad \forall i \in I, i = H_2O \tag{3.28}$$

$$y_{i,n}^{fms} P_n^{rt} - P_i^{sat} = 0 \qquad \forall i \in I, i = H_2O, n \in N \tag{3.29}$$

Equation (3.30) gives the feed mole flowrate of the stream that is fed to the membrane. It is the sum of the flue gas permeate mixture and the retentate recycle stream.

$$R_{i,n}^{fs} = R_{i,n}^{fms} + \sum_{rr} x_{n,rr}^{rtr} R_{i,n}^{rt} \qquad \forall i \in I; n \in N \tag{3.30}$$

Equation (3.31) states that the flowrate of component *i* in the residue stream (*ro)* is a fraction of the retentate stream. The material balance around the residue mixer is given by Equation (3.32)and it states that the flowrate of component *i* in the total residue stream is a sum of the component flowrate from the various membrane stages *n.*

$$R_{i,n}^{ro} = x_n^{rto} R_{i,n}^{rt} \qquad \forall i \in I, \forall\ n \in N \tag{3.31}$$

$$R_i^{oa} = \sum_n R_{i,n}^{ro} \qquad \forall i \in I \tag{3.32}$$

Figure 3.6 shows the process streams from the permeate side of the membrane. Water that has

permeated can be removed from the permeate stream by condensation. Equation (3.33) gives the flowrate of component *i* after the sweep gas recovery or the vacuum system. Equation (3.34) ensures that it is only water that leaves the permeate stream, and the flowrate of the other components remains unchanged.

$$R_{i,n}^{pm} = R_{i,n}^{pms} - R_{i,n}^{wo} \qquad \forall n \in N, i \in I, i = H_2O \tag{3.33}$$

$$R_{i,n}^{pm} = R_{i,n}^{pms} \qquad \forall n \in N, i \in I, i \neq H_2O \tag{3.34}$$

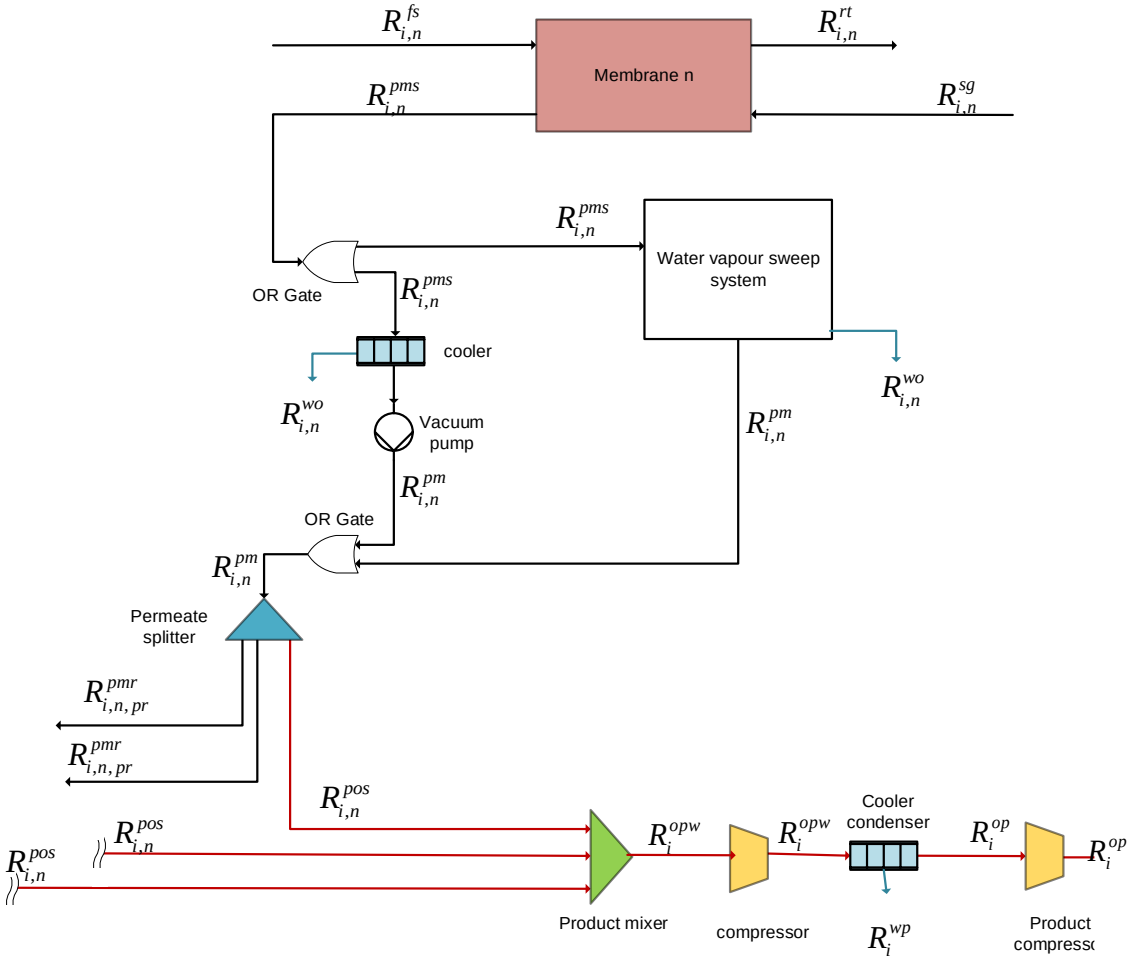

Figure 3.6 Material balance around the permeate condenser, permeate splitter, product mixer and product condenser

Each permeate stream can be split into multiple streams for recycling and/or can be sent to the final product mixer for storage. Equation (3.35) shows that the sum of the split fraction for the permeate recycle stream and product stream is 1.

$$x_n^{pos} + \sum_{pr} x_{n,pr}^{pmr} = 1 \qquad \forall n \in N \tag{3.35}$$

Equation (3.36) states that the flowrate of component *i* from membrane stage *n* towards the product mixer is a product of the flowrate in the permeate stream and the split fraction. The material balance around product mixer is described by Equation (3.37) and gives the flowrate of component *i* in the product stream. Equation (3.37) states that the product stream is a sum of all product streams from membrane stages *n*. The CO_2 rich stream is compressed to pressure (P^{ppw}) and then cooled to 25 °C and water condenses and is separated from the gas stream which has attained the target purity. The material balance around the separator is presented by Equation (3.38) and Equation (3.39). Equation (3.39) ensures that only water leaves the gas stream. Equation (3.40) gives the mole fraction of the water swept along in the gas stream and also the pressure of the product compressor responsible for removing extra water before the final staged compression.

$$R_{i,n}^{pos} = \quad x_n^{pos} R_{i,n}^{pm} \qquad \forall i \in I, \forall\ n \in N \tag{3.36}$$

$$R_i^{opw} = \quad \sum_n R_{i,n}^{pos} \qquad \forall i \in I \tag{3.37}$$

$$R_i^{op} = \quad R_i^{opw} - R_i^{wp} \qquad \forall i \in I, i = H_2O \tag{3.38}$$

$$R_i^{op} = \quad R_i^{opw} \qquad \forall i \in I, i \neq H_2O \tag{3.39}$$

$$y_{i,n}^{op} P^{ppw} = P_i^{sat} \qquad \forall i \in I, i = H_2O, n \in N \tag{3.40}$$

The total molar flowrate of a stream in membrane stage *n* is the sum of the component flowrates as stated by the general Equation (3.41).

$$R_n = \sum_i R_{i,n} \qquad \forall n \in N \tag{3.41}$$

3.3.4 Inequality constraints

The optimisation problem is set to achieve a certain recovery and desired purity of the CO_2 stream captured. The desired CO_2 recovery ratio and desired purity of the product stream are given by Equation (3.42) and Equation (3.43) respectively. Equation (3.42) states that the recovery of component *i* should be greater than the ratio of the flowrate of *i* in the product stream to that in the feed flue gas. The purity of a component *i* in the product stream is the fraction of that component with respect to the total flowrate of all the components in the product stream. Equation (3.43) allows the desired purity of the final product stream to be set.

$$DR_i \geq \frac{R_i^{op}}{R_i^{ftg}} \qquad \forall i \in I \tag{3.42}$$

$$DP_i \geq \frac{R_i^{op}}{\sum_i R_i^{op}} \qquad \forall i = I \tag{3.43}$$

Feasible bounds

The area of each membrane unit is set within a feasible range as given by Equation (3.44). The operating permeate pressure range is different for a vacuum pump and sweep gas set up hence Equations (3.45) and (3.46). Equation (3.45) allows a feasible possible minimum vacuum condition to be set for the vacuum pump operation and the atmospheric pressure is set as the upper bound for the permeate pressure. From the water phase diagram it is ascertained that at the membrane temperature (35 °C) gaseous H_2O exist at the pressure range (0.025 bar to 0.125 bar) which is described by Equation (3.46) (Glasser, 2004; Hussain and Hägg, 2010). Equation (3.47) ensures that the retentate side operating pressure is at least equal to the atmospheric pressure and not vacuum conditions.

$$A^L \leq A_n^{mem} \leq A^U \qquad \forall n \in N \tag{3.44}$$

$$P^L Z_n^{vac} \leq P_n^{pms} \leq Z_n^{vac} P^{atm} \qquad \forall n \in N \tag{3.45}$$

$$P^L Z_n^{sg} \le P_n^{pms} \le Z_n^{sg} P^U \qquad \forall n \in N \tag{3.46}$$

$$1 \le P_n^{rt} \ge P^U \qquad \forall n \in N \tag{3.47}$$

3.3.5 Logic constraints

Either a vacuum pump or a sweep gas system is in operation on the permeate side in each membrane stage and denoted by binary variable *Z*. Equation (3.48) ensures that either a vacuum pump or sweep gas is employed in membrane stage *n*.

$$Z_n^{vac} + Z_n^{sg} = 1 \qquad \forall n \in N \tag{3.48}$$

Equation (3.49) indicates that the molar flowrate of the sweep gas supplied to the membrane *n* is a fraction (g) of the total feed supplied to the retentate side of the membrane.

$$\sum_i R_{i,n}^{sg} = g_n Z_n^{sg} \sum_i R_{i,n}^{fs} \qquad \forall n \in N \tag{3.49}$$

3.3.6 Compressors

Adiabatic compression is assumed for the compressors and vacuum pumps are modelled similarly. The power consumption of the feed compressors and vacuum pumps is given by Equations (3.50) - (3.53). The adiabatic expansion coefficient *(γ)* is taken to be 1.4 and the vacuum pump discharges the permeate gas streams at atmospheric pressure (1.0 bar) as previously assumed (Hasan et al., 2012; Uppaluri et al., 2006, 2004). The power generated by the residue expander and sweep gas expander turbines is given by Equations (3.54) –(3.56) (Bounaceur et al., 2006; Douglas, 1989; Favre, 2011). Equation (3.57) gives the power consumed by the compressor that raises the pressure of the product stream so that more water can be removed at the elevated pressure.

$$Q_n^{cft} = \frac{1}{\eta}\left[\left(\sum_i R_{i,n}^{ms}\right)\cdot 8.314\cdot T^{atm}\left(\frac{\gamma}{\gamma-1}\right)\left(\left(\frac{P_n^{rt}}{P^{atm}}\right)^{\left(\frac{\gamma-1}{\gamma}\right)}-1\right)\right] \qquad \forall n\in N \qquad (3.50)$$

$$Q_{n,np}^{cr} = \frac{1}{\eta}\left[\left(\sum_i R_{i,n,rr}^{rtr}\right)\cdot 8.314\cdot T^{atm}\left(\frac{\gamma}{\gamma-1}\right)\left(\left(\frac{P_{np}^{rt}}{P_n^{rt}}\right)^{\left(\frac{\gamma-1}{\gamma}\right)}-1\right)\right]\cdot \mathrm{Z}_{n,np}^{cr} \qquad \forall n\in N, rr\in RR \qquad (3.51)$$

$$Q_n^{csg} = \frac{1}{\eta}\left[\left(\sum_i R_{i,n}^{pms}\right)\cdot 8.314\cdot T^{mem}\left(\frac{\gamma}{\gamma-1}\right)\left(\left(\frac{P^{atm}}{P_n^{pms}}\right)^{\left(\frac{\gamma-1}{\gamma}\right)}-1\right)\right]\cdot \mathrm{Z}_n^{sg} \qquad \forall n\in N \qquad (3.52)$$

$$Q_n^{vac} = \frac{1}{\eta}\left[\left(\sum_i R_{i,n}^{pms}\right)\cdot 8.314\cdot T^{mem}\left(\frac{\gamma}{\gamma-1}\right)\left(\left(\frac{P^{atm}}{P_n^{pms}}\right)^{\left(\frac{\gamma-1}{\gamma}\right)}-1\right)\right]\cdot \mathrm{Z}_n^{vac} \qquad \forall\ n\in N \qquad (3.53)$$

$$Q_n^{exr} = \eta\left[\left(\sum_i R_{i,n}^{rto}\right)\cdot 8.314\cdot T^{atm}\left(\frac{\gamma}{\gamma-1}\right)\left(1-\left(\frac{P^{atm}}{P_n^{rt}}\right)^{\left(\frac{\gamma-1}{\gamma}\right)}\right)\right] \qquad \forall n\in N \qquad (3.54)$$

$$Q_n^{exs} = \eta\left[\left(\sum_i R_{i,n}^{sg}\right)\cdot 8.314\cdot T^{atm}\left(\frac{\gamma}{\gamma-1}\right)\left(1-\left(\frac{P_n^{pms}}{P^{atm}}\right)^{\left(\frac{\gamma-1}{\gamma}\right)}\right)\right]\cdot \mathrm{Z}_n^{sg} \qquad \forall n\in N \qquad (3.55)$$

$$Q_{n,np}^{xr} = \eta\left[\left(\sum_i R_{i,n,rrr}^{rtr}\right)\cdot 8.314\cdot T^{atm}\left(\frac{\gamma}{\gamma-1}\right)\left(1-\left(\frac{P_{np}^{rt}}{P_n^{rt}}\right)^{\left(\frac{\gamma-1}{\gamma}\right)}\right)\right]\cdot \mathrm{Z}_{n,np}^{xr} \qquad \forall n\in N \qquad (3.56)$$

$$Q_n^{ppw} = \frac{1}{\eta}\left[\left(\sum_i R_{i,n}^{opw}\right)\cdot 8.314\cdot T^{atm}\left(\frac{\gamma}{\gamma-1}\right)\left(\left(\frac{P^{ppw}}{P^{atm}}\right)^{\left(\frac{\gamma-1}{\gamma}\right)}-1\right)\right] \qquad \forall n\in N \qquad (3.57)$$

The captured CO_2 is compressed so that it liquefies and then it is pumped and sent for storage. The power consumed in this process is determined by Equation (3.58). The compression ratio

is given by Equation (3.59) (Arias et al., 2016). Equation (3.60) gives the power consumed by the pump.

$$Q^{icp} = \frac{1}{\eta}\left[\left(\sum_i R_i^{OP}\right)\cdot 8.314\cdot T^{mem}\left(\frac{\gamma}{\gamma-1}\right)\left((CR)^{\left(\frac{\gamma-1}{\gamma}\right)}-1\right)\right] \tag{3.58}$$

$$CR = \left(\frac{P^{cut}}{P^{ppw}}\right)^{1/stagecut} \tag{3.59}$$

$$Q^{pump} = \frac{1}{\eta}\sum_i\left(\frac{Mr_i}{\rho_i}R_i^{op}\right)\cdot\left(P^{storage}-P^{cut}\right) \tag{3.60}$$

3.3.7 CO_2 permeance and relative humidity

Zhang et al. (2013) developed an expression for permeance in relation to partial pressure for facilitated transport membranes. The function was validated against experimental results and is applicable to both liquid facilitated transport and fixed site carrier membranes. The permeance of the target component is expressed in terms of its diffusivity, Henry's constant, equilibrium constant, the total carrier concentration and retentate and permeate pressure. The expression can be implemented in simulation work as the parameters can be obtained and determined from literature. Equation (3.61) gives the permeance of CO_2 through the FSC membrane. The CO_2 permeance is a sum of the contribution of the solution diffusion mechanism and that of reaction diffusion mechanism. It is apparent that CO_2 permeance is inversely proportional to the membrane thickness (l) and partial pressure. The parameters used in Equation (3.61) are determined for the polyvinlyamine/polysulfone (PVAm/Psf) FSC membrane presented in literature (T. J. Kim et al., 2013).

$$\varphi_{i,n,k} = \frac{D_i}{lHC_i} + \frac{D_{iAm}K_{eq}CR_T HC_i}{l(HC_i + K_{eq}P_n^{rt}\cdot y_{i,n,k}^{rt})(HC_i + K_{eq}P_n^{pms}\cdot y_{i,n,k}^{pms})} \tag{3.61}$$
$$\forall n\in N, k\in K, i\in I, i = CO_2$$

The N_2, H_2O and O_2 permeance is assumed to be constant and is taken as 1.84×10^{-7}, 2.48×10^{-5}, 8.26×10^{-7} kmol/ (m^2.bar.s) respectively as assumed previously (He and Hägg, 2014).

The relative humidity of the stream that is fed to the membrane is given by the ratio of the water partial pressure $\left(y_{i,n}^{fs}P_n^{rt}\right)$ to the saturation vapour pressure at the membrane operating temperature (35° C) as described by Equation (3.62) Saturation pressure is a parameter in the model since the membrane operating temperature is assumed beforehand. The water saturation pressure is determined from the Antoine equation (Perry and Green, 1997).

$$RH_n.P^{sat} = y_{i,n}^{fs}P_n^{rt} \qquad \forall n \in N, i \in I, i = H_2O \tag{3.62}$$

3.3.8 Water condensation

Water condensation is modelled as previously described elsewhere (Crabtree et al., 1998; Dunn and El-Halwagi, 1994; El-Halwagi et al., 1995). The process stream that exits the compressor is cooled and if the water partial pressure exceeds the water saturation pressure at that temperature *(T)* then condensation occurs. For instance the mole fraction of the water that remains in the gas stream after the flue gas-permeate recycle condenser is computed by Equation (3.63).

$$y_{i,n}^{fms}P_n^{rt} = P^{sat} \quad (T) \qquad i \in I,\ i = H_2O \tag{3.63}$$

An increase in pressure will, therefore, allow more water to be removed as condensate. The gas stream supplied to the compressors has water content at less than or equal to saturation pressure. As the gas is compressed, the temperature of the gas increases and consequently the saturation pressure increases, thereby preventing the condensation of the water vapour in the compressor (Pfister et al., 2017). Water is then separated from the gas stream when it has been cooled down. The compressed feed is cooled to 35 °C, and thus serves as the membrane operating pressure. The product streams are cooled to 25 °C and corresponding saturation pressure is used in the different cases.

3.3.8.1 Vacuum condensers

The vacuum cooler condenser is modelled by Equation (3.64) gives the mole flowrate of the water vapour that is swept in the gas stream together with the non-condensables (*nc*). Equation (3.65) gives the mass of steam *(kg)* used as the sweep gas.

$$R_{H_2O,n}^{rps} = \frac{Z_n^{rwvc} \sum_i^{nc} R_{i,n}^{rps} \cdot P^{sat}}{Z_n^{rwvc} (PP_n - P^{sat})} \qquad \forall n \in N \tag{3.64}$$

$$m_{n,steam} = R_{i,n}^{sg} Mr_i \cdot Z_n^{sg} \qquad \forall\ n \in N, i \in I, i = H_2O \tag{3.65}$$

3.3.8.2 Coolers

The temperature of the gas stream as it exits flue gas -permeate compressor is given by Equation (3.66). Equations (3.67) and (3.68) give the heat transfer area of the flue gas permeate compressor cooler A_n^{clf} and the logarithmic mean temperature difference (lmt_n^{clf}) of the cooler respectively.

$$T_n^{cft} = T_n^{ms} \left(\frac{P_n^{rt}}{P^{atm}} \right)^{\left(\frac{\gamma-1}{\gamma}\right)} \qquad \forall n \in N \tag{3.66}$$

$$A_n^{clf} = \frac{\sum_i R_{i,n}^{ms} \cdot Cp \left(T_n^{cft} - T^{mem} \right)}{Ulmt_n^{clf}} \qquad \forall n \in N \tag{3.67}$$

$$lmt_n^{clf} = \frac{(T_n^{cft} - T^{hw}) - \left(T^{mem} - T^{cw} \right)}{ln \frac{\left(T_n^{cft} - T^{hw} \right)}{\left(T^{mem} - T^{cw} \right)}} \qquad \forall n \in N \tag{3.68}$$

3.3.9 The objective function

The objective is to minimise the total annualised cost (TAC) of the CO_2 capture membrane process. TAC is a sum of the annualised costs associated with each process unit and is generalised by Equation (3.69) which shows that TAC is a sum of annualised operating cost (OPEX) and annualised capital cost (CAPEX). The bare module cost method (CAPECOST) is adopted in this work to allow for comparison with other FSC membrane works (Chu and He, 2018; He et al., 2015; He and Hägg, 2014). The costing method is based on the contribution of major equipment such as compressors and the membrane area. The contribution of minor equipment such as condensers to the total cost is not considered.

$$min\left[TAC\right] = OPEX + CAPEX \tag{3.69}$$

The net power consumed is a sum of the power consumed by the compressors and vacuum pumps less the power generated by the expanders as given by Equation (3.70).

$$\begin{aligned} TNQ = \sum_n Q_n^{cft} + \sum_n Z_n^{vac} Q_n^{vac} + \sum_n Z_n^{sg} Q_n^{csg} + Q_n^{ppw} + Q^{icp} + Q^{pump} - \\ \sum_n Z_n^{sg} Q_n^{exs} - \sum_n Q_n^{exr} - \sum_n \sum_{rr} Z_{n,rr}^{xr} Q_{n,rr}^{xr} + \sum_n \sum_{rr} Z_{n,rr}^{cr} Q_{n,rr}^{cr} \end{aligned} \tag{3.70}$$

The capital cost related to the membrane is computed by Equation (3.71). It is the sum of the purchase price and the cost of replacement of the membrane modules. The membrane is replaced every five years at 20% of the initial cost.

$$TCC^{mem} = C^{mem} TMA + C^{rpl} TMA \tag{3.71}$$

The total purchasing cost of the units is given by Equation (3.72). The 2012 US dollar cost prices are adjusted for inflation to 2018 prices by use of chemical engineering process overall indexes of 2012 and 2018 (Chemengonline, 2019; Chu and He, 2018).

$$TCCU = {}^{603.1}\!/_{584.6}\left(\begin{array}{l} TCC^{mem} + \sum_n CC_n^{comp} + \sum_n CC_n^{clf} + \sum_n CC_n^{exr} \\ +CC^{ico} + \sum_n \mathrm{CC}_n^{vac} \cdot Z_n^{vac} + \sum_n CC_n^{csg} \cdot Z_n^{sg} + \\ +\sum_n CC_n^{exs} \cdot Z_n^{sg} + \sum_n \sum_{rr} Z_{n,rr}^{xr} CC_{n,rr}^{xr} + \sum_n \sum_{rr} Z_{n,rr}^{cr} CC_{n,rr}^{cr} \end{array}\right) \quad (3.72)$$

The total capital cost is a sum of the purchase cost and installation, labour and unforecastable costs which are assumed to be 18 % of the purchase cost. It is also assumed that the annual capital related charge *(CRF)* is 0.2 (He & Hägg, 2014). Equation (3.73) gives the annual capital cost. The annual operational cost consists of the net electricity consumed in running the compressors and vacuum pump, the labour cost per year and the cost of steam when sweep vapour is present as stated by Equation (3.74). It is assumed that steam from the boiler is used in the CO_2 capture rather than including a steam generation specifically for the CO_2 capture plant.

$$CAPEX = CRF\left(1.18\right)TCCU \quad (3.73)$$

$$OPEX = C^{el} \cdot TNQ \cdot EY + CLB \cdot EY + C^{stm} \cdot Z_n^{sg} \quad (3.74)$$

The total capital cost of compressors and vacuum pumps is given by Equation (3.75). Equation (3.76) gives the capital cost of expanders. The cost of the CO_2 rich product pump is given by Equation (3.77). The calculation is based on the power consumption of each unit. The coolers capital cost is evaluated based on the size of the heat transfer area as given by Equation (3.78)

$$CC^{comp} = C^{comp} Q^{comp} \quad (3.75)$$

$$CC^{exp} = C^{exp} Q^{exp} \quad (3.76)$$

$$CC^{pump} = C^{pump} Q^{ump} \quad (3.77)$$

$$CC^{h/exch} = A^{h/exch} C^{h/exch} \quad (3.78)$$

3.4 Illustrative example

Equations (3.1) - (3.74) make up an MINLP problem. The model is implemented and solved by the solver GAMS/BARON on the online NEOS servers (Puranik and Sahinidis, 2017). To validate the membrane model the work of Pan was simulated with acceptable differences as presented in Appendix A1 (Pan, 1986). The two stage cascading FSC membrane process operating at 2.5 bar retentate and 0.25 bar permeate was also reproduced to validate the entire simulation process (membrane, equipment models and balances) with acceptable differences (He and Hägg, 2014). The power plant considered in this study is a plant that produces 819 MW of electricity from coal of lower heat value (LHV) of 1657.1MW/t. The plant flue gas flowrate is 26.61 kmol/s and comprises 12.7% CO_2, 72.9% N_2, 9.7% H_2O and 3.7% O_2. The CO_2 emission rate is 763kg/MWh_{net}. (Broutin et al., 2014; CESAR, 2011; He and Hägg, 2014).

The membrane properties are obtained from literature (Kim et al., 2013b). Kim et al. (2013b) presented the results for the study of CO_2/N_2 separation using a PVAm/Psf membrane. The membrane was synthesised by casting a PVAm solution onto poly-sulfone support to make a 1% PVAm/Psf membrane. The synthesised membrane was characterised and tested for CO_2 capture from a mixture of CO_2 and N_2 gas which had been humidified. The permeation experiments were carried out at 35°C and at different operating pressure and relative humidity. The effect of feed gas humidity and the pressure was investigated. Scanning electron microscopy showed that the selective PVAm layer was 0.8μm to 1.2μm thick. It was shown that the highest permeance and selectivity was realised at the highest relative humidity (90%) as other studies before had shown. The permeance was also highest at the lowest feed pressure (Deng et al., 2009). The sweep gas flowrate was not reported in the study and therefore the permeate partial pressure could be regarded negligible It can be considered that permeation experiments are carried out at close to zero CO_2 permeate partial pressure since the sweep gas flowrate is usually much greater than the permeate (Zhang et al., 2013).

In this study, the thickness of the effective layer of the membrane is assumed to be 0.8μm, and the relative humidity of the feed is considered to vary from 90% to 100%. The total carrier concentration is determined for 1% PVAm. The Henry's constant for CO_2 is determined at the membrane operating temperature (35°C) from Equation (3.79). The equilibrium constant and

diffusivities of CO_2 and CO_2 –amine complex are considered similar to that determined for polyalyamine/polyvinlyalcohol /PSf membrane (Zhang et al., 2013).

Table 3.1 shows other values of the parameters used in the simulation as determined. The parameters give a modest CO_2 permeance of 3.8×10^{-5} kmol/m^{2}bar.s at feed pressure 1.1 bar and CO_2 concentration of 10% and negligible permeate pressure. In this work, the permeance varies with varying partial pressure across the membrane as the CO_2 concentration changes along the discretised membrane profile. From Equation (3.1) and Equation (3.61), it is apparent that a trade-off should be achieved between CO_2 permeance which is enhanced by a low partial pressure difference and the overall flux that is enhanced by a high pressure partial pressure difference.

$$HC_{CO_2} = \left\{ \exp\left(22.2819 - \frac{138.306\times10^2}{T} + \frac{691.346\times10^4}{T^2} - \frac{155.895\times10^7}{T^3} + \frac{120.037\times10^9}{T^4} \right) \right\} \Big/ 7.5001 \tag{3.79}$$

Table 3.1: PVAm/Psf membrane parameters used in simulation

Parameter	
l(m)	0.8×10^{-6}
CR_T (kmol/m^3)	27.1
H_{CO_2} (barm^3/kmol)	37.95
D_{CO_2} (m^2/s)	9.4×10^{-11}
D_{CO_2Am} (m^2/s)	4.34×10^{-13}
K_{eq} (m^3/kmol)	122

The cost parameters used in the simulation are listed in Table 3.2 (He and Hägg, 2014). The prices in the table are in US dollars for the year 2012.

Table 3.2: Economic data for the case study

Parameter	symbol	Value
Membrane price (US$/m^2)	C^{mem}	35
Membrane replacement cost	C^{rep}	0.2% C^{mem}
Flue gas and recycle compressor unit cost (US$ /KW)	C^{comp}	850
Inter-stage compression and pump cost (US$ /KW)	C^{icp}	1800
Product pump cost (US$ /KW)	C^{icp}	1350
Expander unit cost (US$ /KW)	C^{exp}	630
Vacuum pump unit cost (US$ /KW)	C^{vac}	1300
Reference heat exchanger (US$/m^2)	C^{hx}	300
Electricity cost (US$ /KW-h)	C^{el}	0.04
Labour cost (US$/hr)	C^{lb}	37
Capital recovery factor (yr)	*CRF*	0.2
Compressor, vacuum, expander efficiency %	η	85
Adiabatic compression coefficient	γ	1.4
Gas constant	R	8.134
Membrane lifetime (yr)		5
Project lifetime (yr)		25
Operating time (h/yr)		7500
Cost of electricity generation at the reference plant (US$/MWh)		40

3.5 Results and discussion

The results are presented in two sections. The first section considers the permeate pressure from 0.2 to 1 bar and this is considered as practically feasible as driven by vacuum pumps only on the permeate side. The second section considers the use of water vapour as sweep and this calls for a lower permeate pressure from 0.025-0.095 bar. The separation targets for all the simulation runs are set at a CO_2 recovery of 90% and purity of 95% for the product stream.

3.5.1 Case 1: Vacuum only driven process

Three scenarios are considered to show the benefits of optimisation. Scenario 1 is a 2 stage cascading process which has no recycle streams and operate at uniform retentate and permeate pressure in both stages. Scenario 2 extends scenario 1 to allow for non-uniform operating pressure both on the retentate and permeate side. Scenario 3 is a 3 stage process based on the superstructure and allows non-uniform pressure operation and multiple recycle streams. The upper bound for the membrane area is set at 1 000 000 m^2 for scenario 3 whilst scenario 1 and 2 could not yield a solution and in that case the membrane area size is unrestricted. Upper bound values considered in literature to varying from 50 000 m^2 to 1 500 000 m^2 (Hasan et al., 2012; He et al., 2015; Lee et al., 2018). The lower bound on operating pressure of vacuum pumps is 0.2 bar and the upper bound is 1 bar.

The comparison of the solutions for the different scenarios of case 1 is presented in Table 3.3 and the optimum pressure values in Table 3.4.

Table 3.3: Computational results of scenario 1, 2 and 3.

Case 1	**Scenario 1**	**Scenario 2**	**Scenario 3**
Number of membrane stages	2	2	3
Recovery	0.9	0.9	0.9
Purity	0.95	0.95	0.95
CO_2 capture rate, (ton/h)	521	521	521
Total membrane ($x\ 10^6\ m^2$)	3.3	2.6	1.75
Total power (MW)	204.1	215.3	224.6
Total net power (MW)	168.0	191.7	171.1
Power recovered (MW)	36.0	23.6	53.5
Operating costs ($x\ 10^6$ US$)	50.5	57.5	51.5
Capital costs ($x\ 10^6$ US$)	113.7	100.3	89.4
TAC ($x\ 10^6$ US$)	164.2	157.0	140.9
Specific capture cost (US$/ton)	42.0	40.1	36.0

Cost of CO_2 avoided (US$/ton)	55.7	55.8	48.1
% saving CO_2 avoided	-	4.5	14.2

In the first scenario, the 2-stage cascading process with uniform pressure ratio in the stages has the highest total cost of CO_2 capture. The resultant process flowsheet is shown in Figure 3.7. The composition of only CO_2 and water is shown for brevity, however the balance of streams is due to N_2 and O_2 composition. Scenario 2 in which a variable pressure ratio is enabled results in a 4.5% reduction in membrane area but the net power increased by 7%. The capital cost decreased because of the decrease in the membrane area requirement and a smaller increase in operating costs as a result of the increased power demand. This led to a specific capture cost saving of 4.5%. The change in the cost of CO_2 avoided was negligible from scenario 1 to scenario 2. This is attributed to the increase in the power consumption which neutralised the annual cost savings.

Figure 3.8 shows the optimum process flowsheet for scenario 3. The resultant process flow sheet of scenario 3 shows that the flue gas stream is combined with a retentate recycle stream and fed to the first stage. The retentate is subsequently fed to a second stage for further stripping. The third stage is solely dedicated to processing the permeate recycle streams from the other 2 stages. This third stage has a high CO_2 driving force since the CO_2 concentration is high and therefore the pressure ratio is lower than the other stages. This results is a more energy efficient system. The variable pressure ratio in each stage and recycling results in a more energy efficient CO_2 capture process and a smaller membrane area which makes the process economical. Scenario 3 therefore has the lowest cost of CO_2 avoided at US$/ton 48.1.

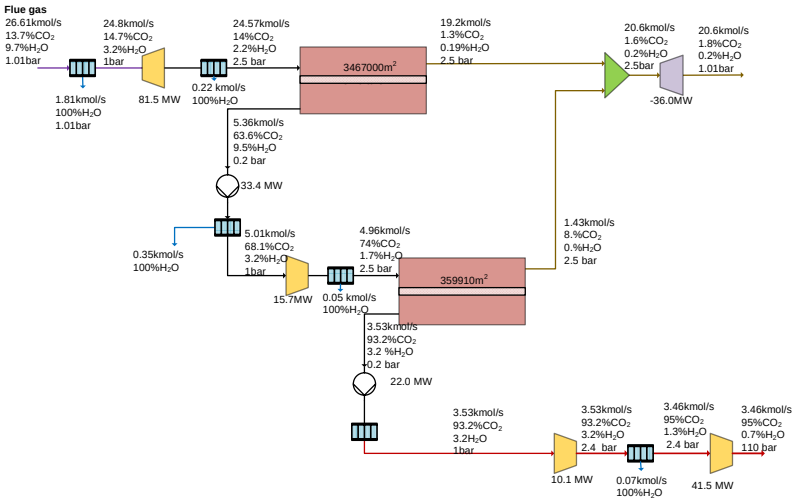

Figure 3.7. Scenario 1 process flowsheet, 2 stage membrane process operating at uniform operating pressure.

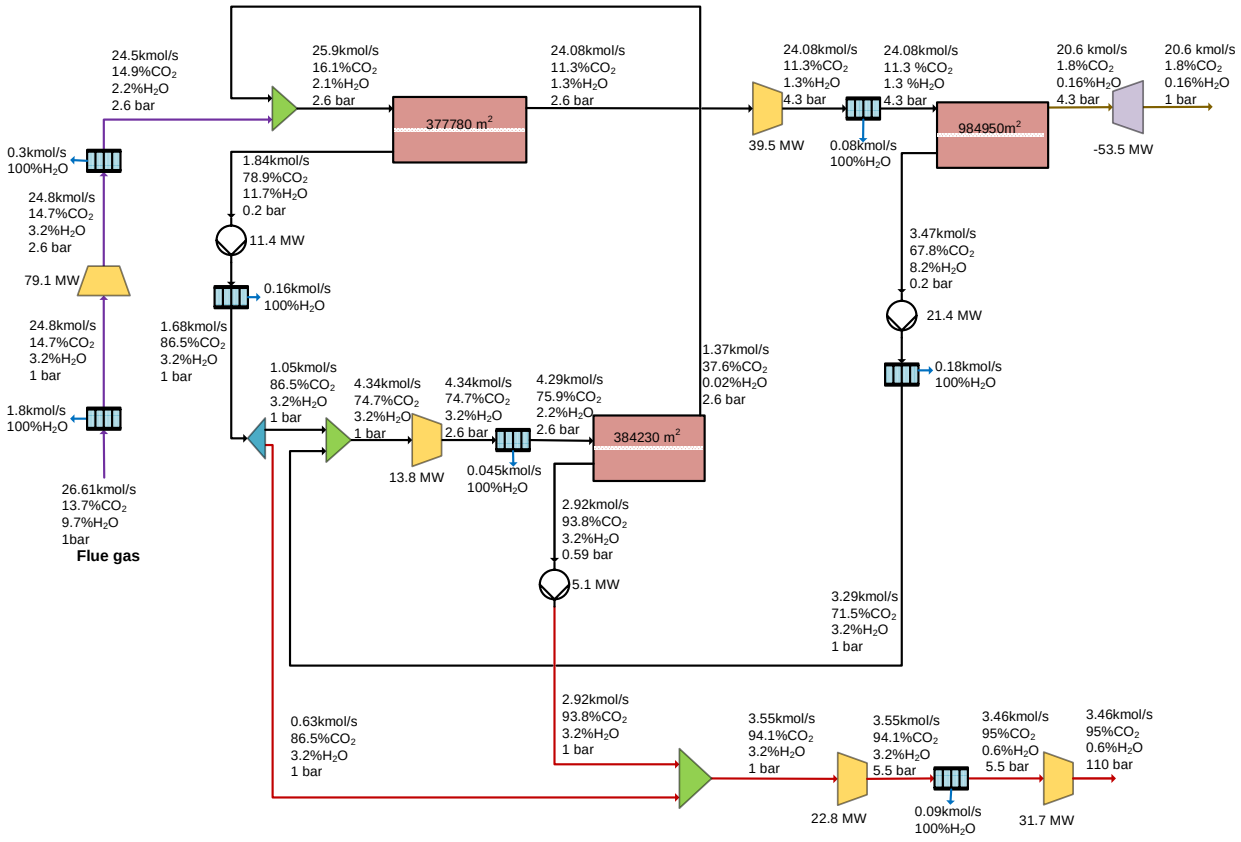

Figure 3.8. Process flowsheet of scenario 3 which is a 3 stage vacuum driven with non-uniform operating pressure.

Table 3.4 shows the optimum pressure ratio and the optimum feed humidity of each membrane stage. Solution to scenario 3 has two membrane stages that operate at high pressure ratio, thereby resulting in a smaller membrane area required to achieve the desired separation targets. For scenario 2 and scenario 3, which allow non-uniform pressure ratio, a lower pressure ratio stage is observed and this results in more energy efficient process systems.

Table 3.4: Optimum pressure values

	Scenario 1		**Scenario 2**		**Scenario 3**		
Membrane stages	1	2	1	2	1	2	3
Retentate (bar)	2.52	2.52	3.19	1.79	2.59	4.29	2.59
Permeate (bar)	0.2	0.2	0.2	0.3	0.59	0.2	0.2
Ratio (P^{rt}/P^{pms})	12.6	12.6	15.9	6.0	4.4	21.4	12.9
RH(%)	99.7	99.7	99	99	99.7	100	94.5
Mol fraction (%)	2.2	2.2	1.8	3.2	1.3	1.2	2.0

Table 3.5 shows that scenario 1 and scenario 3 have comparable overall plant power efficiencies (35%). This indicates a 10% efficiency penalty which is comparable to several studies (He and Hägg, 2014; Zhai and Rubin, 2013).

Table 3.5: Comparative study on overall plant energy consumption

	Reference	**Scenario1**	**Scenario 2**	**Scenario 3**
Recovery (%)	0	90	90	90
CO_2 product purity (%)	-	90	95	95
Gross power (MW)	819.0	819.0	819.0	819.0
Auxiliary (MW)	65.0	233.1	256.7	236.1
Net power output (MW)	754.0	585.9	562.3	582.9
Efficiency %LHV	45.5	35.4	33.9	35.2
Specific power (KWh/ton)	-	322	368	328

CO_2 emitted (kg/MWh)	763.0	89.3	92.9	89.6
CO_2 avoided (US$/ton)	-	55.7	55.8	48.1

From Table 3.6 it is evident that the optimisation model presented results in significantly less membrane area required for CO_2 capture process than that previously reported for FSC membranes (He and Hägg, 2014, He et al., 2015). A smaller membrane area results in significant overall cost savings. Scenario 3 is recommended since it achieves the separation targets at relatively the same power plant efficiency but at a lower cost.

Table 3.6: Comparison with other studies

Variable	**(He et al., 2015)**	**(He & Hägg, 2014)**	**Scenario 1**	**Scenario 3**
Number of stages	2	2	2	3
CO_2 Purity	0.95	0.957	0.95	0.95
Recovery	0.80	0.90	0.90	0.90
Specific membrane m^2/ton.h	8189	7904	5049	3351
Specific power, kWh/ton	284.3	316	368	328
Specific cost, US$/ton	47.87	45.6	40.1	36.0
Plant power efficiency %	-	35.5	33.9	35.2

3.5.2 Case 2: Consideration for water vapour sweep

This section evaluates the benefit of incorporating a sweep strategy into the design. For comparison purposes, the 3-stage vacuum-only driven optimisation is carried out under the permeate pressure range (0.025 - 1 bar) and compared to the sweep pressure range (0.025 – 0.095 bar) where water can exist as vapour at the membrane operating temperature; and then the third case considers the possible use of both sweep strategy and vacuum-only in different

membrane stages. Scenario 4 has vacuum pumps only in the permeate side in all the 3 stages; scenario 5 has sweep gas in all the 3 stages; and scenario 6 is the case for having a combination of vacuum-only and sweep gas in different membrane stages. Scenarios 4, 5 and 6 allow non-uniform operating pressure in the membrane stages, and therefore have variable retentate/pressure ratio. Results of the 3 scenarios of case 2 are presented in Table 3.7.

Table 3.7: Results for Case 2

	Scenario 4	**Scenario 5**	**Scenario 6**
Number of membrane stages	3	3	3
Recovery	0.9	0.9	0.9
Purity	0.95	0.95	0.95
CO_2 capture rate, (ton/h)	521	521	521
Total membrane ($x10^6$ m^2)	1.68	1.06	1.30
Total power (MW)	174.5	204.3	190.9
Total net power (MW)	150.7	174.5	159.3
Power recovered (MW)	23.7	29.8	31.5
Operating costs ($x10^6$ US$)	45.3	53.0	48.4
Capital costs ($x10^6$ US$)	77.5	68.3	70.4
TAC ($x10^6$ US$)	122.9	121.3	118.8
Specific cost of capture (US$/ton)	31.4	31.0	30.3
Cost capture- CO_2 avoided(US$/ton)	40.3	41.7	39.6
% saving on specific cost	-	0.9	3.5

The use of a sweep (scenario 5) reduces the membrane area requirement by 37% when compared to scenario 4. A smaller membrane area translates to lower capital cost. The use of the sweep however results in an increase in the power consumption by 15.8% thereby increases the operating costs. The difference in the total annual cost is minimal, as it decreases by 1.3%

for scenario 5 due to the larger decrease in capital cost which outweighs the decrease in operating cost. The decrease in membrane area when sweep gas is used has been documented (Hussain and Hägg, 2010). The sweep gas dilutes the permeate and keeps the partial pressure of the CO_2 low thus enhancing the driving force and hence the smaller membrane area achieves the recovery. However, the use of the sweep gas increases the power consumption as higher permeate flowrates need to be compressed. Vacuum only (scenario 4) also has a larger permeate pressure range which enables efficient distribution of power consumption in the membrane stages. The cost of CO_2 avoided increases for the sweep driven compared to the non-sweep set up due to the higher power consumption.

A combination of sweep and vacuum pumps (scenario 6) gave the most economic result with annual cost of US$118.8 million compared to the vacuum only system (US$122.9 million). The process flow comprises of 2 stages that are sweep driven and a stage which is vacuum only driven.

Figure 3.9 shows the process flowsheet. This optimum process flowsheet leads to 3.9 % and 2.1 % reduction in total annual costs in comparison with the vacuum only and sweep strategy respectively. The cost of CO_2 avoided also is lowest for scenario 6 at US$39.6 compared to scenario 4 and scenario 5. The use of sweep in the 2 stages reduces the membrane area and the vacuum only stage makes up for moderate power consumption as it operates at a low pressure ratio as illustrated in Table 3.8. The presence of a sweep lowers the CO_2 permeate partial pressure which enhances the driving force. This enables a higher stage cut to be achieved by a smaller membrane area. Water vapour sweep regeneration consumes a lot of energy during compression of the permeate from the permeate side operating pressure (0.025-0.095 bar) to 1 bar. Scenario 6 operates at relatively lower feed pressure in two of the three stages which results in high CO_2 permeance since the sweep gas generates the driving force and therefore a simpler network can achieve the set separation targets.

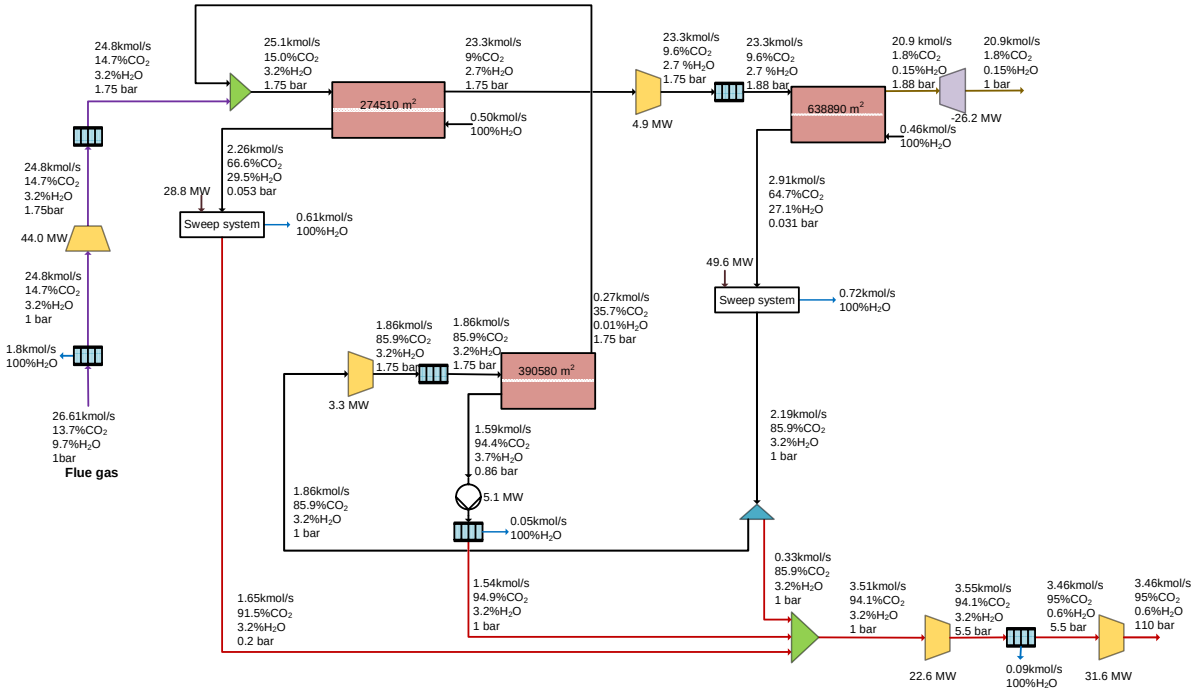

Figure 3.9. Scenario 6 Optimum process flowsheet for 3-stage, combined sweep and vacuum with non-uniform operating pressure.

Table 3.8: Optimum pressure values

Membrane stages	Scenario 4			Scenario 5			Scenario 6		
	1	2	3	1	2	3	1	2	3
	Z^{vac}	Z^{vac}	Z^{vac}	Z^{sg}	Z^{sg}	Z^{sg}	Z^{vac}	Z^{sg}	Z^{sg}
Retentate (bar)	1.77	1.76	1.77	1.76	1.76	1.76	1.75	1.75	1.88
Permeate (bar)	0.51	0.044	0.052	0.095	0.056	0.03	0.86	0.053	0.031
Ratio (P^{rt}/P^{pms})	3.4	40.7	34.4	18.5	31.4	5.85	2.04	33.0	60.5
RH(%)	99.7	99.7	99.4	99.1	99.7	90.0	98.7	98.6	90.0
Mol fraction (%)	3.2	3.3	3.1	3.2	3.2	2.9	3.2	3.2	2.7
g (%)	-	-	-	9.6	2.1	2.0	-	2.0	2.0

3.5.3 Relative humidity profiles

Figure 3.10 shows the relative humidity profiles on the retentate side of the membrane. The profiles indicate that de-humidification occurs, which would contribute to a lower permeance of CO_2 along the membrane length. This has not been accounted for in this study. The extent of dehumidification is less for sweep driven stages. The presence of water vapour on the permeate side lowers the partial pressure difference across the membrane and hence reduces the water driving force so that less water permeates. Whilst this study has considered a generalised CO_2 permeance for FSC membranes, the dependency of permeance on the humidity is membrane specific. Several simulation studies of carbon capture from humidified gases have not reported humidity profiles within the FSC membrane modules, but only gave the relative humidity of the feed gas as it is fed into the membrane (He and Hägg, 2014; Hussain and Hägg, 2010; Low et al., 2013; Pfister et al., 2017). The de-humidification of the membrane module and the consequent decrease in CO_2 permeance could be one of the reasons the FSC showed lower CO_2 permeance during a pilot study compared to the experimental study (He et al., 2017; T. J. Kim et al., 2013).

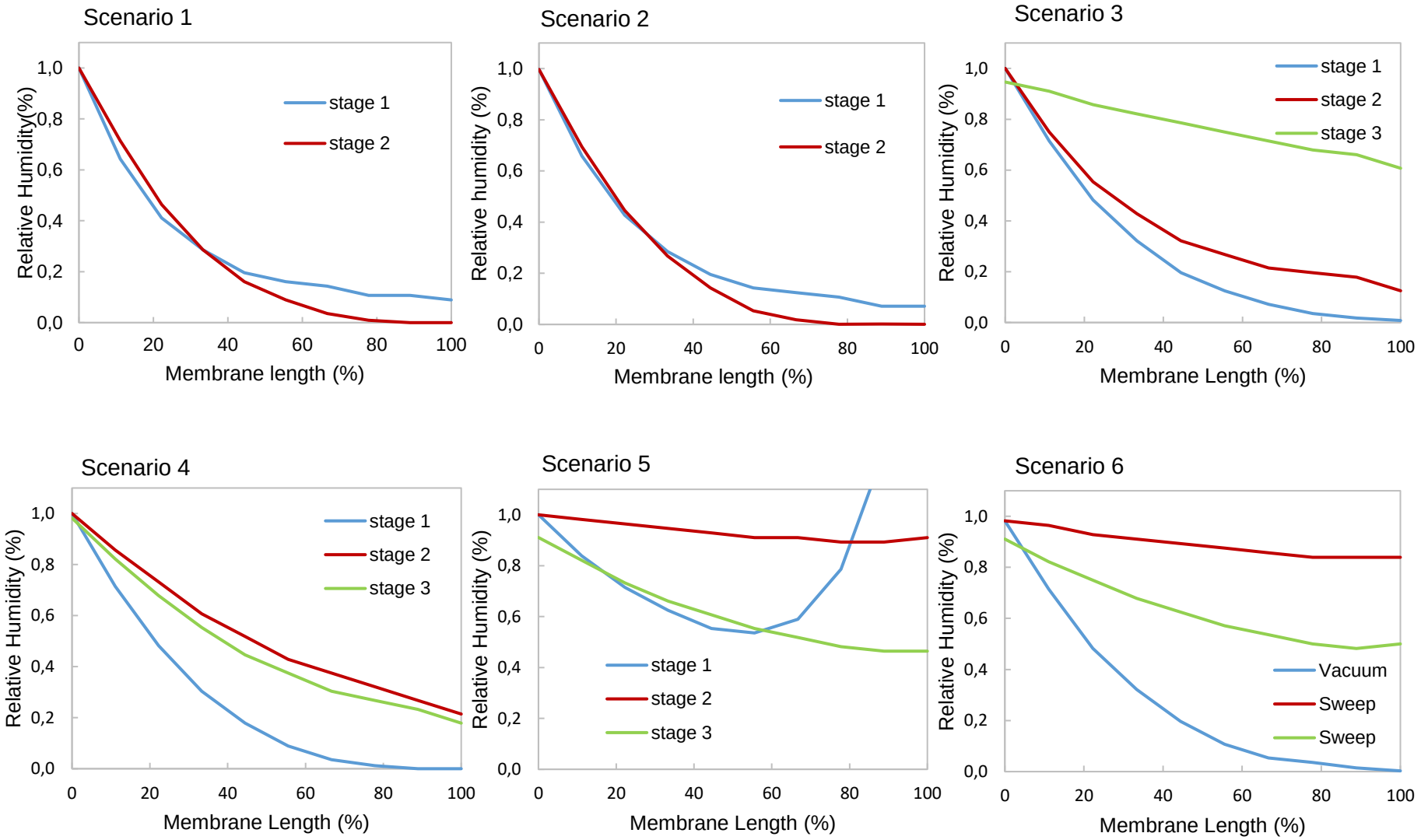

Figure 3.10. Humidity profiles along the membrane

Table 3.9 and Table 3.10 shows the comparative statistics. The results indicates a highly non-linear model and the computational times to be relatively short. Scenario 6 has significantly longer time since the model searches a solution from sweep option, then vacuum driven only and also a combination of these in the different stages.

Table 3.9: Comparative model statistics for different scenarios- Case 1

	Scenario 1	**Scenario 2**	**Scenario 3**
No. constraints	1202	1200	1922
No. variables	888	888	1480
No. binary variables	4	4	24
Non-linear terms	1987	1987	3320
CPU(s)	17.12	34.39	356.5

Table 3.10: Comparative model statistics for different scenarios- Case 2

	Scenario 4	**Scenario 5**	**Scenario 6**
No. constraints	1940	2030	2192
No. variables	1480	1552	1558
No. binary variables	24	24	30
Non-linear terms	3512	3743	4910
CPU(s)	500.9	121.6	1275.2

3.5.4 In-depth analysis of the FSC membrane application for CO_2 capture from coal plant flue gas

Technical and economic analysis of the various factors that affect the feasibility of CO_2 capture based on the FSC membrane is discussed. These include the flow pattern, the effect of uniform or non-uniform pressure operation, and the water permeance value. The impact of the cost of the membrane and the cost of electricity on the optimisation results are also investigated. The model presented in section 3.3 is the basis of the results presented in this section. The

superstructure involved the use of vacuum conditions on the permeate side, as indicated in Case 2 presented in section 3.5.1.

3.5.4.1 Effect of flow pattern

Optimisation of the CO_2 capture process is carried out based on three membrane flow patterns. The flow patterns are countercurrent, cocurrent and crossflow. The recovery and purity were set to 90% and 95%, respectively. The results presented in Figure 3.11 indicate that the countercurrent flow results in the lowest annualised cost.

Optimising the process based on a cocurrent flow pattern in all the stages would result in a 20% increase in the annual cost of capture compared to an optimisation run based on the countercurrent flow pattern. This is due to significantly higher power consumption in the cocurrent flow configuration that results in an optimum power consumption of 212 MW. A more energy efficient process system results when a countercurrent flow pattern is adopted as this consumes 171.1 MW, as illustrated in Figure 3.12. The cocurrent flow pattern results in a slightly lower membrane area than the other flow patterns. Khalilpour et al. (2012) reported that a longer fibre length resulted in less pure permeate for the countercurrent flow. As the membrane profile becomes longer, this increases the permeances of other components as their composition increase with a decrease in the target component and hence the other components increase in driving force. Hence, in this case, a lower membrane area is desirable for cocurrent and is compensated by higher power consumption to achieve the required recovery targets.

An optimisation run based on the cross flow pattern results in an annual cost that is 4% lower than the cocurrent flow pattern. This is due to the lower energy requirement of the cross flow pattern process. The countercurrent has an inbuilt difference in partial pressure, where the feed point on the retentate side corresponds to the permeate outlet. The CO_2 composition is highest at the initial membrane profile on the retentate side, the permeate at the same point is diluted and has a relative low CO_2 composition. The countercurrent flow pattern has been shown to achieve higher stage cuts and purer permeate streams (He et al., 2014; Lock et al., 2015; Makaruk and Harasek, 2009). Uppaluri et al. (2004) also found that the countercurrent configuration gave the lowest gas processing cost in their superstructure based optimisation of the recovery of H_2 from syngas (H_2+CO_2). The crossflow pattern also costed 4.29% less than

the cocurrent flow that is comparable to 4.43% realised in this case. The cost savings of the countercurrent flow was 6% in comparison to the cocurrent flow pattern, which is much less than the 20% of cost savings realised in this work. Merkel et al. (2010) also observed that the countercurrent flow pattern reduced the energy demand by 18% and enhanced the CO_2 recovery of a single stage membrane by 12% compared to the crossflow pattern. Thus the process has an inate source of driving force. Thus the counterflow pattern requires less energy to achieve the targets. A low permeate CO_2 partial pressure on the permeate side also increases the CO_2 permeance in FSC membrane.

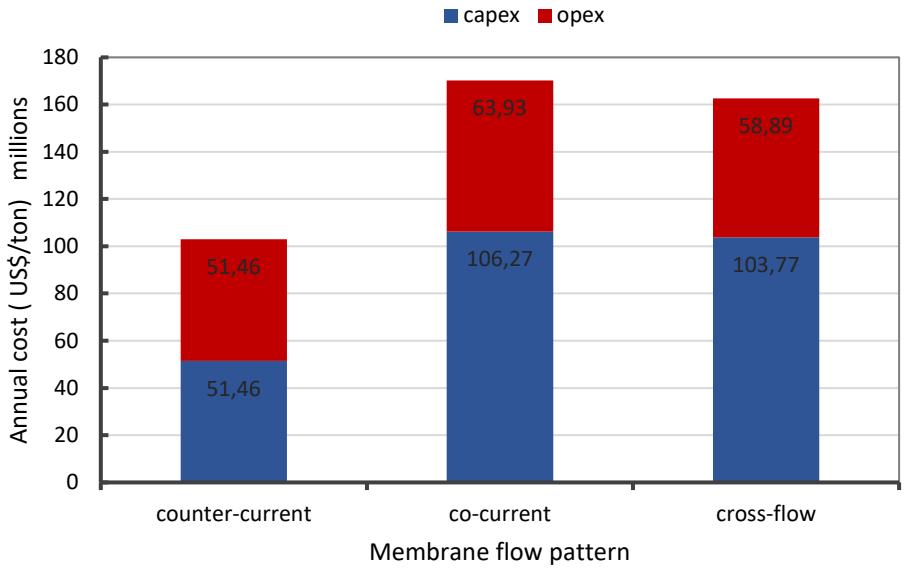

Figure 3.11. Figure showing the annual cost, CAPEX and OPEX of the three flow patterns

The total membrane area and net power consumption for the three stage process simulated in the optimisation runs is presented in Figure 3.12. Appendix B shows the CO_2 partial pressure profiles along the membranes. The differences in the results is due to the differences in the partial pressure of CO_2 on the retentate and permeate sides of the membrane for the different flow patterns. The gap between the retentate and permeate curves indicate the difference the CO_2 partial pressure which is an indication of the quatity of the driving force. It is observed that the countercurrent flow has a larger gap between the two curves. The gap between the two curves narrow earlier at about 40% of the cocurrent and cross flow patterns compared to > 60% for the countercurrent pattern. The retentate CO_2 partial pressure falls more rapidly for the

cocurrent and crosscurrent than the countercurrent flow which decreases at a lower rate. This makes up for a purer CO_2 permeate and higher stage cut as the driving force remains higher than in the other flow patterns (Khalilpour et al., 2012).

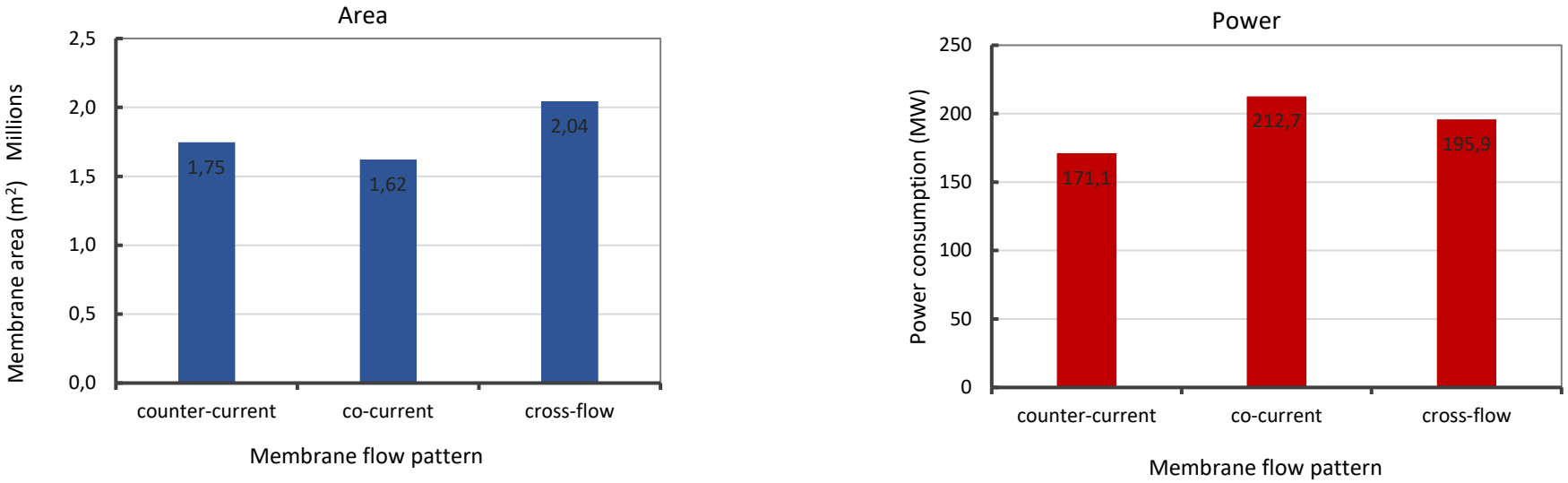

Figure 3.12.Showing optimum membrane area and optimum power consumption for the different flow patterns

3.5.4.2 Effect of fixed pressure ratios and variable pressure values

The effect of using uniform pressure and non-uniform operating pressure in the different stages was analysed to assess the impact of pressure on the process economics. Four scenarios were studied, and these are uniform retentate pressure operation (fpr), uniform permeate pressure (fpp), variable permeate pressure (vpp) and variable retentate pressure (vpr). An optimisation run that is set to operate at uniform permeate pressure and variable retentate pressure is therefore termed (fpp-vpr). The various combinations are simulated for two stage and three stage membrane processes.

Figure 3.13 shows the resulting annual cost requirement for each membrane stage. The results show that increasing the degrees of freedom by non-uniform pressure variable reduces the cost of capture for both two and three stage operations even for the FSC where a multicomponent flue gas is being processed for CO_2 capture. The cost of capture decreases by 6.7% and 13.1% for the two and three stage membrane process when both the retentate and permeate pressure is made non-uniform in the different stages compared to uniform pressure operation on the permeate and retentate sides. A non-uniform pressure ratio is essential for an efficient membrane process operation (Arias et al., 2016; Mores et al., 2019). The cost saving is greater for a three stage process as it has potential for more recycle streams. Recycling increases the CO_2 composition in the feed streams. The variable pressure operations allow the model to choose a lower pressure ratio in those stages that can have a driving force due to higher CO_2 composition. This makes the process more energy efficient. This is depicted in Figure 3.14, where the power consumption for the three stage process for the three scenarios with a non-uniform pressure ratio is almost equal. However, the total membrane area becomes smaller. This smaller membrane area results in the cost savings that are realised.

Having non-uniform pressure operation on either the retentate side or permeate sides also reduces the capture cost more significantly in the three stage process. Previous simulation studies have shown that vacuum operation would be more energy efficient than feed compression but would result in a higher membrane area as the generated driving force is likely to be low (Belaissaoui et al., 2012b; Ling et al., 2015; Zhao et al., 2008). This is consistent with the results presented in this study, where a non-uniform permeate pressure results in a lower

cost of capture than non-uniform retentate pressure. The lower energy requirement is traded off by the slightly higher membrane area observed.

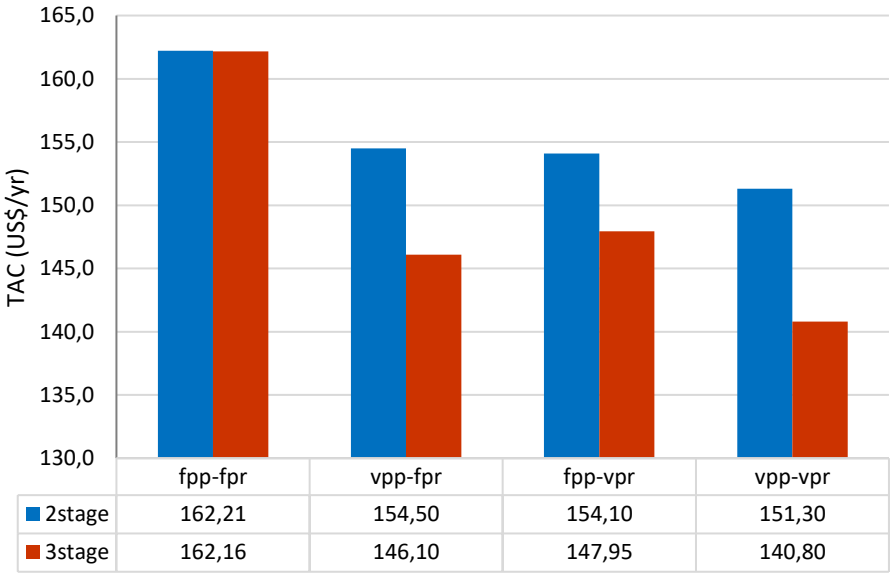

	fpp-fpr	vpp-fpr	fpp-vpr	vpp-vpr
2stage	162,21	154,50	154,10	151,30
3stage	162,16	146,10	147,95	140,80

Figure 3.13 Annual cost for uniform operation versus non-uniform operation.

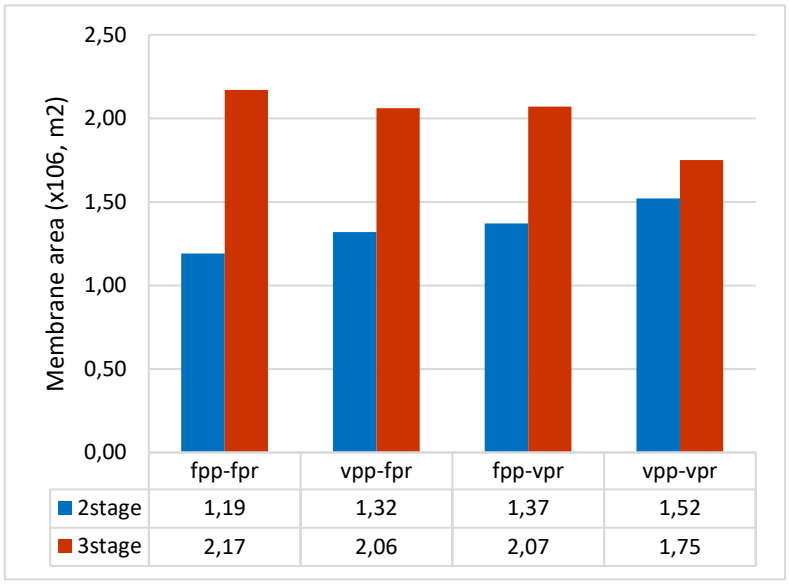

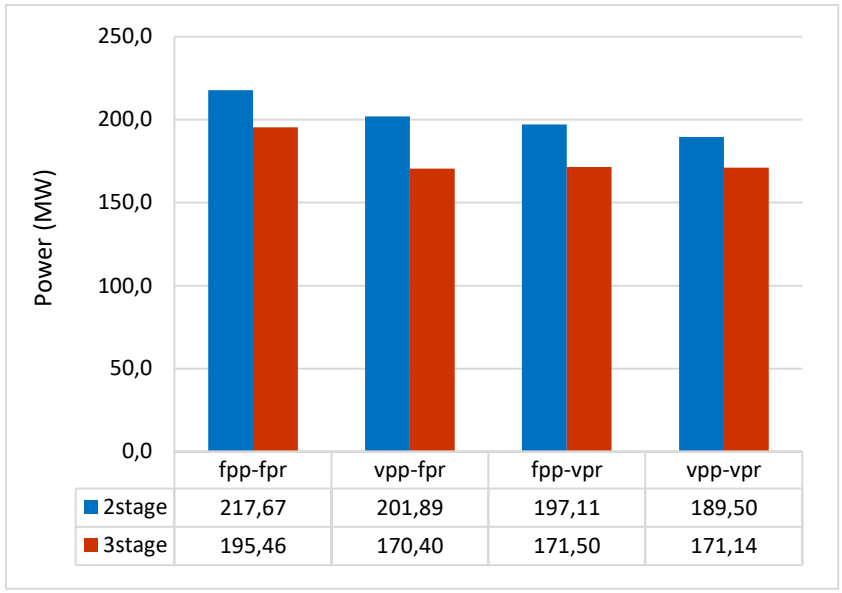

Figure 3.14.Membrane area (a) and power consumption (b) of two and three stage processes with uniform pressure values vs non-uniform pressure values

.

3.5.4.3 Effect of increased recovery and purity targets

The specific cost of a unit mass of CO_2 increases with increase in the recovery fraction and increase in product purity as shown in Figure 3.15. The results for optimisation of a two stage process to obtain a product stream of 95% purity is termed 2sp95 and likewise the results for a four stage process at purity target of 99% is named 4sp99.

The two stage process results in a higher cost of capture than the three and four stage membrane processes for all the set separation targets with the least recovery of 90%. Solution for 100% recovery could not be obtained for the two stage process and is thus assumed to be infeasible. The process system is limited in terms of membrane area as well as recycle streams which deter from achieving higher recovery and higher purity targets.

At a purity of 95% the difference in the cost between the three stage and four stage is negligible. Three membrane stages have been previously reported to be optimum for CO_2 capture from flue gas (Lee et al., 2018; Ramírez-Santos et al., 2018). Increasing the CO_2 recovery from 90% to 100% (zero emission) would increase the specific cost of capture by 23%. This is mainly attributed to the increase in power consumption which increases significantly. At 98% to 100% recovery, the increase in the cost is sharper as it increases by 12%.

Increasing the product purity from 95% to 99% at a recovery of 90% would increase the cost of capture by 17.8%. Increasing the product purity from 95% to 99% at 100% recovery would cost 9.7% more for the optimal solution which is a four stage process. A higher purity stream is desirable for CO_2 capture by membranes to compete with solvent absorption that produces 99% purity of the product stream. At a higher purity target, i.e. 99%, the optimum process involves four stages for CO_2 capture. The three stage process results in a suboptimal solution. As is shown in the chart the trend line for 3sp99 is above that of 4sp99. The 4sp99 utilises a larger membrane area and is more energy-efficient than the two and three stage processes.

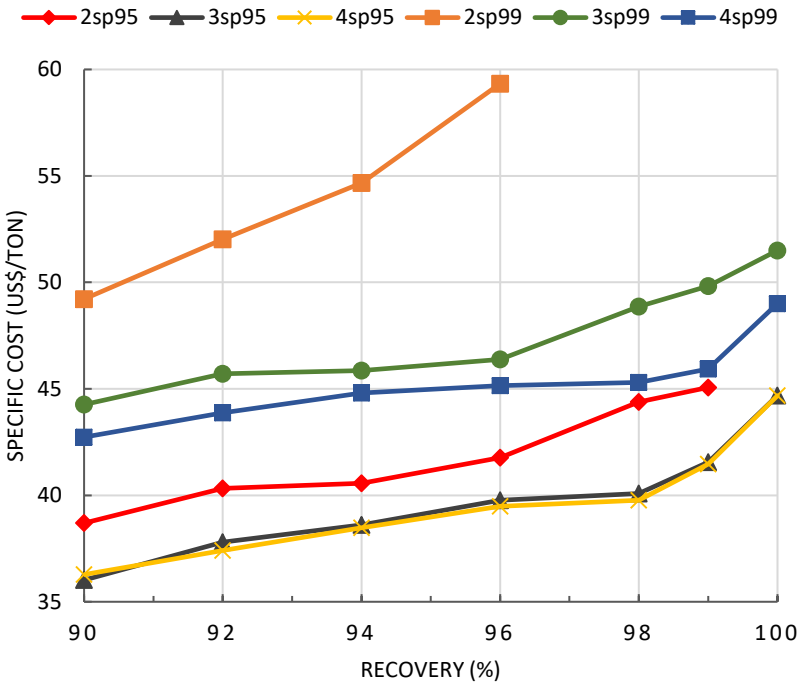

Figure 3.15. Variation of specific cost with increased recovery and purity

3.5.4.4 Effect of membrane cost

Figure 3.16 shows the net power consumption and membrane area required to achieve the separation targets as the cost of the membrane is increased. The membrane price is doubled from US$35 to US$70 and thereafter, the initial price is multiplied by an increased integer factor up to six times. When the price is initially doubled the total membrane area drops by 18 %. The model selects to increase power consumption and reduce the membrane area to reduce the capital cost.

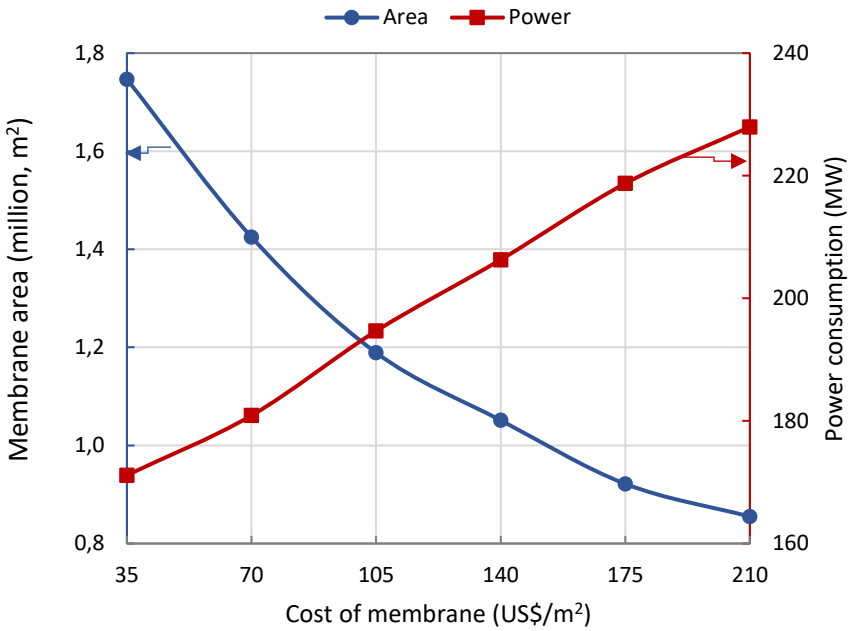

Figure 3.16. Effect of increasing the cost of membrane on the membrane area and power consumption

Figure 3.17 shows the capital costs generally dominates the total annual cost. The capital costs is influenced by the capital recovery charge and the cost model used. In this study, a high capital recovery charge factor (0.2) considered make capital costs dominant. The annual cost increases in accordance with the increase in both the capital cost and operational cost. Though the membrane area decreases, the capital cost continues to increase due to the increase in membrane price. The total annual cost of capture rises with an increase in the cost of the membrane. This expected result confirms the results of previous studies (He et al., 2015; Lee et al., 2018; Van Der Sluijs et al., 1992). Simulation studies showed a direct proportionality with the rate of increase in the cost of capture being a straight line (He et al., 2015; Van Der Sluijs et al., 1992).

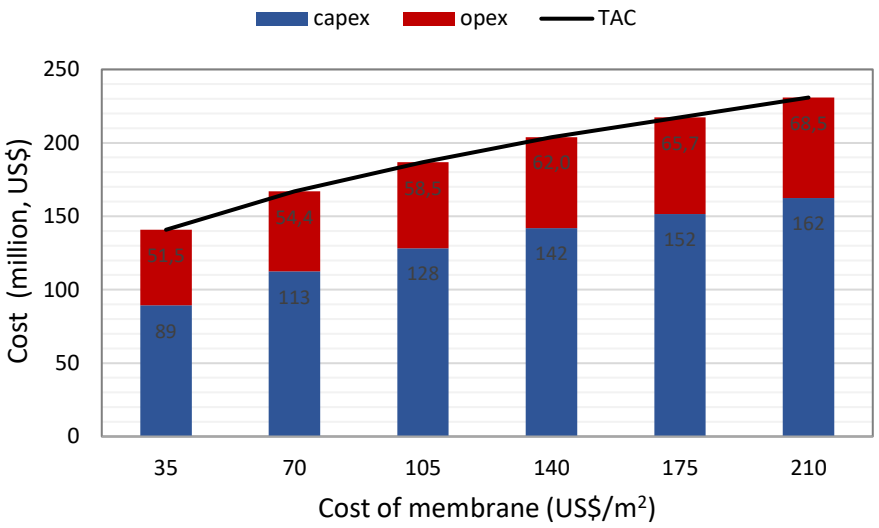

Figure 3.17. Effect of increasing the cost of membrane on the OPEX, CAPEX and TAC.

3.5.4.5 Effect of the increase in the cost of electricity

Figure 3.18 depict the effect of increasing the price of electricity by 20 US$/MW. As expected, the membrane area generally increases with an increase in electricity price as the system seeks to reduce the power consumption by employing a larger membrane area. The increase is sharper from 60 US$/MW to 80 US$/MW from where it slows down a bit. The power consumed decreases with the increase in the price of electricity but the rate slows down at prices greater than 60 US$/MW.

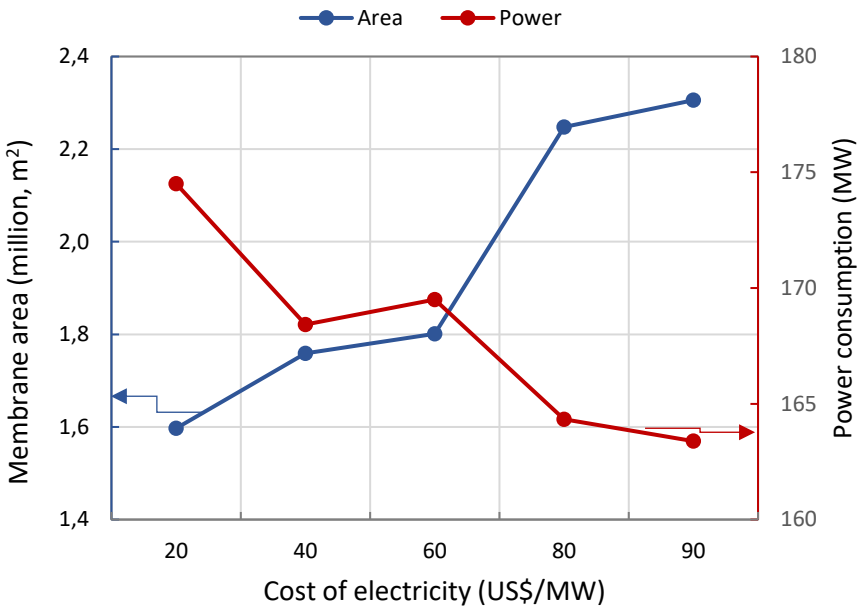

Figure 3.18. Effect of increasing the cost of electricity on the membrane area and power consumption.

Figure 3.19 shows that the annual cost follows an upward trend as a result of the increase in price of electricity. The rate of increase is higher for operational costs that are primarily electricity cost. A small increase is noted in the capital cost as a result of the increase in membrane area. When the price of electricity is doubled from 40 US$/MW to 80 US$/MW the operational cost increases by 95% and consequently causes the total annual cost to increase by 37%.

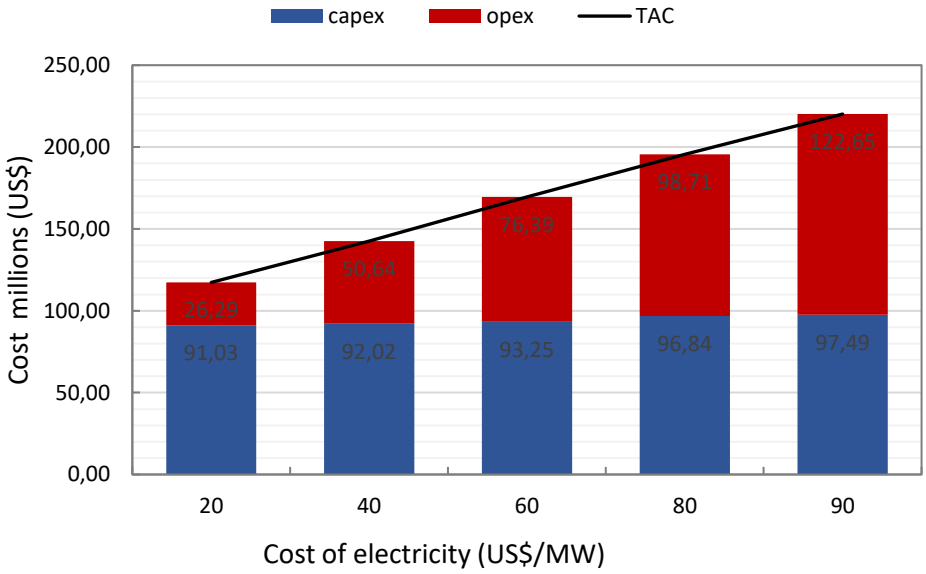

Figure 3.19. Effect of increasing the cost of electricity on OPEX, CAPEX and TAC.

3.5.4.6 Effect of water permeance value

It has been known that water is relatively highly permeable in polymeric FSC membranes (Deng and Hägg, 2010; Li et al., 2014). He et al. (2017) in the study of an FSC membrane on pilot scale, found out that the H_2O/CO_2 selectivity was 5. Feasibility studies on the FSC membranes have assumed a CO_2/H_2O selectivity of 1 or less for amine FSC membranes (Hussain and Hägg, 2010; He and Hägg, 2014) when a multicomponent gas is treated instead of the standard CO_2/N_2 binary gas. In a recent study, He et al. assumed water permeance that is double that of the CO_2 permeance (He et al., 2020).

In this study, the optimisation is carried out for a 3 stage membrane system with a recovery rate of 90% and product purity of 95% but each time with a different water permeance value. Figure 3.20 shows that when the water permeance is tripled or more, both the membrane area size required and the power consumption also increases. This leads to an increase in capital and operational cost and consequently, the annual cost as depicted in Figure 3.21. The rate of increase is higher for the operational cost (electricity bill) more than the increase in the membrane area. The system depends on the saturated flue gas to achieve the required humidity levels of the feed for optimal function of the FSC membrane. In the highly water permeable membrane, the water composition in the retentate recycle stream is very low. To meet the

humidity constraints of the feed in subsequent membrane stages, a higher pressure has to be utilised to achieve the minimum required relative humidity for the feed stream.

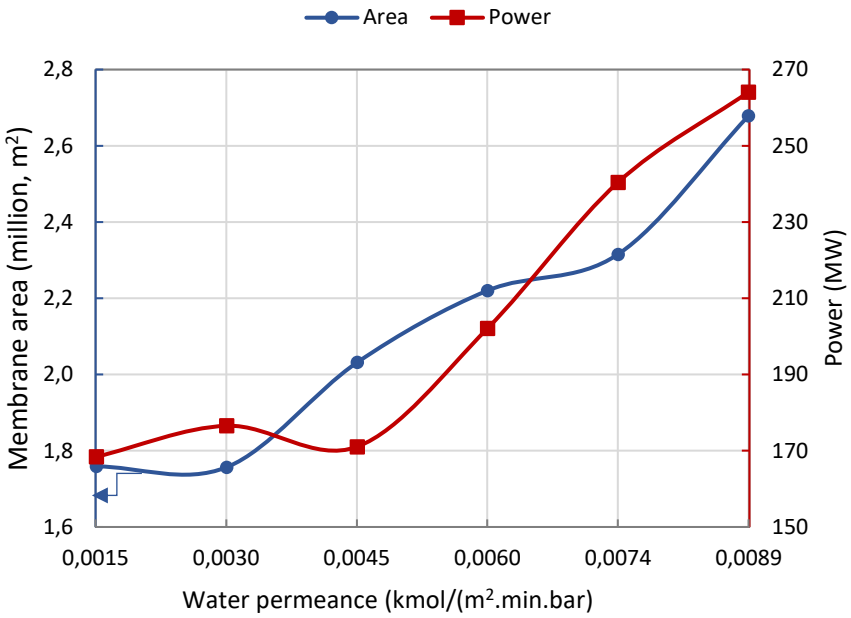

Figure 3.20. Effect of the membrane area and power consumption.

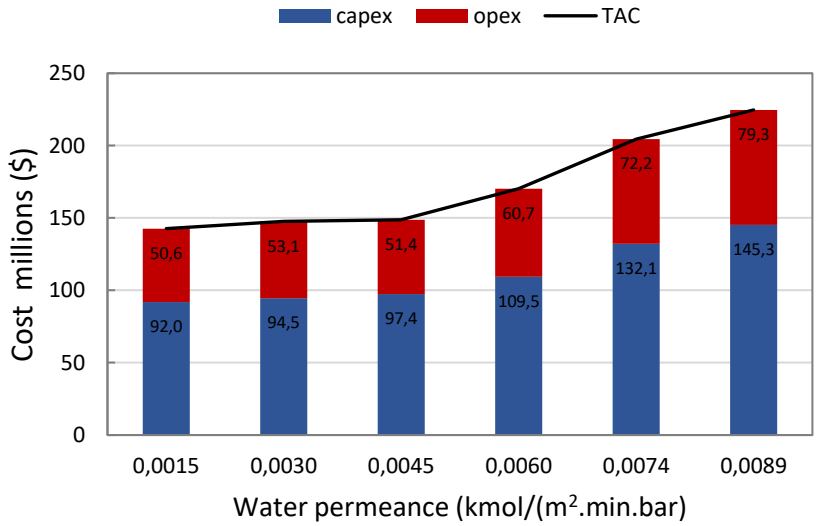

Figure 3.21. Effect of increased water permeance on OPEX, CAPEX and TAC.

3.6 Concluding remark

Optimisation of CO_2 capture from a coal-fired power plant using a fixed site carrier membrane has been carried out and reported in this article. It was shown that allowing non-uniform operating pressure in the different membrane stages increases the energy efficiency of the process by optimisation of the power consumption by the compressors and thereby reducing the operating cost. Therefore, it is beneficial to use an accurate FSC permeation model so that the operating pressure can be optimised. Increasing membrane stages and allowing recycle stream further reduces the membrane area and therefore results in cost reduction for the CO_2 capture process. The use of vacuum and water vapour as sweep on the permeate side was also investigated. The use of a sweep reduces the membrane area significantly, however, the energy consumption also increases due to the need to compress the higher permeate volumes from very low permeate operating pressure. The increase in driving force allows the membrane to operate at low feed pressure at which the CO_2 permeance is much higher than at higher feed pressure. Therefore, the membrane area required is significantly reduced and thus reduces the capital cost requirements of the process and the overall total annual cost. The energy consumed by the compressor that generates the initial sweep has not been taken into account, the energy maybe significant and may increase the cost of the scenerios with the sweep strategy.

An analysis of the FSC membrane based CO_2 capture has been carried out to study the impact of increasing product purity and recovery. At the conventional separation targets of recovery 90% and purity 95%, the three stage is optimal and the four stage processs does not bring further improvement in terms of annual cost and specific cost. At increased purity of 99%, the four stage is more economical and more energy efficient. Experimental work is carried out based on significantly low flowrates and usually the goal is to determine the CO_2 permeance and CO_2/ N_2 seperation. It is process design that can determine the possibility of 100% recovery. A review of literature showed that 100% recovery had not been analysed for CO_2 capture. Chapter 6 proposes a process design framework that can achieve 100% CO_2 recovery and hence zero CO_2 emission from coal fired power plant.

A high assumed water permeance will result in increased cost of capture if the water in the flue gas is the sole source of humidification for meeting the FSC feed humidity constraints. Having a non-uniform pressure ratio is essential to reduce the energy consumption of the membrane

process for CO_2 capture. When the cost of electricity doubles, the increase in the annual cost of capture can increase by 37%; meanwhile, doubling the cost of the membrane would result in only an 18.5% increase in annualised capture.

3.7 Nomenclature

Sets

N	{n|n membrane stage}
NP	{np|np alias of membrane stage}
I	{i|i component in a process stream} $i \in I = \{CO_2, N_2, H_2O, O_2\}$
K	{k|k compartments in membrane stage n}
RR	{rr|rr retentate recycle stream}
PR	{pr|pr permeate recycle stream}

Parameters

A^L	Lower bound of the membrane area size, m^2
A^U	Upper bound of the membrane area, m^2
C^{el}	Electricity cost, $/KW
C^{mem}	Cost of membrane, $/m^2$
C^{rpl}	Cost of replacing membrane modules, $/m^2$
CLB	Cost of labour
CP_i	Heat capacity, KJ/kmol.K
CR_T	Total carrier concentration, kmol/m^3
D_i	Diffusivity of component i in membrane, m^2/s
$D_{i,Am}$	Diffusivity of component and carrier complex in membrane, m^2/s
EY	Effective time the plant is online per year, s/year
HC_i	Henry's constant of component i, bar.m^3/kmol
K_{eq}	Equilibrium constant of the CO_2 and amine reaction m^3/kmol
l	Thickness of membrane, m
Mr_i	Relative molecular weight of component i, kg/kmol
P^{atm}	Atmospheric pressure (1 bar),bar

P^L Pressure lower bound, *bar*

P^U Pressure upper bound, *bar*

R_i^{ftg} Flowrate of component *i* in the flue gas stream, *kmol/s*

T^{atm} Atmospheric temperature (298 K), *K*

T^{ftg} Temperature of the flue gas stream as supplied to the capture plant, *K*

T^{mem} Operating temperature of the membrane, *K*

TMA Total membrane area, m^2

U Heat transfer coefficient, KW/m^2. *K*

γ Specific heat ratio

η Efficiency of compressor, vacuum, expander

Binary Variables

Z_n^{vac} Defines the existence of a vacuum pump in membrane stage n

Z_n^{sg} Sweep gas exist on the permeate side

Z_n^{rwf} Flue-permeate mixture condenser exists in membrane stage n

Z_n^{rwvc} Vacuum condenser is in use in membrane stage n

Z_n^{rwo} Vacuum condenser is in use in membrane stage n

Z_n^{cr} Compressor on retentate recycle stream in membrane stage n

Z_n^{xr} Expander on retentate recycle is in use in membrane stage n

Continuous variables

A_n^{mem} Membrane area of stage n, m^2

A_n^{clf} Heat transfer area of the feed compressor cooler in stage *n*, m^2

DP_i Desired purity of the CO_2 enriched stream

DR_i Desired recovery of CO_2,

g_n Flowrate of sweep gas in membrane *n* is a fraction *g* of the feed gas

lmt_n^{clf} Logarithm mean temperature of feed cooler in membrane stage *n*

$m_{n,steam}$ Amount of steam required to vaporise sweep gas in membrane stage *n*, *kg*

P_n^{pms} Pressure on the permeate side in membrane stage *n, bar*

P_n^{rt} Pressure on the retentate side in membrane stage *n, bar*

P_n^{ppw} Pressure of the product compressor in, *bar*

P^{sat} Saturation pressure at a particular temperature

Q_n^{cft} Duty of flue permeate compressor *(cft)* in membrane stage *n, KW*

Q_n^{csg} Power consumed by the compressor of permeate with sweep in stage *n , KW*

Q^{comp} Power consumed by product compressor, *KW*

Q^{pump} Power consumed by product compressor, *KW*

Q_n^{exr} Power recovered by expander of residue stream OA in membrane stage *n,K*

Q_n^{exs} Power generated by sweeping expander in membrane stage *n, KW*

Q_n^{ppw} Power generated by product first compressor, *KW*

Q^{icp} Power consumed by product inter-stage compressor, *KW*

Q_n^{clf} Heat removed by cooler placed after feed compressor in stage *n, KW*

Q_n^{vac} Power consumed by the vacuum pump in stage *n* of membrane, *KW*

$Q_{n,np}^{xr}$ Power recovered by expander of retentate recycle membrane stage *n, K*

$Q_{n,np}^{cr}$ Power consumed by compressor of retentate recycle membrane stage *n ,K*

$R_{i,n}^{f}$ Flowrate of *i* in flue gas supplied to membrane stage *n, kmol/s*

R_i^{ft} Flowrate of component *i* exiting the flue gas condenser, *kmol/s*

$R_{i,n}^{fs}$ Flowrate of component *i* in the feed supplied to membrane stage *n, kmol/s*

$R_{i,n}^{ms}$ Flowrate of component *i* exiting flue permeate mixer in membrane stage *n, kmol/s*

$R_{i,n}^{fms}$ Flowrate of component *i* exiting flue-permeate condenser, stage *n, kmol/s*

R_i^{op} Flowrate of component *i* from product mixer *kmol/s*

R_i^{oa} Flowrate of component *i* from residue mixer, *kmol/s*

R^{opt} Total flowrate of the product stream, *kmol/s*

R_i^{opw} Flowrate of component *i* in the stream exiting the product mixer, *kmol/s*

$R_{i,n,k}^{pms}$ Flowrate *i* from compartment k on the membrane permeate side of stage n, *kmol/s*

$R_{i,n}^{pm}$ Flowrate of component *i* in permeate stream from condenser to splitter, *kmol/s*

$R_{i,n,pr}^{pmr}$ Flowrate of component *i* in recycled permeate stream *pr* from stage *n kmol/s*

$R_{i,n}^{pos}$ Flowrate of component *i* in the product stream from membrane stage *n, kmol/s*

$R_{i,n}^{rto}$ Flowrate of component *i* in residue stream in membrane stage *n kmol/s*

$R_{i,n}^{rt}$ Flowrate of component *i in* retentate in membrane stage *n kmol/s*

$R_{i,n,k}^{rt}$ Flowrate component *i* from compartment *k* on the retentate side of stage *n, kmol/s*

$R_{i,n,rr}^{rtr}$ Flowrate of component *i in* retentate recycle stream *rr* from stage *n, kmol/s*

$R_{i,n}^{sg}$ Flowrate of the sweep gas supplied to membrane stage *n, kmol/s*

RH_n Relative humidity in membrane stage *n*

R_i^{wc} Flowrate of component *i* condensed in the flue gas condenser, *kmol/s*

$R_{i,n}^{wf}$ Flowrate of component *i* condensed in the feed gas condenser, *kmol/s*

$R_{i,n}^{wo}$ Flowrate of *i* condensed in the permeate condenser in membrane stage *n, kmol/s*

R_i^{wcp} Flowrate of water condensed in the product condenser, *kmol/s*

TAC Total annual cost, $/year

TLC Total levelised cost, $/ton

TNQ Total net power consumed by the capture process, *KW*

T_n^{cft} Temperature of gas at outlet of flue permeate compressor from membrane *n, K*

T_n^{csg} Temperature of gas at outlet of sweep compressor from membrane *n, K*

T^{hw} Temperature of cooling water as it leaves cooler, *K*

T^{cw} Temperature of cooling water as supplied to the cooler, *K*

x_n^f Split fraction of flue gas flowing to membrane stage *n,*

x_n^{pos} Split fraction for stream towards product from permeate splitter in stage *n*

$x_{n,pr}^{pmr}$ Split fraction of the recycle streams from permeate splitter in membrane stage *n*

$x_{n,rr}^{rtr}$	Split fraction of recycle streams from retentate splitter in membrane stage *n*
x_{n}^{rto}	Split fraction of residue stream towards residue mixer *n*
$y_{i,n,k}^{pms}$	Mole fraction of component *i* at point k on the permeate side of membrane stage *n*
$y_{i,n,k}^{rt}$	Mole fraction of component *i at point k* on the retentate side of membrane *n*
$y_{i,n}^{fms}$	Mole fraction of component *i* in stream that exits the flue-permeate cooler of *n*
$y_{i,n}^{fs}$	Mole fraction of component *i* in feed stream to the membrane *n*
$y_{i,n}^{sg}$	Mole fraction of component *i* at point k on the is sweep gas in membrane stage *n*
φ_i	Permeance of component *i, kmol/m^2.bar.s*

Superscript

atm	Atmosphere
clf	Feed cooler
cft	Compressor feed
cr	retentate recycle compressor
cw	Cooling water
csg	Compressor sweep gas
comp	compressor
el	Electricity
exs	Expander sweep gas
exr	Expander on residue
f	Feed from flue gas splitter to membrane stage
ft	Total feed after flue gas condenser
fs	Feed supply to membrane
ftg	Total flue gas
icp	product inter-stage compressor
mem	Membrane
ms	stream exiting flue-permeate mixer
oa	Residue output to atmosphere
op	Output product

opw	Product output with water before product condenser
pm	Permeate after condenser
pms	Permeate exiting membrane
pmr	Permeate recycle stream
pos	Product output stream from splitter
ppw	product compressor for removing and adjusting water from product stream
pump	pump
rpl	Replacement
rto	Residue to atmosphere
rt	Retentate
rtr	Retentate recycle
sg	Sweep gas
sat	Saturation
L	Lower bound
U	Upper bound
wat	Water
wc	Water from flue condenser
wf	water from flue-permeate condenser
wo	Water from permeate condenser
wp	Water from product condenser
nc	non condensable gases

Chapter 4 - Techno-economic evaluation of membrane-based carbon capture and storage from a coal power plant in South Africa

4.1 Introduction

The Electricity Power Commission (ESKOM) produces the bulk of electricity in South Africa (ESKOM, 2013). Medupi and Kusile power stations in Limpopo and Mpumalanga respectively represent the state of the art technology in terms of coal power plants in South Africa. Medupi has been designed and constructed to be 'capture ready'(Maccoll, 2010). 95% of electricity in South Africa comes from coal (DOE SA, 2018; Surridge and Cloete, 2009). The government of South Africa has reported that coal use for power generation remains in the foreseeable future. However, it is committed to reducing carbon emissions by employing both renewable energy sources and mitigation technologies (IRP, 2019). It is planned that coal use for power generation will be reduced down to 30% by 2030 and further down to 20% by 2050 (DOE SA, 2019).

Surridge and Cloete, (2009) reported that 61% of the 400 mL/year of CO_2 produced in SA can be captured from large points of emission such as power plants, cement manufacturer and coal to liquid production plants (Surridge and Cloete, 2009). The South Africa Centre for Carbon Capture (SACCS) under the Department of Energy (DOE) is responsible for technical assessment, implementing and supporting CO_2 capture and related technologies. However, the SACCS was recently moved to 'The Council for Geoscience' in a streamlining exercise by the government of South Africa. The SACCS roadmap however has not changed and includes a geological survey to determine the storage capacity as a first step (SANEDI, 2019). The next step would be the test injection and then followed by the setup and operating of a CO_2 capture and storage demonstration plant. Thereafter, large-scale deployment of CCS in South Africa is envisioned to be in effect by 2025. Two major geological sites are potentials for CO_2 storage. The Kwa Zulu Natal offshore basin and the orange basin in the southwestern of South Africa these have a capacity to store CO_2 for an excess of 100 years. (Beck et al., 2013; Viljoen et al., 2010)

South Africa uses coal of higher ash content and lower calorific value for local electricity generation and exports the higher grade bituminous coal (Maccoll, 2010). Medupi units are

supercritical plants with a capacity to produce 794 MW. The plant is the 4th largest air-cooled power plant in the world due to the water scarcity in South Africa (ESKOM, 2013). The South African context is unique in terms of CCS cost as the conditions differ from the other regions such as the USA, China and Europe. Cheaper labour and cheaper coal could lower the cost of power generation in SA (Maccoll, 2010). However, coal with high ash content, low calorific value and higher ambient temperatures could result in a higher cost of producing electricity. Furthermore, air cooling reduces the efficiency of a coal power plant by about 1- 5% compared to water-cooled power plants and CO_2 capture will further reduce this efficiency (Zhai and Rubin, 2010).

Research carried out by academic institutions in South Africa has been mainly on finding suitable storage sites, a few have been on the capture of CO_2 as applied to the South Africa context (Chabangu et al., 2014; EPRI, 2015; Tot et al., 2011; Viebahn et al., 2015; Viljoen et al., 2010). Tot et al, (2011) carried out a techno-economic assessment for the deployment of Carbon capture and storage in Southern Africa with a particular focus on South Africa, Namibia, Botswana and Mozambique. All these four countries have potential storage sites. The study sought to determine the effect of introducing a carbon tax. For three-carbon prices, US$25/ton, US$50/ton and US$100/ton, it was observed that over a period of time, CO_2 emissions would drop as industry moved to more greener energies such as wind and solar. A survey of the potential storage sites was carried out. The feasibility study showed that for the long term South Africa will have to utilise the storage sites in Mozambique. The results of the modelling study showed that power plant generation with CCS would make economic sense if the Carbon tax is set at US$ 100/ton. Below that, nuclear energy is more competitive in terms of cost. Enhanced coal bed methane and enhanced oil recovery offered economic benefits.

A techno-economic study was carried out by the Parsons Brinckerhoff as engaged by the World Bank for the possible deployment of CO_2 capture in South Africa for the long term period 2030 to 2050. (Parsons Brinckerhoff and Group, 2013). The techno study was all-inclusive of all the CO_2 producing industries in South Africa, ranging from coal power plants, cement manufacturing plants, steel making, refineries, synthetic fuel production and other smaller emitters such as paper making companies. The comprehensive study reviewed the sources of emissions in South Africa. A thorough review of the possible storage sites was also carried out and a pipeline network was proposed which involved a national trunk line with branch lines

attached to it carrying CO_2 to the storage sites. Emitters would then have smaller pipelines connected to the main trunk line. Though the Zululand basin is closer to the areas where the largest emitters which are coal power plants are located, it offers limited storage capacity. This would necessitate transportation of the CO_2 to the orange basin which is the biggest storage site but is located further. This would raise the cost of transporting the CO_2 captured. Two trunk lines were suggested, one which would transport to the Zululand and the other to the Orange basin. The results from the modelling studies showed that South Africa would need a total expenditure of ZAR 3.2 trillion to capture CO_2 from all the CO_2 point emissions with capturable CO_2. Power plants showed the highest levelized cost of CO_2 capture followed by cement making, steel, paper and refinery ranked the lowest cost of CO_2 capture. The findings indicated that CO_2 capture from power plants would increase the cost of producing electricity by 500 ZAR/Kwh. Much of this cost is attributed to the alternative greener power generation. This method makes up for the power loss due to the CO_2 capture process.

The few techno-economic studies on CO_2 capture in South Africa in the public domain have been based on chemical absorption (EPRI, 2015; Parsons Brinckerhoff and Group, 2013; Tot et al., 2011). None as far as to our knowledge has explored the feasibility of CO_2 capture based on other technologies such as membranes. CO_2 capture by use of membranes is cheaper and more environmentally friendly when compared to chemical absorption (He and Hägg, 2014; Zhai and Rubin, 2013). Furthermore, CO_2 capture by absorption would require additional water (20-80%) which may not be available since SA is an arid country (Magneschi et al., 2017; Tu et al., 2019; Zhai and Rubin, 2011). CO_2 capture by chemical absorption consumes more water than other technologies such as membrane and absorption methods. In the chemical absorption method, a significant quantity of water is consumed as make-up water to the absorber to keep the solvent concentration constant (Magneschi et al., 2017). In this work, a techno-economic evaluation of CO_2 capture from a coal power plant in South Africa by use of membranes is carried out. Based on the specifications that could be found in the open literature, the asibilityof retrofitting a membrane capture system to a certain power plant in South Africa is investigated.

4.2 Method

The flue gas characteristics together with the total capital requirement and operating and maintenance costs (O&M) are determined, these are then made parameters for the membrane-

based CO_2 capture and storage system model. A Mixed Integer Non-Linear Program is formulated to optimise the membrane-based CO_2 capture, transport and storage system. It is implemented in GAMS and solved by BARON and ANTIGONE. The objective was to minimise the levelized cost of electricity (COE). The calculation of the COE was based on constant dollar with no escalation cost and inflation neglected which makes it equal to the cost of electricity.

4.2.1 Coal power plant modelling

Figure 4.1 illustrates the steps in the methodology. It also illustrates the process units for the power plant. The coal-fired power plant without carbon capture and storage is modelled by the software International Environmental Control Model (IECM) which has cost models related to engineering models embedded within. The IECM has been used extensively for modelling and evaluation of the feasibility of CCS for power plants around the world (Hu and Zhai, 2017; Rao and Kumar, 2014; Singh and Rao, 2016; Ye et al., 2019; Zhai and Rubin, 2013). The IECM includes sub-modules representing each process unit. These units are; base plants, which involves the boiler, the cooling system, fly ash control, de NOx control unit and the flue gas desulphurisation unit (FGD). Each unit is modelled and the material balances are given and the capital requirement and operating and maintenance costs (O&M) associated with each unit are given depending on the set parameter values. The costs are evaluated based on 2017 constant dollars. Medupi power station is considered in this study. It operates a supercritical boiler-based coal pulverised power plant. Medupi does not operate an FGD unit but may do so in future. It is assumed in this study that CCS will be implemented after the implementation of the FGD unit.

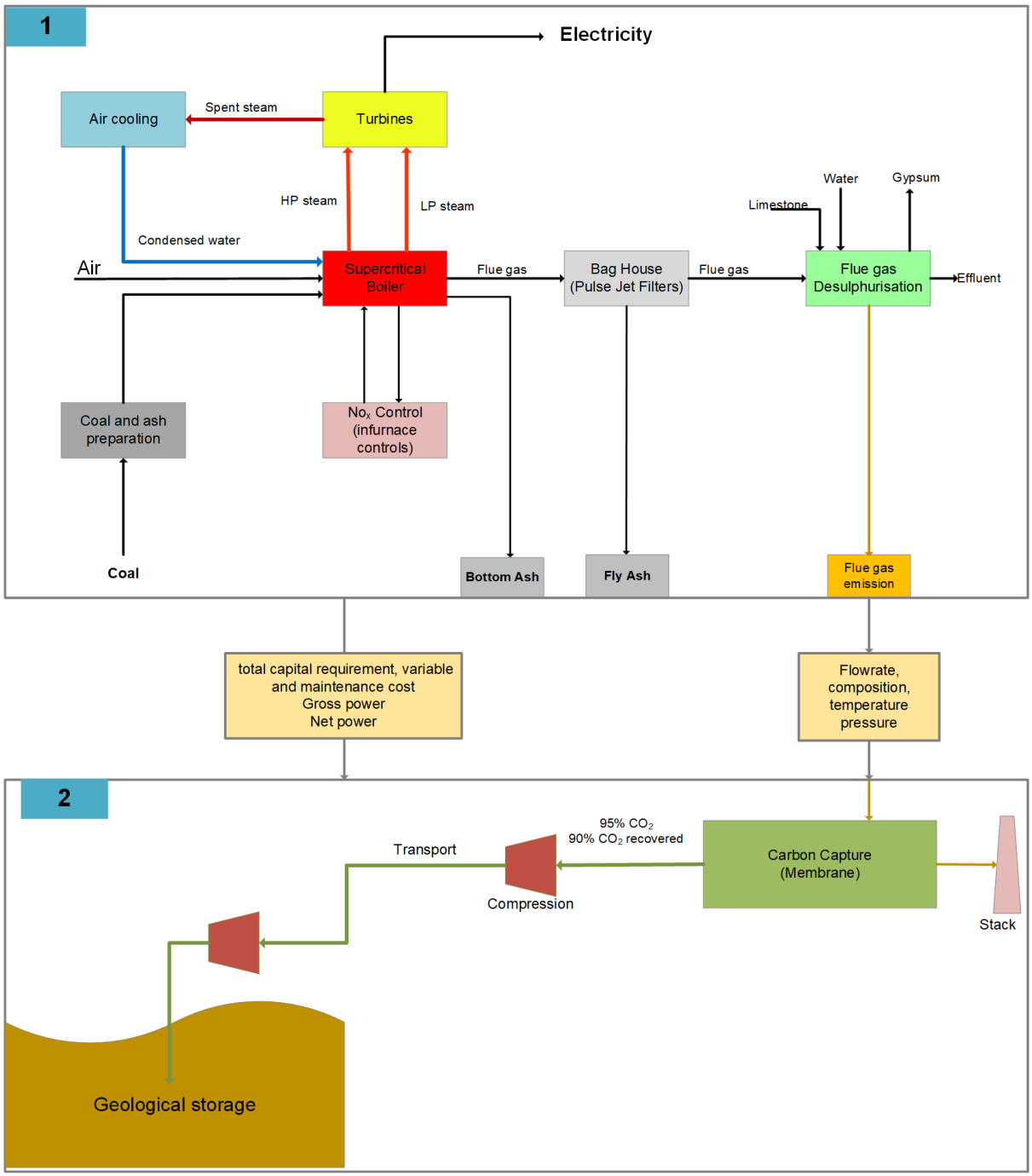

Figure 4.1.Methodology for assessing membrane based CCS (Riboldi et al., 2014)

Table 4.1 shows the parameters specific for Medupi power plant in South Africa such as ambient temperature and humidity, type of cooling system and the discount rate.

Table 4.2 gives the coal composition and the ash properties for Medupi power plant (EPRI, 2015).

Table 4.1: Power plant and cost specifications

Parameter	Assumption	Reference
Plant type	Pulverised coal	(ESKOM, 2013)
Type of coal	Bituminous	(ESKOM, 2013)
Boiler	Supercritical	(ESKOM, 2013)
Capacity	804MW	(EPRI, 2015)
Air temperature °C	32.2	(EPRI, 2015)
Annual relative humidity %	60	(EPRI, 2015)
NO_x control	None	(ESKOM, 2013)
Fly Ash control	Pulse-jet bags	(ESKOM, 2013)
SO_2 control	Wet FGD	(ESKOM, 2013)
Cooling system	Air cooling	(ESKOM, 2013)
CCS system	FSC membrane	
Capacity factor, %	85	(EPRI, 2015)
Construction time, years	4	(EPRI, 2015)
Cost base	Constant US$, 2017	
Discount rate,%	8%	(EPRI, 2015; Tot et al., 2011)
Fixed charge factor	0.105	
Coal Price, US$/ton	24.9	(DOE SA, 2018)
US$/MJ- HHV	1712	(DOE SA, 2018)
CCS recovery efficiency	90	(Zhang et al., 2014)
Electricity cost, US$/MWh	24.09	(DOE SA, 2018)
South Africa carbon tax, US$/ton	7.94	(SARS, 2019)
Cost of transport, US$/(ton.km)	1	(Viebahn et al., 2015)
Distance to storage site, km	794	(Google maps)

Cost of storage, US$/ton	12	(Viebahn et al., 2015)
Plant Life, years	45	(ESKOM, 2013)

Table 4.2: Coal composition

Coal	**Composition,%**	**Ash**	**Composition,%**
Carbon	46.92	SiO_2	58.00
Hydrogen	2.25	Al_2O_3	22.00
Oxygen	7.79	Fe_2O_3	3.80
Chlorine	0.0	CaO	1.80
Sulphur	0.83	MgO	1.40
Nitrogen	1.05	Na_2O	0.45
Ash	31.16	K_2O	0.79
Moisture	10.0	TiO2	1.80
Total	100	P_2O_5	0.40
		SO_3	5.20
		Other	4.36
HHV(kJ/Kg)	17850	Total	100

The default capital-related costs computed are based on a plant in the USA and the equivalent cost for a SA power plant is determined by location correction factors for the equipment, machinery, labour costs and labour productivity. The correction factors used are listed in

Table 4.3 (EPRI, 2015). There is an option to input direct cost values of materials, if these are not specified, then default values multiplied by the correction factors apply. The cost values specified were first converted to 2017 based on the CEIPC (Chemengonline, 2019). Prices in South Africa Rand (ZAR) were converted using the year exchange rate. The coal price is obtained from reports gazetted by the government, prices of chemicals are collected from websites of various suppliers. The labour price is determined by the correction factor. The number of jobs needed per plant is assumed to be similar to that in the US, as given by the

IECM default values. A three-hour shift per day is assumed, which translate to 8 hours per shift.

Table 4.3: Correction factors applied to USA cost values (EPRI, 2015)

Sector	Factor
Equipment	1
Materials	1
Labour	0.56
Labour productivity	2.3

Table 4.4 specifies the environmental constraints imposed by the government (DEA SA, 2010). This work is modelled with the assumption that the power plant achieves these targets by installing an FGD before installing the CCS system. The emission limits are specified in the IECM model.

Table 4.4: South Africa emission restrictions (DEA SA, 2010).

Parameter	Value
Particulates, mg/Nm^3	50
SO_3, mg/Nm^3	500
NO_x, mg/Nm^3	750

The LCOE is determined by dividing the total annual cost by the net energy *(MW_{net})* in that year. The total capital-related charge (TCR) is also determined, which consists of the purchase price, insurance, contingency fees and installation costs. The TCR is annualised by the fixed charge factor *(fcf)* which is a function of the interest rate. The total operational and maintenance *(OM) costs* is a sum of fixed costs such and variable cost per year. The variable cost for the base plant consists of the cost of coal used to produce electricity and other consumables such as chemicals. The levelised cost of electricity is computed as shown;

$$LCOE_{wocc} = \left(\frac{(fcf.TCR) + (OM)}{(cf \cdot 365.52 \cdot 24)(MW_{net})} \right) \quad (4.1)$$

4.2.2 Membrane based CO_2 capture system model description

The results from the first stage indicate that the flue gas that exits the FGD unit is saturated with water. The flue gas that exits the FGD unit is saturated with water at 48 °C as is fed to the CO_2 capture process plant at ambient pressure (0.81 bar). The model presented in Chapter 3 for Scenario 3 is also applied in this section. However the model is extended to include transport and storage cost and the objective is to determine the levelised cost of electricity. The superstructure for automatic process synthesis by a membrane includes numerous possible process flow routes as illustrated in Figure 4.2. The flue gas is cooled to 35 °C and some water is allowed to condense and be removed by a condenser. The flue gas is then split and sent to the membrane stages where it is combined with retentate and permeate recycle and reuse streams. This stream is then compressed to at least 1.0 bar which is the set minimum membrane operating pressure. The temperature of the gas stream increases and needs to be cooled to the membrane operating temperature (35 °C). More water can be condensed out at that elevated pressure to further adjust the water content and consequently the relative humidity of the stream to be fed to the retentate side of the membrane. Components then permeate through the membrane where a vacuum enables sub-ambient pressure operation. The operating pressure range is 0.2 to 0.81 bar. The permeate can be split into the product stream or recycle and reuse streams. The retentate stream is at high pressure as it exits the membrane hence some power is recovered by a turbine expander. The retentate is then split and a portion of it can be sent to the stack for emission and some can be recycled. The product stream is further pumped and cooled to allow condensation and removal of water through condensation. This allows the product stream to easily reach the target purity. The product stream is then pumped to 150 bar and transported by pipeline to the storage facility. The lower and upper bounds of the membrane area per stage are set at 1000 m^2 and 1.5 million m^2, respectively which is an acceptable range based on previous studies (Lee et al., 2018; Mores et al., 2019).

.

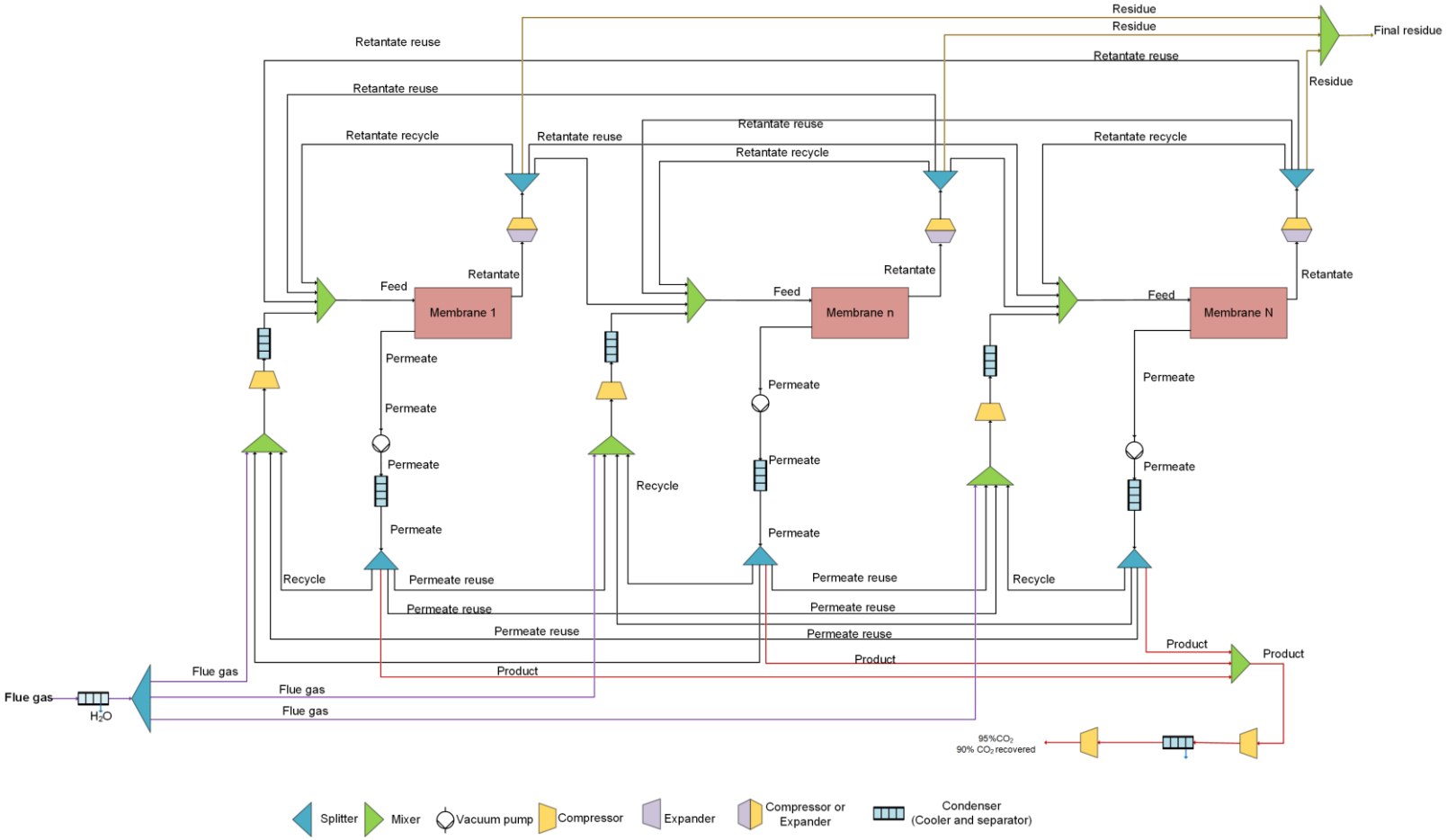

Figure 4.2. Superstructure for the membrane flue gas separation process

CO_2 permeation through the membrane is facilitated by amino carriers fixed on the polymer polyvinyl structure. The permeation model for CO_2 transport through the fixed site carrier membrane transport is described elsewhere (Zhang et al., 2013). CO_2 permeance is a sum of the permeance by the solution diffusion mechanism and by the facilitation reaction between the CO_2 and the amines group within the polymer structure. It is assumed that pressure drop is negligible both on the permeate and retentate sides and that the permeation of components is independent of other components and pressure except CO_2 (Chiwaye et al., 2021; Micari et al., 2021; Ren et al., 2020).

In the model the retentate and permeate pressures are variables that are non-uniform. The overall balance around the membrane shows that the flowrate of a component fed to the membrane is equal to the retentate and permeate that leaves the membrane module. The net power consumption (*TNQ*, MW) of the membrane system is equal to the total consumption of the compressors and vacuum pumps but is less than that recovered by the expanders. Material balances are carried out around the mixers and splitters and around the cooler condensers where water is removed. The mole fraction that remains in the gas being processed is determined from the model presented previously. Condensation commences when the partial pressure of the water vapour in the gas stream equals the saturation vapour pressure at the operating temperature. (Crabtree et al., 1998; Dunn and El-Halwagi, 1994; El-Halwagi et al., 1995). Compressor, vacuum and Expander models commonly used for membrane-based CC studies were used (Bounaceur et al., 2006; Zhai and Rubin, 2013).

4.2.2.1 Objective function

The Equation (4.2) shows that the objective of the optimisation is to minimise the levelised cost of electricity ($LCOE_{ccs}$) of the plant with CCS. In the Equation (4.2), TNQccs refers to the net power consumed by the CCS process.

$$min[LCOE_{ccs}] = \left[\left(\frac{fcf + (TCR + tcr_{ccs}) + (OM + OM_{ccs})}{(cf \cdot 365.52 \cdot 24)(MW_{net} - TNQ_{ccs})} \right) \right] \tag{4.2}$$

The membrane-based CCS process optimisation model was implemented in the General Algebraic Modelling Systems (GAMS) and solved by the solvers BARON and ANTIGONE

(Misener and Floudas, 2014; Puranik and Sahinidis, 2017). Both solvers are based on the branch and bound procedure to solve MINLPs such as developed in this work. BARON converts the MINLP into a relaxed linear form by adding auxiliary variables such that the reformulated problem consists of nonconvex terms. Hence it uses linear programs for bounding in the branch instead of the conventional non-linear programs that other solvers based on the branch and bound algorithm use (GAMS Development Corp., 2014). Meanwhile, ANTIGONE makes use of mixed integer programs for bounding in the branch and bound procedure (Misener and Floudas, 2014). BARON is useful in that it is capable of finding solutions faster and does not need a starting solution to work with. However, it can take long computational periods to terminate. In this solution strategy, BARON generates a solution which is used by ANTIGONE as a starting point.

4.2.2.2 Economic evaluation

Table 4.5 gives the parameter values used for evaluating the cost associated with the membrane gas separation process.

Table 4.5. Membrane Cost parameters

Parameter	**Value**
Compressor, vacuum, expander efficiency, %	85
Inter-stage compression and pump, %	80
Adiabatic compression coefficient,	1.4
Capital recovery factor, yr^{-1}	0.105
Membrane price, US$/$m^2$	37
Reference frame cost, US$/KW	2.3
Compression unit cost, US$/KW	850
Inter-stage compression and pump cost, US$/KW	1350
Expander unit cost, US$/KW	630
Equipment cost factor for housing,	1.80
Electricity cost, US$/KWh	0.024

Process facilities capital cost, %	37
Maintenance cost of membrane	1%TCC^{mem}
Maintenance cost of compressors	3.6% of CC^{unit}
Membrane lifetime, yr	5
Project lifetime, yr	25
Operating time, h/yr	7451.1

The cost of CO_2 avoided is thereafter computed from the COE obtained for the plant with CCS and the plant without CCS. The specific cost of capture (US$/ton) is reported mainly for CO_2 capture study and it is the cost involved with the separation of CO_2 from flue gas and does not include CO_2 transport nor storage.

$$C_{capture} = \frac{Total\ cost\ of\ capture\ (US\$/yr)}{Total\ CO_2\ captured\ (ton/yr)} \tag{4.3}$$

4.3 Results and discussion

The assumed operation capacity factor per year of 85% equals 7451.1 hours of operation per year. Table 4.6 shows the power output of the plant with the coal used. The plant was modelled with a full load capacity of 804 MW of electricity. It shows that for a pulverised coal plant (PC) without FGD, the auxiliary load is 60.2 MW, and 743.8 MW of electricity can be delivered to the grid. The overall efficiency based on HHV is 37.33%. The efficiency of supercritical plants is about 40%. The plant considered in this study loses a further 3% of efficiency due to air cooling, which is more energy-intensive (Zhai and Rubin, 2010). The introduction of an FGD to the plant (PC+FGD) will cause a further loss of 16.56 MW and reduce the electricity output to 727.3 MW which is equal to an efficiency of 36.5%. The output efficiencies are relatively close to that reported before for similar coal properties and a full load capacity of 804 MW for Medupi power unit. The efficiency reported was 37.1% and 36.7% for the PC and for the PC+FGD, respectively (EPRI, 2015).

Table 4.6 Power Consumption of different sub-modules of the power plant

Parameter	PC	PC+FDG
Gross Electrical Output, MW	804	804
Base Plant Use, MW	34.59	34.59
In furnace NOx control, MW	0.0	0.0
Fabric Filter, MW	0.59	0.59
Air cooled condenser, MW	24.98	24.98
Wet FGD, MW	-	16.56
Total Auxiliary Load, MW	60.16	76.72
Net Output, MW	743.84	727.3
Efficiency, % HHV	37.33	36.5

Table 4.7 shows that 30.9 kmol/s of flue gas leaves the baghouse and is emitted into the atmosphere. The introduction of an FGD would increase the flue gas to 34.0 kmol/s mainly due to a gain of water vapour that occurs in the SO_2 scrubber during desulphurisation. Table 4.*7* shows the composition of the main components in the flue gas produced that exits the FGD unit and is sent to the membrane-based CO_2 capture process plant. It is assumed that the CCS will be retrofitted only after the FGD unit has been added to the plant. The Flue gas flowrate (34kmol/s) is higher compared to other supercritical plants producing similar gross electrical output (CESAR, 2011; He and Hägg, 2014). The low calorific value of the coal used dictates a higher feed amount to produce the required capacity of the plant of 804 MW. The CO_2 mole fraction is 12.9% and the water composition is 14.4% which is within the reported range for coal power plants flue gas (Sreenivasulu et al., 2015). These compositions and the cost parameters presented in Table 4.7 are set as parameters in the superstructure based optimisation of the CCS process. The objective is to minimise the levelised cost of electricity based on the cost of producing the electricity, membrane CO_2 capture process, transportation and storage.

Table 4.7: Flue gas emissions without carbon capture

	PC		PC +FGD	
Parameter	**Composition**	**ton/h**	**Composition**	**ton/hr**
Flowrate, kmol/s	30.9kmol/s	3295.6	34kmol/s	3496.1
CO_2	0.141	690.9	0.129	694.4
N_2	0.743	2320	0.686	2323
H_2O	0.061	121.5	0.144	316.7
O_2	0.045	163.2	0.041	162.0

Figure 4.3 shows the resulting optimal membrane process flowsheet for the CCS process system. The optimum membrane network consists of 4 membrane stages. The flue gas is supplied to the first stage as a pre-concentration step. The retentate from this stage is split and sent to two succeeding membrane stages that operate at a higher pressure ratio. The permeate from all three membrane stages has greater than 50% CO_2 concentration permeate and is sent to a fourth membrane stage. The permeate from the fourth stage is at 91% CO_2 and the purity of the stream is increased by removing water through 2 stages of condensation and collected as the product stream. Power is recovered from the retentate streams from the two high pressure stages and then are sent to the stack for emission. The retentate from the fourth membrane is fed to the first stage as retentate recycle. The optimum permeate pressure of the three stages is 0.2 bar which is the lowest possible, however, the final stage operates at 0.57 bar. It is energy efficient to increase the pressure ratio across the membrane by operating at lower permeate pressure as the vacuum pumps handle relatively lower flowrates than the feed compressors (Favre et al., 2009). Gabrielli et al. (2017) found three stages to be optimum and four stages did not exhibit improved results. Arias et al. found four stages to be optimal, giving lower membrane area and lower net power consumption based on the superstructure that was presented (Arias et al. 2016). In this study, 4 membrane stages are found to be optimum. The flue gas processed is higher than that considered in Chapter 3 and also in previous reports found in the literature. The high flue gas flowrates are due to the low calorific values and the high ash content of the coal used in South Africa. The upper bound of the membrane area in each stage is set at 1 500 000 m^2. Hence to increase the total membrane area as required to achieve the separation targets more membrane stages are required. In this study a three stage process was

found to be suboptimal and a four stage membrane process was found to be optimal whilst a five stage membrane process did not yield a better solution.

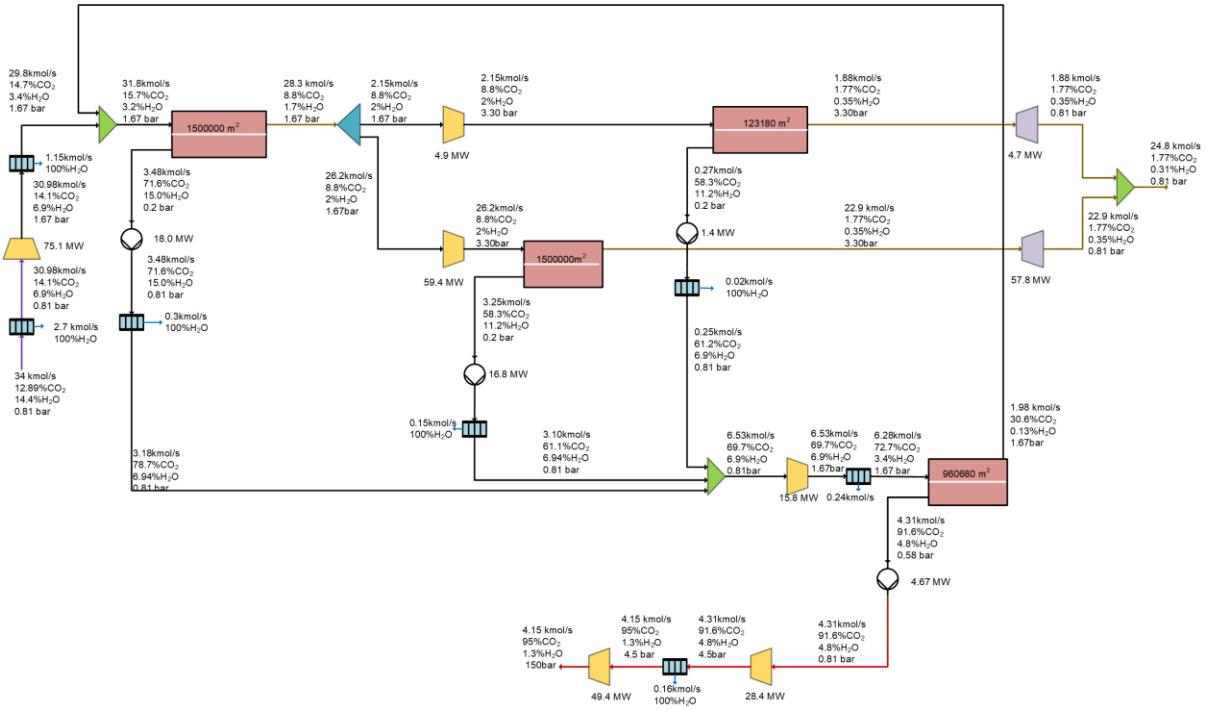

Figure 4.3.Optimum membrane process flowsheet

Table 4.8 shows the results obtained from the optimisation for the CO_2 separation by membrane and compression up to 150 bar for transportation by pipeline (without transport and storage). This gives the cost of capture as given by several reports on the feasibility of CO_2 capture by use of membranes (Arias et al., 2016; Gabrielli et al., 2017; He et al., 2015; Mores et al., 2019). A total membrane area of 4.08 x10^6 m^2 and a net power of 211.3 MW is required to achieve the set targets of 90% recovery and 95% purity. 62.6 MW of electricity is recovered by the turbines. The total annual cost of capture is US$125.4 million.

The specific membrane area requirement of 6531.4 m^2/(ton.hr) is higher than that previously reported by Arias et al. (2016). The authors reported an area of 3510 m^2/(ton.hr) but is lower than the results of He and Hägg, (2014) that showed a specific membrane area of 7904 m^2/(ton/hr) (Arias et al., 2016; He and Hägg, 2014). The specific power consumption of 338.0 KW/ton is realised. A higher membrane area is needed for CCS to lower the power required by the system as there is a trade-off between the power which is a source of driving force and

the membrane area. Despite the high specific membrane area and comparable specific power consumption, a lower specific cost of capture of 26.9 US$/ton is realised. The levelised cost of capture is lower than that reported for other membrane-based CO_2 capture in the USA and Europe (Arias et al., 2016; Zhai and Rubin, 2013). A more efficient optimisation model presented recently shows similar specific cost of capture about US$31 for similar capture targets (Mores et al., 2019).

Comparison of cost is not straightforward because of the different cost models employed by different authors. The lower specific cost realised in this study can be attributed to the lower cost of electricity in South Africa which in this case was US$0.024/ KWh compared to US$0.04/ KW h assumed in several membrane-based CO_2 capture studies (Arias et al., 2016; Lee et al., 2018; Mores et al., 2019)

Table 4.8: Optimum design values for variables for the membrane process with storage

Parameter	**PC +FGD+CCS**
Number of membrane stages	4
Desired recovery,%	90
Desired purity,%	95
Objective	LCOE
CO_2 capture rate, (ton/h)	625.3
Total membrane ($\times 10^6$ m^2)	4.08
Total power (MW)	273.9
Total net power (MW)	211.3
Power recovered (MW)	62.6
Operating costs ($\times 10^6$ US$)	49.5
Capital costs ($\times 10^6$ US$)	75.9
TAC ($\times 10^6$ US$)	125.4
Specific cost of capture (US$/ton)	26.9
Cost of transport ($\times 10^6$ US$/year)	35.8

Cost of storage ($\times 10^6$ US$/year)	60.1
Total cost of retrofitting ($\times 10^6$ US$/year)	221.3
Cost of capture including transport and storage (US$/ton)	47.50

The total cost of transport and storage is US$95.9 million and 62.6% of this is storage cost. A high cost of storage per ton was assumed in this study due to the uncertainties related to the storage site (Viebahn et al., 2015). Retrofitting the membrane-based CCS would require US$221.3 million annually to sequestrate 4. 65 million tonnes of CO_2. Figure 4.4 shows that the capture of CO_2 from flue gas contributes 51% of the total costs of CCS whilst transport and storage contribute 49%. The cost of storage alone contributes 25% of the total cost associated with CCS. This is in contrast to the other reports for the cost of capture where the membrane capture process constitutes a bigger share of the total CCS cost even up to 90% and transport and storage contribute only about 10% (Hu and Zhai, 2017; Zhai and Rubin, 2013). In this study, a high cost of storage US$12/ ton is assumed compared to US$5/ ton assumed by Zhai and Rubin for both transport and storage for power plants located in Pittsburgh, USA (Zhai and Rubin, 2013).

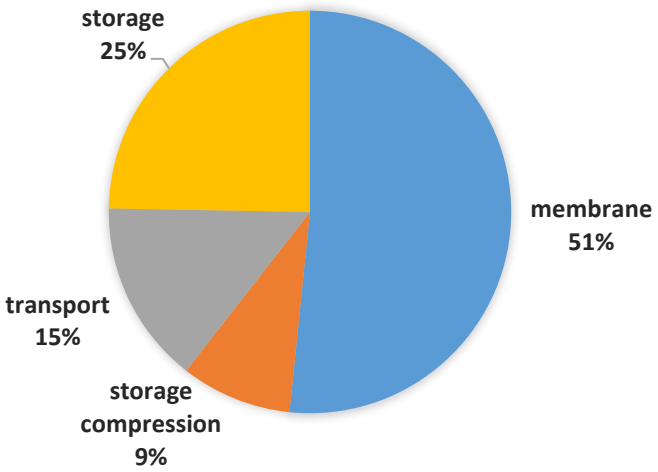

Figure 4.4. Cost-share of the aspects of CCS.

Figure 4.5 shows that the base plant (PC+FGD) would contribute 60% of the total annual cost whereas the capture, transport and storage process would contribute the balance of 40%.

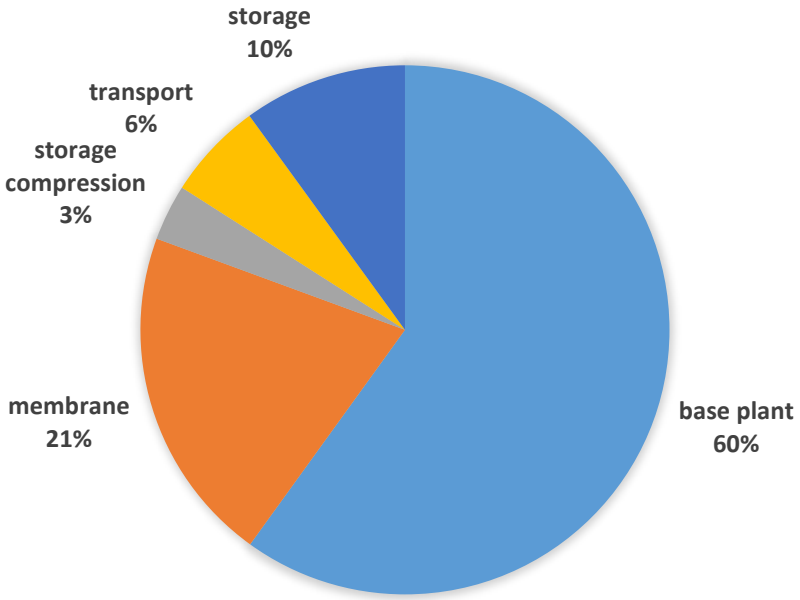

Figure 4.5. Cost-share of the total annual cost (PC + FGD + CCS)

Table 4.9 gives the effect of retrofitting the CCS system on the power plant electricity output. The optimum LCOE obtained from the membrane-based CCS is 151.2 US$/MW. This is an increase of US$84.8 /MW compared to the plant without CCS. The high cost associated with CCS coupled with the loss of net power output in the system results in an increase of 127.7% of the cost of electricity. CCS results in 10.6% penalty on the efficiency of the plant. The penalty of the efficiency of the plant is consistent with other membrane-based techno feasibility studies. He and Hägg, (2014) reported a decrease in efficiency of 10.0 whilst (Zhai and Rubin, 2013) reported a loss of 10.1%. An increase of 130% on the COE was noted for the Medupi power plant when absorption-based CCS technical study was carried out (EPRI, 2015). It could not be ascertained which section of the CCS contributed the most to the increase in COE as this was not reported.

Table 4.9: Plant performance

Parameter	PC+FGD	PC +FGD+CCS
Gross Electrical Output, MW	804	804
Auxiliary Load, MW	76.72	76.72
CC, MW	-	211.3
Solar Power, MW	-	-
Net Electrical output, MW	727.3	515.9
Efficiency,%- HHV	36.50	25.9
CO_2 captured, (ton/yr)$\times 10^6$	-	4.66
CO_2 emitted, (ton/yr)$\times 10^6$	5.2	0.53
LCOE, US$/MW	66.4	151.2
CO_2 avoided, US$/ton	-	103.68

The cost of CO_2 avoided for the whole CCS process results in US$103.68 /ton. The introduction of the carbon tax reduces the cost of CO_2 avoided for the CCS scenario as shown in Table 4.10. This is due to the LCOE of the plant without CCS that increases as the penalty cost of emitting CO_2 is introduced.

Table 4.10 shows the effect of the carbon tax on the LCOE. The carbon tax has been gazetted to be US$7.79/ton (2017 equivalent) of CO_2 emitted. The introduction of the carbon tax to the PC+FGD results in the COE increasing by which is 11.1%. However, the introduction of the carbon tax results in a negligible increase in LCOE for the plant with CCS. Much less CO_2 is emitted; hence the lower carbon tax paid for the plant with CCS system is also minimal. The CO_2 avoided indicates the price of carbon which would make CCS economic sense (Rubin, 2012). At the current price of carbon, it is economical to pay the carbon tax than implement CCS. Tot et al, (2011) reported that carbon tax would need to be set at US$96.9 (2017 equivalent) to motivate for investment in CCS for a power plant in South Africa. This was based on CCS based on absorption.

Table 4.10: Table showing the effect of adding carbon tax at the gazetted price

Parameter	PC+FGD	PC+FGD+CCS
CO_2 emitted, %	100	10
CO_2 emitted, (ton/yr)$\times 10^6$	5.2	0.52
Annual cost, (US$/yr)$\times 10^6$	360	581
Carbon tax, (US$/yr)$\times 10^6$	40.3	4.03
Total annual cost, US$/yr	400.3	585.3
Net Electrical output, MW	727.3	515.9
Efficiency,%- HHV	36.50	25.9
LCOE,US$/MW	73.87	152.2
CO_2 avoided, US$/ton	-	95.8

4.4 Concluding remark

A techno-economic study for carbon capture by use of membrane technology from a South Africa coal power plant is carried out. The base plant is modelled based on the coal type and ambient conditions of the location of the plant. The output from this step is the cost of producing electricity without CCS, the flue gas composition, flowrate and temperature. CO_2 capture from the flue gas produced is then carried out by a superstructure based optimisation model in the GAMS environment. The objective is to minimise the levelized cost of electricity for power plant with CO_2 capture, transport and storage. The resulting process flow and corresponding optimum conditions give the COE of 151.2 US$/MW which is a 127.8% increase in the cost of producing electricity. The bulk (49%) of the cost of CCS is incurred in transportation and storage. The specific cost of capture by a membrane at a South Africa plant at 26.9 US$/ton is lower than in other parts of the world such as the USA and Norway. It is therefore recommended that efforts be put into investigating the feasibility of implementing sequestration methods other than geological storage in the Zululand basin such as carbon utilisation and enhanced gas and oil recovery to make CO_2 capture more economically favourable. A 127% increase in LCOE for membrane-based CCS realised in this study is lower than 130% increase previously reported for absorption-based CCS for the SA context. CO_2

absorption technology would increase the water consumption by 38.6% whereas the membrane process can recover over 90% of the water vapour in flue gas which would otherwise be emitted via the stack for the case without CCS. Therefore, it is recommended that membrane-based CO_2 capture, though currently at the pilot stage, be considered in South Africa. Further study should consider embedding a detailed transport and storage model based on the potential storage sites to lower the associated cost. An analysis based on the full six-unit train may result in a lower cost of electricity as some costs are shared.

4.5 Nomenclature

LCOE	Levelised cost of electricity, US$/MWh
COE	Cost of electricity
$C_{avoided}$	Cost of CO_2 avoided, US$/ton
$C_{capture}$	Cost of CO_2 capture, US$/ton
cf	Levelized capacity factor
E	CO_2 emission, ton/MWh
FOM	Annual fixed operating and maintenance cost, US$
fcf	Fixed charge factor
OM	Operation and maintenance cost, US$/year
VOM	Annual variable operating and maintenance cost, US$/year

Chapter 5 – On Optimisation of N_2 and CO_2 selective membrane hybrid process system for CO_2 capture from coal power plants flue gas

This study has been published

Chiwaye, N., Majozi, T., Daramola, M.O., 2021. On Optimisation of of N_2 and CO_2 selective membrane hybrid process system for CO2 capture from coal power plants flue gas. Int. J. Mem. Scie (2021) https://doi.org/10.1016/j.memsci.2021.119691

5.1 Introduction

The use of N_2-selective membrane has opportune advantages in that it exploits the already high N_2 content in coal power plants flue gas and also collects the high CO_2 pure stream from the high pressure side. Both factors may reduce the energy required for final product compression before being sent for storage. As far as could be ascertained, a superstructure based model for automated synthesis and optimisation of a multi-stage N_2-selective and CO_2–selective hybrid membrane system for post-combustion CO_2 capture from a humidified multicomponent flue gas is presented for the first time. Cellulose acetate with silica backbone functionalised with p-tetranitrocalix(4)arene to form a CA/Si_CL membrane is considered as the N_2-selective membrane (Hussain et al., 2015). A polymer membrane as the CO_2 selective membrane (White et al., 2015). The superstructure involves recycle streams from both the retentate and permeate. The product can be collected from both the recycle and or the permeate side. The model simultaneously achieves a synthesis of the process flowsheet and gives the optimum operating conditions of process streams, membrane area and membrane feed side pressure and permeate side pressure. An analysis of the potential of the N_2-selective membrane for CO_2 capture is firstly carried out and compared to the established Polaris membrane. The N_2/CO_2-selective hybrid process is then evaluated and the results compared to the performance of the CO_2 membrane.

5.2 Problem statement

The problem statement is described below;

Given;

(i) Flowrate, temperature, composition and pressure of the flue gas produced from a coal power plant
(ii) A choice to use either N_2-selective membrane or CO_2-selective membrane
(iii) Set of membrane stages
(iv) A known desired recovery
(v) A known desired product purity

Determine;

(i) The optimum process network
(ii) The optimum power consumption
(iii) The optimum membrane area
(iv) The minimum total annualised cost of CO_2 capture

5.3 Model description

Assumptions guiding the development of the model as follows.

(i) The plug flow regime is assumed on both permeate and retentate sides (Arias et al., 2016).
(ii) The permeance of a component is constant and is not affected by pressure nor changes in concentration (Uppaluri et al., 2006).
(iii) Pressure drop is considered negligible (Zhai and Rubin, 2013).
(iv) Membrane operation is isothermal (Bocciardo et al., 2013).
(v) Counter-current configuration (Bocciardo et al., 2013).
(vi) The flue gas only contains CO_2, N_2, O_2 and H_2O (Merkel et al., 2010).

5.3.1 Superstructure description

The Figure 5.1 presents the superstructure from which the model is formulated. Flue gas from the power plant is delivered to the CO_2 capture plant and cooled to 25 °C and 1 bar and some of the water condenses out. The flue gas is then split and sent to the different flue-permeate mixers in different membrane stages. The flue gas is mixed with the permeate recycle streams also and is compressed to membrane feed pressure which increases the temperature of the gas. The stream is then passed through a separator to remove excess water. The stream can be cooled

or heated to bring the temperature to the membrane operating temperature (40 °C). The flue and permeate mixture is mixed with retentate recycle streams and fed to the membrane. The gas is separated and the more permeable gas permeates to the permeate side of the membrane. The less permeable gas is collected on the retentate side. The retentate stream is made to pass through a separator if it is saturated with water and is split into recycle stream and residue or product stream. It is then passed through a compressor or an expander depending on the pressure of the destination of the retentate stream. The permeate side can operate at atmospheric pressure or vacuum conditions as generated by a vacuum pump which discharges the gas at atmospheric pressure. The permeate stream passes through a cooler/condenser to adjust the water content. The stream is then split into recycle streams that are sent to any of the membrane stages and also to the residue and product streams. The product streams are compressed to enable more water to condense out at a higher pressure. The final product stream pressure is increased to 73.8 bar by an interstage compressor with interstage cooling. The pressure of the CO_2 stream is then further increased to 150 bar and is then ready for transportation to the storage sites. The splitters in the superstructure allow for partial recycling of the permeate and the recycle streams and the flowrates of these streams are simultaneously optimised with the other variables in the model.

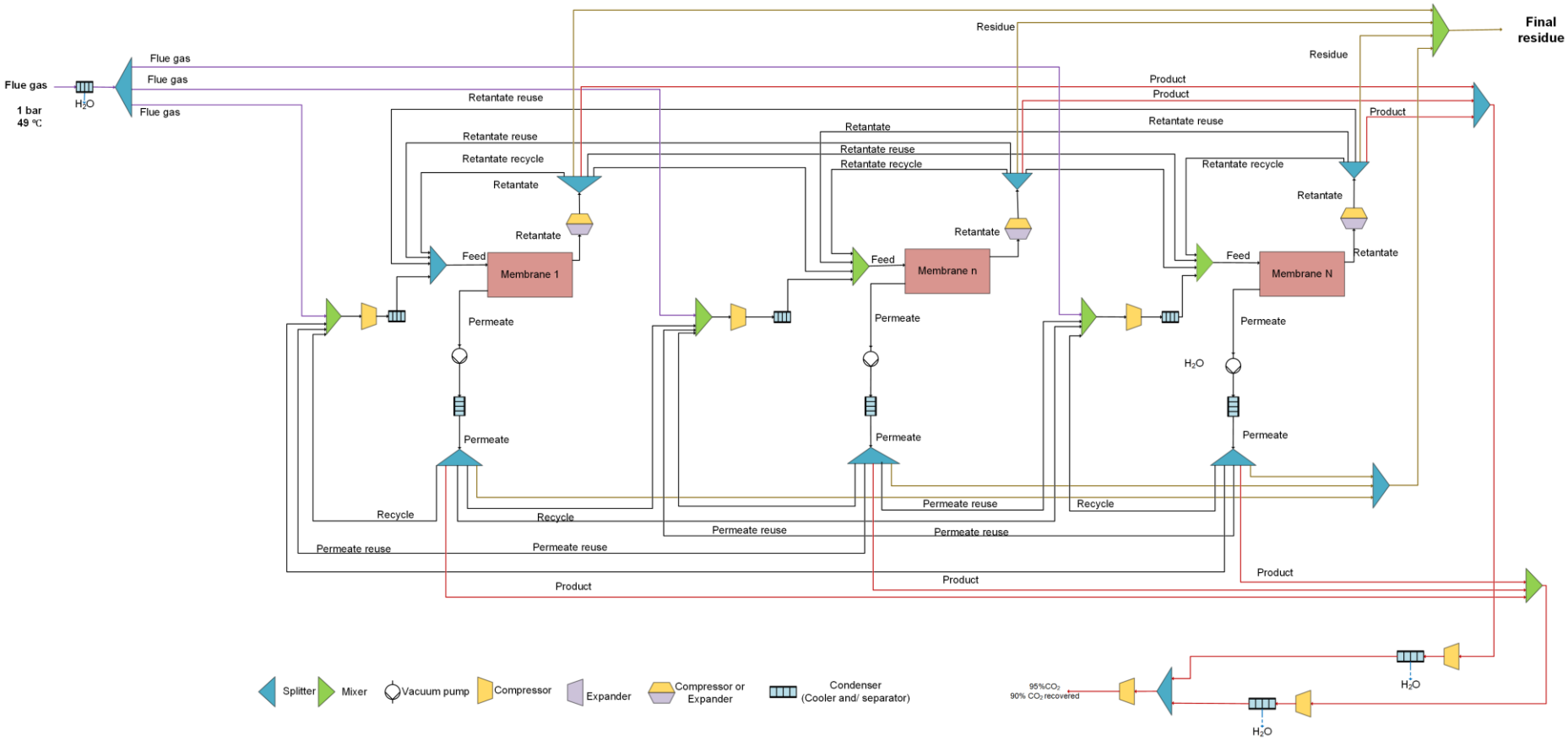

Figure 5.1. Superstructure for the N_2/CO_2 hybrid membrane system

5.3.2 Membrane permeation model

Figure 5.2 shows the basis of the material balance of component *i* across a small area dA_n^{mem} in the membrane stage *n.* The flow is the countercurrent flow.

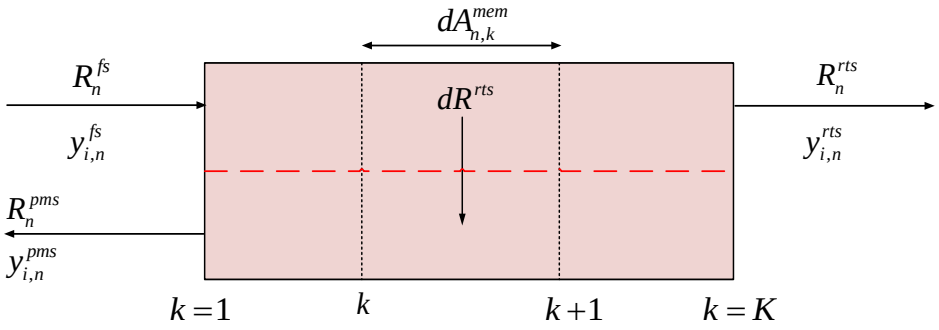

Figure 5.2.Countercurrent flow in a membrane module (without a sweep gas)

A material balance based on the solution diffusion mechanism results in Equation (5.1). The molar flowrate *(R)* of component *i* that permeates through the membrane dA_n^{mem} is equal to the product of the permeance and the difference in the partial pressure in the retentate and permeate side. The retentate partial pressure is the product of the retentate pressure and the mole fraction of the component, i.e. ($P_n^{rts} \cdot y_{i,n}^{rts}$). The Equation (5.1) is discretised as previously described in section 3.3.2 to give Equations (5.2) and (5.3).

$$-\frac{d(R_n^{rts} \cdot y_{i,n,}^{rts})}{dA_n^{mem}} = \varphi_i \left(P_n^{rts} \cdot y_{i,n}^{rts} - P_n^{pms} \cdot y_{i,n}^{pms} \right) \qquad \forall n \in N, i \in I \tag{5.1}$$

Equations (5.2) and (5.3) compute the flowrates of component *i* at the discretisation points and also gives the membrane area of stage *n.*

$$\frac{K-1}{2A_n^{mem}} \left(-R_{n,k-1}^{rts} \cdot y_{i,n,k-1}^{rts} + R_{n,k+1}^{rts} \cdot y_{i,n,k+1}^{rts} \right) + \varphi_i \left(P_n^{rts} \cdot y_{i,n,k}^{rts} - P_n^{pms} \cdot y_{i,n,k}^{pms} \right) = 0$$
$$\forall n \in N, i \in I, k \in K; k = 2 \tag{5.2}$$

$$\frac{K-1}{2A_n^{mem}}\left(R_{n,k-2}^{rts}\cdot y_{i,n,k-2}^{rts}-4R_{i,n,k-1}^{rts}\cdot y_{i,n,k-1}^{rts}+3R_{n,k}^{rts}\cdot y_{i,n,k}^{rts}\right)$$
$$+\,perm_i\left(P_n^{rts}\cdot y_{i,n,k}^{rts}-P_n^{pms}\cdot y_{i,n,k}^{pms}\right)=0\quad \forall n\in N, i\in I, \forall k\in K, k>2 \tag{5.3}$$

The Equation (5.4) is the material balance around the area bound by the points *k* and *K*. It shows that the flowrate of *i* at any point k on the retentate side is equal to the sum of component *i* that exits the membrane from the retentate sides and the flowrate of *i* on the permeate side at point *k*. Equation (5.5) is the total stream flowrate balance around the same boundary. The Equation (5.6) is the overall material balance around the whole membrane module. It shows that the gas flowrate supplied to the membrane should be equal to the amount that leaves module.

$$R_{n,k}^{rts}\cdot y_{i,n,k}^{rts}=R_{n,K}^{rts}\cdot y_{i,n,K}^{rts}+R_{n,k}^{pms}\cdot y_{i,n,k}^{pms}\qquad \forall n\in N, i\in I, k\in K \tag{5.4}$$

$$R_{n,k}^{rts}=R_{n,K}^{rts}+R_{n,k}^{pms}\qquad \forall n\in N, k\in K \tag{5.5}$$

$$R_{i,n}^{fs}=R_{i,n,K}^{rts}+R_{i,n,k=1}^{pms}\qquad \forall n\in N, i\in I, k\in K \tag{5.6}$$

Equation (5.7) states that the sum of the mole fractions of the components is 1.

$$\sum_i y_{i,n,k}^{pms}=1\qquad \forall n\in N, k\in K \tag{5.7}$$

$$\sum_i y_{i,n,k}^{rts}=1\qquad \forall n=N, k\in K \tag{5.8}$$

The boundary conditions at *k=1* are stated by Equations (5.9) and (5.10) for the retentate and permeate sides, respectively. The flowrate of the stream that leaves membrane stage *n* at the retentate side is given by Equation (5.11).

$$R_{i,n,k=1}^{rts}=R_{i,n,}^{fs}\qquad \forall n\in N, i\in I \tag{5.9}$$

$$R_{i,n,k=1}^{pms}=R_{i,n,}^{pms}\qquad \forall n\in N, i\in I \tag{5.10}$$

$$R^{rts}_{i,n,k=K} = R^{rts}_{i,n,} \qquad \forall n \in N, i \in I, k = K \tag{5.11}$$

5.3.3 Material balance constraints

Material balances are carried out around the splitters namely; flue gas splitter, retentate splitter, permeate splitter and the condensers. Figure 5.3 shows that the flue gas passes through a condenser before it can be split and sent to different membrane stages (Chiwaye et al., 2021; Uppaluri et al., 2006, 2004). A contact cooler condenser has been suggested in several studies and assumed that traces of NO_x and SO_x and the remaining ash is washed away in the process (Hasan et al., 2012; Ren et al., 2020).

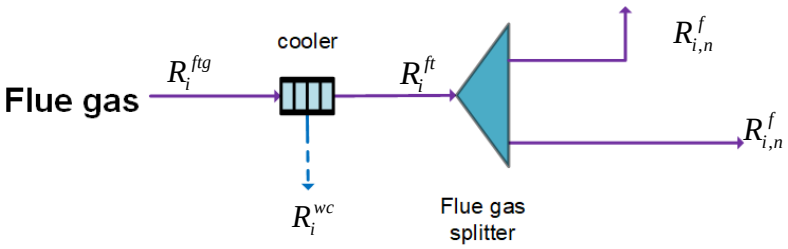

Figure 5.3. Balance around flue gas condenser and flue gas splitter

Equations (5.12) and (5.13) give the material balance around the flue gas condenser. Only water can condense when the saturated flue gas stream is cooled to 25 °C. The flue gas can then be split. The component flowrate of the flue gas after the flue gas splitter is a product of the split *(x^f)* fraction and the flowrate of *i* in the flue gas supplied to the capture process plant. This is shown by Equation (5.14). Equation (5.15) constrains the sum of the split fractions to 1.

$$R_i^{ftg} = R_i^{ft} + R_i^{wc} \qquad i \in I,\ i = H_2O \tag{5.12}$$

$$R_i^{ftg} = R_i^{ft} \qquad \forall i \in I,\ i \neq H_2O \tag{5.13}$$

$$R_{i,n}^{f} = x_n^f R_i^{ft} \qquad \forall i \in I \tag{5.14}$$

$$\sum_n x_n^f = 1 \tag{5.15}$$

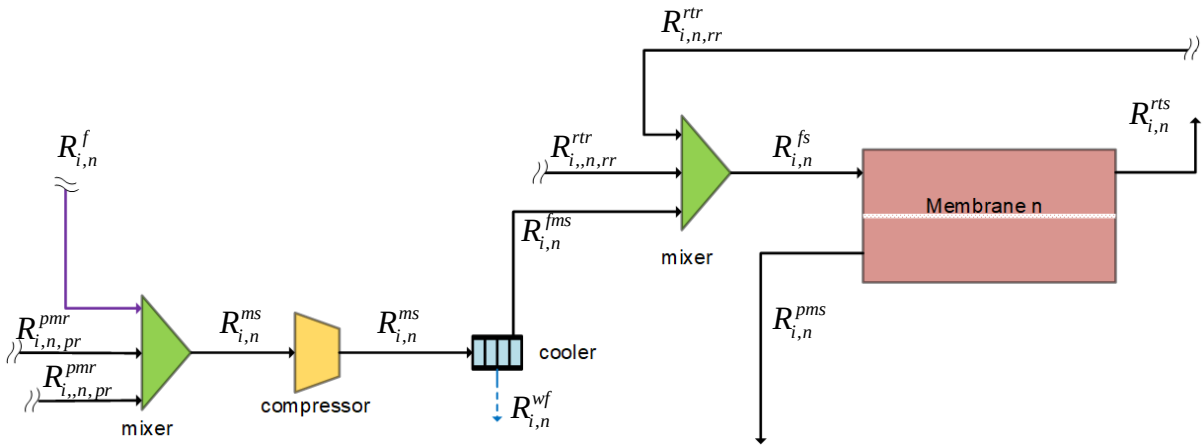

Figure 5.4. Balance around the flue gas-permeate recycle and feed mixer

The flue gas sent to membrane stage n is mixed with the permeate recycle streams and compressed to membrane operating pressure. Figure 5.4 illustrates in detail the possible streams. At high pressure, more water can condense. The Equation (5.16) shows that the flowrate of a component as it leaves the flue gas-permeate mixer is a sum of the flue gas and permeate recycle streams sent to that membrane stage. Equations (5.17) and (5.18) give the material balance around the condenser.

$$R_{i,n}^{ms} = R_{i,n}^{f} + \sum_{pr} x_{n,pr}^{pmr} R_{i,n}^{pmr} \qquad \forall i \in I; n \in N \tag{5.16}$$

$$R_{i,n}^{ms} = R_{i,n}^{fms} - R_{i,n}^{wf} \qquad \forall i \in I, i = H_2O \tag{5.17}$$

$$R_{i,n}^{ms} = R_{i,n}^{fms} \qquad \forall i \in I, i \neq H_2O \tag{5.18}$$

Only water may condense under these conditions. If the stream is not saturated at the target temperature, condensation will not occur. A binary variable (Z^{wf}) depicts the existence or non-existence of the separator. Equation (5.19) ensures a feasible water flowrate to be removed.

Equation (5.20) ensures that the partial pressure of water in the gas stream that leaves the condenser is not more than the saturation pressure of water at that temperature.

$$R^L Z_n^{wf} \le R_{i,n}^{wf} \le R^U Z_n^{wf} = 0 \qquad \forall i \in I, i = H_2O \tag{5.19}$$

$$y_{i,n}^{fms} P_n^{rt} - P_i^{sat} = 0 \qquad (T) \quad \forall i \in I, i = H_2O, n \in N \tag{5.20}$$

The feed stream to the membrane ($R_{i,n}^{fs}$) is a sum of the flue gas, the retentate recycle and, the combined permeate recycle and flue gas stream ($R_{i,n}^{fms}$) as described by Equation (5.21). The flowrate of component *i* in the permeate recycle stream from membrane stage *n* supplied to stage *pr* is determined by the spit fraction $x_{n,pr}^{pmr}$. The split fraction $x_{n,rr}^{rt}$ determines the flowrate of the retentate streams of component *i* in the retentate of membrane stage *n* that is recycled and sent to membrane stage.

$$R_{i,n}^{fs} = \sum_{rr} x_{n,rr}^{rtr} R_{i,n}^{rt} + R_{i,n}^{fms} \qquad \forall i \in I, n \in N \tag{5.21}$$

The Equation (5.22) states that the flowrate of component *i* in the retentate recycle stream is equal to the split fraction multiplied by the flowrate in the retentate stream. Equation (5.23) states that the flowrate of component *i* in the permeate recycle stream is equal to the split fraction multiplied by the flowrate in the permeate stream

$$R_{i,n,rr}^{rtr} = x_{n,rr}^{rtr} R_{i,n}^{rt} \qquad \forall i \in I, n \in N, rr \in RR \tag{5.22}$$

$$R_{i,n,pr}^{pmr} = x_{n,pr}^{pmr} R_{i,n}^{pm} \qquad \forall i \in I, n \in N, pr \in PR \tag{5.23}$$

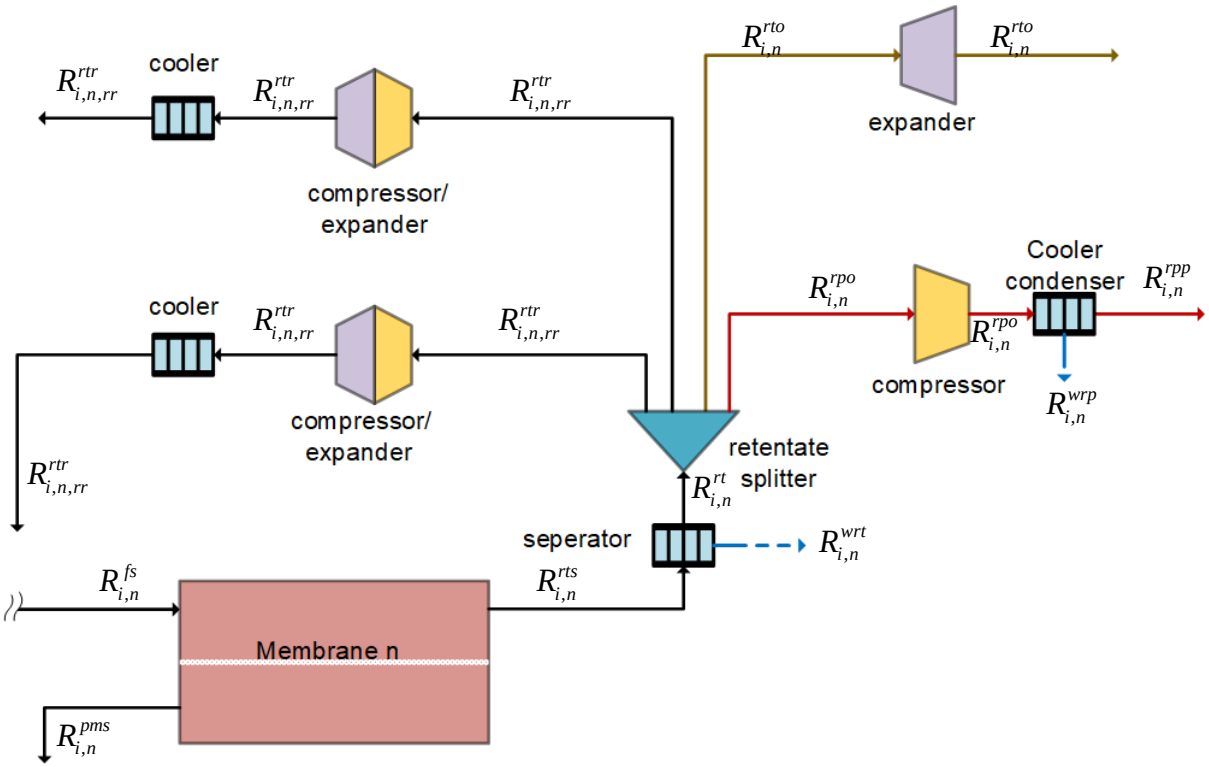

Figure 5.5. The process design of the streams from the stream that leaves the retentate side

Whilst information on the permeance of water through the N_2-selective membrane is barely available, reasonable assumptions can be made. Previous techno-economic studies on the use of the N_2-selective membrane have assumed that water is almost impervious in the membrane since this presents the most severe scenario in separating CO_2 and N_2 and achieving desired separation targets (Ren et al., 2020). A similar assumption is made in this study, and it means that most of the water is retained on the retentate side and its concentration increases as the N_2 and some CO_2 permeates the membrane. It is therefore, likely that the retentate stream is highly saturated as it leaves the membrane and thus, a knockout separator is placed just after the membrane as shown in Figure 5.5. The design has been adopted previously for N_2 selective membranes. Equation (5.24) and (5.25) gives the balance around this separator.

$$R_{i,n}^{rt} = R_{i,n}^{rts} - R_{i,n}^{wrt} \qquad \forall i \in I, i = H_2O \tag{5.24}$$

$$R_{i,n}^{rt} = R_{i,n}^{rts} \qquad \forall i \in I, i \neq H_2O \tag{5.25}$$

The retentate stream can be split into the recycle stream *(rtr)*, a fraction can be sent to the residue mixer *(rto)* and another fraction sent to the product mixer *(rpo)*. Equation (5.26) constraints the sum of these fractions to one. Equations (5.27) and (5.28) give the flowrates of the stream that goes to the residue mixer and product mixer respectively according to their respective split fractions.

$$x_n^{rto} + \sum_{rr} x_{n,rr}^{rtr} + x_n^{rpo} = 1 \qquad \forall n \in N \tag{5.26}$$

$$R_{i,n}^{rto} = x_n^{rto} R_{i,n}^{rt} \qquad \forall n \in N; \forall i \in I \tag{5.27}$$

$$R_{i,n}^{rpos} = x_n^{rpo} R_{i,n}^{rt} \qquad \forall n \in N; \forall i \in I \tag{5.28}$$

The retentate that is sent to the residue mixer *(rto)* is at high pressure and the energy is recovered by expander turbines *en-* route to the residue mixer. On the other hand, the stream that is sent to the product mixer *(rpo)* may have excess water which may need to be removed to meet CO_2 purity targets, therefore it may be compressed to pressure (P^{pw}) which is a variable to be optimised in the model *en-* route the product mixer. Equation (5.29) and (5.30) shows the balance around the cooler condenser.

$$R_{i,n}^{rpp} = R_{i,n}^{rpo} - R_{i,n}^{wrp} \qquad \forall i \in I, i = H_2O \tag{5.29}$$

$$R_{i,n}^{rpp} = R_{i,n}^{rpo} \qquad \forall i \in I, i \neq H_2O \tag{5.30}$$

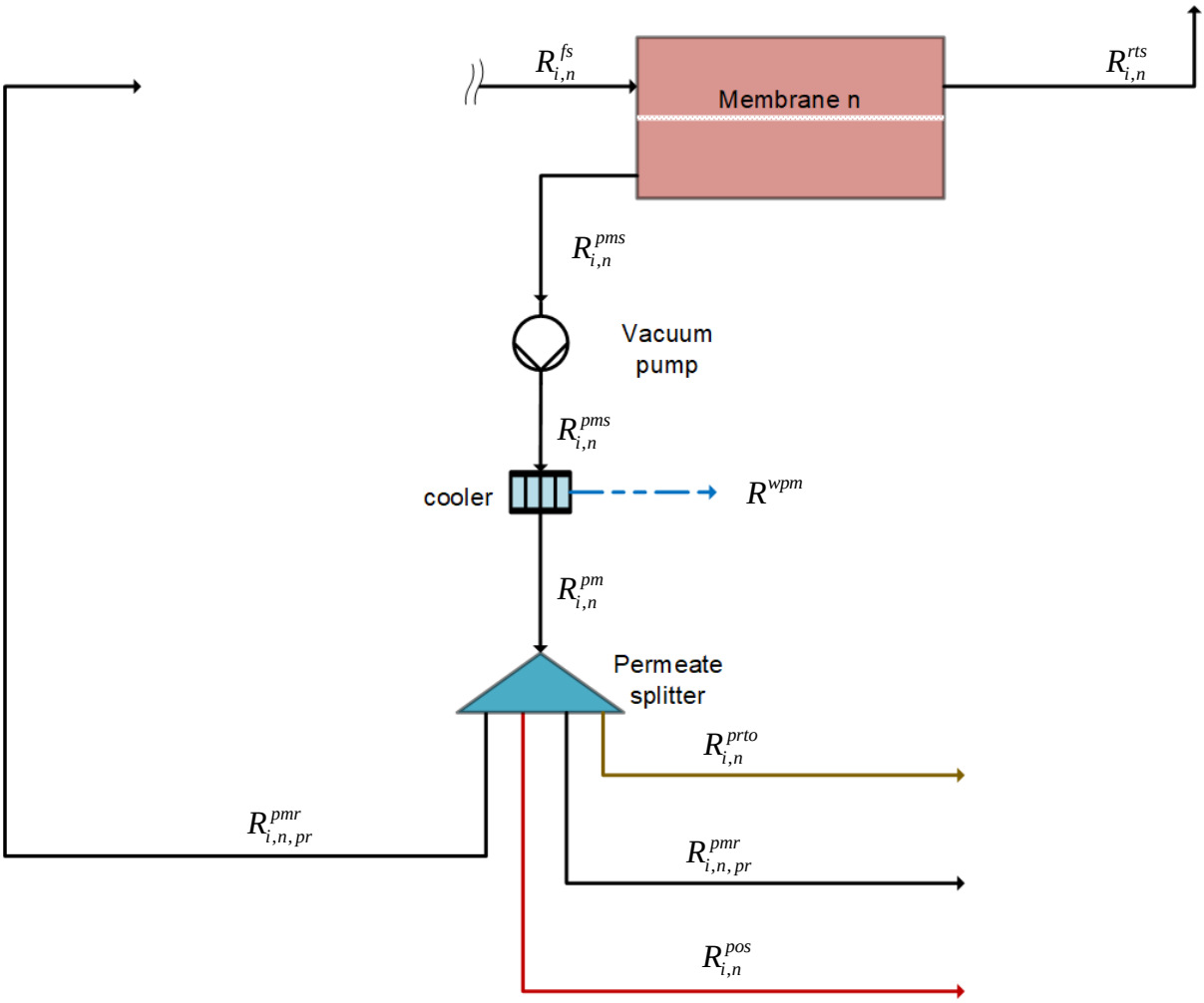

Figure 5.6. Streams on the permeate side

Figure 5.6 shows the process streams that can be generated from the permeate side of the membrane. Water is highly permeable in the CO_2 selective membrane used and much of it will appear in the permeate. The permeate is cooled in a cooler/condenser and some water also condenses and is removed from the stream. Equations (5.31) and (5.32) give the balances around the cooler condenser.

$$R_{i,n}^{pm} = R_{i,n}^{pms} - R_{i,n}^{wpm} \qquad \forall i \in I, i = H_2O \tag{5.31}$$

$$R_{i,n}^{pm} = R_{i,n}^{pms} \qquad \forall i \in I, i \neq H_2O \tag{5.32}$$

The permeate splitter generates recycle streams *(pmr)* that are fed to the different membrane stages and also sent to the product mixer *(pos)* and residue mixer *(prto)*. The sum of these split

fractions should be equal to one as given by Equation (5.33). Equation (5.34) shows that the component flowrate of the stream that goes to the product mixer is equal to the split fraction multiplied by the flowrate of that component in the permeate stream. The component flowrate of the stream sent to the residue mixer from the permeate side is given by Equation (5.35).

$$x_n^{pos} + \sum_{pr} x_{n,pr}^{pmr} + \sum_{n} x_n^{prto} = 1 \qquad \forall n \in N \tag{5.33}$$

$$R_{i,n}^{pos} = x_n^{pos} R_{i,n}^{pm} \qquad \forall n \in N; \forall i \in I \tag{5.34}$$

$$R_{i,n}^{prto} = x_n^{prto} R_{i,n}^{pm} \qquad \forall n \in N; \forall i \in I \tag{5.35}$$

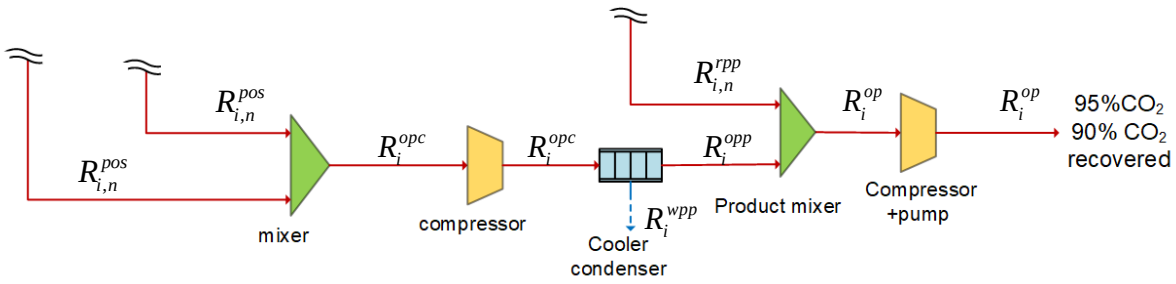

Figure 5.7. Streams that make up the product that is sent for sequestration.

Figure 5.7 shows the streams that make up the final product that is compressed to 150 bar and sent to storage. The product streams *(pos)* from the permeate side are mixed and then compressed to enable further dewatering of the stream. Equation (5.36) shows that the sum of these permeate streams results in the stream *(opc)* which is compressed and cooled and after the knockout drum the stream *(opp)* results.

$$R_i^{opc} = \sum_{n} R_{i,n}^{pos} \qquad \forall i \in I \tag{5.36}$$

Equations (5.37) give the material balance around the cooler condenser and Equation (5.38) ensures that it is only water that is removed from the product stream.

$$R_i^{opp} = R_i^{opc} - R_i^{wpp} \qquad \forall i \in I, i = H_2O \tag{5.37}$$

$$R_i^{opp} = R_i^{opc} \qquad \forall i \in I, i \neq H_2O \tag{5.38}$$

Equation (5.39) shows that the water composition is determined by the pressure *(P^{pw})* to which the stream is compressed to.

$$y_i^{opp} P^{pw} - P_i^{sat} = 0 \qquad (T^{atm}) \quad \forall i \in I, i = H_2O, n \in N \tag{5.39}$$

Equation (5.40) shows that the flowrate of the final product *(op)* is a sum of the permeate product *(opp)* and the total product streams that come from the retentate side of the membrane stages.

$$R_i^{op} = R_i^{opp} + \sum_n R_{i,n}^{rpp} \qquad \forall i \in I \tag{5.40}$$

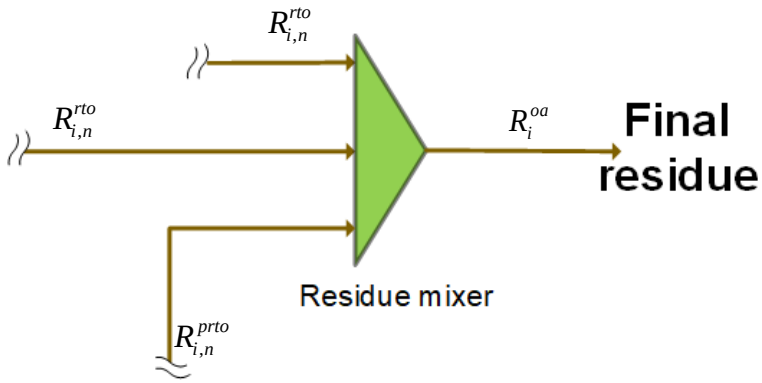

Figure 5.8. Streams that make up the final residue released into the atmosphere

The permeate that is sent to the residue mixer *(prto)* is already at 1 bar after being discharged by the vacuum pumps and from there is cooled and sent straight to the residue mixer. The flowrate of the gas that exits the residue mixer is a sum of the streams from the retentate *(rto)* and permeate splitter *(prto)* as shown by Equation (5.41). This is the residue stream that is sent to the stack as waste.

$$R_i^{oa} = \sum_n R_{i,n}^{rto} + \sum_n R_{i,n}^{prto} \qquad \forall i \in I \tag{5.41}$$

Equation (5.42) ensures that the feed fed to any membrane stage *(n)* is not saturated with water by constraining the water partial pressure not to exceed the staturatation pressure.

$$y_{i,n}^{fs} P_n^{rt} \le P_i^{sat} \qquad \forall i \in I, i = H_2O, n \in N \tag{5.42}$$

The mole fraction of any stream (y_i) is a fraction of the mole flowrate of that component to the total mole fraction of all the components in that gas stream as given by the generalised Equation (5.43).

$$y_i = \frac{R_i}{\sum_i R_i} \qquad \forall i \in I \tag{5.43}$$

Binary variables also are used to set the permeance of the components of either an N_2-selective membrane or that of CO_2-selective membrane. Equation (5.44) shows that in each membrane stage either an N_2-selective membrane or CO_2-selective membrane exists. Equation (5.45) sets the permeance of the component *(i)* to its actual values (q) which are parameters in the model.

$$Z_n^{N_2} + Z_n^{CO_2} = 1 \qquad \forall n \in N \tag{5.44}$$

$$\varphi_{i,n} = Z_n^{N_2} \cdot q_i^{N_2} + Z_n^{CO_2} \cdot q_i^{CO_2} \qquad \forall n \in N; i \in I \tag{5.45}$$

5.3.4 Compressors

The duties of the compressors, vacuum pumps and expander turbines are determined in the previous section 3.3.6 (Arias et al., 2018; Favre, 2007). The adiabatic ratio is assumed to be 1.4. The vacuum pump and the expander turbine discharge the gas streams at atmospheric pressure (1.0 bar). The final product stream is compressed to 73.8 bar in stages and further pumped to 150 bar. The compressor and the vacuum pumps duties are computed by Equation (5.46) and the expanders by Equation (5.47).

$$Q_n^{comp} = \frac{1}{\eta}\left[\sum_{i=1}^{I} R_{i,n} \cdot 8.314 \cdot T^l \left(\frac{\gamma}{\gamma - 1}\right)\left(\left(\frac{P_n^h}{P_n^l}\right)^{\left(\frac{\gamma-1}{\gamma}\right)} - 1\right)\right] \qquad \forall n \in N \tag{5.46}$$

$$Q_n^{exp} = \eta \left[\sum_{i=1}^{I} R_{i,n} \cdot 8.314 \cdot T^l \left(\frac{\gamma}{\gamma - 1} \right) \left(1 - \left(\frac{P_n^l}{P_n^h} \right)^{\left(\frac{\gamma - 1}{\gamma} \right)} \right) \right] \qquad \forall n \in N \qquad (5.47)$$

5.3.5 Cooling

The partial pressure $(y_{i,n}P_n)$ of the water that is swept along in the gas stream (R) is equal to the water saturation pressure at the temperature as illustrated by Equation (5.48).

$$y_{i,n}P_n = P_i^{sat} \quad (T) \qquad \forall \in N;\ i \in I,\ i = H_2O \qquad (5.48)$$

5.3.6 Separation targets

Equation (5.49) shows that the desired recovery is a fraction given by the amount of the component in the final product stream (op) divided by the amount in the flue gas supplied to the capture process plant (ftg). Equation (5.50) computes the composition of the components in the product stream. Equation (5.49) and Equation (5.50) allow the setting of the desired CO_2 recovery and purity of the product stream, respectively.

$$DR_i = \frac{R_i^{op}}{R_i^{ftg}} \qquad \forall i \in I \qquad (5.49)$$

$$DP_i = \frac{R_i^{op}}{\sum_i R_i^{op}} \qquad (5.50)$$

The cooling of gas streams is carried out by cooling water from the cooling tower at a cost that is deemed negligible in comparison to the cost of the membrane and the compressors.

5.3.7 Cost Model

The cost method by (Zhai and Rubin, 2013) is adopted. The total annualised cost (TAC) is a sum of the annualised costs associated with each process unit. Equation (5.51) states that the annual capital expenditure (CAPEX) is the total cost of the operational units including installation cost per year and this is multiplied by a capital recovery factor *(CRF*). The cost associated with the purchase cost of the membrane and replacement (TCC^{mem}) is given by Equation (5.52). A factor of 1.37 is included to account for facilities and process contingencies.

$$CAPEX = CRF(1+0.37)\left(\begin{array}{l} TCC^{mem} + \sum_n CC^{comp} + \sum_n CC^{coolers} \\ + \sum_n CC^{vac} + \sum_n CC^{exr} + CC^{pump} \end{array}\right) \tag{5.51}$$

The total membrane area required is a sum of the membrane area of each stage. The total membrane purchase cost includes the cost of purchase of the membrane module as well as the cost of the frame as shown in Equation (5.52).

$$TCC^{mem} = C^{mem}\sum_n A_n^{mem} + \left(C^{mf}\left(\frac{\left(\sum_n A_n^{mem}\right)}{2000} \right)^{0.7} \right) \tag{5.52}$$

The purchase cost (*CC*) associated with compressors, vacuum pumps, expander and CO_2 product pump is given generally by Equation (5.53). The capital cost of each heat exchanger is determined from the heat transfer areas as shown by Equation (5.54).

$$CC^{unit} = C^{unit}Q^{unit} \tag{5.53}$$

$$CC^{exch} = C^{hxc}A^{cl} \tag{5.54}$$

The operating cost per year is the sum of the operational and maintenance cost (*COM*) which is taken as a fraction of the capital cost and the cost of the net electricity consumed by the compressors. This is described by Equation (5.55). Equation (5.56) gives the cost of

maintenance. The cost of maintaining the membrane modules is 1 % its cost and that of maintaining the rest of the units is 3.6% of the purchase cost.

$$OPEX = COM + EC \tag{5.55}$$

$$COM = \left(0.01 TCC^{mem}\right) + \left[0.036\left(\begin{array}{l} TCC^{mem} + \sum_n CC^{comp} + \sum_n CC^{coolers} \\ + \sum_n CC^{vac} + \sum_n CC^{exr} + CC^{pump} \end{array}\right)\right] \tag{5.56}$$

The total cost of the electricity required by the process is given by Equation (5.57). It is the net power consumption multiplied by the cost of electricity C^{el}.

$$EC = C^{el}\left(\sum_n Q^{comp} + Q^{pump} + \sum_n Q^{vac} - \sum_n Q^{exr}\right) \tag{5.57}$$

5.3.8 Objective function

The objective is to minimise the levelized cost of CO_2 capture per ton.

$$min\ [TAC] = \left[OPEX + CAPEX\right]$$

$$min[TAC] = \left[\begin{array}{l} \left(CRF(1+0.37)\left(\begin{array}{l} TCC^{mem} + \sum_n CC^{comp} + \sum_n CC^{coolers} \\ + \sum_n CC^{vac} + \sum_n CC^{exr} + CC^{pump} \end{array}\right)\right) + \\ \left(C^{el}\left(\sum_n Q^{comp} + Q^{pump} + \sum_n Q^{vac} - \sum_n Q^{exr}\right) + \right. \\ \left.\left(\left(0.01 TCC^{mem}\right) + \left[0.036\left(\begin{array}{l} TCC^{mem} + \sum_n CC^{comp} + \sum_n CC \\ + \sum_n CC^{vac} + \sum_n CC^{exr} + CC^{pump} \end{array}\right)\right]\right)\right) \end{array}\right] \tag{5.58}$$

5.4 Illustrative example

Table 5.1 shows the flue gas characteristics similar to that of a power plant that generates 550MW of electricity from a supercritical boiler.

Table 5.1: Flue gas composition

Parameter	**Value**
Flue gas flowrate, $kmols^{-1}$	22.321
Flue gas pressure, bar	1.0
CO_2 mole fraction	0.135
N_2 mole fraction	0.689
H_2O mole fraction	0.152
O_2 mole fraction	0.024

Table 5.2 gives the permeance of the gaseous components through the 2 types of membrane considered in the study. The N_2-selective membrane previously reported is considered (Hussain et al., 2015). The N_2 permeance observed from the experimental study is presented in Table 5.2. The N_2/O_2 and N_2/H_2O selectivity is assumed to be 1000 in this work as the permeance was not reported. At such high selectivity, negligible amounts of O_2 and water permeate and report to the permeate stream. High selectivity for O_2 and water was chosen since little permeance of these components would present a more severe case in terms of achieving product purity (Ren et al., 2020). A common polymer membrane is considered as the CO_2 selective membrane (White et al., 2015).

Table 5.2: Gas permeance through the different membranes

Membrane parameter	Permeance kmol/(m^2.s.bar)
CO_2-selective membrane	
CO_2	$3.39x10^{-5}$
N_2	$6.78x10^{-7}$
H_2O	$6.79x10^{-5}$
O_2	$1.36x10^{-6}$
N_2-selective membrane	
CO_2	$2.78x10^{-6}$
N_2	$6.53x10^{-5}$
H_2O	$6.53x10^{-8}$
O_2	$6.53x10^{-8}$

Table 5.3 shows the prices of compressors, expanders, vacuum pumps and the assumed efficiency. The cost of the membrane is assumed to be US\$50/m^2 (Lee et al., 2018; Zhai and Rubin, 2013). Prices in the Table 5.3 are presented for the year 2013 and were adjusted to 2018 prices in this study using the chemical engineering index (Chemengonline, 2019).

Table 5.3: Economic data

Parameter	Value
Capacity factor %	75
Compressor, vacuum, expander efficiency %	85
Adiabatic compression coefficient,	1.4
Capital recovery factor, yr^{-1}	0.113
Membrane price, US\$$m^{-2}$	50
Reference frame cost, US\$	2,300,000.00
Compression unit cost, US\$ KW^{-1}	670

Inter-stage compression and pump cost, US$ KW^{-1}	902
Expander unit cost, US$ KW^{-1}	500
Equipment cost factor for housing,	1.80
Reference heat exchanger, US$$m^{-2}$	300
Electricity cost, US$ KW-h^{-1}	0.05
Process facilities capital cost, %	37
Maintenance cost of membrane	1%TCC^{mem}
Maintenance cost of compressors and heat exchangers	3.6% of CC^{unit}
Membrane lifetime, yr	5
Project lifetime, yr	25
Operating time, h yr^{-1}	6570

The levelized cost is calculated as given by Equation (5.59). It is the total annualised cost divided by the quantity of CO_2 recovered from the flue gas per annum.

$$TLC = \left(\frac{OPEX + CAPEX}{6570 \cdot DR_{CO_2} \cdot mCO_{2\,fluegas}} \right) \tag{5.59}$$

The lower and upper bounds of the membrane area are set to 1000 m^2 and 1000000 $m^{2,}$ respectively. Previous works have assumed membrane areas from 5 m^2 to 1 500 000 m^2 (Al-Marzouqi et al., 2002; Lee et al., 2018). The lower bound for the permeate pressure is 0.2 bar (Kim et al., 2020). The optimisation runs based on exclusively the CO_2-selective membrane have the CO_2 product collected from the permeate streams side only. Likewise, the exclusively N_2-selective membrane process optimisation runs have the retentate streams contribute to the CO_2 product stream.

The model is an MINLP problem and is solved in the GAMS environment by the solver DICOPT. The relaxed MINLP (RMINLP) is first solved by BARON and then the first solution generated is used as initial values for solving the MINLP in DICOPT, running CPLEX as the MIP solver and CONOPT as the NLP solver.

5.5 Results and discussion

The results are presented in two sections. The first case shows the results where recovery and purity are set at 90% and 80%, respectively. This is to highlight the optimisation of the capture process by the N_2-selective membrane. The second case is when the purity targets are set at the conventional capture targets of 90% recovery and 95% purity for membrane capture. In order to highlight the benefit of superstructure based optimisation, a predetermined two stage (PRD-2) process design previously shown to require the least power consumption and smallest membrane area were optimised first (Ren et al., 2020). In the optimisation run, the membrane, the operating pressure, and flowrates were optimised whilst the recycle streams were fixed as predetermined. The results of the PRD-2 process were compared to the superstructure based optimisation results. The PRD-2 did not include partial recycle streams, whereas the superstructure based model embeds the possibility of partial recycle streams. The third and fourth sections of the results section show the effect of the N_2 permeance and N_2/CO_2 selectivity of the N_2-selective membrane on the optimisation results obtained for the hybrid system.

5.5.1 Case 1: Recovery 90% and purity 80%

Considering that O_2 is almost impermeable in the N_2-selective membrane at the set selectivity, most of the O_2 will appear in the retentate together with CO_2, thereby making it infeasible to achieve the common purity target of 95%. From Table 5.1, it can be deduced that CO_2 make up 84.9% of the sum of these two components. Therefore, in this first section, a CO_2 purity target of 80% is set to study the multistage optimisation of the carbon capture process by the use of an N_2-selective membrane.

5.5.1.1 Optimisation of carbon capture by an N_2-selective membrane

Table 5.4 presents the results for the optimisation run where an N_2-selective membrane was employed in all the membrane stages when the recovery was set at 90% and purity was set at 80%.

Table 5.4: Results obtained for the N_2-selective membrane recovery 90% and purity 80%

Variable		**Values**		
Number of membrane stages	PRD-2	2	3	4
Desired recovery,%	90	90	90	90
Desired purity,%	90	80	80	80
Total membrane ($\times 10^6$ m^2)	0.42	0.42	0.43	0.44
Total net power (MW)	161.5	161.5	150.25	149.9
Operating costs ($\times 10^6$ US$)	57.80	57.80	53.7	53.7
Capital costs ($\times 10^6$ US$)	25.38	25.38	23.5	24.1
Annual cost ($\times 10^6$ US$)	83.17	83.17	77.1	77.7
Specific cost (US$/ton)	29.47	29.47	27.33	27.55
% specific cost difference	-	0	7.26	6.52
CO_2 avoided (US/ton)	46.0	46.0	41.03	41.31
% CO_2 avoided difference	-	0	10.3	9.68

The optimum process, which is three stages, results in energy savings of 11 MW compared to two stage process that is predetermined (PRD-2) beforehand. Changes in membrane area requirement are minimal. The optimisation based on the superstructure where only two stages are involved yielded the same result as the predetermined process. However, multistage optimisation involving three or four stages gave more energy efficient processes. The energy efficient process reduces the operating cost significantly. The energy savings resulted in a 7.3% decrease in annualised capture cost. This is consistent with observations in the previous optimisation studies based on CO_2 selected membrane for CO_2 capture where three stages gave the optimum, and two stages gave sub-optimal results (Lee et al., 2018; Ramírez-Santos et al., 2018). Four-stage membrane processes have also been found to be optimum in other studies (Arias et al., 2016; Mores et al., 2019). The use of three stages or four stages gives more recycle and reusable streams which increase the concentration of the target component in the feed streams. This in turn, increases the driving force and reduces the operating pressure ratio to reduce energy consumption.

Figure 5.9 represents the optimum membrane network for the N_2-selective membrane optimisation. From the membrane network, it is seen that in the case of a three-stage process, it is the permeate streams that are reused in the preceding stages to increase the N_2 concentration and to further recover the CO_2 that would have permeated. The retentate is passed onto succeeding stages for further purification as N_2 permeates through the membrane.

For efficient energy use, the first stage operates at 1 bar on the permeate side to avoid having the vacuum pump processing large flowrates. The lowest retentate pressure is adopted in this stage also because of the large flue gas flowrate. The subsequent stages operate at a higher retentate pressure due to the lower N_2 concentration in those stages. The final stage employs vacuum operation to further create the needed driving force to process the lowest N_2 content in the flue gas. Ren et al. (2020) reported that for two stage configurations they studied, a successive compression without vacuum operation yielded lower energy consumption and a smaller membrane area. However, in the study, a binary gas CO_2/N_2 was studied.

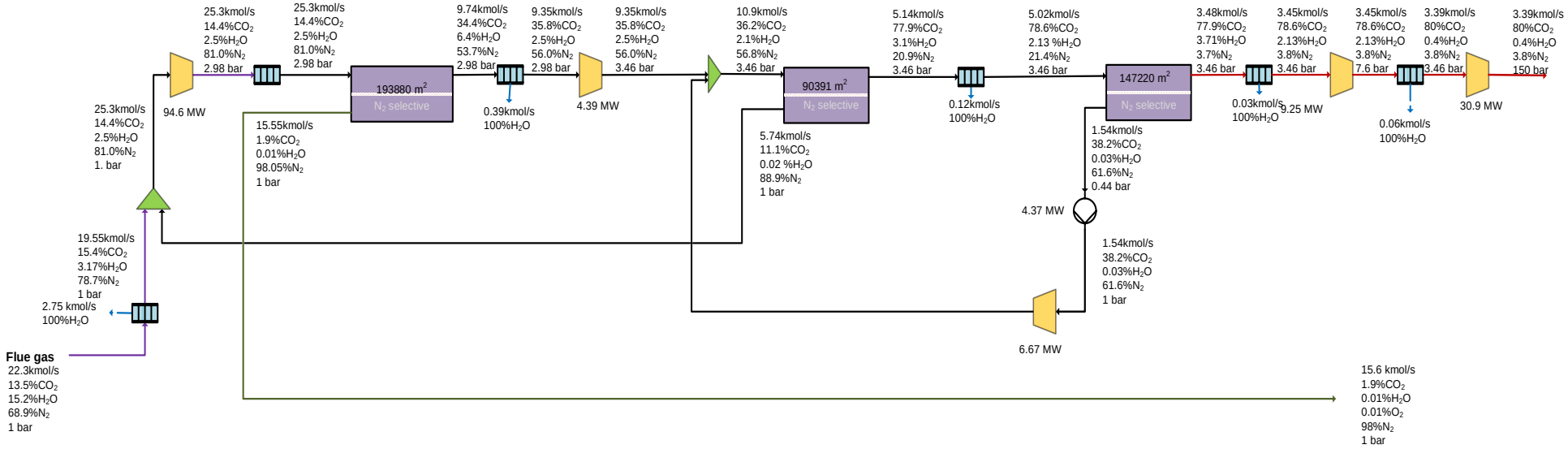

Figure 5.9. Optimum membrane network for N_2-selective membrane system, CO_2 recovery 90% and purity 80%. The balance of the composition is O_2

5.5.1.2 Optimisation of carbon capture by N_2-selective CO_2 selective hybrid membrane system

Optimisation of the CO_2-selective membrane process is based on the superstructure presented previously (Chiwaye et al., 2021). Table 5.5 gives the results for the CO_2-selective membrane process for recovery 90% and purity 80%. The multistage optimisation results in a lower cost of capture (2.9%) than the PRD-2 process. For the superstructure multistage optimised processes, the annualised cost did not vary significantly for the CO_2-selective membrane. Increasing the membrane stages, from two stages through to four stages gave results with minor variances of less than 1%, which can be attributed to computational discrepancies. This is expected since the purity target is low in this case and thus, a two stage process is also competitive.

Table 5.5: Results obtained for the CO_2- selective membrane recovery 90% and purity 80%

Variable			**Values**	
Number of membrane stages	PRD-2	2	3	4
Desired recovery,%	90	90	90	90
Desired purity,%	80	80	80	80
Total membrane ($\times 10^6$ m^2)	1.21	1.16	1.09	1.07
Total net power (MW)	133.7	133.0	133.6	131.7
Operating costs ($\times 10^6$ US$)	50.5	50.2	50.3	49.6
Capital costs ($\times 10^6$ US$)	39.7	39.0	38.3	37.9
Annual cost ($\times 10^6$ US$)	90.14	89.1	88.6	87.5
Specific cost (US$/ton)	31.9	31.59	31.40	31.01
% specific cost difference	-	1.13	1.7	2.91
CO_2 avoided US$/ton	43.75	44.83	44.62	43.84
% CO_2 avoided difference	-	1.31	1.72	3.44

Table 5.5 shows that at the same assumed cost for both membranes at similar capture targets, the annualised cost of CO_2 capture is higher for the CO_2-selective membrane than the N_2-selective membrane. The CO_2-selective membrane requires larger membrane areas (153%) and thus has a higher capital cost than the N_2-selective membrane process. However, the power

consumption for the N_2-selective membrane exceeds that of the CO_2-selective membrane by 12% and thus gives a higher operational cost. The value of the N_2 permeance in the N_2-selective membrane is twice that of CO_2 permeance in the CO_2-selective membrane. The high permeance of N_2 in the N_2-selective membrane together with the high N_2 composition in the flue gas enables the N_2-selective membrane process to easily achieve the required recovery over a very small membrane area. The higher N_2 composition in the flue gas provides an inherent driving force that enables a higher flux and thus reduces the membrane area required.

However, due to the high rejection of O_2 and water in the N_2-selective membrane, the N_2-selective membrane process is highly constrained in terms of achieving the required purity and requires a higher pressure ratio in downstream stages to achieve the set purity target. A large membrane area would allow more CO_2 to permeate and further dilute the permeate. Thus a lower membrane area is employed. This lower membrane area is traded with high pressure ratio which results in high energy consumption for the N_2-selective membrane. The CO_2-selective process also includes the residue expanders, which recover energy from the high pressure and high flowrate retentate streams which reduces the net power consumption of the membrane process. The N_2-selective membrane does not have these residue expanders as the residue is collected on the permeate side at 1 bar. The benefit of compressing the product to the final product pressure from a high pressure retentate for transportation in the N_2-selective membrane process is outdone by the recovery of energy in the CO_2-selective membrane process.

A smaller membrane area was also shown to achieve a higher N_2 purity of the permeate for the N_2-selective membrane compared to the CO_2-selective membrane when simulation was carried out in previous work (Ren et al., 2020). Meanwhile, for the CO_2-selective membrane, a larger membrane area is required to increase the flux in light of the low CO_2 composition in the flue gas which translate to a low driving force.

From the results shown in Table 5.6, it is apparent that an N_2/CO_2 selective hybrid system is beneficial. A PRD-2 N_2/CO_2 hybrid process reduces the cost of capture by 8.0% compared to the multistage CO_2 selective membrane process. Superstructure based hybrid optimal network reduces the cost saving by 2.91% compared to the PRD-2 process. The multistage optimisation reduces the cost of capture by 15.8% compared to the CO_2 selective membrane process. The

optimum hybrid process gives a more energy efficient process with a smaller membrane area than a CO_2-selective membrane. Ren et al. (2020) observed that the N_2-selective membrane process and the hybrid system gave more energy efficient process flow with smaller membrane areas than the CO_2-selective membrane process (Ren et al., 2020). The two stage hybrid process, which involved compression without vacuum use, was more energy efficient than the N_2-selective membrane though it had a slightly larger membrane area.

Table 5.6: Results for the CO_2 /N_2 hybrid process; recovery 90% and purity 80%

Variable				**Values**	
Process system	CO_2	N_2	CO_2-N_2	CO_2-N_2	CO-N_2
Number of membrane stages	Optimum	Optimum	PRD-2	2	3-optimum
Desired recovery,%	90	90	90	90	90
Desired purity,%	80	80	80	80	80
Total membrane ($x\ 10^6\ m^2$)	1.07	0.43	0.43	0.49	0.86
Total net power (MW)	131.7	150.3	144.8	142.2	124.9
Operating costs ($x\ 10^6$ US$)	49.6	53.7	52.8	51.7	45.7
Capital costs ($x\ 10^6$ US$)	37.8	23.5	27.8	27.8	28.2
Annual cost ($x\ 10^6$ US$)	87.5	77.1	80.5	78.9	73.9
Specific cost (US$/ton)	31.01	27.3	28.53	27.95	26.1
% specific cost difference	-	12.0	8	9.9	15.8
CO_2 avoided (US$/ton)	42.25	39.24	40.33	39.21	35.00
% CO_2 avoided difference	-	7.12	4.5	7.20	17.2

The membrane network produced by optimisation shows that the N_2-selective membrane is the first stage to process the flue gas. This first stage takes advantage of the high N_2 concentration that translates to driving force in membrane separation thus resulting in a more energy efficient process. This study, therefore, is consistent with the pre-assumption that an N_2-selective membrane in the first stage results in lowered cost of CO_2 capture, as presented in Figure 5.10 (Hussain et al., 2015; Ren et al., 2020). However, in this work, the CO_2-selective stages operate at a vacuum on the permeate side. This could be because the optimisation model allows for

retentate and permeate optimisation, unlike in the previous study when the operating pressure was selected beforehand (Ren et al., 2020). The approach taken in this work facilitates a more energy efficient process for CO_2 capture from coal-fired power plants by membranes.

Table 5.7 illustrates that the N_2-selective membrane stage operates at a lower pressure ratio than CO_2-selective membrane stages in the hybrid process system.

Table 5.7: Optimum pressure values for recovery 90% and purity 80%

Process	**CO_2 Optimum**				**N_2 Optimum**			**Hybrid Optimum**		
Membrane stages	1	2	3	4	1	2	3	1	2	3
Membrane type	Z^{CO2}	Z^{CO2}	Z^{CO2}	Z^{CO2}	Z^{N2}	Z^{N2}	Z^{N2}	Z^{N2}	Z^{CO2}	Z^{CO2}
Retentate (bar)	2.85	1.8	2.85	2.85	2.98	2.46	3.46	2.34	2.34	2.34
Permeate (bar)	0.27	1	0.76	0.2	1	0.44	1	1	0.2	0.33
Ratio (P^{rt}/P^{pms})	10.6	1.8	3.8	14.3	2.98	5.6	3.5	2.3	11.7	7.09

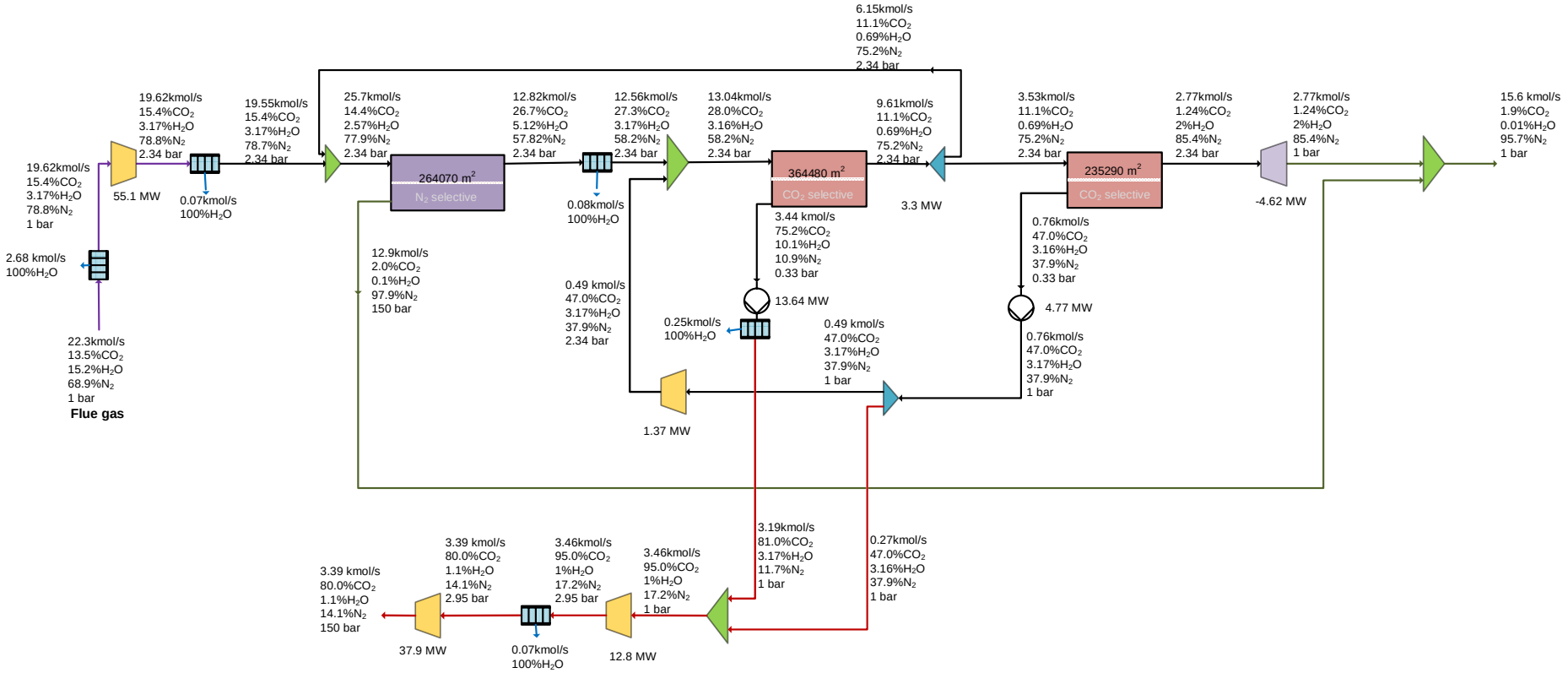

Figure 5.10. Optimum membrane network for N_2/CO_2-selective hybrid membrane system, CO_2 recovery 90% and purity 80%.The balance of the composition is O_2

5.5.2 Case 2: Recovery 90% and purity 95%

Case 2 presents the results of the hybrid optimisation and compares it to the use of CO_2-selective membrane capture at the conventional capture targets of recovery 90% and purity of 95%. The N_2-selective membrane alone cannot achieve the high purity of 95% CO_2 at the assumed N_2/O_2 selectivity. Optimisation of the CO_2-selective membrane process yields the results presented in Table 5.8. The difference in the results between the different membrane stages is minimal. A three stage process is optimal. The general trend in all the cases is that the total annual cost is dominated by operational cost.

Table 5.8: Results obtained for the CO_2-selective membrane, recovery 90% and purity 95%

Variable		**Values**		
Number of membrane stages	PRD-2	2	3	4
Desired recovery,%	90	90	90	90
Desired purity,%	95	95	95	95
Total membrane ($\times 10^6$ m^2)	1.13	1.13	1.16	1.15
Total net power (MW)	137.0	137.1	133.0	135.4
Operating costs ($\times 10^6$ US$)	51.7	51.7	50.5	51.1
Capital costs ($\times 10^6$ US$)	39.5	39.7	39.5	39.3
Annual cost ($\times 10^6$ US$)	91.2	91.15	90.1	90.4
Specific cost (US$/ton)	32.30	32.30	31.92	32.03
% specific cost difference	-	0	1.2	0.8
CO_2 avoided US$/ton	44.66	44.66	43.65	44.09
% CO_2 avoided difference		0	2.3	1.3

From Table 5.9, it is apparent that the N_2-CO_2 hybrid membrane process is more economical than the CO_2-selective membrane process. The optimum hybrid process combines the advantages of the N_2-selective membrane and that of the CO_2-selective membrane. Optimisation of the hybrid system saves 1% of the energy requirements and reduces the membrane area by 42% compared to the CO_2-selective membrane process.

Table 5.9: Results for the CO_2 /N_2 hybrid process; recovery 90% and purity 95%

Variable		Hybrid		
Process system	CO_2	CO_2/N_2	CO_2/N_2	CO_2/N_2
Number of membrane stages	Optimum (3)	2	3	4
Recovery,%	90	90	90	90
Purity,%	95	95	95	95
Total membrane ($x\ 10^6\ m^2$)	1.16	1.06	0.74	0.67
Total net power (MW)	133.0	148.7	146.2	131.6
Operating costs ($x\ 10^6$ US$)	50.5	55.8	53.74	48.1
Capital costs ($x\ 10^6$ US$)	39.5	40.3	32.3	28.9
Annual cost ($x\ 10^6$ US$)	90.0	96.1	86.0	77.0
Specific cost (US$/ton)	31.92	34.05	30.48	27.29
% specific cost difference	-	-6.7%	4.4%	14.5%
CO_2 avoided (US$/ton)	43.7	48.7	43.26	37.17
% CO_2 avoided difference	-	-11.4%	1.0%	14.9%

Table 5.10 gives the pressure ratios across the membrane stages and Figure 5.11 shows the novel process flowsheet of the optimum hybrid process for CO_2 capture. The optimum network involves an N_2-selective membrane and three CO_2-selective membrane stages. The residue that is sent to the stack is a sum of the retentate stream from a CO_2-selective membrane and the permeate from the N_2-selective membrane. This is similar to the hybrid process presented in Figure 5.10. The product is collected from the CO_2-selective membrane stages.

The smaller stage membrane areas (smaller than 300 000 m^2) exhibited in Figure 5.11 are desirable as this could reduce energy losses through pressure drop along the membrane profile. Optimisation studies have previously presented membrane networks with at least one membrane stage with an area of more than 1 million m^2 for CO_2-selective membrane for similar flue gas flowrates (Arias et al., 2016; Lee et al., 2018; Mores et al., 2019). The total area of 673 000 m^2 is slightly higher than that previously reported for a two stage hybrid membrane process. Hussain et al. (Hussain et al., 2015) reported a total membrane area of 643 000 m^2 for a two stage hybrid membrane process. It is important to note that a higher N_2/CO_2-selectivity of 200 was assumed (Hussain et al., 2015). However, in this study, the selectivity is much lower at 23.5.

CO_2 capture by CO_2 selective membranes is characterised by large membrane areas (> 1 million m^2). For instance, Merkel et al. (Merkel et al., 2010) reported a total membrane area requirement of 1.3 million m^2 for the whole process CO_2 capture integrated design where the air is used as a sweep in the membrane process before being fed to the boiler (Merkel et al., 2010). Even at high CO_2 permeance such as 3000 GPU, the total membrane area needed was shown to be higher than 1 million m^2 (Ramasubramanian et al., 2012). The smaller membrane area achieved by the hybrid process system results in a 14% reduction in the specific cost of capture compared to the CO_2-selective membrane process. The optimum specific cost at $US27.29 is lower than that reported in previous optimisation studies (Arias et al., 2016; Lee et al., 2018).

Ren et al. (2020) reported a higher membrane area (1.42 million m^2) for a higher recovery of 98%, a purity of 90% CO_2 and an N_2/CO_2 selectivity of 200. The N_2-selective membrane stage had a bigger membrane area (1.28 million m^2) than the subsequent CO_2-selective membrane (0.135 million m^2). This large membrane area was observed for a two-stage hybrid system in this work (1.06 million m^2), of which the cost of capture was higher than the CO_2-selective membrane. Similarly, the first N_2-stage had a larger membrane area (0.9 million m^2), and the second stage CO_2-selective membrane had a lower membrane area (0.066 million m^2). In both studies, an N_2-selective membrane was employed as the first stage to process the flue gas, which is similar to the process flowsheet resulting from optimisation carried out in this work for the two stage hybrid system. In the previous studies, a direct comparison of the performance of the CO_2-selective membrane process to the hybrid process under the same assumptions was

not provided for the more realistic multicomponent flue gas and large scale flowrates (Hussain et al., 2015; Ren et al., 2020).

The pressure values presented in Table 5.10 indicate a combination of the use of compressors and vacuum pumps in various stages. The N_2-selective membrane stages *(Z^{N2})* operate at a lower pressure ratio than the CO_2-selective membrane stages *(Z^{CO2}).*

Table 5.10: Optimum pressure values for recovery 90% and purity 95%

	CO_2 Optimum			**Hybrid Optimum**			
Membrane stages	1	2	3	1	2	3	4
Membrane	Z^{CO2}	Z^{CO2}	Z^{CO2}	Z^{N2}	Z^{CO2}	Z^{CO2}	Z^{CO2}
Retentate (bar)	1.88	2.73	2.73	2.50	2.73	3.35	2.50
Permeate (bar)	0.218	0.2	0.76	1	0.44	0.2	1
Ratio (P^{rt}/P^{pm})	8.62	13.7	3.6	2.5	6.2	16.8	2.5

The configuration that exhibited the least energy requirement involved enriching CO_2 stream by the N_2-selective membrane first and then increasing the CO_2 purity to 95% by the CO_2-selective membrane in the second stage. The N_2-selective membrane operates at a high pressure achieved by compression and sub-ambient pressure on the permeate side. The second stage also involves both a compressor and vacuum, in addition, some energy is recovered by expander turbines from the high pressure N_2 rich retentate.

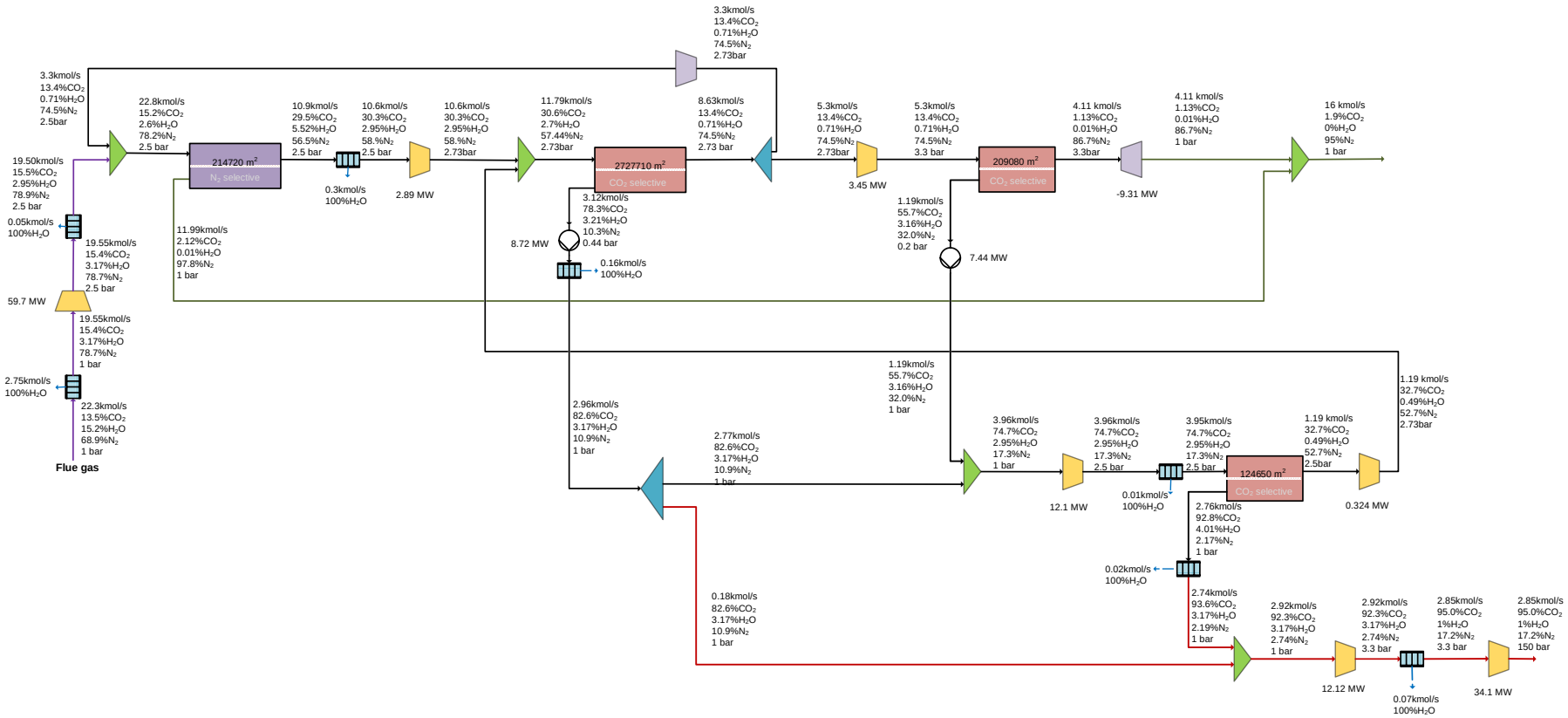

Figure 5.11. Optimum membrane network for N_2/CO_2 selective hybrid membrane system, CO_2 recovery 90% and purity 95%. The balance of the composition is O_2

Table 5.11 and Table 5.12 show the model statistics and also shows that the computational time required is short because of the strategy used to solve a RMINLP first before solving the MINLP.

Table 5.11: Statistics for Case 1 – Recovery 90% and purity 80 %

	CO_2	N_2	CO_2/N_2	CO_2/N_2
Membrane stages	Optimum(4)	Optimum(3)	Hybrid (2)	Optimum(3)
No. variables	1923	1417	987	1498
No. binary variables	4627	3361	2518	3932
Non-linear terms	44	27	20	36
CPU(s)	2.875	11.36	0.093	0.063
Iterations	3460	39270	4	4

Table 5.12: Statistics for Case 2 – Recovery 90% and purity 95 %

	CO_2	CO_2/N_2	CO_2/N_2	CO_2/N_2
Membrane stages	Optimum (3)	2	3	Optimum (4)
No. variables	1406	987	1498	2043
No. binary variables	27	20	36	56
Non-linear terms	3299	2518	3932	5466
CPU(s)	0.078	1.126	0.141	0.63
Iterations	4	5175	8	4

5.5.3 Sensitivity to N_2 permeance on the hybrid process

The effects of varying N_2 permeance in the N_2 selective membrane for CO_2 capture is carried out. The N_2-selective membrane considered in sections 5.5.1 and 5.5.2 is the reference membrane (presented in Table 5.2). For the purpose of investigating the effect of N_2 permeance on the resulting optimisation, the N_2 permeance was varied whilst the N_2/CO_2, N_2/O_2, N_2/H_2O selectivity was equal in all the runs. The N_2/CO_2 selectivity was 23.5, whilst the N_2/O_2, N_2/H_2O selectivity was set at 1000. The N_2 permeance was considered as products (0.25, 0.5, 1, and 2)

of the permeance of the N_2-selective membrane that is presented in Table 5.2 and consequently the simulated membranes were referred to as 0.25MP, 0.5MP, 1MP and 2MP. Though in the practical, it might difficult to synthesise membranes of exactly similar permeance and assumed N_2/CO_2, N_2/O_2, N_2/H_2O selectivity, the difference will be small. Table 5.13 shows the permeance of the N_2-selective membrane that is used in the optimisation runs.

Table 5.13 Permeance of N_2 in the different N_2-selective membranes simulated #

Membrane Name	**Fraction of reference membrane**	**N_2 Permeance (kmol/(m^2.s.bar))**
0.25MP	**0.25**	1.63×10^{-5}
0.5MP	**0.5**	3.26×10^{-5}
1MP	**1**	6.53×10^{-5}
2MP	**2**	1.31×10^{-4}

 # Selectivity, N_2/CO_2 =23.5; N_2/O_2, = 1000; N_2/H_2O=1000 for all optimisation runs

The recovery and purity targets were set at 90% and 95%, respectively, and all the optimisation runs were carried out based on a four membrane stage superstructure. Each run is set to involve at least one N_2-selective membrane stage to ensure an N_2/CO_2 hybrid process. The CO_2 selective membrane considered in previous sections and permeance presented in Table 5.2 was also considered as the CO_2-selective membrane in all the optimisation runs.

Figure 5.12 presents the results of the optimisation based on the N_2-selective membranes of differing N_2 permeance. The figure shows that both the membrane area and the power consumption initially decreases as the N_2 permeance in the N_2-selective membrane is increased. However, the changes in membrane area and power consumption become minimal. The variation in the operational and capital cost is illustrated in Figure 5.13. Initially, doubling the N_2 permeance from 1.63×10^{-5} to 3.26×10^{-5} kmol/(m^2.s.bar) reduces the annual cost of capture by 6.3%. However, further increases result in lower-cost reductions. For instance, increasing the N_2 permeance by two-fold from 6.53×10^{-5} to 1.31×10^{-4} results in a negligible decrease in the cost of CO_2 capture. Similar behaviour was reported before (Lee et al., 2018; Zhao et al., 2010). The N_2/CO_2 selectivity of the N_2-selective membrane is identical in all the optimisation

runs carried out. Therefore, as the N_2 permeance is increased, the CO_2 permeance also increases and thus, higher quantities of CO_2 also reports on the permeate side of the N_2 –selective membranes. This would constrain the system in terms of recovery, as CO_2 that is in permeate stream of the N_2-selective membrane may need to be recovered. Thus, no further reduction in cost is observed. The results also show that even when the N_2 permeance in the N_2-selective membrane is as low as 1.63×10^{-5} kmol/(m^2.s.bar) (25% of the reference), the N_2/CO_2 hybrid system is more cost-effective than the CO_2-selective process by 6%.

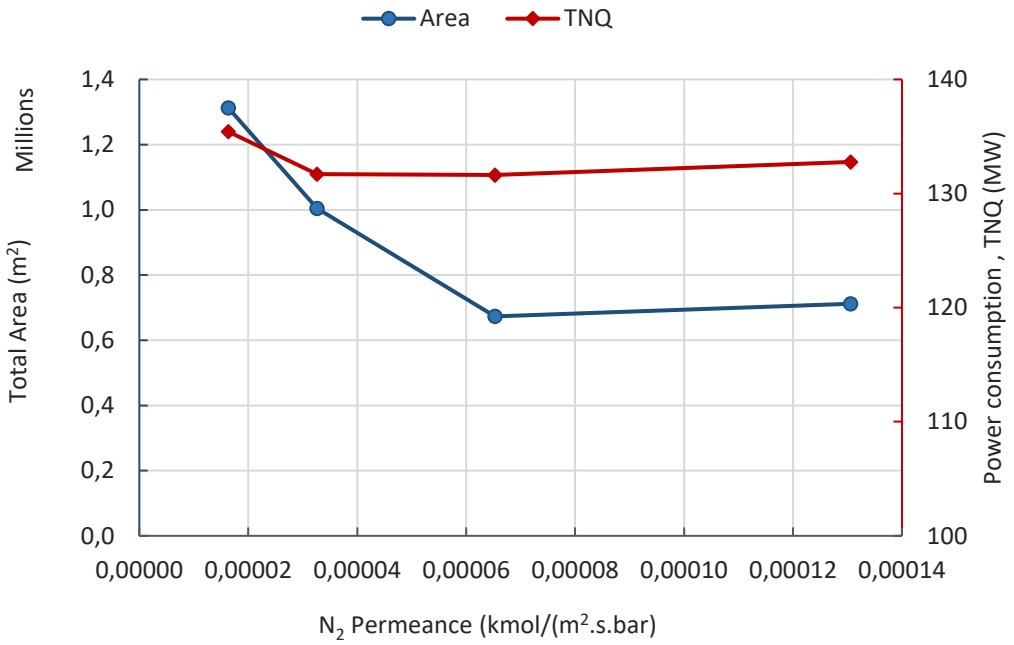

Figure 5.12. Effect of increased N_2 permeance in the N_2 selective membrane on the membrane area and power consumption of the N_2-CO_2 hybrid system

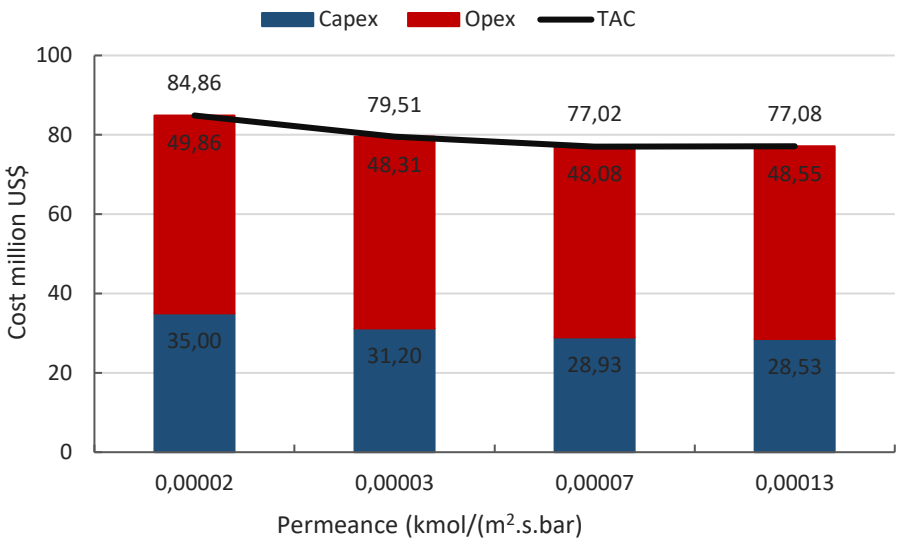

Figure 5.13. Impact of N_2 permeance in the N_2 selective membrane on the total annual cost of the N_2-CO_2 hybrid system

5.5.4 Sensitivity to N_2/CO_2 selectivity on the hybrid process

Table 5.14 shows the membranes of differing N_2/CO_2 selectivity simulated in multiple optimisation runs. The N_2, O_2, and H_2O permeance were not changed as presented in Table 5.2, so only the CO_2 permeance was the different parameter in each optimisation run. The membranes considered have the N_2/CO_2 selectivity varied as shown in Table 5.14. In each optimisation run, a membrane stage is fixed to operate an N_2- selective membrane to ensure a N_2/CO_2 selective membrane hybrid system.

Table 5.14: Selectivity of N_2/CO_2 in the different N_2 selective membranes#

Membrane name	Fraction of reference membrane	N_2/CO_2 selectivity
0.25MS	**0.25**	5.86
0.5MS	**0.5**	11.73
1MS	**1**	23.5
2MS	**2**	46.9

#Permeance, N_2= 6.53x10^{-5}; Selectivity, N_2/O_2, = 1000; N_2/H_2O=1000

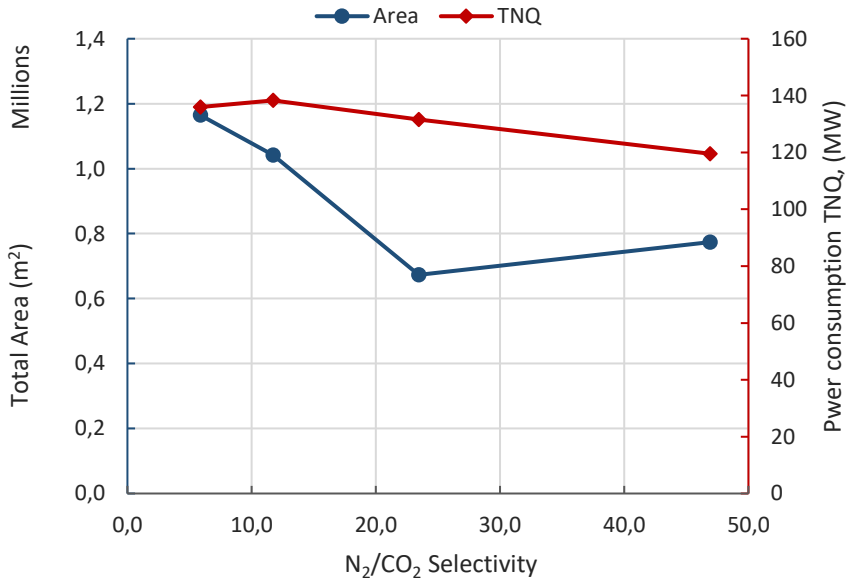

Figure 5.14. Effect of N_2/CO_2 selectivity in the N_2 selective membrane on the membrane area and power consumption of the N_2-CO_2 hybrid system

Figure 5.14 depicts the variation of the total membrane area and power consumption as the N_2/CO_2 selectivity increases. It is shown that the membrane area required initially decreases as the N_2/CO_2 selectivity is increased and then increases. While a lower N_2/CO_2 selectivity would result in insufficient N_2-CO_2 separation, very high N_2/CO_2 selectivity would increase CO_2 driving force, since the CO_2 composition is lower on the permeate side. Thus the membrane

area required initially decreases and then increases. This is consistent with the reports for CO_2 capture by use of a CO_2-selective membrane (Merkel et al., 2010; Zhao et al., 2010). The power consumption generally decreases with increasing N_2/CO_2 selectivity in the N_2 selective membrane. Figure 5.15 shows a general decrease in capital cost and operational cost. As a result, the annual cost of capture also decreases with increasing N_2/CO_2 selectivity of the N_2-selective membrane in the range investigated in this study. Increasing the N_2/CO_2 selectivity from 5.86 to 46.91 reduces the cost of capture by 26%. Doubling the N_2/CO_2 selectivity from 23.45 to 46.9 would further reduce the annualised cost by 11%, from US$77.02 million to 68.49. This is due to the reduced power consumption that consequently reduces operational costs. The results also show that the hybrid system is still more cost-competitive than the CO_2-selective membrane process, even at lower N_2/CO_2 selective such as 5.86 (25 % of the base case). Similar behaviour was observed in a simulation computational studies by Favre et al. (2009). It was noted that a low N_2/CO_2 selectivity in an N_2-selective membrane would be able to achieve higher capture targets even at a lower pressure ratio where a CO_2 selective membrane with higher CO_2/N_2 selectivity would fail.

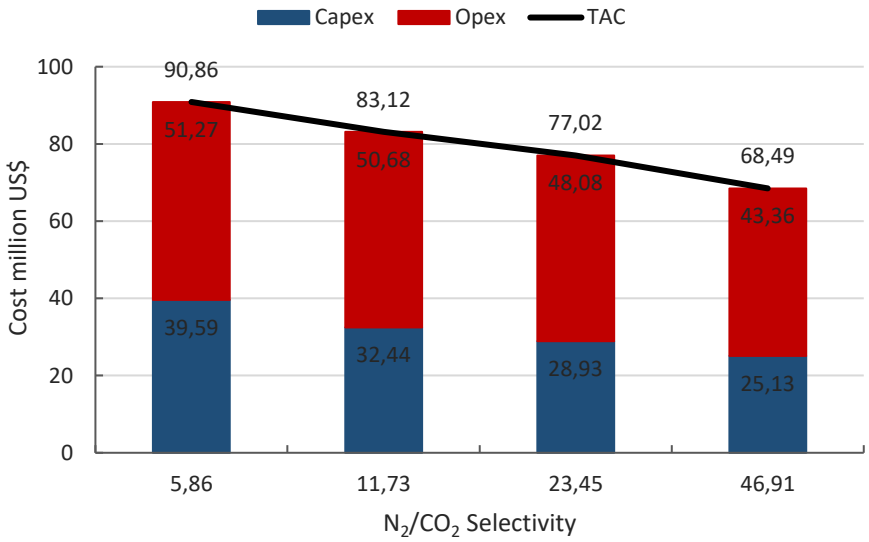

Figure 5.15. Impact of N_2/CO_2 selectivity in the N_2 selective membrane on the annual cost of the N_2-CO_2 hybrid system

The optimum process flow sheet shows that even at the lowest selectivity, the flue gas is first processed and separated by the N_2-selective membrane. With only one N_2-selective membrane being involved in the process and thus treating the flue gas first.

Investigations on the influence of CO_2/N_2 selectivity of the CO_2 selective membranes show that the cost of capture initially decreases with increasing selectivity up to about 50, and thereafter, insignificant changes in the cost is noted. Further work should be undertaken to further investigate the effects of selectivity and permeance beyond the range investigated in this study. Further study should assess the suitability of the hybrid system when CO_2 selective membranes of different permeance and selectivity values are considered.

5.6 Concluding remark

This study has presented a framework for the optimisation of membrane systems that can be used for the evaluation of new N_2-selective membranes and N_2-CO_2 hybrid system for CO_2 capture from coal-fired power plants. A superstructure based model was developed to optimise the CO_2 capture process from power plants when an N_2-selective membrane is employed. The model allows for the collection of the residue streams and product streams from both the retentate and permeate sides. Binary variables are included for automated determination of whether a stage operates an N_2-selective membrane or a CO_2-selective membrane. The model simultaneously optimises the operating membrane area, the retentate and permeate pressure.

The results indicate that superstructure based multistage optimised integrated process design is beneficial for further reduction of the cost associated with membrane carbon capture process. The N_2-selective membrane process results in a lower cost of carbon capture than the CO_2-selective membrane at low purity targets. Stripping the flue gas of N_2 with an N_2-selective membrane as the first stage in membrane based carbon capture reduces the total membrane requirement for the process significantly even at low N_2/CO_2 selectivity. The N_2-CO_2-selective hybrid membrane process results in the lowest cost of capture compared that of the N_2-selective membrane process and of the CO_2-selective membrane process. Therefore, the hybrid system is recommended for CO_2 capture though more experimental work on the development of N_2-selective membranes for CO_2 capture is required.

5.7 Nomenclature

Sets

N	{n|n membrane stage}
NP	{np|np alias of membrane stage}
I	{i|i component in a process stream} $i \in I = \{CO_2, N_2, H_2O, O_2\}$
K	{k|k compartments in membrane stage n}
RR	{rr|rr retentate recycle stream}
PR	{pr|pr permeate recycle stream}

Parameters

A^L	Lower bound of the membrane area size, m^2
A^U	Upper bound of the membrane area, m^2
C^{el}	Electricity tariff, *$/KW*
C^{mem}	Cost of membrane, *$/$$m^2$*
C^{rpl}	Cost of replacing membrane modules, *$/$$m^2$*
Mr	Relative molecular weight of component *i*, *kg/kmol*
P^{atm}	Atmospheric pressure (1 bar),*bar*
P^L	Pressure lower bound, *bar*
P^U	Pressure upper bound, *bar*
q_i	Permeance value of component i, *kmol/(m^2.br.s)*
R_i^{ftg}	Flowrate of component *i* in the flue gas stream, *kmol/s*
T^{atm}	Atmospheric temperature (298 K), *K*
T^{mem}	Operating temperature of the membrane, *K*
TMA	Total membrane area, m^2
γ	Specific heat ratio
η	Efficiency of compressor, vacuum, expander

Binary Variables

$Z_n^{CO_2}$ CO_2 selective membrane applies in membrane stage n

$Z_n^{N_2}$ N_2 selective membrane applies in membrane stage n

Z_n^{rwf} Flue-permeate mixture condenser exists in membrane stage n

Z_n^{wpm} Permeate condenser is in use in membrane stage n

Z_n^{wrt} Retentate knock out drum is in use in membrane stage n

Z_n^{wrp} Condenser on the retentate stream that is sent to product mixer

Z_n^{cr} Compressor on retentate recycle stream in membrane stage n

Z_n^{xr} Expander on retentate recycle is in use in membrane stage n

Continuous variables

A_n^{mem} Membrane area of stage n, m^2

DP_i Desired purity of the CO_2 enriched stream

DR_i Desired recovery of CO_2,

P_n^{pms} Pressure on the permeate side in membrane stage *n*, *bar*

P_n^{rts} Pressure on the retentate side in membrane stage *n*, *bar*

P_n^{ppw} Pressure after the dewatering product compressor in, *bar*

P^{sat} Saturation pressure at a particular temperature

Q_n^{cft} Duty of flue-permeate compressor *(cft)* in membrane stage *n*, *KW*

Q^{comp} Power consumed by product compressor, *KW*

Q^{pump} Power consumed by product pump, *KW*

Q_n^{exr} Power recovered by expander of residue stream *rto* in stage *n*, *KW*

Q_n^{ppw} Power consumed by the dewatering compressor of permeate product, *KW*

Q^{icp} Power consumed by product inter-stage compressor, *KW*

Q_n^{vac} Power consumed by the vacuum pump in stage *n* of membrane, *KW*

$Q_{n,np}^{xr}$ Power recovered by expander of retentate recycle membrane stage *n, K*

$Q_{n,np}^{cr}$ Power consumed by compressor of retentate recycle membrane stage *n ,K*

$R_{i,n}^{f}$ Flowrate of *i* in flue gas supplied to membrane stage *n, kmol/s*

R_{i}^{ft} Flowrate of component *i* exiting the flue gas condenser, *kmol/s*

$R_{i,n}^{fs}$ Flowrate of component *i* in the feed supplied to membrane stage *n, kmol/s*

$R_{i,n}^{ms}$ Flowrate of component *i* exiting flue permeate mixer in membrane stage *n, kmol/s*

$R_{i,n}^{fms}$ Flowrate of component *i* exiting flue-permeate condenser, stage *n, kmol/s*

R_{i}^{op} Flowrate of component *i* from final product mixer *kmol/s*

R_{i}^{oa} Flowrate of component *i* from residue mixer, *kmol/s*

$R_{i,n,k}^{pms}$ *F*lowrate *i* from compartment k on the membrane permeate side of stage n, *kmol/s*

$R_{i,n}^{pm}$ Flowrate of component *i* in permeate stream from condenser to splitter, *kmol/s*

$R_{i,n,pr}^{pmr}$ Flowrate of component *i* in recycled permeate stream *pr* from stage *n kmol/s*

$R_{i,n}^{pos}$ Flowrate of component *i* in the product stream from membrane stage *n, kmol/s*

$R_{i,n}^{rto}$ Flowrate of component *i* in residue stream in membrane stage *n kmol/s*

$R_{i,n}^{rt}$ Flowrate of component *i* in retentate after separator in membrane stage *n kmol/s*

$R_{i,n,rr}^{rtr}$ Flowrate of component *i in* retentate recycle stream *rr* from stage *n, kmol/s*

$R_{i,n}^{rts}$ Flowrate of component *i* from retentate side of membrane stage *n kmol/s*

$R_{i,n,k}^{rts}$ Flowrate component *i* from compartment *k* on the retentate side of stage *n, kmol/s*

R_{i}^{wc} Flowrate of component *i* condensed in the flue gas condenser, *kmol/s*

$R_{i,n}^{wf}$ Flowrate of component *i* condensed in the flue permeate gas condenser, *kmol/s*

$R_{i,n}^{wpm}$ Flowrate of *i* condensed in the permeate condenser in membrane stage *n, kmol/s*

R_{i}^{wpp} Flowrate of water condensed in the permeate product condenser, *kmol/s*

R_{i}^{wrp} Flowrate of water condensed in the retentate product condenser, *kmol/s*

R_i^{opc}	Flowrate of component *i* in stream from permeate product mixer, *kmol/s*
R_i^{opp}	Flowrate of component *i* in the final product stream, *kmol/s*
$R_{i,n}^{rpp}$	Flowrate of component *i* in retentate product stream after condenser, *n kmol/s*
$R_{i,n}^{rpo}$	Flowrate of component *i* in retentate product from retentate splitter, *n kmol/s*
TAC	Total annual cost, $/year
TLC	Total levelised cost, $/ton
TNQ	Total net power consumed by the capture process, *KW*
T_n^{cft}	Temperature of gas at outlet of flue permeate compressor from membrane *n, K*
x_n^f	Split fraction of flue gas flowing to membrane stage *n,*
x_n^{pos}	Split fraction for stream towards product from permeate splitter in stage *n*
$x_{n,pr}^{pmr}$	Split fraction of the recycle streams from permeate splitter in membrane stage *n*
$x_{n,pr}^{prto}$	Split fraction of the residue stream from permeate splitter in membrane stage *n*
$x_{n,rr}^{rtr}$	Split fraction of recycle streams from retentate splitter in membrane stage *n*
x_n^{rto}	Split fraction of residue stream towards residue mixer *n*
x_n^{rpo}	Split fraction of product stream from retentate splitter residue mixer *n*
$y_{i,n,k}^{pms}$	Mole fraction of component *i* at point k on the permeate side of membrane stage *n*
$y_{i,n,k}^{rts}$	Mole fraction of component *i at point k* on the retentate side of membrane *n*
$y_{i,n}^{rt}$	Mole fraction of component *i after the condenser* on the retentate side
$y_{i,n}^{fms}$	Mole fraction of component *i* in stream that exits the flue-permeate cooler of *n*
$y_{i,n}^{fs}$	Mole fraction of component *i* in feed stream to the membrane *n*
y_i^{opp}	Mole fraction of component *i* in permeate product from condenser
$\varphi_{i,n}$	Permeance of component *i* that applies in membrane stage *n, kmol/(m^2.bar.s)*

Chapter 6 – An assessment of the various strategies used in modelling, optimisation and techno-economic evaluation of membrane based CO_2 capture

6.1 Introduction

Several techno-economic studies for CO_2 capture by membranes have been carried out before (Cao et al., 2013; He et al., 2015; He and Hägg, 2011a; Shao et al., 2013; Zhai and Rubin, 2013). A review of the cost methods was carried out, and recommendations on how to calculate and report the cost of capture was presented (Rubin et al., 2013a; Rubin, 2013b). Khalilpour et al. (2014) reviewed techno-economic strategies and made a discussion on the economic evaluation of CO_2 capture by use of membranes. It was noted that there are variances in the cost methods and scope studied. The cost model by Van Der Sluijs et al. (1992) was found to be more comprehensive and closer to practical terms and has been adopted in a number of studies (Arias et al., 2016; Ramasubramanian et al., 2013; Van Der Sluijs et al., 1992; Zhai and Rubin, 2013). There are variances in the parameters used as input data for techno-economic feasibility studies and modelling and simulation of membrane based CO_2 capture processes. Whilst these are adequate in investigating and understanding the parameters that influence the economics of the membrane based CO_2 capture, comparison of the results of one study to the other is difficult, so is the comparison of membrane based CO_2 capture with amine absorption CO_2 capture.

There are differences in the set lower bound pressure when vacuum pumps are employed on the permeate side. Some studies have set 0.1 bar as possible minimum pressure (Hasan et al., 2012; Lee et al., 2018; Shao et al., 2013). However, several reports set 0.2 bar as the practical minimum pressure. The lower efficiency and the huge footprints of vacuum pumps may make the application of very low pressure such as 0.1 bar less economic (Merkel et al., 2010; Ramírez-Santos et al., 2018). There are also variations in the final storage pressure of the captured CO_2 when membrane based feasibility studies are undertaken. The final storage pressure reported varies between 80 bar to 150 bar (Arias et al., 2016; He et al., 2015; Shao et al., 2013). The membrane stage limit also varies with the feasibility report, ranging from a possible minimum of 5 m^2 to a maximum possible of 2 000 000 m^2 (Arias et al., 2016; Hasan et al., 2012; He and Hägg, 2014). A large membrane stage upper bound may lead to less energy consumed by the compressors. The definition of membrane stage seems to be different in some

reports where the first stage is referred to as pre-concentration even if two membrane units are used (Shao et al., 2013). However, most reports refer to a stage as a membrane unit (Hussain and Hägg, 2010; Murad Chowdhury et al., 2005).

Mathematical optimisation methods based on superstructures have been applied to understand CO_2 capture by use of membrane gas separation from power plants (Arias et al., 2016; Lee et al., 2018). However, as far as we could ascertain, none has reported the cost of zero CO_2 emission in detail. Arias et al. (2016) reported optimum results based on a range of set separation targets of CO_2 recovery of 90-98% and purity of 90-98%. Lee et al. (2018) reported on CO_2 recovery up to 99% at 95% purity. (Mores et al. (2019) reported high separation targets of recovery up to 98% recovery and 98% purity. A few reports have considered superstructure optimisation of CO_2 capture of multicomponent flue gas mixtures from coal power plants with numerous selecting to study CO_2/N_2 binary mixture (Arias et al., 2016; Hasan et al., 2012; Lee et al., 2018; Mores et al., 2019). Flue gas from coal power stations has a moisture content that is highly permeable in polymeric membranes, and it needs to be taken into account (Merkel et al., 2010). The removal of water from the process stream also results in lower flowrates of flue gas being handled by the compressors and can reduce the cost of capture (Pfister et al., 2017). Furthermore, CO_2/O_2 selectivity is comparable to that of CO_2/N_2 (Zamarripa et al., 2018). These factors have an impact on the process design by superstructure based optimisation.

In this study, the optimisation of post-combustion CO_2 capture by a common polymeric membrane from multicomponent flue gas from a coal-fired power plant is carried out in order to minimise the total annual cost of CO_2 capture. By carefully selecting reasonable and practical operating parameters, a superstructure based optimisation is carried out to achieve high separation targets similar to those achieved by chemical absorption of 99% and recovery ranging from 90% to 100% is imposed. An analysis of the cost associated with attaining zero CO_2 emission from coal-fired power plants is given. This is followed by a comparative study of the effect of cost models, allowable stages, allowable maximum membrane area, allowable minimum permeate pressure, permeation models on the global optimum and optimum operating conditions. The aim is for the differences to be known and for the comparison of one study to another to be made easier.

6.2 Problem statement

The problem statement is described below;

Given;

(i) A flue gas of known flowrate, components, composition, temperature and pressure
(ii) A predefined desired CO_2 product purity and desired minimum recovery of CO_2.
(iii) The permeance, selectivity and operating temperature of the membrane to be known.

Determine;

(i) Optimum membrane network system,
(ii) Optimum flowrates of the streams,
(iii) Optimum power consumption of the equipment,
(iv) Optimum membrane area of each stage and the
(v) Operating pressure on the feed and permeate sides of the membrane.
(vi) Minimum total annualised costs (TAC) for the membrane-based CO_2 capture system

6.3 Model description

The proposed superstructure is based on the framework presented by Uppaluri et al. (2004). The superstructure presented embeds numerous process routes. It allows feed to be sent to each membrane stage and also allows retentate and permeate recycle streams to be sent to any of the membrane stages. However, there are differences in the arrangement of splitters and mixers involved in the recycling of the permeate streams and the inclusion of the product condenser and residue expander. In this section, the superstructure and the description of the process, including the model constraints are presented. The model consists of flux constraints, mass balance, inequality expressions, logic constraints, the objective function, and finally, the cost models.

The following assumptions guide the development of the model;

(i) The plug flow regime is assumed, and concentration polarisation on the membrane is considered negligible (Arias et al., 2016).
(ii) Permeability of a component is constant and is not affected by pressure nor changes in concentration (Uppaluri et al., 2006);
(iii) Membrane operates isothermal and pressure drop is considered negligible along the membrane (Zhai and Rubin, 2013).

6.3.1 Superstructure description

Figure 6.1 gives the superstructure upon which the model is built. It shows several routes to process the flue gas and capture CO_2 and possible compressor vacuum options for the various stages. Flue gas from the de-sulphurising chamber at 40 °C and at a pressure of 1 bar is supplied to the CO_2 capture plant. The flue gas is cooled to 25 °C in a cooler condenser where some of the water condenses out of the flue gas stream. The flue gas can then be split and sent to the various membrane stages. The flue gas combines with permeate and product recycle streams is then compressed to membrane retentate pressure and cooled. The stream can be cooled or heated to bring the temperature to the membrane operating temperature (40 °C). This flue gas permeate recycle mixture is mixed with the retentate and residue recycle streams to become the membrane feed and is passed onto the feed side chamber of the membrane. The different components permeate according to the permeability. The un-permeated gas is the retentate and the permeated is the permeate. The permeate side operates at vacuum pressure as generated by vacuum pumps and the vacuum pumps discharge the permeate at 1 bar. The permeate is cooled and water can be condensed out. The permeate that exits the cooler condenser can be split and sent to the various stages as recycle or can be sent to a product mixer. The CO_2 concentrate from the product mixer passes through a splitter where the gas can be split and some of the product can be sent to the final product compressor and/or some to the recycle mixer to be processed again in the membrane. The first compressor raises the product pressure to enhance water removal by a subsequent cooler condenser for water to be removed from the gas stream. The captured CO_2 is compressed to 75 bar by an inter-stage compressor and then pumped to 150 bar before being sent for storage.

The retentate is also split and sent to the membrane stages as recycle stream and can also be sent to the retentate residue mixer. The stream from the residue mixer can be split and be

recycled to any membrane stage, and some or all of that gas can also be emitted into the atmosphere via an expander turbine that recovers some of the energy from the high-pressure stream. The residue is released into the atmosphere at 1 bar. *R* denotes the stream flowrate, *P* denotes the pressure of the stream, *y* is the mole fraction of component *i* and *n* refers to the membrane stage.

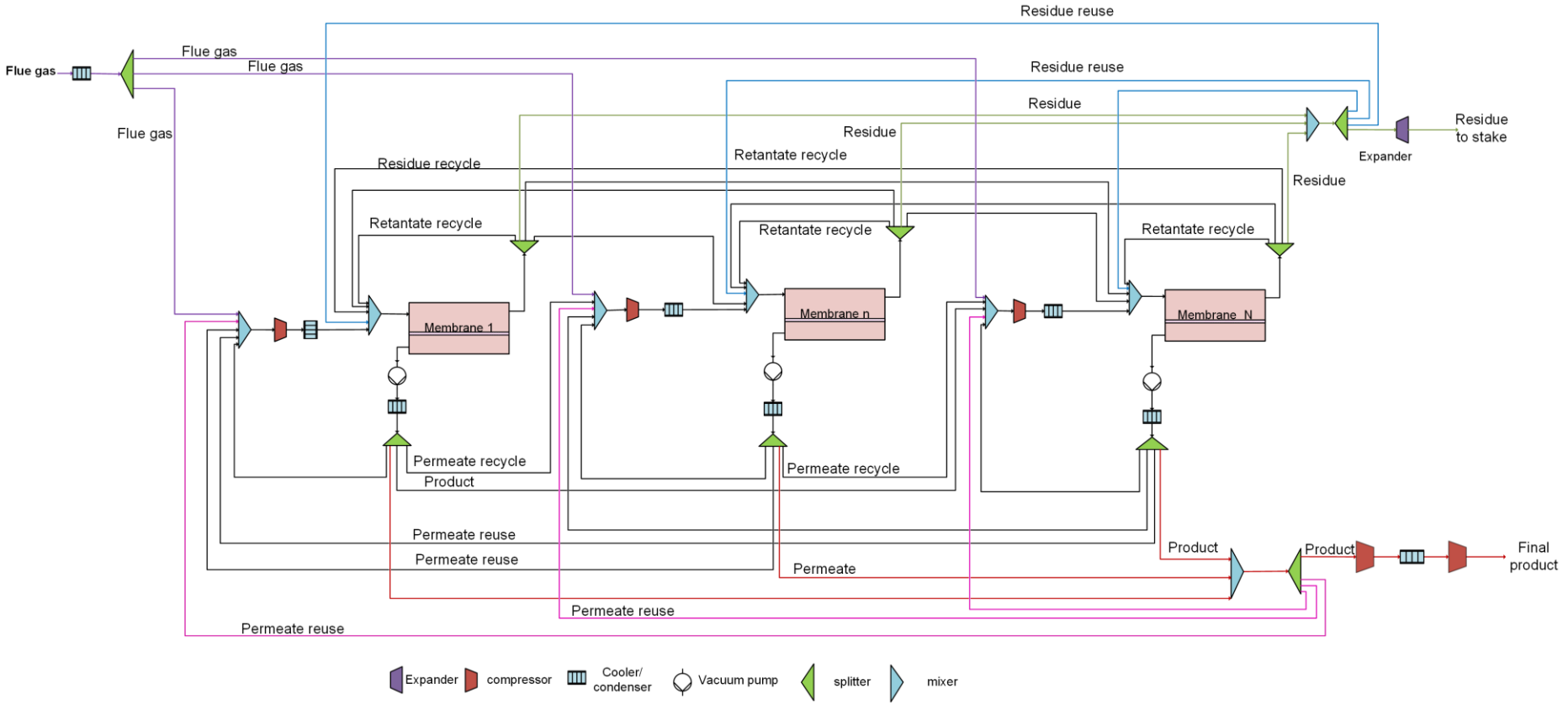

Figure 6.1. Superstructure representation of the membrane process system for CO_2 capture

6.3.2 Membrane permeation models

A countercurrent mode of operation is adopted for this work since it has been proven to yield better permeance than the cocurrent mode of operation (Pan, 1986). Three gas separation models for determining flux in membrane based CO_2 capture are given;

(i) The model previously presented and adapted for algebraic modelling software (permeation model A) (Arias et al., 2016)
(ii) A dedicated model for the treatment of multicomponent feed gas (Li et al., 1990) (permeation model B),
(iii) An approximate model widely used for gas separation by membranes (permeation model C) (Hasan et al., 2012; Uppaluri et al., 2006, 2004).

6.3.2.1 Permeation model A

The permeation model A is presented previously in section 5.3.2.

6.3.2.2 Permeation model B

The flux of gas component *i* through a differential area dA_n^{mem} of membrane stage *n* for a certain driving force is given by Equation (6.1). The flux is equal to the difference in the partial pressure of the component on the retentate and permeate sides of the membrane multiplied by the permeance (φ_i) of that component.

$$-\frac{d(R_n^{rt} \cdot y_{i,n,}^{rt})}{dA_n^{mem}} = \varphi_i \left(P_n^{rt} \cdot y_{i,n}^{rt} - P_n^{pms} \cdot y_{i,n}^{pms} \right) \qquad \forall i \in I,\, n \in N \tag{6.1}$$

Equation (6.2) states that the mole fraction of component *i* in the permeate is equal to the rate of change of the flowrate of that component with a change in the total flowrate in the gas stream.

$$y_{i,n}^{pms} = \frac{d(R_n^{rt} \cdot y_{i,n}^{rt})}{dR_n^{rt}} \qquad \forall i \in I, n \in N \tag{6.2}$$

Rearranging Equations (6.1) and (6.2) gives the differential equation shown in Equation (6.3). A sum of the permeate flow for all the components is given by Equation (6.4)

$$\frac{dy_{i,n}^{rt}}{dA_n^{mem}} = -\frac{1}{R_n^{rt}}\left[y_{i,n}^{rt} \cdot \frac{dR_n^{rt}}{dA_n^{mem}} + \varphi_i \left(P_n^{rt} y_{i,n}^{rt} - P_n^{pms} y_{i,n}^{pms} \right) \right] \qquad \forall i \in I, n \in N \tag{6.3}$$

$$\frac{d(R_n^{rt})}{dA_n^{mem}} = -\sum_i \varphi_i \left(P_n^{rt} y_{i,n}^{rt} - P_n^{pms} y_{i,n}^{pms} \right) \ \forall i \in I, n \in N \tag{6.4}$$

Figure 6.2 shows the flow of gas through a membrane area dA^{mem} of membrane stage *n*.

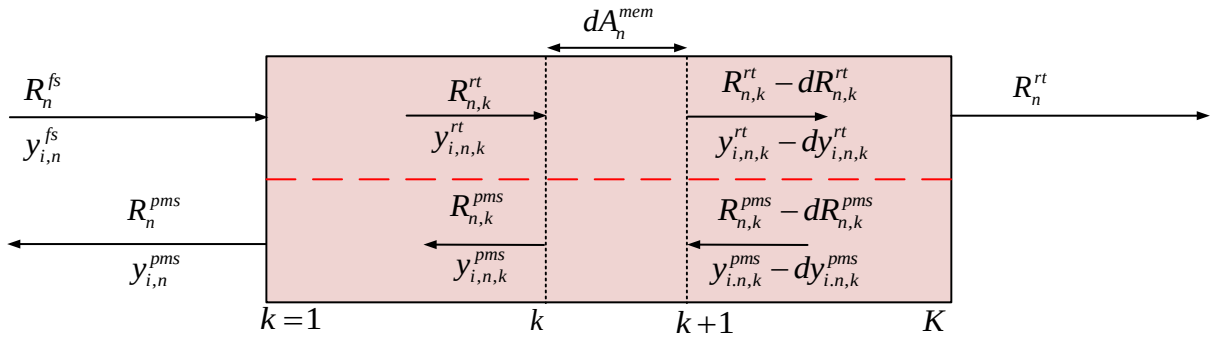

Figure 6.2. Flow of components through the membrane for countercurrent set

The discretisation of the term $\frac{d\left(y_{i,n}^{rt}\right)}{dA_n^{mem}}$ based on the central finite difference method in order to estimate the mole fraction of component *i* at $k=2$ yields Equation (6.5):

$$\frac{y_{i,n,k+1}^{rt} - y_{i,k-1}^{rt}}{2dA_n^{mem}} = \frac{(K-1)\left(y_{i,n,k+1}^{rt} - y_{i,k-1}^{rt}\right)}{2A_n^{mem}} \tag{6.5}$$

Applying backward finite difference method to discretise $\frac{d\left(y_{i,n}^{rt}\right)}{dA_n^{mem}}$ in order to compute the mole fraction of the components at k >2 results in Equation (6.6):

$$\frac{y_{i,n,k-2}^{rt} - 4y_{i,n,k-1}^{rt} + 3y_{i,n,k}^{rt}}{2dA_n^{mem}} = \frac{(K-1)\left(y_{i,n,k-2}^{rt} - 4y_{i,n,k-1}^{rt} + 3y_{i,n,k}^{rt}\right)}{2A_n^{mem}} \quad \forall i \in I \tag{6.6}$$

Similarly applying the discretisation to $\frac{d(R_n^{rt})}{dA_n^{mem}}$ and substituting in Equation (6.4) for the solution to points *k=2* and *k> 2* give Equations (6.7) and (6.8) respectively. Equations (6.7) and (6.8) describe the total retentate flowrate at the discretisation point k of membrane stage *n.*

$$\frac{K-1}{2A_n^{mem}}\left(-R_{i,n,k-1}^{rt}+R_{i,n,k+1}^{rt}\right)=-\sum_i \varphi_i\left(P_{i,n,k}^{rt}\cdot y_{i,n,k}^{rt}-P_{i,n,k}^{pms}\cdot y_{i,n,k}^{pms}\right) \qquad \forall n\in N, i\in I, \in K, k=2 \tag{6.7}$$

$$\frac{K-1}{2A_n^{mem}}\left(R_{i,n,k-2}^{rt}-4R_{i,n,k-1}^{rt}+3R_{i,n,k}^{rt}\right)=-\sum_i \varphi_i\left(P_{i,n,k}^{rt}\cdot y_{i,n,k}^{rt}-P_{i,n,k}^{pms}\cdot y_{i,n,k}^{pms}\right) \qquad \forall n\in N, \forall i\in I, \forall k\in K; k>2 \tag{6.8}$$

Substituting Equation (6.3) with the discretised expressions given in Equations (6.5) - (6.8) give Equations (6.9) and (6.10). Equations (6.9) and (6.10) give the mole fraction of component *i* at the discretisation points.

$$\frac{K-1}{2A_n^{mem}}\left(\left(-y_{i,n,k-1}^{rt}+y_{i,n,k+1}^{rt}\right)R_{n,k}^{rt}\right)=-\left[\begin{array}{l} y_{i,n,k}^{rt}\left(\frac{K-1}{2A_n^{mem}}\left(-R_{n,k-1}^{rt}+R_{n,k+1}^{rt}\right)\right)+ \\ \varphi_i\left(P_n^{rt}\cdot y_{i,n,k}^{rt}-P_n^{pms}\cdot y_{i,n,k}^{pms}\right)\end{array}\right] \qquad \forall n\in N, i\in I, k\in K; k=2 \tag{6.9}$$

$$\frac{K-1}{2A_n^{mem}}\left(\left(y_{i,n,k-2}^{rt}-4y_{i,n,k-1}^{rt}+3y_{i,n,k}^{rt}\right)R_{n,k}^{rt}\right)=-\left[\begin{array}{l} y_{i,n,k}^{rt}\left(\frac{K-1}{2A_n^{mem}}\left(R_{n,k-2}^{rt}-4R_{n,k-1}^{rt}-3R_{n,k}^{rt}\right)\right)+ \\ \varphi_i\left(P_n^{rt}\cdot y_{i,n,k}^{rt}-P_n^{pms}\cdot y_{i,n,k}^{pms}\right)\end{array}\right] \qquad \forall n\in N, i\in I, k\in K; k>2 \tag{6.10}$$

The ratio of the total permeate flowrate to the feed flowrate in a membrane stage is known as the stage cut. The stage cut (ϕ) of membrane stage *n* is given by Equation (6.11).

$$\phi_n=\frac{R_n^{pms}}{R_n^{fs}} \qquad \forall n\in N \tag{6.11}$$

Equation (6.12) gives the overall material balance around the membrane in stage *n*. It shows that the sum of the permeate and the retentate is equal to the gas fed to the membrane. Similarly, Equation (6.13) gives the component balance over the area bounded from *k=k to k= K*.

$$R_{n,k}^{rt} = R_{n,K}^{rt} + R_{n,k}^{pms} \qquad \forall n \in N, k \in k \tag{6.12}$$

$$R_{n}^{fs} \cdot y_{n}^{fs} = R_{n,K}^{rt} \cdot y_{i,n,K}^{rt} + R_{n,k}^{pms} \cdot y_{i,n,k}^{pms} \qquad \forall n \in N, i \in I, k \in K \tag{6.13}$$

Substituting Equation (6.12) into Equation (6.13) gives Equation (6.14).

$$y_{i,n,k}^{rp} = \frac{y_{i,n,k}^{rt} \cdot R_{n,k}^{rt} - ((1-\phi_n) \cdot R_{n}^{fs} \cdot y_{i,n,K}^{rt})}{R_{n,k}^{rt} - ((1-\phi_n) \cdot R_{n}^{fs})} \qquad \forall n \in N, i \in I, \forall k \in K \tag{6.14}$$

The summation of the mole fraction of the components can only be equal to 1 as stated by Equation (6.15).

$$\sum_{i} y_{i,n,k}^{rt} = 1 \qquad \forall n \in N, \forall k \in K \tag{6.15}$$

Permeate output flowrate of component *i* from membrane stage *n* and the retentate output of component *i* from membrane stage *n* is given by Equation (6.16) and Equation(6.17).

$$R_{i,n}^{pms} = R_{i,n,k=1}^{pms} \qquad \forall n \in N, i \in I, k \in K; k = 1 \tag{6.16}$$

$$R_{i,n}^{rt} = R_{i,n,k=K}^{rt} \qquad \forall n \in N, i \in I, k \in K; k = K \tag{6.17}$$

6.3.2.3 Permeation model C

The ‘compartmentalisation’ method used by Shah and Kokossis (1997) in improving the synthesis of plug flow and well mixed multiphase reactors was adopted in modelling membrane gas permeation by Uppaluri et al. (2004). The model was specifically applied to membrane based CO_2 capture by Hasan et al. (2012). The approximate model assumes that the membrane can be divided into compartments. Figure 6.3 shows the schematic illustration of the membrane.

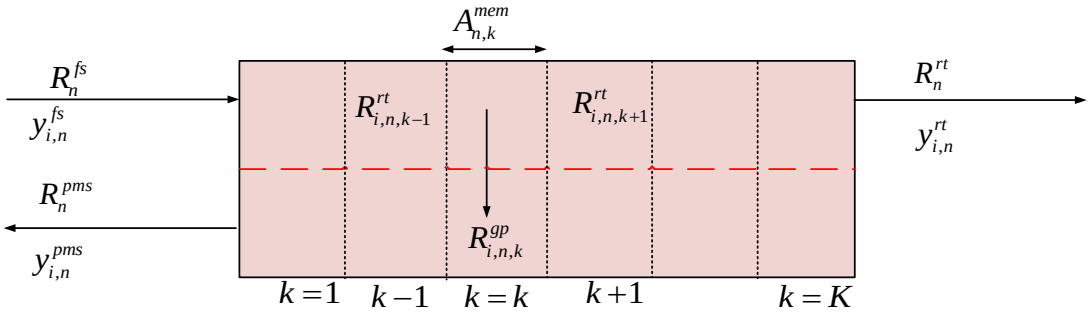

Figure 6.3. Countercurrent mode of flow in a membrane module

Permeation of gas component *i* from the high pressure (retentate) side to the low pressure (permeate) side of the compartment is given by Equation (6.18). It states that the flowrate of gas component *i* across the membrane of compartment *k* is a product of the permeance, area and the difference in the partial pressure of component *i* on the retentate and permeate side.

$$R_{i,n,k}^{gp} = \varphi_i (P_n^{rt} \cdot y_{i,n,k}^{rt} - P_n^{pms} \cdot y_{i,n,k}^{pms}) A_{n,k}^{mem} \qquad \forall n \in N, i \in I, k \in K \tag{6.18}$$

The total membrane area of membrane stage n is then a sum of the area of each 'compartment' as given by Equation (6.19).

$$A_n^{mem} = \sum_{K=1}^{K} A_{n,k}^{mem} \qquad \forall n \in N \tag{6.19}$$

Equation (6.20) - (6.22) are material balances of component i on the retentate side. Equation (6.20) states that the flowrate of *i* that has permeated is equal to the loss in flowrate of *i* on the retentate side compartment *k*. Equation (6.21) shows the component balance around the first compartment $k=1$. Equation (6.22) is the component balance around compartments $k-1$ and *k*.

$$R_{i,n,k}^{gp} = -R_{i,n,k}^{rt} \qquad \forall n \in N, i \in I, k \in K \tag{6.20}$$

$$R_{i,n,k=1}^{rt} = R_{i,n}^{fs} - R_{i,n,k=1}^{gp} \qquad \forall n \in N, i \in I \tag{6.21}$$

$$R_{i,n,k}^{rt} = R_{i,n,k-1}^{rt} - R_{i,n,k}^{gp} \qquad \forall n \in N; i \in I, k \in K; k > 1 \tag{6.22}$$

Equation (6.23) and (6.24) give the material balance of component *i* on the permeate side. The flowrate of *i* at *k=K* is equal to that which has permeated across the membrane. Equation (6.24) provides the flowrate of *i* at *k* as a sum of the flowrate of *i from k+1* and the flow that permeated in *k*.

$$R_{i,n,k=K}^{pms} = R_{i,n}^{gp} \qquad \forall n \in N, i \in I, k \in K; k = K \tag{6.23}$$

$$R_{i,n,k}^{pms} = R_{i,n,k+1}^{pms} + R_{i,n,k}^{gp} \qquad \forall n \in N, i \in I, k \in K; k < K \tag{6.24}$$

Equations (6.25)and (6.26) are constraints that ensure that the sum of the mole fractions of all the components is equal to one.

$$\sum_i y_{i,n,k}^{pms} = 1 \qquad \forall n \in N, k \in K \tag{6.25}$$

$$\sum_i y_{i,n,k}^{rt} = 1 \qquad \forall n \in N, k \in K \tag{6.26}$$

Permeate output flowrate of *i* from membrane stage *n* and the retentate output of *i* from membrane stage *n* is given by Equation (6.27) and Equation (6.28) respectively.

$$R_{i,n}^{pms} = R_{i,n,k=1}^{pms} \qquad \forall n \in N, i \in I, k \in K, k = 1 \tag{6.27}$$

$$R_{i,n}^{rt} = R_{i,n,k=K}^{rt} \qquad \forall n \in N, i \in I, k \in K, k = K \tag{6.28}$$

6.3.3 Material balance constraints

Material balances are carried out around splitters; flue gas splitter, retentate splitter and permeate splitter and the condenser. Equations (6.29) and (6.30) give the balance on the flue gas around the condenser.

$$R_i^{ftg} = R_i^{ft} + R_i^{wc} \qquad i \in I,\ i = H_2O \tag{6.29}$$

$$R_i^{ftg} = R_i^{ft} \qquad \forall i \in I,\ i \neq H_2O \tag{6.30}$$

Equation (6.31) shows that the sum of the split fractions of the flue gas is equal to one. The flowrate of the flue gas sent to membrane *n* is a product of the split fraction and the total flue gas flowrate from the power plant (R^{ft}) as given by Equation (6.32). Equation (6.33) gives the flowrate of component *i* as the product of the split fraction and the flowrate of *i* in the feed flue gas (R_i^{ft}).

$$\sum_n x_n^f = 1 \tag{6.31}$$

$$R_{i,n}^f = x_n^f R_i^{ft} \qquad \forall i \in I, n \in N \tag{6.32}$$

$$R_i^{ft} = \sum_n R_{i,n}^f \qquad \forall i \in I \tag{6.33}$$

The material balance around the membrane feed mixer is given by Equation (6.34). The flowrate of component *i* supplied to the retentate side of the membrane is a sum of the flowrate of that component in the flue gas received from the flue gas splitter, permeate recycle streams *(pmr)* and product recycle streams *(opr)* sent to the membrane stage *n*.

$$R_{i,n}^{ms} = x_n^f R_i^{ft} + \sum_{pr} x_{n,pr}^{pmr} R_{i,n}^{pm} + x_n^{opr} R_i^{opc} \qquad \forall i \in I, \forall n \in N \tag{6.34}$$

The stream is compressed to membrane retentate pressure and thereafter, if the water partial pressure exceeds the saturation pressure the cooler condenser condenses out the excess water and the balances are given by Equation (6.35) and Equation (6.36).

$$R_{i,n}^{msw} = R_{i,n}^{ms} - R_{i,n}^{wf} \qquad \forall i \in I, i = H_2O, \forall n \in N \tag{6.35}$$

$$R_{i,n}^{msw} = R_{i,n}^{ms} \qquad \forall i \in I, i \neq H_2O, \forall n \in N \tag{6.36}$$

The permeate recycle and flue gas combine with the retentate *(rtr)* and residue *(oar)* recycle to make up the feed to the membrane *(fs)* as depicted by Equation (6.37).

$$R_{i,n}^{fs} = R_{i,n}^{msw} + \sum_{rr} x_{n,rr}^{rtr} R_{i,n}^{rt} + x_n^{oar} R_i^{oac} \qquad \forall i \in I, \forall n \in N \tag{6.37}$$

Equation (6.38) gives the flowrate of component *i* in the retentate recycle stream. Equation (6.39) gives the flowrate of component *i* in the permeate recycle streams.

$$R_{i,n,rr}^{rtr} = x_{n,rr}^{rtr} R_{i,n}^{rt} \qquad \forall i \in I, \forall rr \in RR \tag{6.38}$$

$$R_{i,n,pr}^{pmr} = x_{n,pr}^{pmr} R_{i,n}^{rt} \qquad \forall i \in I, \forall pr \in PR \tag{6.39}$$

Equation (6.40) shows that the sum of the split fractions of the retentate stream splitter always amounts to one.

$$x_n^{rto} + \sum_{rr} x_{n,rr}^{rtr} = 1 \qquad \forall n \in N \tag{6.40}$$

The flowrate of component *i* that is sent to the residue mixer is a product of the split fraction and the flowrate of component *i* in the retentate stream as stated by Equation (6.41). The material balance around the residue mixers is given by Equation (6.42). It states that the stream that exits the mixer is a sum of the residue streams.

$$R_{i,n}^{rto} = x_n^{rto} R_{i,n}^{rt} \qquad \forall n \in N, \forall i \in I \tag{6.41}$$

$$R_i^{oac} = \sum_n R_{i,n}^{rto} \qquad \forall i \in I \tag{6.42}$$

The sum of the split fraction for the residue stream that is emitted (x^{oa}) and the split fraction of the residue streams that are recycled (x_n^{oar}) is equal to one as ensured by Equation (6.43). The flowrate of the residue stream that is emitted to the atmosphere is given by the product of the residue split fraction and the total residue stream as shown by Equation (6.44):

$$x^{oa} + \sum_{n} x_n^{oar} = 1 \tag{6.43}$$

$$R_i^{oa} = x^{oa} R_i^{oac} \qquad \forall i \in I \tag{6.44}$$

The permeate *(pms)* that leaves the membrane passes through a cooler and as separator to remove water that can condense out at the cooling temperature. The resultant permeate stream *(pm)* is sent to the permeate splitter. Equation (6.45) is the water molar balance around the condenser and Equation (6.46) ensures that it is only water that leaves the permeate stream and the flowrates of the other components remain the same as the stream exits the condenser. The molar fraction of the water that is swept by the gas is given by the partial pressure as given by Equation (6.56). The binary variable, Z^{wo} denotes the existence or non-existence of the condenser depending on a feasible water flowrate as given by the lower and upper bounds described by Equation (6.48).

$$R_{i,n}^{pm} = R_{i,n}^{pms} - R_{i,n}^{wo} \qquad \forall n \in N, i \in I, i = H_2O \tag{6.45}$$

$$R_{i,n}^{pm} = R_{i,n}^{pms} \qquad \forall n \in N, i \in I, i \neq H_2O \tag{6.46}$$

$$y_{i,n}^{pm} P_n^{pm} - P_i^{sat} = 0 \qquad (T) \qquad \forall i \in I, i = H_2O, n \in N \tag{6.47}$$

$$R^L Z_n^{wo} \leq R_{i,n}^{wo} \leq R^U Z_n^{wo} = 0 \qquad \forall i \in I, i = H_2O \tag{6.48}$$

Equation (6.49) states that the sum of the split fraction for the product stream and the permeate recycle streams is one.

$$x_n^{pos} + \sum_{pr} x_{n,pr}^{pmr} = 1 \qquad \forall n \in N \tag{6.49}$$

Equation (6.50) shows that the flowrate of component *i* in the product stream from membrane stage n is a product of the split fraction and the permeate flowrate. The product streams ($R_{i,n}^{pos}$)

are summed before being sent to a cooler condenser to give a resultant flowrate of component *i*, (R_i^{opw}) as given by Equation (6.51):

$$R_{i,n}^{pos} = x_n^{pos} R_{i,n}^{pm} \qquad \forall n \in N, \forall i \in I \tag{6.50}$$

$$R_i^{opc} = \sum_n R_{i,n}^{pos} \qquad \forall i \in I \tag{6.51}$$

Equation (6.52) ensures that the sum of split fraction for the product stream that is sent for storage (x^{op}) and the split fraction of the streams that are recycled (x_n^{opr}) is equal to one. The flowrate of the product stream that is sent for storage is equal to the product of the product recycle split fraction and the total product stream as given by Equation (6.53).

$$x^{op} + \sum_n x_n^{opr} = 1 \tag{6.52}$$

$$R_i^{opw} = x^{op} R_i^{opc} \qquad \forall i \in I \tag{6.53}$$

The material balance around the condenser is given by Equation (6.54). Equation (6.55) ensures that it is only water that is removed by the condenser. Equation (6.56) optimises the pressure of the stream that exits the product compressor which is dependent on the water mole fraction and the saturation pressure at the temperature of the cooled stream.

$$R_i^{opw} = R_i^{wp} + R_i^{op} \qquad i \in I \tag{6.54}$$

$$R_i^{opw} = R_i^{op} \qquad i \in I,\ i \neq H_2O \tag{6.55}$$

$$yR_i^{op} \cdot P^{pw} = P^{sat}\ (T) \qquad i \in I,\ i = H_2O \tag{6.56}$$

6.3.4 Objective function

The objective of this study was to minimise the total annualised cost (TAC) of the CO_2 capture during post-combustion capture using a membrane process at set capture targets as described

in previous chapters. The TAC is a sum of the annualised capital costs and the operating costs (Equation (6.57)). The annualised capital costs usually include the cost of purchase and installation. The operating cost is dominated mainly by the cost of electricity that is used for driving the compressors and to a less extent, the cost of labour and maintenance.

$$\min\left[TAC\right] = OPEX + CAPEX \tag{6.57}$$

6.3.5 Cost Models

Three cost models (designated in this study as A, B and C) were considered for a comparative study to investigate the impact of a cost model on the resulting global optimum. Cost model A has been used extensively for the estimation of the cost of membrane based CO_2 capture (Van Der Sluijs et al., 1992; Zhai and Rubin, 2013). The annual capital expenditure (CAPEX) is the total cost of the operational units including installation cost per year and this is annualised by a capital recovery factor (CRF). Cost model A considers a factor of 1.37 to account for general facilities such as offices and contingencies that may arise whereas the other cost models do not explicitly factor this in. The model as reported takes into account the heat transfer area of coolers as capital expense. The operating cost per year is the sum of the operational and maintenance cost (COM) which is taken as a fraction of the capital cost and the cost of the net electricity consumed by the compressors. The cost of maintaining the membrane modules is 1 % of its purchase cost and that of maintaining the rest of the units is 3.6% of the purchase cost.

Cost model B has been applied and reported for membrane based gas separation (Uppaluri et al., 2006, 2004). It was also specifically applied to CO_2 capture in several works (Hasan et al., 2012; Zamarripa et al., 2018). The capital cost of compressors and vacuum pumps is estimated by Guthrie's correlation which includes the purchase and installation cost (Douglas, 1989; Hasan et al., 2012). The cost of membrane includes the purchase cost and the cost of replacement. The model considers the quantity of cooling water as an operational expense.

Cost model C has also been used for CO_2 capture techno-economic studies (Chu and He, 2018; He et al., 2015; He and Hägg, 2014). The cost model C is less complex and less non-linear than cost model B. It considers the total capital cost as a sum of the purchase cost and installation, and unforecastable costs that are assumed to be 18 % of the purchase cost. It is also assumed

that the annual capital recovery factor is 0.2. The cost of the membrane used in the carbon capture process is a sum of the purchase cost and the cost incurred in replacing the membrane and. The sum is considered to be part of the capital cost. The annual operational cost is a sum of the net electricity consumed in running the compressors and vacuum pump and the labour cost incurred for the number of hours the plant is online per year. The model considers the cost of only major equipment and considers the contribution cost of minor units such as heat exchangers as negligible.

6.3.5.1 Cost model A

Cost model A has been presented in the previous chapter 5, section 5.3.7.

6.3.5.2 Cost model B

The Capex is given by the sum of the equipment purchase cost and the cost of membrane multiplied by an annualisation factor of 0.154 as given by Equation (6.58). The capital cost of compressors and vacuum pumps is estimated by Guthrie's correlation which includes the purchase and installation cost (Douglas, 1989; Hasan et al., 2012). The cost of membrane includes the purchase cost and the cost of replacement.

$$CAPEX = 0.154(EPC + (C^{mem} \cdot TMA)) \tag{6.58}$$

The annualised cost of the membrane includes the purchase cost of the permeator case and actual membrane, the cost of installation as well as the cost involved in the replacement of the membrane module inside the permeator.

$$EPC = (CC^{cft} Z^{pr}) + CC^{comp} + CC^{pump} + \sum_n CC^{vac} + (CC^{exr} Z^{pr}) + \sum_n CC_n^{cfr} Z^{pr} \tag{6.59}$$

The capital cost of a compressor is given by Equation (6.60). This is applicable to the flue gas compressor, permeate recycle compressor and CO_2 product inter-stage compressor *(ico)* and the vacuum pumps (Equations (6.60)-(6.61)). The cost of the expander was calculated similarly as given in Equation (6.62). The Marshall and Swift index of 1638.2 for the year 2018 was used.

$$CC^{comp} = \left(\frac{M\ \&\ S}{280}\right) + 5.17.5\left(Q^{comp} \cdot C^{comp}\right)^{0.82}\left(2.11 + b^{comp}\right) \tag{6.60}$$

$$CC^{vac} = \left(\frac{M\ \&\ S}{280}\right) + 5.17.5\left(Q^{vac} \cdot C^{vac}\right)^{0.5}\left(2.11 + b^{vac}\right) \tag{6.61}$$

$$CC^{exr} = \left(\frac{M\ \&\ S}{280}\right) + 5.17.5\left(1/\eta\, Q^{exr} \cdot C^{exr}\right)^{0.82}\left(2.11 + b^{exr}\right) \tag{6.62}$$

The sum of the cost of electricity and the cooling water used in the coolers make up the operating cost as stated by Equation (6.63). The electricity cost is given by Equation (6.64) and the cost of cooling water by Equation (6.65). Equation (6.66) shows that the total mass of cooling water required is a sum of the cooling water utilised by each cooler to meet the heat exchange demand of that cooler.

$$OPEX = EC + C^{mcw} \tag{6.63}$$

$$EC = 6570 \cdot 0.05 \cdot TNQ \tag{6.64}$$

$$C^{cw} = mcw\ (3600 * 6570) \tag{6.65}$$

$$mcw = mcw^{cft} + \sum_{n} mcw_{n}^{cfr} + mcw^{clco} + mcw^{clrwp} \tag{6.66}$$

6.3.5.3 Cost model C

Cost model C has been presented previously in Chapter 3, section 3.3.9.

6.4 Illustrative example

The resulting Mixed-Integer Non-Linear Program was implemented in the GAMS 24.3.3 environment and solved by BARON on the NEOS server platform. The model is applied to a case reported in literature (Zhai and Rubin, 2013). The study considers a 550 MW producing power plant with a flue gas flowrate of 22.32 kmol/s. The simulated membrane has a permeance of 1000 GPU (3.4×10^{-5} $kmolm^{-2}s^{-1}bar^{-1}$) and a CO_2/N_2 selectivity of 50, CO_2/O_2 selectivity of 30 and CO_2/H_2O selectivity of 1 (Merkel et al., 2010). These specifications have also been used in other studies with minor variations (Lee et al., 2018; Mores et al., 2019; Zhai and Rubin, 2013).

The Table 6.1 shows the assumed flue gas characteristics and listed in Table 6.2 are the economic specifications. Permeation model A and cost model A are the basis used in the assessment unless stated otherwise. The lower bound for the permeate pressure was set at 0.2 bar unless stated otherwise (Merkel et al., 2010). The upper bound for the membrane area was set at 1 000 000 m^2 considering the various values reported in literature which vary from 600 000 m^2 to 1 500 000 m^2 and other studies do not report on the upper membrane area bound (Arias et al., 2016; He et al., 2015; Lee et al., 2018). The design and model operates a uniform retentate pressure in all the stages and non-uniform permeate pressure and thus the pressure ratio can be non-uniform for the membrane stages.

Table 6.1: Flue gas and membrane specifications

Parameter	Value
Flue gas flowrate, $kmols^{-1}$	22.321
Membrane Temperature, ℃	40
Flue gas pressure, bar	1.013
CO_2 concentration	0.12
N_2 concentration	0.73
H_2O concentration	0.10
O_2 concentration	0.05
Membrane permeance of CO_2 , $kmolm^{-2}s^{-1}bar^{-1}$	0.0000335
Membrane CO_2/N_2 selectivity	50
CO_2/H_2O selectivity	1
CO_2/O_2 selectivity	30

Table 6.2: Cost Model A economic data

Parameter	Value
Capacity factor %	75
Compressor, vacuum, expander efficiency %	85
Adiabatic compression coefficient,	1.4
Capital recovery factor, yr^{-1}	0.113
Membrane price US$$m^{-2}$	50
Reference frame cost, US$	2,300,000.00
Compression unit cost, US$ KW^{-1}	670
Inter-stage compression and pump cost, US$ KW^{-1}	902
Expander unit cost, US$ KW^{-1}	500
Equipment cost factor for housing,	1.80

Reference heat exchanger, US$m^{-2}	300
Electricity cost, US$ KW-h^{-1}	0.05
Process facilities capital cost, %	37
Maintenance cost of membrane	1%TCC^{mem}
Maintenance cost of compressors and heat exchangers	3.6% of CC^{unit}
Membrane lifetime, yr	5
Project life time, yr	25
Operating time, h yr^{-1}	6570

6.5 Results and discussion

The results obtained in this study are split into two sections. The first section highlights the results of optimisation for the reference cases of 95% and 99% final product purity at the different recovery from 90% to 100%. The second section makes an analysis of the assumptions that can affect the cost of CO_2 capture and the corresponding optimum values of the variables. The notation r90p95 refer to an optimisation run where the recovery is set at 90% and desired purity is set at 95%. The permeation model A and cost model A have been the basis of the simulation unless otherwise stated. The investigation carried out in this chapter has been limited to two stage and three stage membrane systems only as carried out in a previous study and also for the purpose comparison and analysis that this work seeks to achieve (Lee et al., 2018). Whilst it is possible that at higher separation targets, four stage membrane system could result in an optimal solution, two and three membrane stages are more practical and likely to be adopted at large scale earlier (Qi and Henson, 1998; Xu et al., 2019). Furthermore, to illustrate the possibility of 100% capture under these more practical conditions is prudent.

6.5.1 Effect of increased recovery and purity and assessment of the cost associated with zero CO_2 emission

Figure 6.4 shows the optimum process flow diagram, optimum stream flowrates; optimum operating pressure values, area of coolers, and the energy consumed by various units for 90%

recovery and 95% purity. The process flow shows a three stage membrane network. The flue gas is not split and is sent to the first membrane stage. The permeate composition is 54% CO_2. This permeate combined with the permeate from the third stage is fed to the second membrane stage for separation. The second stage permeate flows to the condenser to remove water from the final product stream before it is compressed and liquefied for storage.

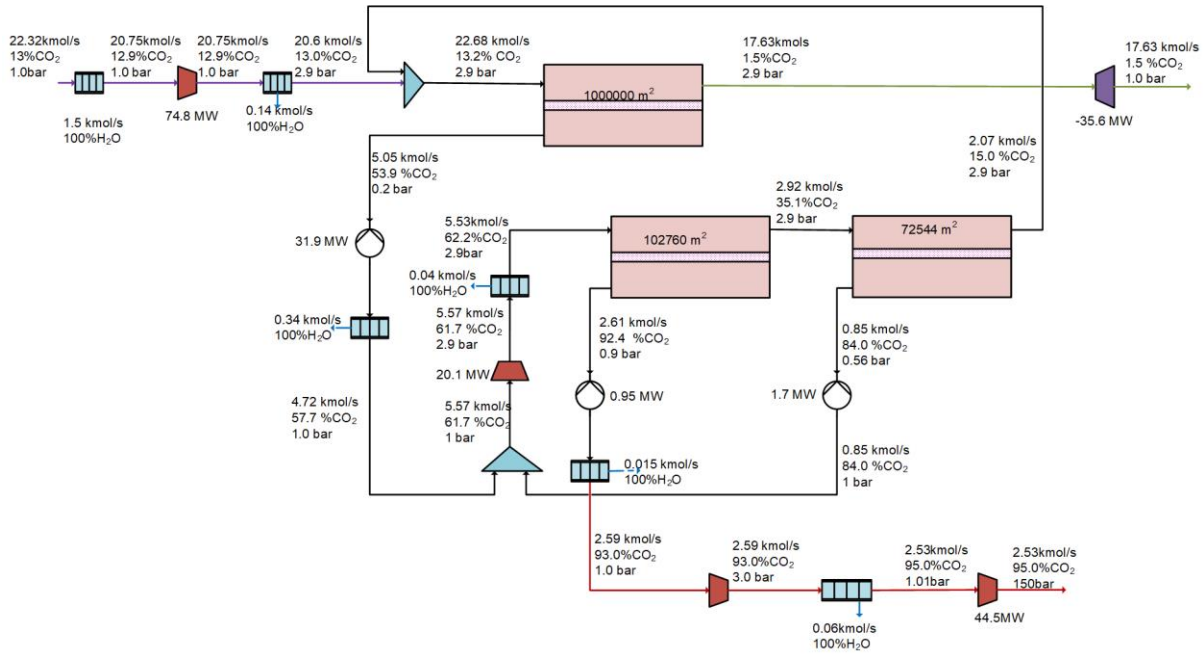

Figure 6.4. Optimum membrane network for CO_2 recovery of 90% and target purity of 95%.

The figures Figure 6.5 and Figure 6.6 are the process flow diagrams obtained to achieve r100p95 and r100p99, respectively. It is observed that the process flow charts are more complex than the one presented for a recovery of 90%. The permeate from the membrane stage that makes up the final product stream is at about 1 bar. The other two stages operate at a higher driving force than the membrane stage from which the product is collected.

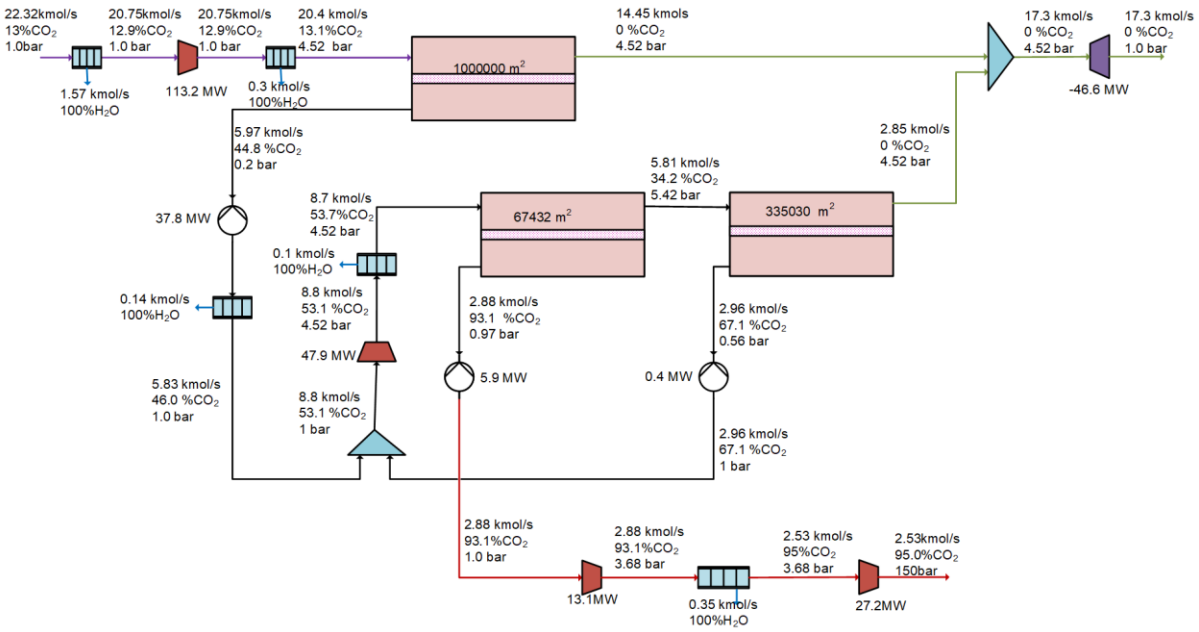

Figure 6.5. Optimum membrane network for CO_2 recovery of 100% and target purity 95%.

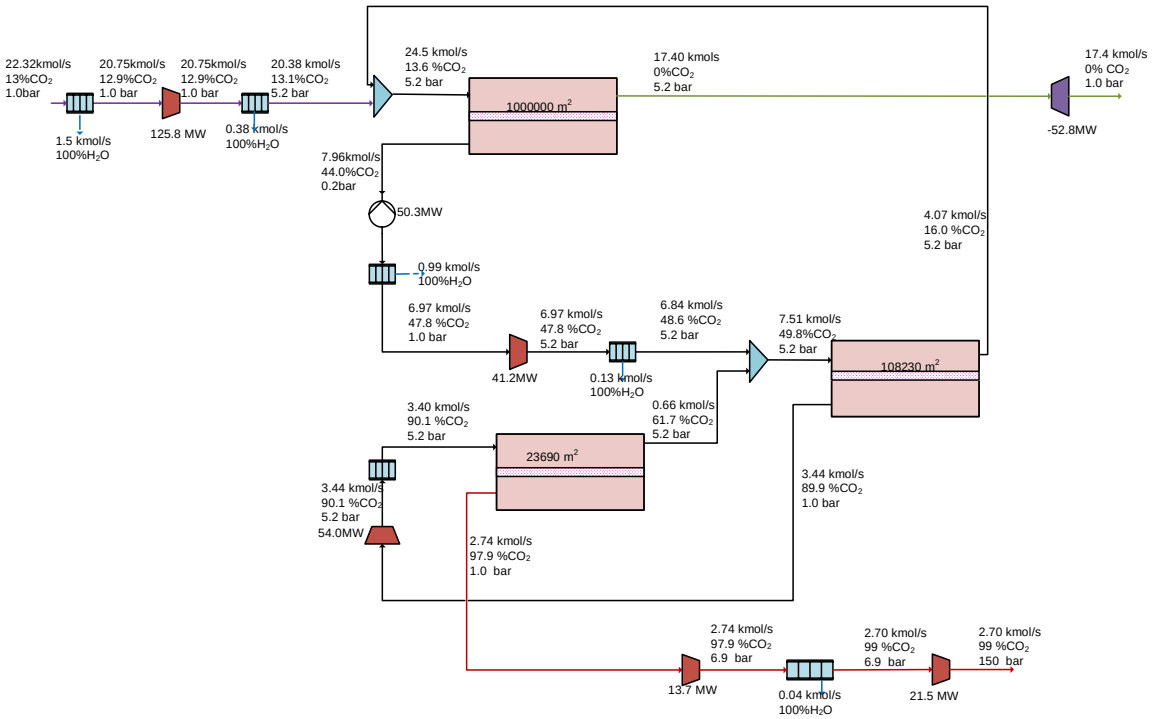

Figure 6.6. Optimum membrane network for CO_2 recovery of 100% and target purity 99%.

Table 6.3 gives the optimum values of important variables for the selected 3 cases of r90p95, r100p95 and r100p99. For the reference case of r90p95, the operating cost contributes 55% of the total annualised costs and the capital cost contribute 45%. High operating cost is attributed to the huge amounts of electricity required to run the compressors and the vacuum pumps. The expander recovers 21% of the total energy consumed. The total membrane area required is 1.8 million m^2. For r100p95 and r100p99 the total membrane area required is 1.4 million m^2 and 1.25 million $m^{2,}$ respectively. The net power consumption increases by 53.5% for r100p95 and by 74.2% for r100p99 compared to r90p95. The annualised cost increases by 29.1% to achieve 100% recovery when the product purity is maintained at 95%. For r100p99, the cost of capture rises by 39.1 % to US$50.1 /ton from US$36.0 for r90p95.

Table 6.3: Comparison of optimum results for 100% recovery at different purities

Parameter	**r90p95**	**r100p95**	**r100p99**
Number of membrane stages	3	3	3
Desired recovery	90	100	100
Desired purity	95	95	99
CO_2 capture rate, (ton/h)	413.70	459.61	459.61
Total membrane ($\times 10^6$ m^2)	1.18	1.40	1.25
Total power (MW)	165.1	245.5	275.8
Total net power (MW)	129.5	198.8	225.6
Power recovered (MW)	35.6	46.6	50.2
Heat transfer area (m^2)	32358.5	39663.2	41935.0
Operating costs ($\times 10^6$ US$)	49.4	74.8	84.3
Capital costs ($\times 10^6$ US$)	41.0	54.6	55.6
TAC ($\times 10^6$ US$)	90.4	129.5	139.8
TLC (US$/ton)	36.02	46.5	50.1
% difference	-	29.1	39.1

Figure 6.7 shows that the optimum membrane area fluctuates as the set recovery is increased. However, the net power consumption steadily increases with increasing set recovery target. A sharp increase is also observed for the change from 99% recovery to 100% recovery.

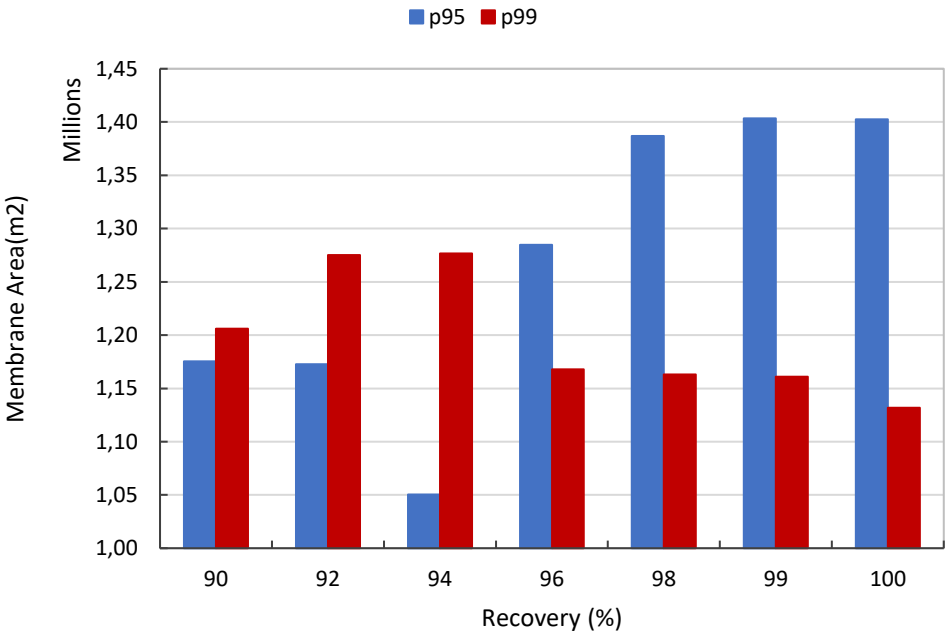

Figure 6.7. Effect of the recovery on the membrane area for purity 95% and 99%.

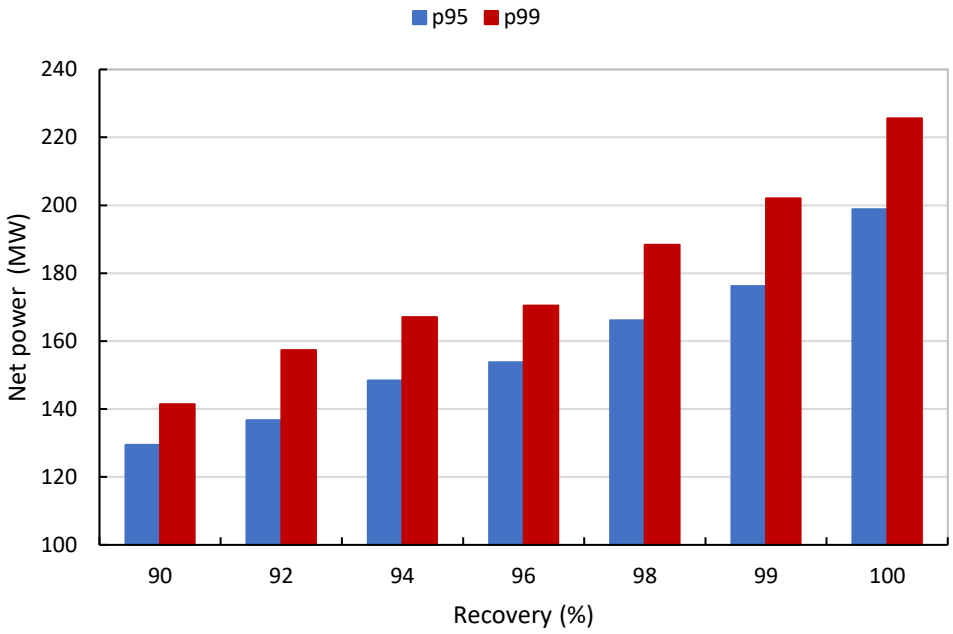

Figure 6.8. Effect of recovery on the net power consumption for purity 95% and 99%.

From Figure 6.8, it is evident that the power consumption increases with an increase in both the purity and recovery. It is apparent that higher energy is needed to achieve higher purity.

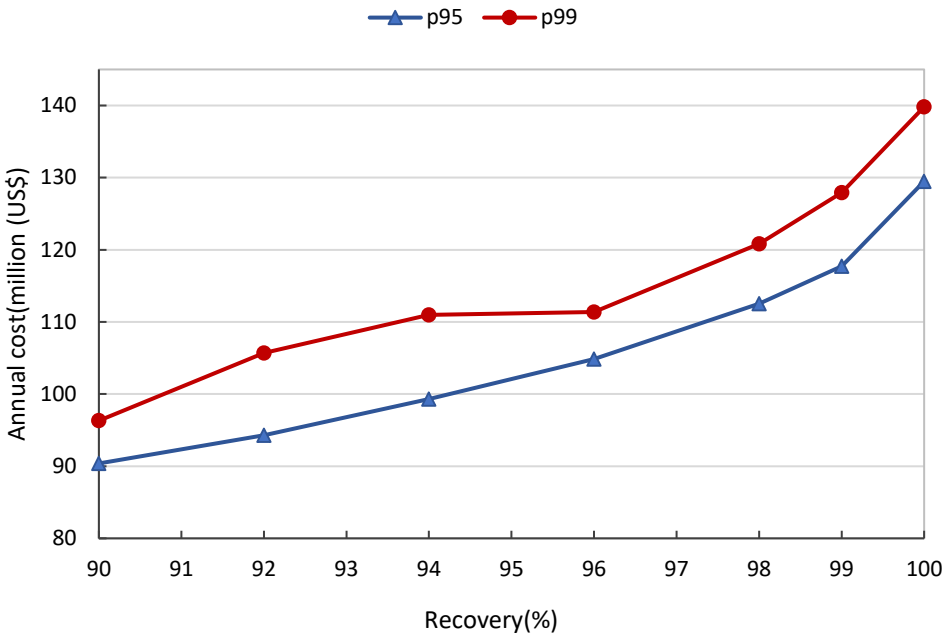

Figure 6.9. Effect of recovery on total annual cost for purity 95% and 99%.

The total annualised cost increases significantly for CO_2 recovery above 98% as shown by Figure 6.9, with r100p99 experiencing a sharper increase than r100p95. A sharp increase is observed from recovery 96% and even steeper from 99% to 100%. This is co-related to power consumption. Higher capture targets (recovery and purity) demand a larger membrane area and higher energy consumption. The pressure difference across the membrane needs to be high in order to meet the driving force required in order to achieve higher recovery.

6.5.2 Assessment of the strategies used in modelling and techno-economic evaluation of membrane based CO_2 capture

In the techno-economic studies, various assumptions on the various parameters were made. The impact of the variation in assumptions on the results of optimisation are presented in this section.

6.5.2.1 Comparison between two stage and three stage results

Figure 6.10 shows the optimum membrane areas for the two stage membrane system and the three stage system at different separation targets. 2sp99 refers to the result obtained for the two

stage system and product purity of 99% and thus, similarly, 3sp95 is for the case considering three membrane stages and product purity of 95%. Figure 6.10 shows that generally, at lower recovery, the two stage configurations require less total membrane area than the three membrane stages. At higher recovery from 96% recovery, the 3sp95 requires the largest membrane area.

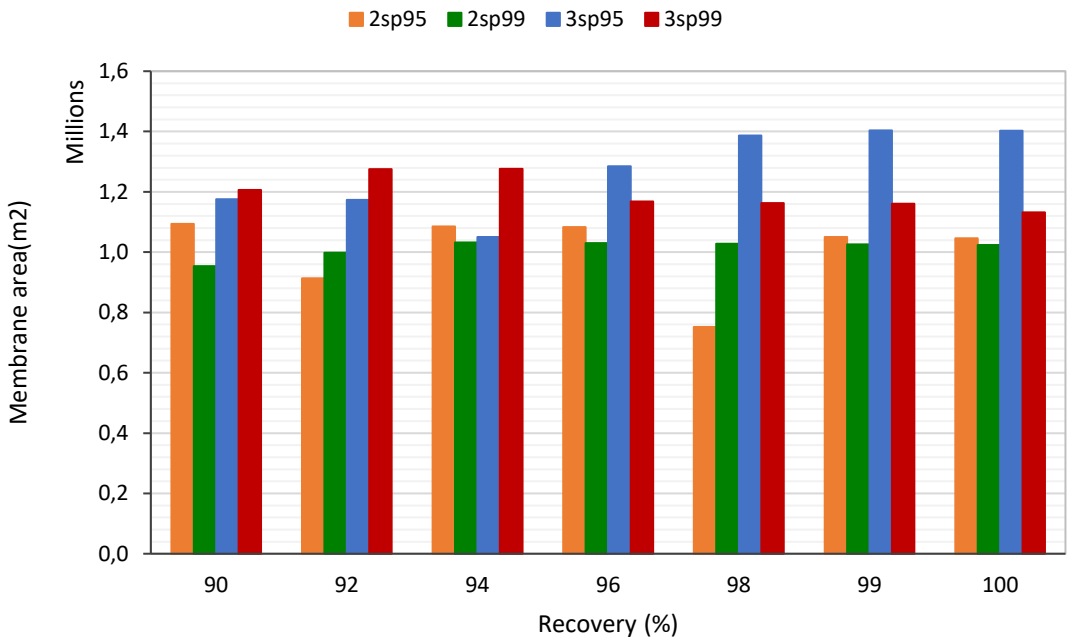

Figure 6.10. Effect of CO_2 recovery on membrane area for 2 stage and 3 stage optimisation at different CO_2 recovery.

Figure 6.11 shows that for a purity of 95%, there is negligible difference in the net power consumption between two membrane stage and three membrane stage systems up to 96 % recovery. As the recovery target reaches 96% the net power consumed in the three stage membrane becomes significantly less than that for a two stage membrane capture process. Significantly higher power consumption is noted for 2sp99.

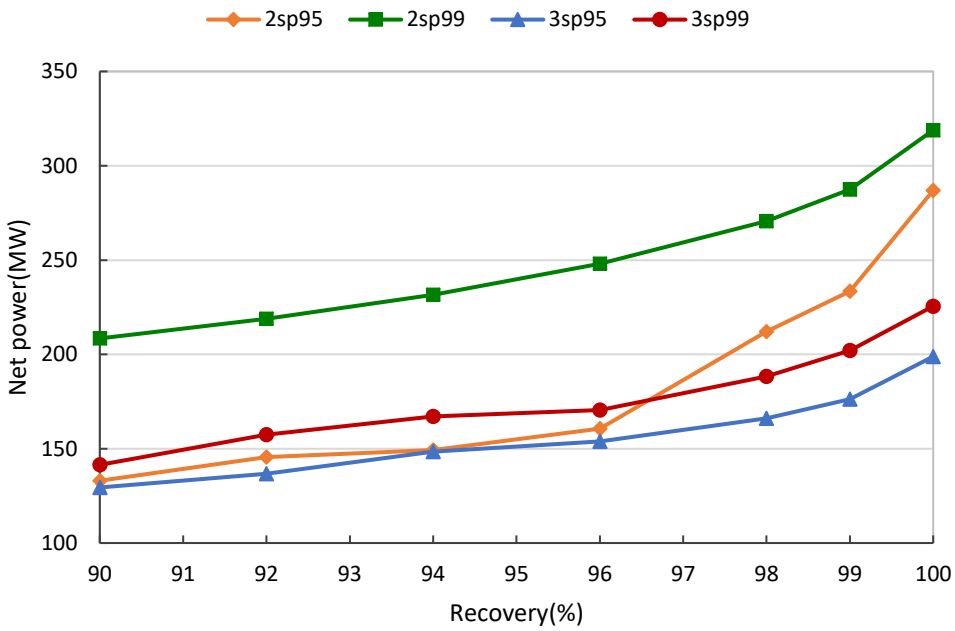

Figure 6.11. Net power consumption for two stage and three stage optimisations at different CO_2 capture targets

Figure 6.12 shows the levelized cost of CO_2 capture as a function of the recovery. It is apparent that the cost of capture is co-related to the energy consumption of the process. At a purity of 95% the difference in the total annual cost of the two stage and three membrane stage processes is small but significant differences are noted from a recovery of 96%.

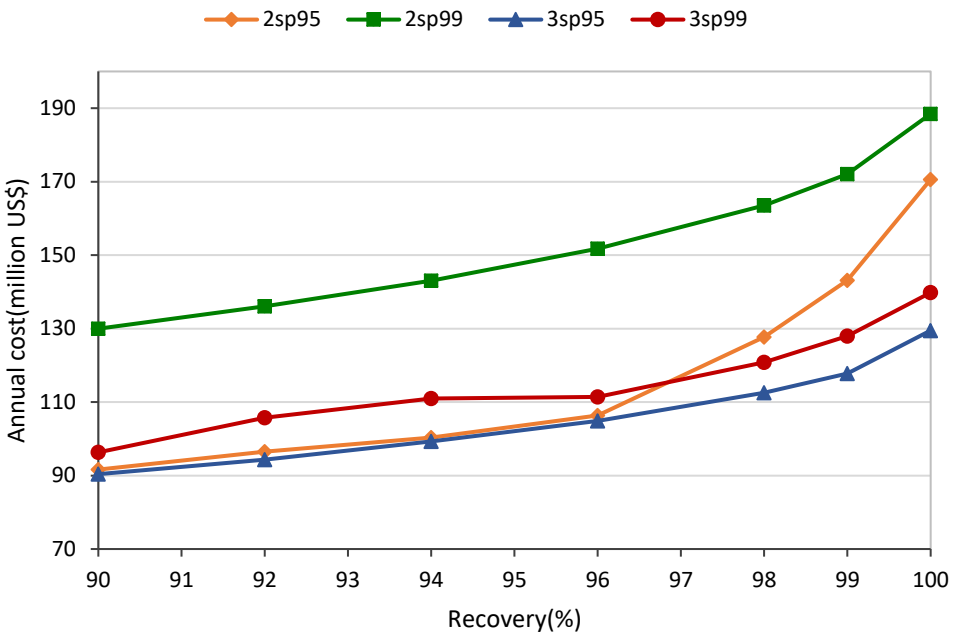

Figure 6.12. Annualised cost capture for two stage and three stage optimisations at different CO_2 capture targets

A two stage membrane is sufficient to achieve a purity of 95% and recovery up to 96%. However, for higher capture targets, i.e. recovery greater than 96% and purity greater than 95% a three stage membrane is desirable since it entails a lower total cost of CO_2 capture.

Lee et al. (2018) realised a higher capture cost for a two stage than a three stage. Arias et al. (2016) found two stage and three stage designs to produce suboptimal solutions. Based on their superstructure 4 stages were found to be optimum. Gabrielli et al. (2017) also analysed two to six membrane stages and found three stages to be the optimal number of stages. An increase in stages increases the possible total membrane area. There is a trade-off between the power requirements of additional compressors to the energy demand of additional recycle streams. After which, the power to process extra recycle streams exceed that required by fewer streams. The introduction of extra membrane stages also increases the possible total membrane. A larger membrane area may be favoured at the expense of higher pressure ratios and this results in lower CO_2 capture cost for three membrane stages than two membrane stages. More membrane stages enable more recycle streams which increases the CO_2 concentration of the streams that are fed to the membrane for separation. A higher CO_2 content translates to a higher partial pressure difference, enabling the process to operate at lower pressure, thus saving energy

consumption that compressors and vacuum pumps would otherwise supply. The superstructure, process design and assumed membrane area upper bound for which the optimisation is based on seem to also have an influence on the optimum number of stages.

6.5.2.2 Effect of selected membrane module size upper bound

Table 6.4 shows the results obtained when optimisation is carried out at different upper bound of the membrane area (UBMA) for the reference case of r90p95. Optimisation runs are carried out with the membrane areas of each stage set at upper bound of 500 000 m^2, 1 000 000 m^2 and 1 500 000 m^2. The range was selected based on a range reported in literature for a comparable flowrate of gas (He et al., 2015; Lee et al., 2018). The maximum total area possible is a product of the membrane upper bound of the stage and the number of stages in the process design. For comparison purposes the optimisation runs were carried out based on a three membrane stage system. The optimisation carried out when the upper bound is set at 500 000 m^2 is here named 0.5M and that carried out at 1 000 000 m^2 and 1 500 000 m^2 are termed 1M and 1.5M respectively. Negligible differences in the CAPEX, OPEX and total annual cost can be noted. The optimisation results show that the total membrane area for the three membrane units for the three cases (0.5M, 1M and 1.5M) is less than 1 500 000 m^2 even though all three stages can reach this potential maximum.

Table 6.4: Comparison of optimum results for varying the upper bound of a stage membrane area

	500 000 m^2	1 000 000 m^2	1 500 000 m^2
Number of mem stages	3	3	3
Recovery	0.90	0.90	0.90
Purity	0.95	0.95	0.95
CO_2 capture rate, (ton/h)	413.68	413.68	413.68
Total membrane ($\times 10^6$ m^2)	1.09	1.18	1.23
Total power (MW)	170.0	165.1	164.1
Total net power (MW)	133.5	129.5	128.9
Power recovered (MW)	38.89	35.6	35.1
Operating costs ($\times 10^6$ US$)	50.9	49.4	49.3
Capital costs ($\times 10^6$ US$)	41.0	41.0	41.4
TAC ($\times 10^6$ US$)	91.9	90.4	90.6
TLC (US$/ton)	36.6	36.02	36.15

Table 6.5 shows the results when separation targets are increased to a recovery of 98% and purity 99%. 0.5M gives a total membrane area of just 0.68 million m^2 which is much less than the maximum possible of 1 500 000 m^2. 1.0M and 1.5M have a total membrane area of 1.6 million m^2 and 1.72 million m^2, respectively. It is clear that the membrane area is a limiting factor in the case of 0.5M. This is compensated by a large pressure difference across the membrane to give a large driving force to meet the high separation targets set for the optimisation. This results in very high power consumption in order to achieve the set recovery and purity of the product stream. The process with membrane size upper bound of 0.5M resulted in the highest net power consumption. The net power consumption was 238.7 MW, and for 1M and 1.5M it was 189.0 MW and 171.3 MW, respectively. The higher power demand

was the major contributor to the total cost as operating cost accounts for 55.1 % at 1.5M; at 1 M it accounts for 58.6%, and at 0.5M it accounts for 62.9%.

Table 6.5: Comparison of optimum results for different maximum membrane areas

Membrane Upper bound	500 000 m^2	1 000 000 m^2	1 500 000 m^2
Number of mem stages	3	3	3
Recovery	0.98	0.98	0.98
Purity	0.99	0.99	0.99
CO_2 capture rate, (ton/h)	450.42	450.42	450.42
Total membrane ($\times 10^6$ m^2)	0.68	1.16	1.72
Total power (MW)	294.8	228.5	209.0
Total net power (MW)	238.7	189	171.3
Power recovered (MW)	56.1	44.5	37.7
Operating costs ($\times 10^6$ US$)	88.5	70.8	64.9
Capital costs ($\times 10^6$ US$)	52.1	50.0	52.8
Total cost ($\times 10^6$ US$)	140.7	120.8	117.7
Levelized cost (US$/ton)	51.49	44.23	43.09
% difference	-	12.1	16.3

Figure 6.13 shows the capital and operating cost and the total annual cost. Increasing the maximum membrane area from 0.5M to 1M and also to 1.5M reduces the cost of CO_2 capture by 12.1% and 16.3% respectively. However, increasing from 1M to 1.5M only reduces the cost of capture by only 2.6 % showing that a further increase in maximum allowable membrane area would not result in much further savings in the cost of capture.

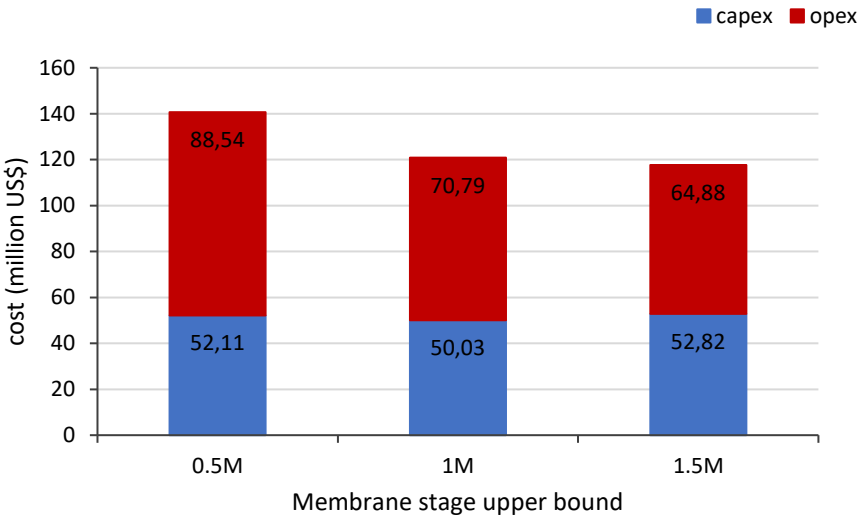

Figure 6.13. Graph showing the capital and operating cost at different maximum membrane areas for CO_2 recovery 98% and purity 99%

6.5.2.3 Effect of choice of cost model

Comparison of the optimum results obtained when three cost models from literature are used is carried out. The cost model total annual cost is a sum of the capital cost and operating cost. The cost model A (CMA), cost model B (CMB) and cost model (CMC) are described in detail in section 6.3.5.

Shown in Table 6.6 is the comparison of the optimum values obtained. The optimum membrane area obtained for CMA is 1.18 million m^2 and that obtained for CMB and CMC is 1.26 million m^2 and 0.97 million m^2, respectively. The capital cost obtained for CMB and CMC is 4.3% and 46.3% more than CMA. For CMB, a greater optimum membrane area, higher CRF and also the Guthrie's correlation for calculation of the cost of compressors contributed to the higher capital cost. CMC involves a higher capital recovery which contributes to the higher capital cost. The capital recovery factor is related to the interest rate.

Figure 6.14 and Figure 6.15 give the annual cost of capture, the total membrane area and net power consumption obtained for the optimisation runs based on the different cost models. There is a small difference in the net power consumed for the three cost models, which is less than 4%. The operating cost obtained for CMA and CMB are comparable, however, the

operating cost for CMC is less than that of CMA by 10%. The operating cost is higher for the optimisation run based on CMA since it includes maintenance cost and the cost of electricity. CMC consider the cost of electricity and the cost of cooling, which is negligible. The cost of CO_2 capture obtained for optimisation carried out based on CMB and CMC is US$37.18 and US$41.63, which is 3% and 16% higher than the CMA. Mores et al. (2019) also noted that the capital recovery factor had a significant impact on the capital cost and had the largest impact on the annualised total cost when they made it a variable with values ranging from 0.113 to 0.226. The capital recovery factor for CMC is 0.2 whilst that of CMA is 0.113; as a result, the capital cost obtained for the optimisation based on CMC is higher than that of CMA despite the lower membrane area.

Table 6.6: Comparison of optimum results for varying cost models

	Cost model A	Cost model B	Cost model C
Number of mem stages	3	3	3
DR	0.9	0.9	0.9
DP	0.95	0.95	0.95
CO_2 capture rate, (ton/h)	414	414	414
Total membrane ($\times 10^6$ m^2)	1.18	1.26	0.97
Total power (MW)	165.1	163.4	174.3
Total net power (MW)	129.5	129.5	135.4
Power recovered (MW)	35.6	33.9	39.1
Operating costs ($\times 10^6$ US$)	49.4	50.5	44.5
Capital costs ($\times 10^6$ US$)	41.0	42.7	59.96
TAC ($\times 10^6$ US$)	90.4	93.3	104.5
TLC (US$/ton)	36.03	37.18	41.63
% difference in TAC	-	3.2	15.6

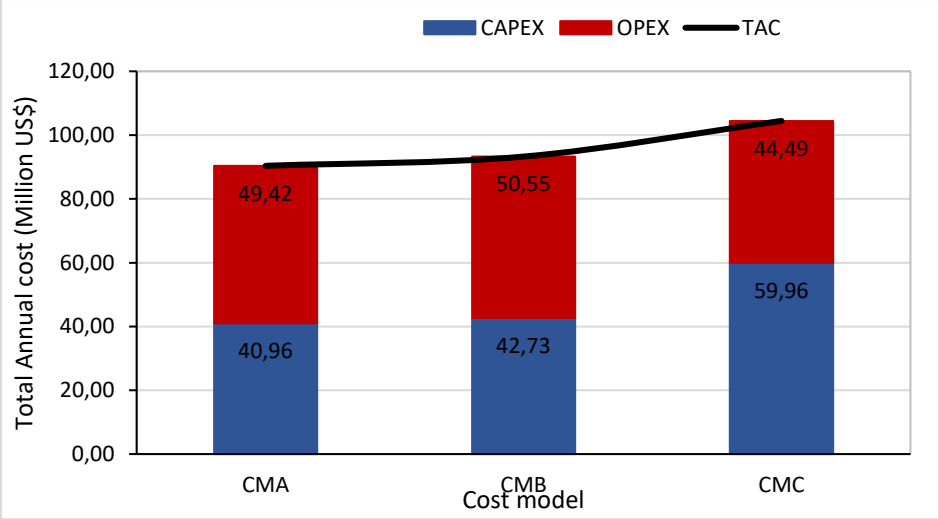

Figure 6.14. CAPEX, OPEX and TAC for the various cost models

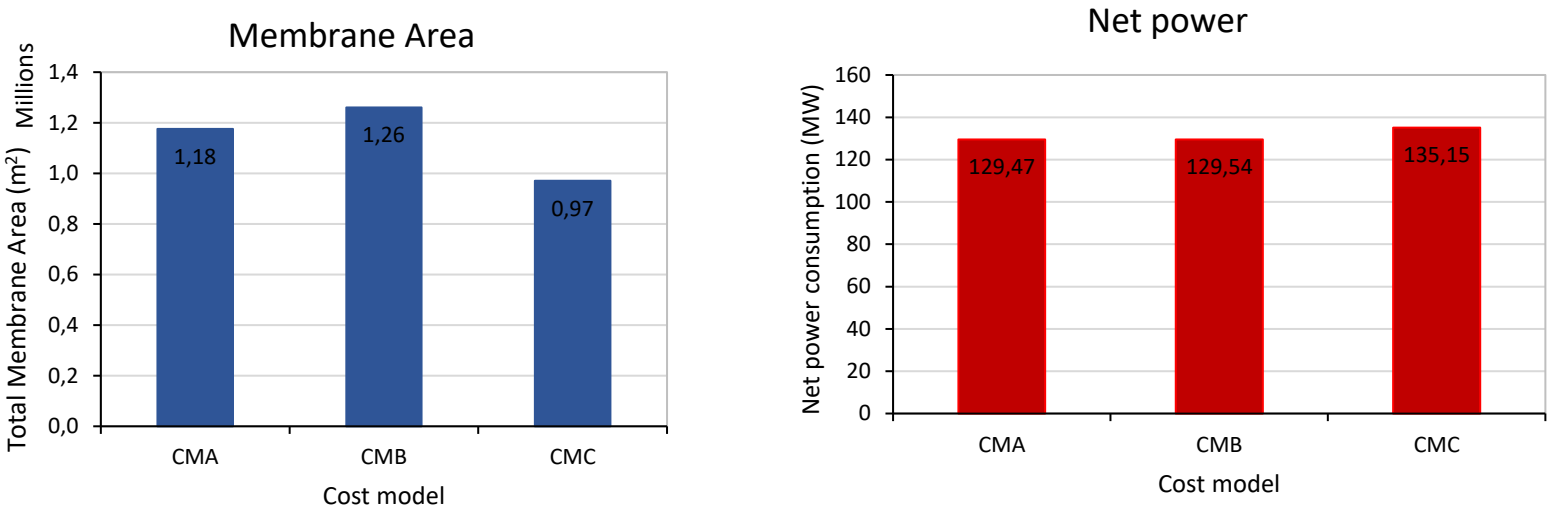

Figure 6.15. Comparison of optimum results for varying cost models

6.5.2.4 Effect of optimisation based on binary vs multicomponent flue gas and choice of permeation model

Optimisation runs are carried out based on two membrane models. Permeation model A (PMA) is based on a dedicated multicomponent model, permeation model B (PMB) is a detailed generic model, and permeation model C (PMC) is an approximate model commonly used in literature. From Figure 6.16, it is evident that minor differences in power consumption are realised for PMA and permeation model B PMB. Permeation model C (PMC) (approximate model) gives a slightly higher power consumption for both the binary flue gas and the multicomponent flue gas.

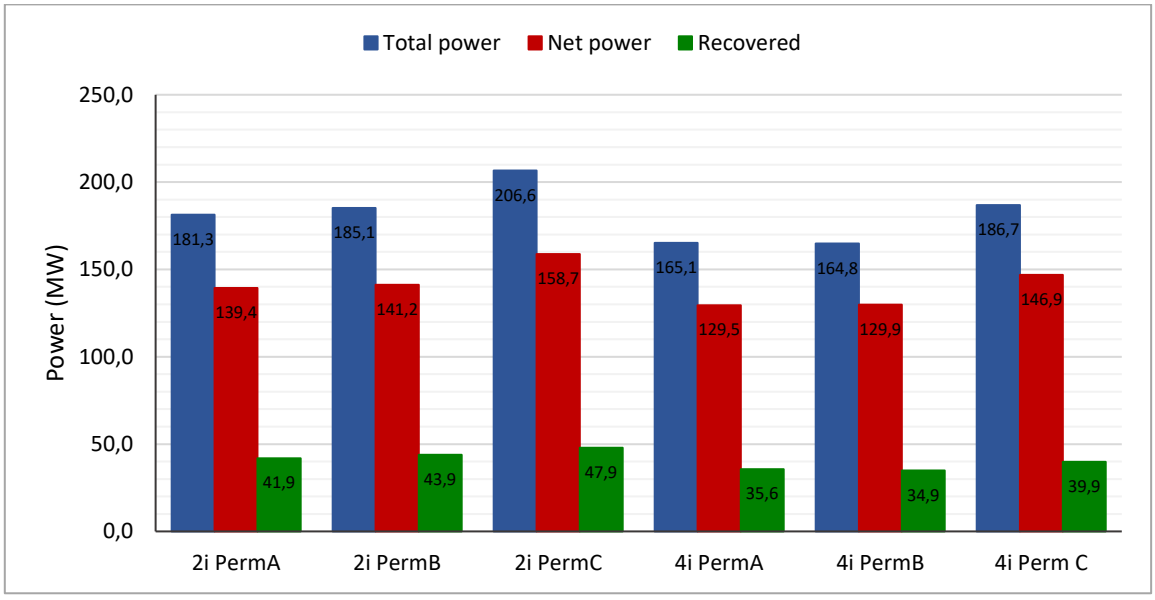

Figure 6.16. Graph showing variation in power consumed for different permeation models for CO_2 recovery 90% and purity 95%

Higher net power consumption is realised when a binary flue gas is considered in the optimisation run than when a four component flue gas is considered. This can be attributed to higher flow rates being processed by compressors when a binary gas is considered in the model. The optimisation based on multicomponent involves cooling which results in some of the water condensing and being removed from the gas streams being processed. For instance, the flue gas is cooled initially before being compressed and sent to the different membrane stages. The water in the feed stream is reduced from 10% to about 3% under the assumed conditions. Thus the gas stream flowrate is reduced by 7%. Water is also highly permeable and can saturate the

permeate. Subsequently, cooling permeate, and the water condenses and is removed from the gas stream. Hence, further reducing the duties of the compressors used for permeate recycle streams. However, when a binary mixture is assumed, H_2O content is usually lumped together as N_2 and is further handled by the subsequent recycle compressors. A few simulation studies also reported on the influence of water composition on the energy consumption of membrane based flue gas separation (Giordano et al., 2016; Pfister et al., 2017).

The difference in the cost of CO_2 capture between the two detailed models (PMA and PMB) is small. However, the approximate model (PMC) results in a higher cost of capture than PMA and PMB. PMC results in the most increased CO_2 capture cost for both binary and multicomponent flue gas. Both the capital and operating costs are higher for the PMC run than for PMA and PMB due to the higher net power consumption.

Table 6.7 shows the membrane area obtained from the different optimisation runs carried out. The membrane area required is also higher for a four-component flue gas than a two-component flue gas. The other components (O_2 and H_2O) are even more permeable than N_2; thus, their permeation reduces the composition of CO_2 in the permeate in each membrane stage. As a result, a lower CO_2 driving force is available in the recycled permeate streams. A larger total membrane area would be required for further separation of the CO_2 from the other components. When a binary gas is treated the O_2 and H_2O compositions are assumed to be N_2 which is less permeable. Thus a smaller membrane area suffices to achieve the purity and recovery set in the optimisation.

It is essential to mention that the superstructure in this work involves a cooler condenser to remove water from the product stream in order to increase the efficiency and capability of the CO_2 capture process system when the multicomponent flue gas is considered. Without the water condenser, the process flow chart would be more complex. For instance, the simulation carried out for a superstructure without the water condenser is unable to achieve 100% CO_2 recovery. When a binary mixture is studied in the synthesis of the post-combustion CO_2 capture process, the resultant process flow may not be applicable for the treatment of real flue gas from a power plant. However, it may be sufficient to analyse the economics of the CO_2 capture process from coal-fired power plants.

Figure 6.17 shows the column graphs for the capital cost, operational costs as well as the annualised cost.

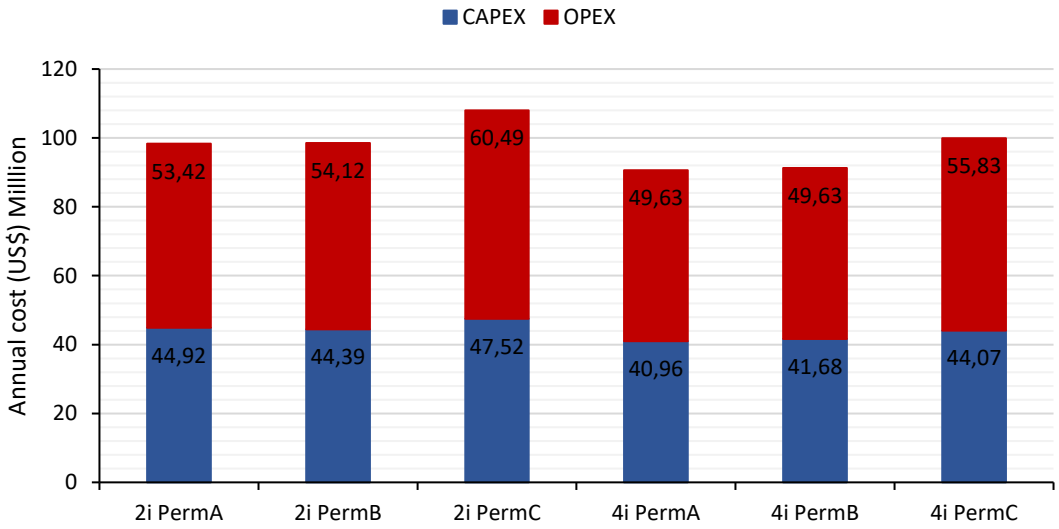

Figure 6.17. Effect of permeation model and flue gas components on the cost of CO_2 capture for recovery 90% and purity 95%

Table 6.7: Results for permeation models, binary and multicomponent flue gas for recovery 90% and purity 95%

	2iPMA	**2iPMB**	**2iPMC**	**4iPMA**	**4iPMB**	**4IPMC**
Number of stages	3	3	3	3	3	3
DP	95	95	95	95	95	95
DR	90	90	90	90	90	90
Specific membrane m^2/ton.h	3287.7	3074.5	3054.4	3077.9	3231.6	3068.0
Specific power, kWh/ton	365.0	370.5	415.7	339.0	340.2	384.7
Levelized cost, US$/ton	39.2	39.3	43.0	36.0	36.4	39.8

6.5.2.5 Effect of selected permeate pressure lower bound

The lower bound of the permeate side pressure (LBPP) is set at 0.1 bar and 0.2 bar at various CO_2 capture targets. 0.1p95 represents the graph of LBPP of 0.1 bar and purity of product stream set at 95%. On the other hand, 0.2p99 denotes the LBPP of 0.2 bar when the purity of the product stream is set at 99%.

Figure 6.18 shows that the power consumed generally increases when the recovery is increased from 90% to 100% for both 0.1 bar, and 0.2 bar set LBPP. Less power is consumed when the LBPP is at 0.1 bar compared to when it is set at 0.2 bar at both 95% and 99% product purity.

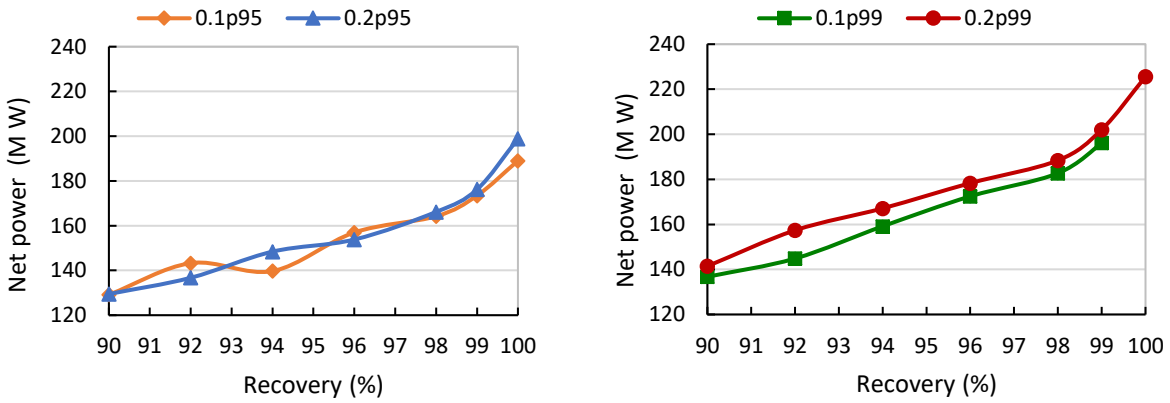

Figure 6.18. Graph showing variation of the power consumption as the recovery is increased with set lower bound of permeate side pressure

Figure 6.*19* illustrates the membrane area requirements. At higher capture targets (DP99), a higher membrane area was observed for the lower LBPP (0.1) than at 0.2 bar. This is consistent with previous simulation studies on membrane based gas separation that observed that a higher vacuum resulted in high membrane areas that are traded by lower energy consumption (Favre, 2007; Zhao et al., 2008).

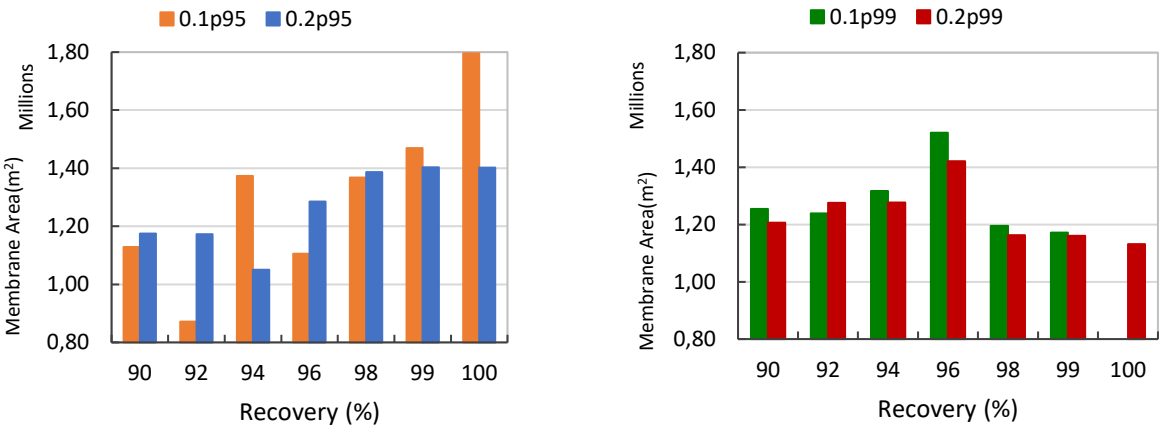

Figure 6.19. Graph showing variation power consumed with set lower bound of permeate side pressure

Figure 6.20 shows the annual cost at the various possible minimum permeate pressure. The annualised cost trends follow the net power consumption trends. From Figure 6.20, it can be observed that when the possible minimum permeate pressure is set at a lower value, the cost of CO_2 also decreases, however slightly. This is observed at all the separation targets of purity and recovery. At a purity of 95%, the percentage difference between 0.1 bar and 0.2 bar LBPP is negligible. However, at the 99% product purity target, the difference is moderately significant. The 0.1 bar LBPP achieves the capture targets at a lower cost of capture than 0.2 bar LBPP

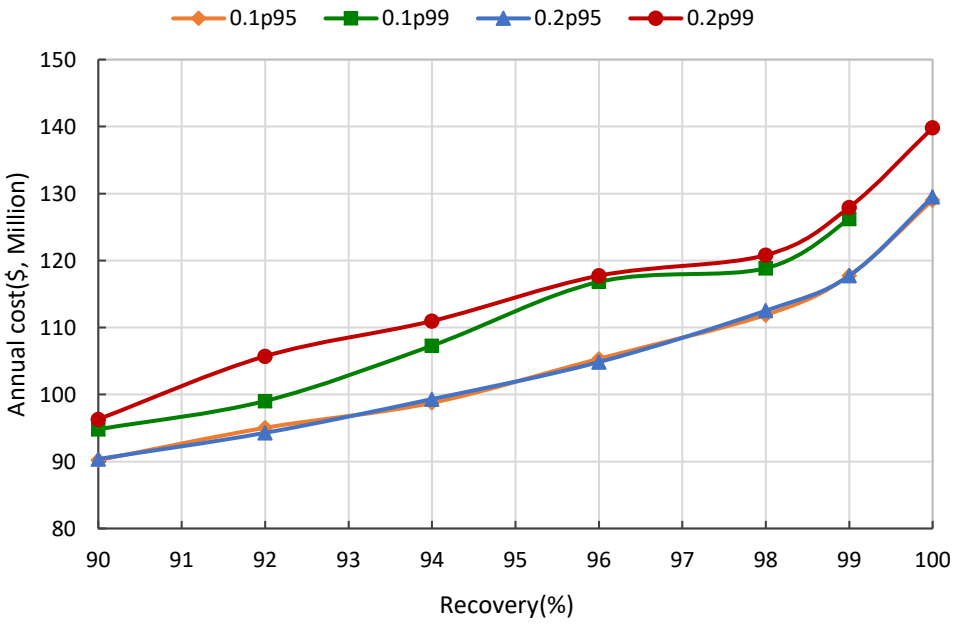

Figure 6.20. Graph showing the variation of annual cost with set lower bound of the permeate side pressure.

The operation of vacuum pumps makes membrane gas processes more energy efficient than compressors alone for driving force generation (Bounaceur et al., 2006). The use of vacuum pumps allows the generation of high pressure ratios at relatively lower energy requirements than compressors alone. The vacuum pump processes the permeate stream, whose flowrate is much less than that of the feed gas handled by the compressors on the feed side of the membrane. In the case of LBPP of 0.1 bar, a higher pressure ratio can be achieved at a relatively cheaper cost. The feed side can operate at a lower pressure, and this reduces the compressor power duty. As a result, the CO_2 capture cost is lower for the optimisation runs that assume LBPP of 0.1 bar than 0.2 bar

6.6 Concluding remark

In this study, optimisation of the membrane based CO_2 capture process for post-combustion CO_2 capture from a coal-fired power plant was carried out. The objective of the optimisation was to establish the minimum total annualised cost when recovery and purity targets is set. The desired product purity is set at 95% and 99% and investigated for recoveries from 90% up to 100% in order to assess the cost of zero CO_2 emission. The energy consumption increases when the recovery is increased, and consequently, the CO_2 capture cost also increases. An increased purity target also results in a higher cost of CO_2 capture. The cost of capture increases by 39% for a 100% recovery and 99% purity compared to 90% recovery and 95% purity. At such stringent capture targets, the process flow chart is more complex with permeate recycle in 2 of the three stages and retentate recycle from one of the stages.

Optimisation was carried out to compare the optimum results when the optimisation is carried out based on three cost methods. The results showed that the choice of the cost model employed had less effect on power consumption. Therefore, minor differences were noted in the operational cost. However, the capital cost was significantly affected mainly because of the different capital recovery factors in each cost model. The choice of the cost method would result in at least 3% and up to 15% difference in the total annualised cost. When the allowable minimum permeate pressure is set at 0.1 bar, a lower CO_2 capture cost is noted than when it is set at 0.2 bar because of the energy savings that are realised when operating at lower permeate

pressure. However, the practicality of low vacuum conditions such as 0.1 bar has been disputed. A higher upper bound of the stage membrane area results in lower CO_2 capture cost. Optimisation based on a humidified multicomponent flue gas results in lower energy requirements and consequently lower cost of capture.

6.7 Nomenclature

N	{n|n membrane stage}
I	{i|i component in a process stream} $i \in I = \{CO_2, N_2, H_2O, O_2\}$
K	{k|k compartments in membrane stage n}
RR	{rr|rr retentate recycle stream}
PR	{pr|pr permeate recycle stream}

Parameters

A^U	Upper bound membrane area, m^2
A^L	Lower bound membrane area, m^2
b_c^{unit}	Design, pressure or material correction factor of unit
C^{el}	Electricity tariff, *US$/KW*
C^{mem}	Cost of membrane, *US$/$m^2$*
C^{rep}	Cost of replacing membrane modules, *US $/$m^2$*
CP_i	Heat capacity of component *i* in gas stream, *KJ/kmol.K*
EY	Effective time the plant is online per year, *s/year*
P^{atm}	Atmospheric pressure, *bar*
R^{ft}	Flowrate of component *i* in the flue gas stream, *kmol/s*
T^{atm}	Atmospheric temperature, *K*
T^{mem}	Operating temperature of the membrane, *K*
U	Heat transfer coefficient, $KW/m^2.K$
ρ_i	Density of component *i*, kg/m^3
γ	Specific heat ratio

η Efficiency of compressor, vacuum, expander

φ_i Permeance of component *i, kmol/m^2.bar.s*

Binary Variables

Z_n^{wo} Permeate water condenser

Continuous variables

A_n^{mem} Membrane area of stage n, *m^2*

A_n^{clf} Heat transfer area of the feed compressor cooler in stage *n*, *m^2*

DP_i Desired purity of the CO_2 enriched stream

DR_i Desired recovery of CO_2,

lmt^{clf} Logarithm mean temperature of feed cooler in membrane stage *n*

P_n^{pm} Pressure on the permeate side in membrane stage *n, bar*

P_n^{rt} Pressure on the retentate side in membrane stage *n, bar*

Q_n^{cft} Duty of feed compressor (cft) in membrane stage *n, KW*

Q^{comp} Power consumed by product compressor, *KW*

Q^{pump} Power consumed by product compressor, *KW*

Q_n^{exr} Power recovered by expander of residue stream OA in membrane stage *n,K*

Q^{icp} Power consumed by product inter-stage cooler, *KW*

Q^{clf} Heat removed by cooler placed after feed compressor in stage *n*, *KW*

Q_n^{vac} Power consumed by the vacuum pump in stage *n* of membrane, *KW*

$R_{i,n}^{f}$ Flowrate of *i* in flue gas supplied to membrane stage *n*, *kmol/s*

$R_{i,n}^{fs}$ Flowrate of component *i* in the feed supplied to membrane stage *n, kmol/s*

$R_{i,n}^{ms}$ Flowrate of *i* in the permeate recycle stream *n* to recycle compressor, *kmol/s*

R^{oat} Total flowrate of *i* in residue stream emitted to the atmosphere, *kmol/s*

R_i^{op} Flowrate of component *i* from product mixer *kmol/s*

R_i^{oa} Flowrate of component *i* from residue mixer, *kmol/s*

R^{opc} Total flowrate of the product stream, *kmol/s*

R_i^{opw} Flowrate of component *i* in the stream exiting the product mixer, *kmol/s*

$R_{i,n}^{pm}$ Flowrate of component *i* in permeate stream from *n* to splitter, *kmol/s*

$R_{i,n,pr}^{pmr}$ Flowrate of component *i* in recycled permeate stream *pr* from stage *n kmol/s*

$R_{i,n}^{pos}$ Flowrate of component *i* in the product stream from membrane stage *n, kmol/s*

$R_{i,n}^{rto}$ Flowrate of component *i* in residue stream in membrane stage *n kmol/s*

$R_{i,n}^{rt}$ Flowrate of component *i in* retentate in membrane stage *n kmol/s*

$R_{i,n,k}^{rt}$ Flowrate component *i* from compartment *k* on the retentate side of stage *n, kmol/s*

$R_{i,n,rr}^{rtr}$ Flowrate of component *i in* retentate recycle stream *rr* from stage *n,* kmol/s

R_i^{wc} Flowrate of component *i* condensed in the flue gas condenser, *kmol/s*

$R_{i,n}^{wo}$ Flowrate of *i* condensed in the permeate condenser in membrane stage *n, kmol/s*

R_i^{wcp} Flowrate of water condensed in the product condenser, *kmol/s*

TAC Total annual cost, US$/year

TNQ Total net power consumed by the capture process, *KW*

T^{cft} Temperature of gas at outlet of feed compressor from membrane *n, K*

T^{hw} Temperature of cooling water as it leaves cooler, *K*

T^{cw} Temperature of cooling water as supplied to the cooler, *K*

x_n^f Split fraction of flue gas flowing to membrane stage *n,*

x_n^{pos} Split fraction for stream towards product from permeate splitter in stage *n*

$x_{n,pr}^{pmr}$ Split fraction of the recycle streams from permeate splitter in membrane stage *n*

$x_{n,rr}^{rtr}$ Split fraction of recycle streams from retentate splitter in membrane stage *n*

$x_{n,rr}^{rto}$ Split fraction of residue stream towards residue mixer *n*

$y_{i,n,k}^{pm}$ Mole fraction of component *i* at point k on the permeate side of membrane stage *n*

$y_{i,n,k}^{rt}$	Mole fraction of component *i at point k* on the retentate side of membrane *n*
$y_{i,n}^{fs}$	Mole fraction of component *i* in feed stream to the membrane *n*

Superscript

unit	Process unit
atm	Atmosphere
clf	Feed cooler
cft	Compressor feed
cw	Cooling water
el	Electricity
exr	Expander residue
f	Feed from flue gas splitter to membrane stage
fs	Feed before bubbling column
ft	Total feed flue gas
fs	Feed supply to membrane
ftg	Total flue gas
hw	Hot water from cooler
mem	Membrane
ms	sum of permeate recycle streams
oa	Residue output to atmosphere
oat	Total output to atmosphere
op	Output product
opt	Total product output
opw	Product output with water before product condenser
rep	Replacement
rto	Residue to atmosphere
rt	Retentate
rtr	Retentate recycle
sg	Sweep gas
pm	Permeate after sweep gas removal
pms	Permeate with sweep gas2
pmr	Permeate recycle stream

pos	Product output stream from splitter
wat	Water
wc	Water from flue condenser
wo	Water from permeate condenser
wp	Water from product condenser

Chapter 7 - General conclusions and recommendations

7.1 General Conclusions

Climate change is a 'super wicked' problem for the 21st century as it is related to energy generation. Energy is the backbone for economic development. For developing countries seeking to lift lives from poverty, fossils as energy sources remain the cheaper option to deliver constant uninterrupted energy that huge industries require for operation. Carbon capture, storage and utilisation will enable continued utilisation of fossil sources such as coal for electricity generation. This study aimed to make membrane based CO_2 capture more affordable and more feasible for large scale use by formulating superstructure based models for automated process synthesis, design and optimisation of CO_2 capture from coal-fired power plants.

The specific objectives are listed below;

- To develop a superstructure based optimisation model for the capture of CO_2 by an FSC from multicomponent saturated flue gas from a coal power plant.
- To assess the feasibility of membrane-based carbon capture from a South African coal power plant.
- To develop an optimisation model for the CO_2 capture from a multicomponent coal plant flue gas by use of an N_2 selective membrane. To optimise the N_2- and CO_2-selective hybrid membrane process for the CO_2 capture process from a coal power plant.
- To assess the possibility of achieving zero CO_2 emissions by membrane-based CO_2 capture. To assess the various strategies employed in the optimisation of the CO_2 capture by membranes from power plants.

7.1.1 Optimisation of post-combustion carbon dioxide capture by use of a fixed site carrier membrane

This thesis reports a process synthesis methodology dedicated to post-combustion carbon capture by a facilitated transport membrane, namely the FSC membrane. To the best of the literature survey, no study reported on the process optimization involving the variable

permeability behaviour of FSC membranes for CO_2 capture from humidified flue gas. Furthermore, the superstructure based model that was developed and implemented in this work included a choice for a process design that operates either a vacuum only or a combined sweep operation or a combination of these. The work is thus novel, both in terms of membrane mass transfer and process type. The use of an FSC transport model facilitated the non-uniform pressure operation of the various membranes in the membrane network. This led to a 13% reduction in the cost of CO_2 avoided compared to a pre-determined two stage membrane process with uniform feed and permeate pressure values and corresponding CO_2 permeance value at the set pressure values. The process design for the case involving a sweep and vacuum operation in the different stages of the membrane process resulted in 3% savings of the cost of capture than the membrane operated by a vacuum pump only on the permeate side in all the membranes. This should motivate future work in the use of sweep as a driving force generation strategy.

7.1.2 Techno-economic evaluation of membrane-based carbon capture and storage from a coal power plant in South Africa

The feasibility of membrane based CO_2 capture from South Africa by a membrane was carried out. A case study of a power plant based in the Limpopo region of South Africa where a relatively high average annual temperature of 33.2 ℃ and a relatively low average atmospheric pressure of 0.81 bar is recorded. The feasibility study was carried out in 2 stages; firstly, the base power plant was modelled and simulated, taking into account the characteristics of coal found in Limpopo and other local conditions to give the power plant flue gas composition, temperature and pressure. The second step involved applying the optimisation model previously developed for the CO_2 capture process from the flue gas. The total annual cost of the plant without CCS and is evaluated and compared to the annual cost of the power plant that include CCS. The CCS process would contribute 40 % to the total annual cost for the power plant with CCS. The results showed that a membrane based CCS system in South Africa would result in an efficiency penalty of 10.7%. The cost of electricity would increase by 127.8 % to US$151.2 /MW. The cost of CCS, therefore, remain high and further research need to be done to reduce the cost. The cost of membrane based capture realised is comparable to solvent absorption. In light of this, membrane based capture would be recommended as it requires less additional water than solvent absorption.

7.1.3 On Optimisation of N_2 and CO_2 selective membrane hybrid process system for CO_2 capture from coal power plants flue gas

This study involved developing a superstructure model that facilitated automated process design and optimisation when both the CO_2-selective and N_2-selective membranes are used for CO_2 capture from flue gas produced in a coal power plant. The results indicated that CO_2 capture based on N_2-selective membrane results in lower total membrane areas than that realised for CO_2 selective membrane. The hybrid system with a combination of N_2 and CO_2-selective membranes results in a smaller membrane area requirement and a more energy efficient system compared to the CO_2 capture system based on CO_2 selective membrane exclusively. The novel multi-stage N_2–CO_2 hybrid membrane process reduces the total membrane area by 46% and the cost of capture by 14% compared to the optimised CO_2-selective membrane process. The study reiterated the benefits of detailed process optimisation.

7.1.4 An assessment of the various strategies used in modelling, optimisation and techno-economic evaluation of membrane based CO_2 capture

A model was developed for the optimisation of CO_2 capture by use of a membrane to assess the impact of the various strategies used in techno-economic feasibility studies. The design achieved 100% CO_2 recovery (zero emission) and ultra-pure CO_2 product purity of 99%. The results showed that increasing the capture targets from the conventionally reported recovery of 90% and product purity of 95% to 100% recovery and 99% purity increases the annual cost of capture by 39.1%. The significant increase in the cost of capture may make zero-emission economically infeasible, in addition, it results in a considerable efficiency penalty. The study also compared the effect of the various assumed parameters and bounds as presented in membrane based CO_2 capture techno economic studies. The results showed that the cost model adopted in the optimisation has a significant impact on the realised cost of capture. The cost model also dictates whether capital costs were greater than operational cost based on the capital recovery charge. This result, therefore, highlights the importance of location-based feasibility studies. Optimisation based on a humidified four component flue gas gives lower cost of capture than a binary (N_2, CO_2) flue gas due to lower energy requirements. It can be therefore adequate to carry out techno-economic feasibility studies based on the binary flue gas as it over estimates the cost involved in membrane based CO_2. However it can be noted that the process

design would not be applicable in practical terms and an accurate process design may need to be carried out in the later stages of the project.

7.2 Limitation of study

This study has assumed negligible pressure drop along the membrane profile both on the retentate and permeate side. Pressure drop may be significant in real life and can reduce the driving force therefore resulting in a less energy efficient system. For the FSC membrane pressure drop on the retentate side may increase the CO_2 permeance, whilst a pressure drop on the permeate side would reduce both the driving force and the CO_2 permeance. This highlighted trade-off needs to be further investigated for the CO_2 capture by a FSC membrane.

In the study for the optimisation of a hybrid N_2/CO_2 selective membrane for CO_2 capture, the cost of the N_2-selective and CO_2-selective membranes has been assumed to be equal which may not be the case when an N_2-selective membrane becomes available commercially.

The efficiency of the vacuum pump assumed in this work could be deemed too high. Therefore, future studies should consider a lower and more practical value. A more detailed model could be used to model the final CO_2 product interstage compressor.

Finding solutions to the developed models was a challenge as shown by the different solvers used for the different models developed and presented in different chapters. Several solvers were used to solve the models and in certain instances necessitated the use of two solvers to get the optimal solution. It was noted that the reformulation of some of the equations prior to implementation in GAMS was influential in finding a solution. The selected bounds for such variables as pressure also impacted the computational times and also influenced the solution obtained. Whilst care and effort has been taken to find the optimal solution, the global optimum cannot be guaranteed and has not been verified for the noncovex MINLPs developed.

Incorporating an equation of state was desirable, instead, the superstructures have been developed in such a way that only streams of identical pressure and temperature mix. This is enabled by expanders, compressors and heat exchangers that the streams have to pass through

en-route mixers. Incorporating an equation of state would offer an opportunity for finding more competitive membrane networks, however the model will become more complex and more difficult to solve.

7.3 Recommendation for future work

The CO_2 membrane permeance model may be extended to make the carrier concentration load a variable whose cost is taken into consideration. Membrane operating temperature can also be made a variable to be optimised. Further work should also consider the pressure drop in the optimisation of FSC membranes for CO_2 capture. A model that takes into account the effect of the loss of humidity along the membrane profile will give more accurate results for CO_2 as the loss of humidity reduces CO_2 permeance, at constant N_2 permeance; this also means a loss of CO_2 /N_2 selectivity. Ideally, a model that simultaneously optimises all these mentioned variables may be closer to real and practical conditions and may further reduce the cost of CO_2 capture. It would be worthwhile to carry out the optimisation of CO_2 capture by membranes by having the cost of CO_2 avoided as the objective function.

More work still need to be done in studying the feasibility of carbon capture in South Africa. Future work should consider the feasibility of using membrane condensers to recover even more water that is usable from the flue gas since South Africa is an arid country. Further study should consider embedding a detailed transport and storage system model in the optimisation model to further lower the cost associated with CCS in South Africa. An analysis based on the full six units train may lower electricity cost due to shared costs.

Based on the smaller membrane area and energy requirements of the N_2/CO_2 selective membranes hybrid system for CO_2 capture, more research effort should be made to confirm the applicability of polymer based N_2 selective membranes for the separation of N_2/CO_2 gas mixtures. The investigations should also determine the O_2 and water permeability and selectivity of the membrane (N_2-selective membrane). Future studies should also consider using a single N_2-selective membrane but vary the CO_2-selective membranes.

An additional technical review should be carried out to determine which of the superstructures presented in the literature is more effective for membrane based CO_2 capture from flue gas. Whereas techno-economic studies in the literature have included the use of a fraction of

retentate or permeate as sweep, this has not been incorporated in the superstructures presented for membrane based CO_2 capture so far. It would be interesting to include this sweep strategy and optimise the flowrate of the stream and investigate the impact on the cost of CO_2 capture.

Advanced techniques and algorithms such as sequential techniques have been developed for solving superstructure based models for water purification. These techniques can also be explored for gas membrane networks.

It would be interesting if pilot plant trials of the process routes designed in this work are carried out. The exercise would investigate the feasibility and practicality of the presented flowsheets.

References

Abanades, J.C., Arias, B., Lyngfelt, A., Mattisson, T., Wiley, D.E., Li, H., Ho, M.T., Mangano, E., Brandani, S., 2015. Emerging CO2 capture systems. Int. J. Greenh. Gas Control 40, 126–166. https://doi.org/10.1016/j.ijggc.2015.04.018

Afkhamipour, M., Mofarahi, M., 2014. Sensitivity analysis of the rate-based CO2 absorber model using amine solutions (MEA, MDEA and AMP) in packed columns. Int. J. Greenh. Gas Control 25, 9–22. https://doi.org/10.1016/j.ijggc.2014.03.005

Al-Marzouqi, M.H., Hogendoorn, K.J.A., Versteeg, G.F., 2002. Analytical solution for facilitated transport across a membrane. Chem. Eng. Sci. 57, 4817–4829. https://doi.org/10.1016/S0009-2509(02)00285-3

Aliaga-vicente, A., Caballero, J.A., Fernandez-Torres, M., 2017. Synthesis and Optimization of Membrane Cascade for Gas Separation via Mixed-Integer Nonlinear Programming. AIChE J. 63, 1989–2006. https://doi.org/DOI 10.1002/aic.15631

Alshehri, A., Khalilpour, R., Abbas, A., Lai, Z., 2013. Membrane Systems Engineering for Post-combustion Carbon Capture. Energy Procedia, GHGT-11 37, 976–985. https://doi.org/10.1016/j.egypro.2013.05.193

Ansaloni, L., Zhao, Y., Jung, B.T., Ramasubramanian, K., Baschetti, M.G., Ho, W.S.W., 2015. Facilitated transport membranes containing amino-functionalized multi-walled carbon nanotubes for high-pressure CO2 separations. J. Memb. Sci. 490, 18–28. https://doi.org/10.1016/j.memsci.2015.03.097

Arias, A.M., Mores, P.L., Scenna, N.J., Caballero, J.A., Mussati, S.F., Mussati, M.C., 2018. Optimal design of a two-stage membrane system for hydrogen separation in refining processes. Processes 6. https://doi.org/10.3390/pr6110208

Arias, A.M., Mussati, M.C., Mores, P.L., Scenna, N.J., Caballero, J.A., Mussati, S.F., 2016. Optimization of multi-stage membrane systems for CO2 capture from flue gas. Int. J. Greenh. Gas Control 53, 371–390. https://doi.org/10.1016/j.ijggc.2016.08.005

Baker, R.W., 2004. Membrane Technology and applications, 2nd ed. Wiley.

Beck, B., Surridge, T., Hietkamp, S., 2013. The South African centre for carbon capture and storage delivering CCS in the developing world. Energy Procedia 37, 6502–6507. https://doi.org/10.1016/j.egypro.2013.06.580

Belaissaoui, B., Cabot, G., Cabot, M.-S., Willson, D., Favre, E., 2012a. An energetic analysis of CO2 capture on a gas turbine combining flue gas recirculation and membrane separation. Energy 38, 167–175. https://doi.org/10.1016/j.energy.2011.12.018

Belaissaoui, B., Willson, D., Favre, E., 2012b. Membrane gas separations and post-combustion carbon dioxide capture: Parametric sensitivity and process integration strategies. Chem. Eng. J. 211–212, 122–132. https://doi.org/10.1016/j.cej.2012.09.012

Bhattacharya, S., Hwang, S.T., 1997. Concentration polarization, separation factor, and Peclet number in membrane processes. J. Memb. Sci. 132, 73–90. https://doi.org/10.1016/S0376-7388(97)00047-1

Biliyok, C., Lawal, A., Wang, M., Seibert, F., 2012. Dynamic modelling, validation and analysis of post-combustion chemical absorption CO2 capture plant. Int. J. Greenh. Gas Control 9, 428–445. https://doi.org/10.1016/j.ijggc.2012.05.001

Blagg, C.R., 2007. The Early History of Dialysis for Chronic Renal Failure in the United States: A View From Seattle. Am. J. Kidney Dis. 49, 482–496. https://doi.org/10.1053/j.ajkd.2007.01.017

Bocciardo, D., Ferrari, M.-C., Brandani, S., 2013. Modelling and Multi-stage Design of Membrane Processes Applied to Carbon Capture in Coal-fired Power Plants. Energy Procedia, GHGT-11 37, 932–940. https://doi.org/10.1016/j.egypro.2013.05.188

Bounaceur, R., Lape, N., Roizard, D., Vallieres, C., Favre, E., 2006. Membrane processes for post-combustion carbon dioxide capture: A parametric study. Energy 31, 2556–2570. https://doi.org/10.1016/j.energy.2005.10.038

Broutin, P., Kvamsdal, H., La Marca, C., Van Os, P., Robinson, L., 2014. OCTAVIUS: A FP7 project demonstrating CO 2 capture technologies. Energy Procedia 63, 6194–6206. https://doi.org/10.1016/j.egypro.2014.11.651

Buabeng-Baidoo, E., Majozi, T., 2015. Effective Synthesis and Optimization Framework for Integrated Water and Membrane Networks: A Focus on Reverse Osmosis Membranes. Ind. Eng. Chem. Res. 54, 9394–9406. https://doi.org/10.1021/acs.iecr.5b01803

Budinis, S., Krevor, S., Dowell, N. Mac, Brandon, N., Hawkes, A., 2018. An assessment of CCS costs, barriers and potential. Energy Strateg. Rev. 22, 61–81. https://doi.org/10.1016/j.esr.2018.08.003

Buzek, L., Warmuziński, K., Tańczyk, M., Janusz-Cygan, A., 1999. Cost analysis for the removal of volatile organic compounds from air using hybrid systems: Membrane separation/condensation versus membrane separation/combustion. Chem. Eng. Process. Process Intensif. 38, 273–279. https://doi.org/10.1016/S0255-2701(99)00010-0

Cao, Y., Song, F., Zhao, Y., Zhong, Q., 2013. Capture of carbon dioxide from flue gas on TEPA-grafted metal-organic framework Mg2(dobdc). J. Environ. Sci. 25, 2081–2087. https://doi.org/10.1016/S1001-0742(12)60267-8

CESAR, 2011. European best practice guidelines for assessment of CO2 capture technologies 1–112.

Chabangu, N., Beck, B., Hicks, N., Botha, G., Viljoen, J., Davids, S., Cloete, M., 2014. The investigation of CO2 storage potential in the Zululand Basin in South Africa. Energy Procedia 63, 2789–2799. https://doi.org/10.1016/J.EGYPRO.2014.11.301

Chemengonline, 2019. www.chemengonline.com [WWW Document]. URL https://www.chemengonline.com/pci-home (accessed 10.31.19).

Chiwaye, N., Majozi, T., Daramola, M.O., 2021. Optimisation of post-combustion carbon dioxide capture by use of a fixed site carrier membrane. Int. J. Greenh. Gas Control 104, 103182. https://doi.org/10.1016/j.ijggc.2020.103182

Chowdhury, M.H.M., Feng, X., Douglas, P., Croiset, E., 2005. A new numerical approach for a detailed multicomponent gas separation membrane model and AspenPlus simulation. Chem. Eng. Technol. 28, 773–782. https://doi.org/10.1002/ceat.200500077

Chu, Y., He, X., 2018. Process Simulation and Cost Evaluation of Carbon Membranes for CO2 Removal from High-Pressure Natural Gas. Membranes (Basel). 8, 118. https://doi.org/10.3390/membranes8040118

Coker, D.T., Allen, T., Freeman, B.D., Fleming, G.K., 1999. Nonisothermal model for gas separation hollow-fiber membranes. AIChE J. 45, 1451–1468. https://doi.org/10.1002/aic.690450709

Coker, D.T., Freeman, B.D., Fleming, G.K., 1998. Modeling multicomponent gas separation using hollow-fiber membrane contactors. AIChE J. 44, 1289–1302. https://doi.org/10.1002/aic.690440607

Crabtree, E.W., El-Halwagi, M.M., Dunn, R.F., 1998. Synthesis of Hybrid Gas Permeation Membrane/Condensation Systems for Pollution Prevention. J. Air Waste Manag. Assoc. 48, 616–626. https://doi.org/10.1080/10473289.1998.10463714

Czyperek, M., Zapp, P., Bouwmeester, H.J.M.M., Modigell, M., Ebert, K., Voigt, I., Meulenberg, W.A., Singheiser, L., Stöver, D., 2010. Gas separation membranes for zero-emission fossil power plants: MEM-BRAIN. J. Memb. Sci. 359, 149–159. https://doi.org/10.1016/j.memsci.2010.04.012

Dai, Z., Aboukeila, H., Ansaloni, L., Deng, J., Giacinti Baschetti, M., Deng, L., 2019. Nafion/PEG hybrid membrane for CO 2 separation: Effect of PEG on membrane micro-structure and performance. Sep. Purif. Technol. 214, 67–77. https://doi.org/10.1016/j.seppur.2018.03.062

Danckwerts, P. V., 1979. The reaction of CO2 with ethanolamines. Chem. Eng. Sci. 34, 443–446. https://doi.org/10.1016/0009-2509(79)85087-3

DEA SA, 2010. National Environmental Management: Air Quality Act, 2004(Act No.39 of

2004)., Government Gazette.

Deng, L., Hägg, M.B., 2010. Swelling behavior and gas permeation performance of PVAm/PVA blend FSC membrane. J. Memb. Sci. 363, 295–301. https://doi.org/10.1016/j.memsci.2010.07.043

Deng, L., Kim, T.-J., Hägg, M.-B., 2009. Facilitated transport of CO2 in novel PVAm/PVA blend membrane. J. Memb. Sci. 340, 154–163. https://doi.org/10.1016/j.memsci.2009.05.019

Deng, L., Kim, T.-J., Hägg, M.-B., 2006. PVA/PVAm blend FSC membrane for CO2-capture. Desalination, Euromembrane 2006Euromembrane 2006 199, 523–524. https://doi.org/10.1016/j.desal.2006.03.118

DOE SA, 2018. 2018 Energy Price Report. https://doi.org/http://www.energy.gov.za/files/media/explained/Energy-Price-Report-2018.pdf

DOE SA, E. department, 2019. Intergrated Resource Plan [WWW Document]. URL http://www.energy.gov.za/files/media/Pub/IRP-2019.pdf (accessed 3.6.20).

DOE, U.S.A., 2005. Carbon Capture and Sequestration Systems Analysis Guidelines.

Douglas, J.M., 1989. Conceptual Design of Chemical.

Dunn, R.F., El-Halwagi, M.M., 1994. Optimal design of multicomponent VOC condensation systems. J. Hazard. Mater. 38, 187–206. https://doi.org/10.1016/0304-3894(94)00014-X

Ebadi Amooghin, A., Moftakhari Sharifzadeh, M.M., Zamani Pedram, M., 2018. Rigorous modeling of gas permeation behavior in facilitated transport membranes (FTMs); evaluation of carrier saturation effects and double-reaction mechanism. Greenh. Gases Sci. Technol. 8, 429–443. https://doi.org/10.1002/ghg.1750

El-Halwagi, M.M., Srinivas, B.K., Dunn, R.F., 1995. Synthesis of optimal heat-induced separation networks. Chem. Eng. Sci. 50, 81–97. https://doi.org/10.1016/0009-

2509(94)00207-8

EPRI, 2015. Power Generation Technology Data for Integrated Resource Plan of South Africa.

ESKOM, 2013. ESKOM Fact sheet Kusile and Medupi coal-fired power stations under construction.

Falbo, F., Brunetti, A., Barbieri, G., Drioli, E., Tasselli, F., 2016. CO2/CH4 separation by means of Matrimid hollow fibre membranes. Appl. Petrochemical Res. 6, 439–450. https://doi.org/10.1007/s13203-016-0164-z

Farmer, T., Cook, J., 2013. Climate Change Science: A modern Synthesis, Springer. https://doi.org/10.1007/978-94-007-5757-8

Favre, E., 2011. Membrane processes and postcombustion carbon dioxide capture: Challenges and prospects. Chem. Eng. J., Special Section: Symposium on Post-Combustion Carbon Dioxide Capture 171, 782–793. https://doi.org/10.1016/j.cej.2011.01.010

Favre, E., 2007. Carbon dioxide recovery from post-combustion processes: Can gas permeation membranes compete with absorption? J. Memb. Sci. 294, 50–59. https://doi.org/https://doi.org/10.1016/j.memsci.2007.02.007

Favre, E., Roizard, D., Bounaceur, R., Koros, W.J., 2009. CO 2/N 2 reverse selective gas separation membranes: Technological opportunities and scientific challenges. Ind. Eng. Chem. Res. 48, 3700–3701. https://doi.org/10.1021/ie801923w

Ferrari, M.-C.C., Bocciardo, D., Brandani, S., 2016. Integration of Multi-Stage Membrane Carbon Capture Processes to Coal-Fired Power Plants using highly permeable polymers. Green Energy Environ. 1, 211–221. https://doi.org/10.1016/j.gee.2016.10.001

Fontalvo, J., 2006. Design and performance of two-phase flow pervaporation and hybrid distillation processes, Dissertation Abstracts International.

Gabrielli, P., Gazzani, M., Mazzotti, M., 2017. On the optimal design of membrane-based gas separation processes. J. Memb. Sci. 526, 118–130.

https://doi.org/10.1016/j.memsci.2016.11.022

GAW, W.M.O., 2014. The State of Greenhouse Gases in the Atmosphere Based on Global Observations through 2013. WMO Greenh. GAS Bull.

Ghosal, K., Chern, R.T., Freeman, B.D., Daly, W.H., Negulescu, I.I., 1996. Effect of basic substituents on gas sorption and permeation in polysulfone. Macromolecules 29, 4360–4369. https://doi.org/10.1021/ma951310i

Giordano, L., Roizard, D., Bounaceur, R., Favre, E., 2017. Evaluating the effects of CO2 capture benchmarks on efficiency and costs of membrane systems for post-combustion capture: A parametric simulation study. Int. J. Greenh. Gas Control 63, 449–461. https://doi.org/10.1016/J.IJGGC.2017.05.002

Giordano, L., Roizard, D., Bounaceur, R., Favre, E., 2016. Interplay of inlet temperature and humidity on energy penalty for CO2 post-combustion capture: Rigorous analysis and simulation of a single stage gas permeation process. Energy 116, Part, 517–525. https://doi.org/10.1016/j.energy.2016.09.129

Glasser, L., 2004. Erratum: Water, water, everywhere: Phase diagrams of ordinary water substance (J. Chem. Educ. (2004) 81, (414-418)). J. Chem. Educ. 81, 645. https://doi.org/10.1021/ed081p414

Goddard, J.D., Schultz, J.S., Suchdeo, S.R., 1974. Facilitated transport via carrier—mediated diffusion in membranes: Part II. Mathematical aspects and analyses. AIChE J. 20, 625–645. https://doi.org/10.1002/aic.690200402

Goldenberg, S., 2014. Canada switches on world's first carbon capture power plant. Guard.

Goto, K., Yogo, K., Higashii, T., 2013. A review of efficiency penalty in a coal-fired power plant with post-combustion CO2 capture. Appl. Energy 111, 710–720. https://doi.org/10.1016/j.apenergy.2013.05.020

Haigh, J.D., 2002. Radiative forcing of climate change. Weather 57, 278–283.

https://doi.org/10.1256/004316502320517362

Han, Y., Ho, W.S.W., 2020a. Design of Amine-Containing CO2-Selective Membrane Process for Carbon Capture from Flue Gas. Ind. Eng. Chem. Res. 59, 5340–5350. https://doi.org/10.1021/acs.iecr.9b04839

Han, Y., Ho, W.S.W., 2020b. Recent advances in polymeric facilitated transport membranes for carbon dioxide separation and hydrogen purification. J. Polym. Sci. 1–15. https://doi.org/10.1002/pol.20200187

Han, Y., Ho, W.S.W.S.W., 2018. Recent advances in polymeric membranes for CO2 capture. Chinese J. Chem. Eng. 26, 2238–2254. https://doi.org/10.1016/j.cjche.2018.07.010

Han, Y., Salim, W., Chen, K.K., Wu, D., Ho, W.S.W., 2019a. Field trial of spiral-wound facilitated transport membrane module for CO2 capture from flue gas. J. Memb. Sci. 575, 242–251. https://doi.org/10.1016/J.MEMSCI.2019.01.024

Han, Y., Wu, D., Ho, W., 2019b. Simultaneous effects of temperature and vacuum and feed pressures on facilitated transport membrane for CO2/N2 separation. J. Memb. Sci. 573, 476–484. https://doi.org/10.1016/j.memsci.2018.12.028

Han, Y., Wu, D., Ho, W.S.W., 2018. Nanotube-reinforced facilitated transport membrane for CO2/N2 separation with vacuum operation. J. Memb. Sci. 567, 261–271. https://doi.org/10.1016/J.MEMSCI.2018.08.061

Han, Y., Yang, Y., Winston Ho, W.S., 2020. Recent progress in the engineering of polymeric membranes for co2 capture from flue gas. Membranes (Basel). 10, 1–35. https://doi.org/10.3390/membranes10110365

Hao, J., Rice, P.A., Stern, S.A., 2008. Upgrading low-quality natural gas with H2S- and CO2-selective polymer membranes. Part II. Process design, economics, and sensitivity study of membrane stages with recycle streams. J. Memb. Sci. 320, 108–122. https://doi.org/10.1016/j.memsci.2008.03.040

Harlacher, T., Wessling, M., 2015. Gas-Gas Separation by Membranes, in: Progress in Filtration and Separation. pp. 557–584. https://doi.org/10.1016/B978-0-12-384746-1.00013-6

Harms, S., Rätzke, K., Faupel, F., Chaukura, N., Budd, P.M., Egger, W., Ravelli, L., 2012. Aging and free volume in a polymer of intrinsic microporosity (PIM-1). J. Adhes. 88, 608–619. https://doi.org/10.1080/00218464.2012.682902

Hasan, M.M.F., Baliban, R.C., Elia, J.A., Floudas, C.A., 2012. Modeling, Simulation, and Optimization of Postcombustion CO 2 Capture for Variable Feed Concentration and Flow Rate. 1. Chemical Absorption and Membrane Processes. Ind. Eng. Chem. Res. 51, 1562–15664. https://doi.org/10.1016/j.compchemeng.2011.08.002

He, X., 2018a. A review of material development in the field of carbon capture and the application of membrane-based processes in power plants and energy-intensive industries. Energy. Sustain. Soc. 8. https://doi.org/10.1186/s13705-018-0177-9

He, X., 2018b. SF Journal of Material and Chemical Engineering The Latest Development on Membrane Materials and Processes for Post-combustion CO 2 Capture : A Review.

He, X., Fu, C., Hägg, M.-B.B., 2015. Membrane system design and process feasibility analysis for CO2 capture from flue gas with a fixed-site-carrier membrane. Chem. Eng. J. 268, 1–9. https://doi.org/10.1016/j.cej.2014.12.105

He, X., Hägg, M.-B., 2014. Energy Efficient Process for CO2 Capture from Flue gas with Novel Fixed-site-carrier Membranes. Energy Procedia, 12th International Conference on Greenhouse Gas Control Technologies, GHGT-12 63, 174–185. https://doi.org/10.1016/j.egypro.2014.11.018

He, X., Hägg, M.-B., 2011a. Hollow fiber carbon membranes: Investigations for CO2 capture. J. Memb. Sci., Membranes for a Sustainable Future Section 378, 1–9. https://doi.org/10.1016/j.memsci.2010.10.070

He, X., Hägg, M.-B.B., Kim, T.-J.J., 2014. Hybrid FSC membrane for CO2 removal from

natural gas: Experimental, process simulation, and economic feasibility analysis. AIChE J. 60, 4174–4184. https://doi.org/10.1002/aic.14600

He, X., Hägg, M.B., 2011b. Optimization of carbonization process for preparation of high performance hollow fiber carbon membranes. Ind. Eng. Chem. Res. 50, 8065–8072. https://doi.org/10.1021/ie2003279

He, X., Kumakiri, I., Hillestad, M., 2020. Conceptual Process Design and Simulation of Membrane Systems for Integra- ted Natural Gas Dehydration and Sweetening. Sep. Purif. Technol. 247, 116993. https://doi.org/10.1016/j.seppur.2020.116993

He, X., Lindbråthen, A., Kim, T.-J., Hägg, M.-B., 2017. Pilot testing on fixed-site-carrier membranes for CO2 capture from flue gas. Int. J. Greenh. Gas Control 64, 323–332. https://doi.org/10.1016/J.IJGGC.2017.08.007

Ho, M.T., Allinson, G.W., Wiley, D.E., 2008. Reducing the cost of CO2 capture from flue gases using membrane technology. Ind. Eng. Chem. Res. 47, 1562–1568. https://doi.org/10.1021/ie070541y

Hoegh-Guldberg O., Jacob D., Taylor M., Bindi M., Brown S., Camilloni I., Diedhiou A., D.R. et al., 2018. Impacts of 1.5°C global warming on natural and human systems., Special Report, Intergovernmental Panel on Climate Change.

Hong, J.-M., Kang, Y.S., Jang, J., Kim, U.Y., 1996. Analysis of facilitated transport in polymeric membrane with fixed site carrier 2. Series RC circuit model. J. Memb. Sci. 109, 159–163. https://doi.org/10.1016/0376-7388(95)00189-1

Hu, B., Zhai, H., 2017. The cost of carbon capture and storage for coal-fired power plants in China. Int. J. Greenh. Gas Control 65, 23–31. https://doi.org/10.1016/j.ijggc.2017.08.009

Huang, J., Zou, J., Ho, W.S.W., 2008. Carbon Dioxide Capture Using a CO2-Selective Facilitated Transport Membrane. Ind. Eng. Chem. Res. 47, 1261–1267. https://doi.org/10.1021/ie070794r

Huang, Y., Paul, D.R., 2007. Effect of film thickness on the gas-permeation characteristics of glassy polymer membranes. Ind. Eng. Chem. Res. 46, 2342–2347. https://doi.org/10.1021/ie0610804

Huang, Y., Rebennack, S., Zheng, Q.P., 2013. Techno-economic analysis and optimization models for carbon capture and storage: a survey. Energy Syst. 4, 315–353.

Hussain, A., Farrukh, S., Minhas, F.T., 2015. Two-Stage Membrane System for Post-combustion CO2 Capture Application. Energy & Fuels 29, 6664–6669. https://doi.org/10.1021/acs.energyfuels.5b01464

Hussain, A., Hägg, M.-B., 2010. A feasibility study of CO2 capture from flue gas by a facilitated transport membrane. J. Memb. Sci., Membranes and CO2 Separation 359, 140–148. https://doi.org/10.1016/j.memsci.2009.11.035

IEA, 2018. Global energy and CO2 status report, International Energy Law. https://doi.org/10.4324/9781315252056

IEA, 2011. CO2 emission from fuel combustion highlights.

IPCC, 2018. Global warming 1.5 Degree Celcius. https://doi.org/10.1017/CBO9781107415324.004

IPCC, 2005. IPCC Special Report on Carbon Dioxide Capture and Storage.

Iulianelli, A., Drioli, E., 2020. Membrane engineering: Latest advancements in gas separation and pre-treatment processes, petrochemical industry and refinery, and future perspectives in emerging applications. Fuel Process. Technol. 206, 106464. https://doi.org/10.1016/j.fuproc.2020.106464

Jaffrin, M., 2015. Membrane filtration processes.

James, R., Zoelle, A., Keairns, D., Turner, M., Woods, M., Kuehn, N., 2019. Cost and Performance Baseline for Fossil Energy Plants Volume 1 : Bituminous Coal and. NETL Rep. Pub-22638 1.

Ji, G., Zhao, M., 2017. Membrane Separation Technology in Carbon Capture. Recent Adv. Carbon Capture Storage. https://doi.org/10.5772/65723

Joseph, K., Chandran, A., George, G., 2018. Gas Transport Through Polymer Composites, in: Transport Properties of Polymeric Membranes. Elsevier Inc., pp. 633–649. https://doi.org/10.1016/B978-0-12-809884-4.00029-X

Kang, Y.S., Hong, J.-M.M., Jang, J., Kim, U.Y., 1996. Analysis of facilitated transport in solid membranes with fixed site carriers 1. Single RC circuit model. J. Memb. Sci. 109, 149–157. https://doi.org/10.1016/0376-7388(95)00190-5

Kanniche, M., Gros-Bonnivard, R., Jaud, P., Valle-Marcos, J., Amann, J.-M., Bouallou, C., 2010. Pre-combustion, post-combustion and oxy-combustion in thermal power plant for CO2 capture. Appl. Therm. Eng. 30, 53–62. https://doi.org/10.1016/j.applthermaleng.2009.05.005

Kemena, L.L., Noble, R.D., Kemp, N.J., 1983. Optimal regimes of facilitated transport. J. Memb. Sci. 15, 259–274. https://doi.org/10.1016/S0376-7388(00)82303-0

Kentish, S.E., 2011. Polymeric membranes for natural gas processing. Adv. Membr. Sci. Technol. Sustain. Energy Environ. Appl. 339–360. https://doi.org/10.1533/9780857093790.3.339

Khalilpour, R., Abbas, A., Lai, Z., Pinnau, I., 2012. Modeling and parametric analysis of hollow fiber membrane system for carbon capture from multicomponent flue gas. AICHE J. 58, 1550–1561. https://doi.org/10.1002/aic

Kim, H.J., Chaikittisilp, W., Jang, K.S., Didas, S.A., Johnson, J.R., Koros, W.J., Nair, S., Jones, C.W., 2015. Aziridine-functionalized mesoporous silica membranes on polymeric hollow fibers: Synthesis and single-component CO2 and N2 permeation properties. Ind. Eng. Chem. Res. 54, 4407–4413. https://doi.org/10.1021/ie503781u

Kim, K.M., Lee, J.W., Lee, J. Bin, 2020. No-mixing-loss design of a multistage membrane carbon capture process for off-gas in thermal power plants. J. Memb. Sci. 598.

https://doi.org/10.1016/j.memsci.2019.117796

Kim, T.-J., Vrålstad, H., Sandru, M., Hägg, M.-B., 2013. Separation performance of PVAm composite membrane for CO2 capture at various pH levels. J. Memb. Sci. 428, 218–224. https://doi.org/10.1016/j.memsci.2012.10.009

Kim, T.-J.J., Uddin, M.W., Sandru, M., Hägg, M.-B.B., 2011. The effect of contaminants on the composite membranes for CO2 separation and challenges in up-scaling of the membranes. Energy Procedia, 10th International Conference on Greenhouse Gas Control Technologies 4, 737–744. https://doi.org/10.1016/j.egypro.2011.01.113

Kim, T.J., Vrålstad, H., Sandru, M., Hägg, M.B., 2013. The effect of pH on CO2-separation from post combustion gas by polyvinylamine based composite membrane. Energy Procedia 37, 986–992. https://doi.org/10.1016/j.egypro.2013.05.194

Kookos, I.K., 2002. A targeting approach to the synthesis of membrane networks for gas separations. J. Memb. Sci. 208, 193–202. https://doi.org/10.1016/S0376-7388(02)00259-4

Kortunov, P. V., Siskin, M., Paccagnini, M., Thomann, H., 2016. CO2 Reaction Mechanisms with Hindered Alkanolamines: Control and Promotion of Reaction Pathways. Energy and Fuels 30, 1223–1236. https://doi.org/10.1021/acs.energyfuels.5b02582

Kumar, P., Kim, S., Ida, J., Guliants, V. V., 2008. Polyethyleneimine-modified MCM-48 membranes: Effect of water vapor and feed concentration on N2/CO2 selectivity. Ind. Eng. Chem. Res. 47, 201–208. https://doi.org/10.1021/ie070700d

Lasseuguette, E., Carta, M., Brandani, S., Ferrari, M.C., 2016. Effect of humidity and flue gas impurities on CO2 permeation of a polymer of intrinsic microporosity for post-combustion capture. Int. J. Greenh. Gas Control 50, 93–99. https://doi.org/10.1016/j.ijggc.2016.04.023

Lau, C.H., Nguyen, P.T., Hill, M.R., Thornton, A.W., Konstas, K., Doherty, C.M., Mulder, R.J., Bourgeois, L., Liu, A.C.Y., Sprouster, D.J., Sullivan, J.P., Bastow, T.J., Hill, A.J.,

Gin, D.L., Noble, R.D., 2014. Ending Aging in Super Glassy Polymer Membranes. Angew. Chemie 126, 5426–5430. https://doi.org/10.1002/ange.201402234

Lawal, A., Wang, M., Stephenson, P., Obi, O., 2012. Demonstrating full-scale post-combustion CO2 capture for coal-fired power plants through dynamic modelling and simulation. Fuel, 8th European Conference on Coal Research and Its Applications 101, 115–128. https://doi.org/10.1016/j.fuel.2010.10.056

Lawal, A., Wang, M., Stephenson, P., Yeung, H., 2009. Dynamic modelling of CO2 absorption for post combustion capture in coal-fired power plants. Fuel, 7th European Conference on Coal Research and Its Applications 88, 2455–2462. https://doi.org/10.1016/j.fuel.2008.11.009

Lee, S.-Y., Park, S.-J., 2015. A review on solid adsorbents for carbon dioxide capture. J. Ind. Eng. Chem. 23, 1–11. https://doi.org/10.1016/j.jiec.2014.09.001

Lee, S., Binns, M., Kim, J.-K., 2018. Automated process design and optimization of membrane-based CO2 capture for a coal-based power plant. J. Memb. Sci. 563, 820–834. https://doi.org/10.1016/J.MEMSCI.2018.06.057

Leperi, K.T., Snurr, R.Q., You, F., 2016. Optimization of Two-Stage Pressure/Vacuum Swing Adsorption with Variable Dehydration Level for Postcombustion Carbon Capture. Ind. Eng. Chem. Res. 55, 3338–3350. https://doi.org/10.1021/acs.iecr.5b03122

Leung, D.Y.C., Caramanna, G., Maroto-Valer, M.M., 2014. An overview of current status of carbon dioxide capture and storage technologies. Renew. Sustain. Energy Rev. 39, 426–443. https://doi.org/https://doi.org/10.1016/j.rser.2014.07.093

Li, K., Acharya, D.R., Hughes, R., 1990. Mathematical modelling of multicomponent membrane permeators. J. Memb. Sci. 52, 205–219. https://doi.org/10.1016/S0376-7388(00)80486-X

Li, S., Wang, Z., He, W., Zhang, C., Wu, H., Wang, J., Wang, S., 2014. Effects of Minor SO2 on the Transport Properties of Fixed Carrier Membranes for CO2 Capture. Ind. &

Eng. Chem. Res. 53, 7758–7767. https://doi.org/10.1021/ie404063r

Liang, C.Z., Chung, T.S., Lai, J.Y., 2019. A review of polymeric composite membranes for gas separation and energy production. Prog. Polym. Sci. 97. https://doi.org/10.1016/j.progpolymsci.2019.06.001

Liguori, S., Lee, K., Wilcox, J., 2019. Innovative N2-selective metallic membranes for the potential use of CO2 capture. J. Memb. Sci. 585, 52–59. https://doi.org/10.1016/j.memsci.2019.05.019

Lin, H., He, Z., Sun, Z., Vu, J., Ng, A., Mohammed, M., Kniep, J., Merkel, T.C., Wu, T., Lambrecht, R.C., 2014. CO2-selective membranes for hydrogen production and CO2 capture – Part I: Membrane development. J. Memb. Sci. 457, 149–161. https://doi.org/10.1016/j.memsci.2014.01.020

Ling, J., Ntiamoah, A., Xiao, P., Webley, P.A., Zhai, Y., 2015. Effects of feed gas concentration, temperature and process parameters on vacuum swing adsorption performance for CO2 capture. Chem. Eng. J. 265, 47–57. https://doi.org/10.1016/j.cej.2014.11.121

Liu, C., 2014. Advances in Membrane Technologies for Drinking Water Purification, Comprehensive Water Quality and Purification. Elsevier Ltd. https://doi.org/10.1016/B978-0-12-382182-9.00030-X

Lock, S.S.M., Lau, K.K., Ahmad, F., Shariff, A.M., 2015. Modeling, simulation and economic analysis of CO2 capture from natural gas using cocurrent, countercurrent and radial crossflow hollow fiber membrane. Int. J. Greenh. Gas Control 36, 114–134. https://doi.org/10.1016/j.ijggc.2015.02.014

Low, B.T., Zhao, L., Merkel, T.C., Weber, M., Stolten, D., Ting, B., Zhao, L., Merkel, T.C., Weber, M., Stolten, D., 2013. A parametric study of the impact of membrane materials and process operating conditions on carbon capture from humidified flue gas. J. Memb. Sci. 431, 139–155. https://doi.org/10.1016/j.memsci.2012.12.014

Maccoll, B., 2010. CO2 Capture - Technicalities of attaching a capture plant to Eskom ' s power stations South Africa Electricity Capacity in 2030 [WWW Document]. URL http://www.sacccs.org.za/wp-content/uploads/2015/CCS Conference/2015 CCS Conference - Retrofit CC - MacColl Eskom.pdf (accessed 5.13.19).

Magneschi, G., Zhang, T., Munson, R., 2017. The Impact of CO2 Capture on Water Requirements of Power Plants. Energy Procedia 114, 6337–6347. https://doi.org/10.1016/j.egypro.2017.03.1770

Makaruk, A., Harasek, M., 2009. Numerical algorithm for modelling multicomponent multipermeator systems. J. Memb. Sci. 344, 258–265. https://doi.org/10.1016/j.memsci.2009.08.013

Marriott, J., Sørensen, E., 2003. The optimal design of membrane systems. Chem. Eng. Sci. 58, 4991–5004. https://doi.org/10.1016/j.ces.2003.07.011

Masson-Delmotte, V., Zhai, P., Pörtner, H.-O., Roberts, D., Skea, J., Shukla, P.R., Pirani, A., Moufouma-Okia, W., Péan, C., Pidcock, R., Connors, S., Matthews, J.B.R., Chen, Y., Zhou, X., Gomis, M.I., Lonnoy, E., Maycock, T., Tignor, M., Waterfield, T., 2018. Intergovernmental Panel on Climate Change-Global Warming of 1.5 Degrees Celcius, IPCC-Summary for Policymakers. https://doi.org/10.1017/CBO9781107415324

Mat, N.C., 2016. Membrane Process Design for Post-Combustion Carbon Dioxide Capture. University of Toledo.

Mat, N.C., Lipscomb, G.G., 2019. Global sensitivity analysis for hybrid membrane-cryogenic post combustion carbon capture process. Int. J. Greenh. Gas Control. https://doi.org/10.1016/j.ijggc.2018.12.023

Mat, N.C., Lipscomb, G.G., 2017. Membrane process optimization for carbon capture. Int. J. Greenh. Gas Control 62, 1–12. https://doi.org/10.1016/j.ijggc.2017.04.002

Mazinani, S., Ramezani, R., Darvishmanesh, S., Molelekwa, G.F., Di Felice, R., Van Der Bruggen, B., 2018. A ground breaking polymer blend for CO2/N2 separation. J. CO2 Util.

27, 536–546. https://doi.org/10.1016/j.jcou.2018.08.024

McDonald, T.O., Akhtar, R., Lau, C.H., Ratvijitvech, T., Cheng, G., Clowes, R., Adams, D.J., Hasell, T., Cooper, A.I., 2015. Using intermolecular interactions to crosslink PIM-1 and modify its gas sorption properties. J. Mater. Chem. A 3, 4855–4864. https://doi.org/10.1039/c4ta06070a

Merkel, T., Lin, H., He, Z., Daniels, R., Thompson, S., Serbanescu, A., Baker, R., 2008. A Membrane Process to Capture CO 2 from Power Plant Flue Gas 1–2.

Merkel, T.C., Lin, H., Wei, X., Baker, R., 2010. Power plant post-combustion carbon dioxide capture: An opportunity for membranes. J. Memb. Sci. 359, 126–139. https://doi.org/10.1016/j.memsci.2009.10.041

Merkel, T.C., Wei, X., He, Z., White, L.S., Wijmans, J.G., Baker, R.W., 2013. Selective exhaust gas recycle with membranes for CO2 capture from natural gas combined cycle power plants. Ind. Eng. Chem. Res. 52, 1150–1159. https://doi.org/10.1021/ie302110z

Micari, M., Dakhchoune, M., Agrawal, K. V., 2021. Techno-economic assessment of postcombustion carbon capture using high-performance nanoporous single-layer graphene membranes. J. Memb. Sci. 624, 119103. https://doi.org/10.1016/j.memsci.2021.119103

Mineral Resources & Energy Department SA, 2020. Coal resources [WWW Document]. URL http://www.energy.gov.za/files/coal_frame.html (accessed 5.14.19).

Misener, R., Floudas, C.A., 2014. ANTIGONE: Algorithms for coNTinuous / Integer Global Optimization of Nonlinear Equations. J. Glob. Optim. 59, 503–526. https://doi.org/10.1007/s10898-014-0166-2

Mores, P.L., Arias, A.M., Scenna, N.J., Mussati, M.C., Mussati, S.F., 2019. Cost-based comparison of multi-stage membrane configurations for carbon capture from flue gas of power plants. Int. J. Greenh. Gas Control 86, 177–190. https://doi.org/10.1016/j.ijggc.2019.04.021

Mourgues, A., Sanchez, J., 2005. Theoretical analysis of concentration polarization in membrane modules for gas separation with feed inside the hollow-fibers. J. Memb. Sci. 252, 133–144. https://doi.org/10.1016/j.memsci.2004.11.024

Müller, N., Handge, U.A., Abetz, V., 2016. Physical ageing and lifetime prediction of polymer membranes for gas separation processes. J. Memb. Sci. 516, 33–46. https://doi.org/10.1016/j.memsci.2016.05.055

Murad Chowdhury, M.H., Douglas, P., Feng, X., Croiset, E., 2005. Design and simulation of membrane based gas separation processes in AspenPlus™ for capturing CO2 from flue gases A2 - Wilson, E.S. RubinD.W. KeithC.F. GilboyM., in: Thambimuthu, T.M.G. (Ed.), Greenhouse Gas Control Technologies 7. Elsevier Science Ltd, Oxford, pp. 1937–1940.

Murphy, D.A., Hockings, L.E., Andrews, R.K., Aubron, C., Gardiner, E.E., Pellegrino, V.A., Davis, A.K., 2015. Extracorporeal membrane oxygenation-hemostatic complications. Transfus. Med. Rev. 29, 90–101. https://doi.org/10.1016/j.tmrv.2014.12.001

Noble, R.D., 1992. Generalized microscopic mechanism of facilitated transport in fixed site carrier membranes. J. Memb. Sci. 75, 121–129. https://doi.org/10.1016/0376-7388(92)80011-8

Noble, R.D., 1991. Analysis of ion transport with fixed site carrier membranes. J. Memb. Sci. 56, 229–234. https://doi.org/10.1016/S0376-7388(00)80811-X

Ohs, B., Lohaus, J., Wessling, M., 2016. Optimization of membrane based nitrogen removal from natural gas. J. Memb. Sci. 498, 291–301. https://doi.org/10.1016/j.memsci.2015.10.007

Oke, D., Majozi, T., Mukherjee, R., Sengupta, D., El-Halwagi, M.M., 2018. Simultaneous Energy and Water Optimisation in Shale Exploration. https://doi.org/10.3390/pr6070086

Pan, C.Y., 1986. Gas separation by high-flux, asymmetric hollow-fiber membrane. AIChE J. 32, 2020–2027. https://doi.org/10.1002/aic.690321212

Pan, C.Y., 1983. GAS SEPARATION BY PERMEATORS WITH HIGH-FLUX ASYMMETRIC MEMBRANES. AIChE J. 29, 545–552.

Parsons Brinckerhoff, Group, W.B., 2013. Techno-Economic Review of CCS Implementation in South Africa.

Perry, Green, 1997. Perry's chemical engineers' handbook, 7th ed. McGraw-Hill, New York.

Pfister, M., Belaissaoui, B., Favre, E., 2017. Membrane gas separation processes from wet postcombustion flue gases for carbon capture and use: A critical reassessment. Ind. Eng. Chem. Res. 56, 591–602. https://doi.org/10.1021/acs.iecr.6b03969

Poth, N., Brusis, D., Stichlmair, J., 2003. Rigorous optimization of reactive distillation in GAMS with the use of external functions. Comput. Aided Chem. Eng. 14, 869–874. https://doi.org/10.1016/S1570-7946(03)80226-2

Puranik, Y., Sahinidis, N. V., 2017. Deletion presolve for accelerating infeasibility diagnosis in optimization models. INFORMS J. Comput. 29, 754–766.

Qi, R., Henson, M.A., 2000. Membrane system design for multicomponent gas mixtures via mixed-integer nonlinear programming. Comput. Chem. Eng. 24, 2719–2737. https://doi.org/10.1016/S0098-1354(00)00625-6

Qi, R, Henson, M.A., 1998. Optimization-based design of spiral-wound membrane systems for CO2/CH4 separations. Sep. Purif. Technol. 13, 209–225. https://doi.org/10.1016/S1383-5866(98)00044-6

Qi, Runhong, Henson, M.A., 1998. Optimal design of spiral-wound membrane networks for gas separations. J. Memb. Sci. 148, 71–89. https://doi.org/10.1016/S0376-7388(98)00143-4

Qi, R., Henson, M.A., 1996. Approximate modeling of spiral-wound gas permeators. J. Memb. Sci. 121, 11–24. https://doi.org/10.1016/0376-7388(96)00156-1

Qiao, Z., Wang, Z., Zhang, C., Yuan, S., Zhu, Y., Wang, J., Wang, S., 2013. PVAm–PIP/PS

Composite Membrane with High Performance for CO2/N2 Separation. AIChE J. 59, 215–228. https://doi.org/10.1002/aic.13781

Quan, S., Li, S.W., Xiao, Y.C., Shao, L., 2017. CO2-selective mixed matrix membranes (MMMs) containing graphene oxide (GO) for enhancing sustainable CO2 capture. Int. J. Greenh. Gas Control 56, 22–29. https://doi.org/10.1016/j.ijggc.2016.11.010

Quintella, C.M., Hatimondi, S.A., Musse, A.P.S., Miyazaki, S.F., Cerqueira, G.S., De Araujo Moreira, A., 2011. CO2 capture technologies: An overview with technology assessment based on patents and articles. Energy Procedia 4, 2050–2057. https://doi.org/10.1016/j.egypro.2011.02.087

Ramasubramanian, K., Ho, W.S.W., 2011. Recent developments on membranes for post-combustion carbon capture. Curr. Opin. Chem. Eng. 1, 47–54. https://doi.org/10.1016/j.coche.2011.08.002

Ramasubramanian, K., Verweij, H., Winston Ho, W.S., 2012. Membrane processes for carbon capture from coal-fired power plant flue gas: A modeling and cost study. J. Memb. Sci. 421–422, 299–310. https://doi.org/10.1016/j.memsci.2012.07.029

Ramasubramanian, K., Zhao, Y., Winston Ho, W. s., 2013. CO2 capture and H2 purification: Prospects for CO2-selective membrane processes. AIChE J. 59, 1033–1045. https://doi.org/10.1002/aic.14078

Ramírez-Santos, Á.A., Bozorg, M., Addis, B., Piccialli, V., Castel, C., Favre, E., 2018. Optimization of multistage membrane gas separation processes. Example of application to CO2 capture from blast furnace gas. J. Memb. Sci. 566, 346–366. https://doi.org/10.1016/J.MEMSCI.2018.08.024

Rao, A.B., Kumar, P., 2014. Cost implications of carbon capture and storage for the coal power plants in India. Energy Procedia 54, 431–438. https://doi.org/10.1016/j.egypro.2014.07.285

Rautenbach, R., Dahm, W., 1985. The separation of multicomponent mixtures by gas

permeation. Chem. Eng. Process. Process Intensif. 19, 211–219. https://doi.org/10.1016/0255-2701(84)80024-0

Rea, R., De Angelis, M.G., Baschetti, M.G., 2019. Models for facilitated transport membranes: A review. Membranes (Basel). 9, 1–55. https://doi.org/10.3390/membranes9020026

Ren, L.X., Chang, F.L., Kang, D.Y., Chen, C.L., 2020. Hybrid membrane process for post-combustion CO2 capture from coal-fired power plant. J. Memb. Sci. 603, 118001. https://doi.org/10.1016/j.memsci.2020.118001

Riboldi, L., Bolland, O., Ngoy, J.M., Wagner, N., 2014. Full-plant Analysis of a PSA CO2 Capture Unit Integrated In Coal-fired Power Plants: Post-and Pre-combustion Scenarios. Energy Procedia, 12th International Conference on Greenhouse Gas Control Technologies, GHGT-12 63, 2289–2304. https://doi.org/10.1016/j.egypro.2014.11.248

Robeson, L.M., 2008. The upper bound revisited. J. Memb. Sci. 320, 390–400. https://doi.org/10.1016/j.memsci.2008.04.030

Robeson, L.M., 1991. Correlation of separation factor versus permeability for polymeric membranes. J. Memb. Sci. 62, 165–185. https://doi.org/10.1016/0376-7388(91)80060-J

Rodrigues, S.C., Sousa, J., Mendes, A., 2018. Facilitated transport membranes for CO2/H2 separation, in: Facilitated Transport Membranes for CO2/H2 Separation. Elsevier, pp. 359–384. https://doi.org/10.1016/B978-0-12-813645-4.00013-1

Roussanaly, S., Anantharaman, R., 2017. Cost-optimal CO2 capture ratio for membrane-based capture from different CO2 sources. Chem. Eng. J. 327, 618–628. https://doi.org/10.1016/j.cej.2017.06.082

Roussanaly, S., Vitvarova, M., Anantharaman, R., Berstad, D., Hagen, B., Jakobsen, J., Novotny, V., Skaugen, G., 2019. Techno-economic comparison of three technologies for precombustion CO2 capture from a lignite-fired IGCC. Front. Chem. Sci. Eng. https://doi.org/10.1007/s11705-019-1870-8

Rubin, E., Booras, G., Davison, J., Ekstrom, C., Matuszewski, M., Mccoy, S., Short, C., 2013. Toward a Common Method of Cost Estimation for CO 2 Capture and Storage at Fossil Fuel Power Plants A White Paper Prepared by the Task Force on CCS Costing Methods 1–43.

Rubin, E.S., 2012. Understanding the pitfalls of CCS cost estimates. Int. J. Greenh. Gas Control 10, 181–190. https://doi.org/10.1016/j.ijggc.2012.06.004

Rubin, E.S., Short, C., Booras, G., Davison, J., Ekstrom, C., Matuszewski, M., McCoy, S., 2013a. A proposed methodology for CO2 capture and storage cost estimates. Int. J. Greenh. Gas Control 17, 488–503. https://doi.org/10.1016/j.ijggc.2013.06.004

Rubin, E.S., Short, C., Booras, G., Davison, J., Ekstrom, C., Matuszewski, M., McCoy, S., 2013b. A proposed methodology for CO 2 capture and storage cost estimates. Int. J. Greenh. Gas Control 17, 488–503. https://doi.org/10.1016/j.ijggc.2013.06.004

Sai Prasad, P.S., Raghavan, K. V., 2012. Techno-economic aspects of the post-combustion CO 2 capture processes. Indian J. Chem. - Sect. A Inorganic, Phys. Theor. Anal. Chem. 51, 1201–1213.

Salim, W., Vakharia, V., Chen, Y., Wu, D., Han, Y., Ho, W.S.W., 2018. Fabrication and field testing of spiral-wound membrane modules for CO2 capture from flue gas. J. Memb. Sci. 556, 126–137. https://doi.org/10.1016/j.memsci.2018.04.001

Sandru, M., Kim, T.J., Capala, W., Huijbers, M., Hägg, M.B., 2013. Pilot scale testing of polymeric membranes for CO2 capture from coal fired power plants. Energy Procedia 37, 6473–6480. https://doi.org/10.1016/j.egypro.2013.06.577

SANEDI, 2019. SACCS [WWW Document]. URL https://www.sacccs.org.za/Home/ (accessed 12.22.19).

Sarfraz, M., Ba-Shammakh, M., 2018. Water-stable ZIF-300/Ultrason® mixed-matrix membranes for selective CO2 capture from humid post combustion flue gas. Chinese J. Chem. Eng. 26, 1012–1021. https://doi.org/10.1016/j.cjche.2017.11.007

SARS, 2019. carbon Tax [WWW Document]. URL https://www.sars.gov.za/ClientSegments/Customs-Excise/Excise/Environmental-Levy-Products/Pages/Carbon-Tax.aspx (accessed 5.1.20).

Scholes, C.A., Ho, M.T., Wiley, D.E., Stevens, G.W., Kentish, S.E., 2013. Cost competitive membrane—cryogenic post-combustion carbon capture. Int. J. Greenh. Gas Control 17, 341–348. https://doi.org/10.1016/j.ijggc.2013.05.017

Scholes, C.A., Kentish, S.E., Stevens, G.W., 2009. Effects of minor components in carbon dioxide capture using polymeric gas separation membranes. Sep. Purif. Rev. 38, 1–44. https://doi.org/10.1080/15422110802411442

Scholz, M., Harlacher, T., Melin, T., Wessling, M., 2013. Modeling gas permeation by linking nonideal effects. Ind. Eng. Chem. Res. 52, 1079–1088. https://doi.org/10.1021/ie202689m

Seyboth, K., Matschoss, P., Susanne, K., Timm, Z., Patrick, E., Gerrit, H., Steffen, S., Christoph, von S., 2011. Renewable Energy Sources and Climate Change Mitigation, Renewable Energy Sources and Climate Change Mitigation. https://doi.org/10.1017/cbo9781139151153

Shah, P.B., Kokossis, A., 1997. Design targets of separator and reactor-separator systems using conceptual programming. Comput. Chem. Eng., Supplement to Computers and Chemical Engineering6th International Symposium on Process Systems Engineering and 30th European Symposium on Computer Aided Process Engineering 21, Supple, S1013–S1018. https://doi.org/10.1016/S0098-1354(97)87635-1

Shakerian, F., Kim, K.-H., Szulejko, J.E., Park, J.-W., 2015. A comparative review between amines and ammonia as sorptive media for post-combustion CO2 capture. Appl. Energy 148, 10–22. https://doi.org/10.1016/j.apenergy.2015.03.026

Shao, P., Dal-Cin, M.M., Guiver, M.D., Kumar, A., 2013. Simulation of membrane-based CO2 capture in a coal-fired power plant. J. Memb. Sci. 427, 451–459. https://doi.org/10.1016/j.memsci.2012.09.044

Singh, U., Rao, A.B., 2016. Techno-Economic Assessment of Carbon Mitigation Options for Existing Coal-fired Power Plants in India. Energy Procedia 90, 326–335. https://doi.org/10.1016/j.egypro.2016.11.200

Smith, S.J.D., Hou, R., Konstas, K., Akram, A., Lau, C.H., Hill, M.R., 2020. Control of Physical Aging in Super-Glassy Polymer Mixed Matrix Membranes. Acc. Chem. Res. 53, 1381–1388. https://doi.org/10.1021/acs.accounts.0c00256

Sreedhar, I., Vaidhiswaran, R., Kamani, B.M., Venugopal, A., 2017. Process and engineering trends in membrane based carbon capture. Renew. Sustain. Energy Rev. 68, 659–684. https://doi.org/10.1016/j.rser.2016.10.025

Sreenivasulu, B., Gayatri, D. V, Sreedhar, I., Raghavan, K. V, 2015. A journey into the process and engineering aspects of carbon capture technologies. Renew. Sustain. Energy Rev. 41, 1324–1350. https://doi.org/10.1016/j.rser.2014.09.029

Stern, S.A., Walawender, W.P., 1969. Analysis of Membrane Separation Parameters. Sep. Sci. 4, 129–159. https://doi.org/10.1080/01496396908052244

Stern, S.A., Wang, S.C., 1978. Countercurrent and cocurrent gas separation in a permeation stage. Comparison of computation methods. J. Memb. Sci. 4, 141–148. https://doi.org/10.1016/S0376-7388(00)83290-1

Suleman, M.S., Lau, K.K., Yeong, Y.F., 2016. Plasticization and Swelling in Polymeric Membranes in CO2 Removal from Natural Gas. Chem. Eng. Technol. 39, 1604–1616. https://doi.org/10.1002/ceat.201500495

Surridge, A.D.D., Cloete, M., 2009. Carbon capture and storage in South Africa. Energy Procedia 1, 2741–2744. https://doi.org/10.1016/j.egypro.2009.02.044

Swaidan, R., Ghanem, B., Litwiller, E., Pinnau, I., 2015. Physical Aging, Plasticization and Their Effects on Gas Permeation in “rigid” Polymers of Intrinsic Microporosity. Macromolecules 48, 6553–6561. https://doi.org/10.1021/acs.macromol.5b01581

Tan, Z., 2014. Air Pollution and Greenhouse Gases, Green Energy and Technology.

Tomé, L.C., Patinha, D.J.S., Freire, C.S.R., Rebelo, L.P.N., Marrucho, I.M., 2013. CO2 separation applying ionic liquid mixtures: The effect of mixing different anions on gas permeation through supported ionic liquid membranes. RSC Adv. 3, 12220–12229. https://doi.org/10.1039/c3ra41269e

Tong, Z., Ho, W.S.W., 2017. Facilitated transport membranes for CO2 separation and capture. Sep. Sci. Technol. 52, 156–167. https://doi.org/10.1080/01496395.2016.1217885

Tot, M., Pešut, D., Alison, H., Catherine, F., Bruno, M., Ajay, T., Jan, D., Helga, F., Arnould, L., 2011. Techno-economic assessment of carbon capture and storage deployment in power stations in the Southern African and Balkan regions.

Tsue, H., Takahashi, H., Ishibashi, K., Inoue, R., Shimizu, S., Takahashi, D., Tamura, R., 2012. Crystallographic analysis of CO 2 sorption state in seemingly nonporous molecular crystal of azacalix[4]arene tetramethyl ether exhibiting highly selective CO 2 uptake. CrystEngComm 14, 1021–1026. https://doi.org/10.1039/c1ce06126g

Tu, T., Cui, Q., Liang, F., Xu, L., He, Q., Yan, S., 2019. Water recovery from stripping gas overhead CO 2 desorber through air cooling enhanced by transport membrane condensation. Sep. Purif. Technol. 215, 625–633. https://doi.org/10.1016/j.seppur.2019.01.058

Ulbricht, M., 2006. Advanced functional polymer membranes. Polymer (Guildf). 47, 2217–2262. https://doi.org/10.1016/j.polymer.2006.01.084

UN, 2015. Paris Agreement 2015, UN reports.

Uppaluri, R., Smith, R., Linke, P., Kokossis, A., 2002. Optimal design of gas permeation membrane & membrane adsorption hybrid systems, in: Schijndel, J.G. and J. van (Ed.), Computer Aided Chemical Engineering, European Symposium on Computer Aided Process Engineering-12 35th European Symposium of the Working Party on Computer Aided Process Engineering. Elsevier, pp. 367–372.

Uppaluri, R.V.S., Smith, R., Linke, P., Kokossis, A.C., 2006. On the simultaneous optimization of pressure and layout for gas permeation membrane systems. J. Memb. Sci. 280, 832–848. https://doi.org/10.1016/j.memsci.2006.03.004

Uppaluri, R.V.S.S., Linke, P., Kokossis, A.C., 2004. Synthesis and Optimization of Gas Permeation Membrane Networks. Ind. Eng. Chem. Res. 43, 4305–4322. https://doi.org/10.1021/ie030787c

Vallieres, C., Favre, E., 2004. Vacuum versus sweeping gas operation for binary mixtures separation by dense membrane processes. J. Memb. Sci. https://doi.org/10.1016/j.memsci.2004.04.023

Van Der Sluijs, J.P., Hendriks, C.A., Blok, K., 1992. Feasibility of polymer membranes for carbon dioxide recovery from flue gases. Energy Convers. Manag. 33, 429–436. https://doi.org/10.1016/0196-8904(92)90040-4

Viebahn, P., Vallentin, D., Höller, S., 2015. Integrated assessment of carbon capture and storage (CCS) in South Africa's power sector. Energies 8, 14380–14406. https://doi.org/10.3390/en81212432

Viljoen, J.H.A., Stapelberg, F.D.J., Cloete, M., 2010. Technical Report on the Geological Storage of Carbon Dioxide.

Wang, M., Wang, Z., Zhao, S., Wang, J., Wang, S., 2017. Recent advances on mixed matrix membranes for CO2 separation. Chinese J. Chem. Eng. 25, 1581–1597. https://doi.org/10.1016/j.cjche.2017.07.006

Wang, S., Li, X., Wu, H., Tian, Z., Xin, Q., He, G., Peng, D., Chen, S., Yin, Y., Jiang, Z., Guiver, M.D., 2016. Advances in high permeability polymer-based membrane materials for CO2 separations. Energy Environ. Sci. 9, 1863–1890. https://doi.org/10.1039/c6ee00811a

Wang, Y.C., Teng, M.Y., Lee, K.R., Lai, J.Y., 2005. Comparison between the pervaporation and vapor permeation performances of polycarbonate membranes. Eur. Polym. J. 41,

1667–1673. https://doi.org/10.1016/j.eurpolymj.2005.01.011

White, L.S., Amo, K.D., Wu, T., Merkel, T.C., 2017. Extended field trials of Polaris sweep modules for carbon capture. J. Memb. Sci. 542, 217–225. https://doi.org/10.1016/j.memsci.2017.08.017

White, L.S., Wei, X., Pande, S., Wu, T., Merkel, T.C., 2015. Extended flue gas trials with a membrane-based pilot plant at a one-ton-per-day carbon capture rate. J. Memb. Sci. 496, 48–57. https://doi.org/10.1016/j.memsci.2015.08.003

Xiao, Y., Chung, T.S., 2011. Grafting thermally labile molecules on cross-linkable polyimide to design membrane materials for natural gas purification and CO2 capture. Energy Environ. Sci. 4, 201–208. https://doi.org/10.1039/c0ee00278j

Xu, J., Wang, Z., Qiao, Z., Wu, H., Dong, S., Zhao, S., Wang, J., 2019. Post-combustion CO2 capture with membrane process: Practical membrane performance and appropriate pressure. J. Memb. Sci. 581, 195–213. https://doi.org/10.1016/j.memsci.2019.03.052

Yave, W., Car, A., Wind, J., Peinemann, K.V., 2010. Nanometric thin film membranes manufactured on square meter scale: Ultra-thin films for CO2 capture. Nanotechnology 21. https://doi.org/10.1088/0957-4484/21/39/395301

Ye, B., Jiang, J., Zhou, Y., Liu, J., Wang, K., 2019. Technical and economic analysis of amine-based carbon capture and sequestration at coal-fired power plants. J. Clean. Prod. https://doi.org/10.1016/j.jclepro.2019.03.050

Ying, Y., Ying, W., Li, Q., Meng, D., Ren, G., Yan, R., Peng, X., 2017. Recent advances of nanomaterial-based membrane for water purification. Appl. Mater. Today 7, 144–158. https://doi.org/10.1016/j.apmt.2017.02.010

Yu, X., Wang, Z., Zhao, J., Yuan, F., Li, S., Wang, J., Wang, S., 2011. An effective method to improve the performance of fixed carrier membrane via incorporation of CO2-selective adsorptive silica nanoparticles. Chinese J. Chem. Eng. 19, 821–832. https://doi.org/10.1016/S1004-9541(11)60062-1

Yuan, M., Narakornpijit, K., Haghpanah, R., Wilcox, J., 2014. Consideration of a nitrogen-selective membrane for postcombustion carbon capture through process modeling and optimization. J. Memb. Sci. 465, 177–184. https://doi.org/10.1016/j.memsci.2014.04.026

Yuan, M., Teichgraeber, H., Wilcox, J., Brandt, A.R., 2019. Design and operations optimization of membrane-based flexible carbon capture. Int. J. Greenh. Gas Control 84, 154–163. https://doi.org/10.1016/j.ijggc.2019.03.018

Zamarripa, M.A., Eslick, J.C., Matuszewski, M.S., Miller, D.C., 2018. Multi-objective Optimization of Membrane-based CO2 Capture, Computer Aided Chemical Engineering. Elsevier Masson SAS. https://doi.org/10.1016/B978-0-444-64241-7.50181-6

Zarca, G., Urtiaga, A., Biegler, L.T., Ortiz, I., 2018. An optimization model for assessment of membrane-based post-combustion gas upcycling into hydrogen or syngas. J. Memb. Sci. 563, 83–92. https://doi.org/10.1016/j.memsci.2018.05.038

Zarca, R., Ortiz, A., Gorri, D., Biegler, L.T., Ortiz, I., 2019. Optimization of multistage olefin/paraffin membrane separation processes through rigorous modeling. AIChE J. 65. https://doi.org/10.1002/aic.16588

Zarca, R., Ortiz, A., Gorri, D., Ortiz, I., 2017a. A practical approach to fixed-site-carrier facilitated transport modeling for the separation of propylene/propane mixtures through silver-containing polymeric membranes. Sep. Purif. Technol. 180, 82–89. https://doi.org/10.1016/j.seppur.2017.02.050

Zarca, R., Ortiz, A., Gorri, D., Ortiz, I., 2017b. Generalized predictive modeling for facilitated transport membranes accounting for fixed and mobile carriers. J. Memb. Sci. 542, 168–176. https://doi.org/10.1016/j.memsci.2017.08.010

Zhai, H., Rubin, E.S., 2013. Techno-Economic Assessment of Polymer Membrane Systems for Postcombustion Carbon Capture at Coal-Fired Power Plants. Environ. Sci. Technol. 47, 3006–3014. https://doi.org/10.1021/es3050604

Zhai, H., Rubin, E.S., 2011. Carbon capture effects on water use at pulverized coal power

plants. Energy Procedia 4, 2238–2244. https://doi.org/10.1016/j.egypro.2011.02.112

Zhai, H., Rubin, E.S., 2010. Performance and cost of wet and dry cooling systems for pulverized coal power plants with and without carbon capture and storage. Energy Policy 38, 5653–5660. https://doi.org/10.1016/j.enpol.2010.05.013

Zhang, C., Wang, Z., Cai, Y., Yi, C., Yang, D., Yuan, S., 2013. Investigation of gas permeation behavior in facilitated transport membranes: Relationship between gas permeance and partial pressure. Chem. Eng. J. 225, 744–751. https://doi.org/10.1016/j.cej.2013.03.100

Zhang, X., Singh, B., He, X., Gundersen, T., Deng, L., Zhang, S., 2014. Post-combustion carbon capture technologies: Energetic analysis and life cycle assessment. Int. J. Greenh. Gas Control 27, 289–298. https://doi.org/10.1016/j.ijggc.2014.06.016

Zhao, L., Riensche, E., Blum, L., Stolten, D., 2011. How gas separation membrane competes with chemical absorption in postcombustion capture. Energy Procedia 4, 629–636. https://doi.org/10.1016/j.egypro.2011.01.098

Zhao, L., Riensche, E., Blum, L., Stolten, D., 2010. Multi-stage gas separation membrane processes used in post-combustion capture: Energetic and economic analyses. J. Memb. Sci., Membranes and CO2 Separation 359, 160–172. https://doi.org/10.1016/j.memsci.2010.02.003

Zhao, L., Riensche, E., Menzer, R., Blum, L., Stolten, D., 2008. A parametric study of CO2/N2 gas separation membrane processes for post-combustion capture. J. Memb. Sci. 325, 284–294. https://doi.org/10.1016/j.memsci.2008.07.058

Zhao, M., Minett, A.I., Harris, A.T., 2013. A review of techno-economic models for the retrofitting of conventional pulverised-coal power plants for post-combustion capture (PCC) of CO_2. Energy Environ. Sci. 6, 25–40. https://doi.org/10.1039/C2EE22890D

Zhao, S., Yan, S., Wang, D.K., Wei, Y., Qi, H., Wu, T., Feron, P.H.M., 2017. Simultaneous heat and water recovery from flue gas by membrane condensation: Experimental investigation. Appl. Therm. Eng. 113, 843–850.

https://doi.org/10.1016/j.applthermaleng.2016.11.101

Zhao, W., He, G., Nie, F., Zhang, L., Feng, H., Liu, H., 2012. Membrane liquid loss mechanism of supported ionic liquid membrane for gas separation. J. Memb. Sci. 411–412, 73–80. https://doi.org/10.1016/j.memsci.2012.04.016

Zhou, F., Tien, H.N., Dong, Q., Xu, W.L., Li, H., Li, S., Yu, M., 2019. Ultrathin, ethylenediamine-functionalized graphene oxide membranes on hollow fibers for CO2 capture. J. Memb. Sci. 573, 184–191. https://doi.org/10.1016/j.memsci.2018.11.080

Zou, J., Ho, W.S.W., 2006. CO2-selective polymeric membranes containing amines in crosslinked poly(vinyl alcohol). J. Memb. Sci. 286, 310–321. https://doi.org/10.1016/j.memsci.2006.10.013

Zylberberg, C., Matosevic, S., 2016. Pharmaceutical liposomal drug delivery: a review of new delivery systems and a look at the regulatory landscape. Drug Deliv. 23, 3319–3329. https://doi.org/10.1080/10717544.2016.1177136

Appendix A. Membrane model validation

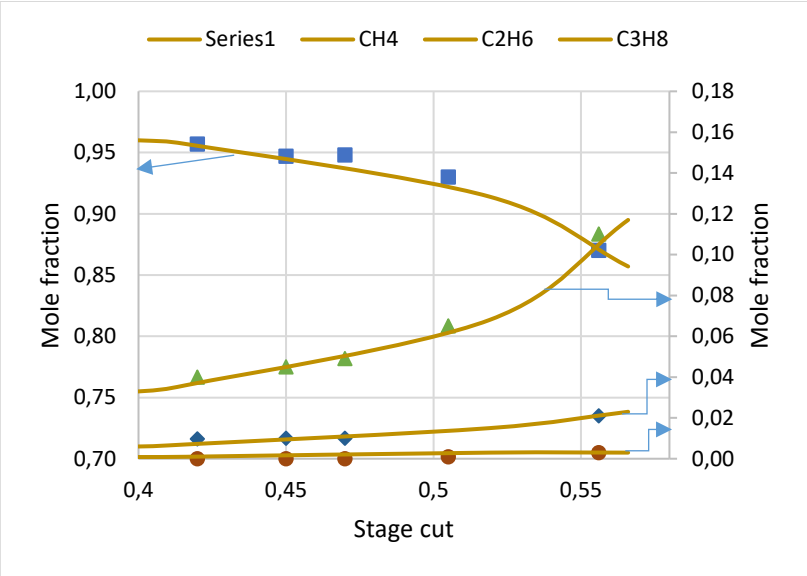

Figure A1. Experimental values (Pan, 1986)(ex) and the values from the simulation

Appendix B. Partial pressure profiles along the membrane profiles of different flow configurations of FSC membrane

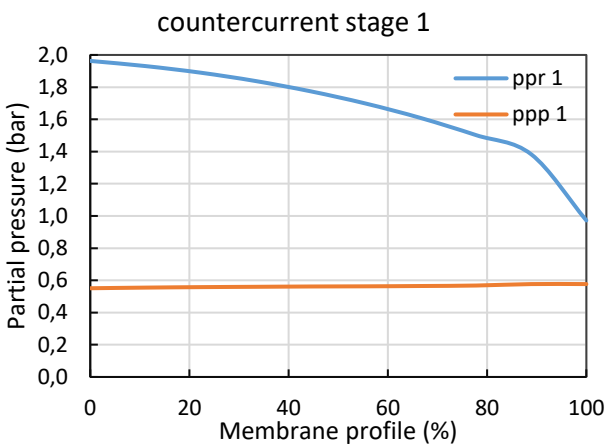

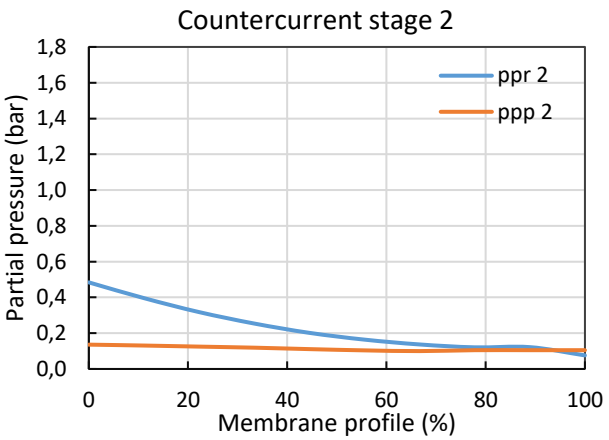

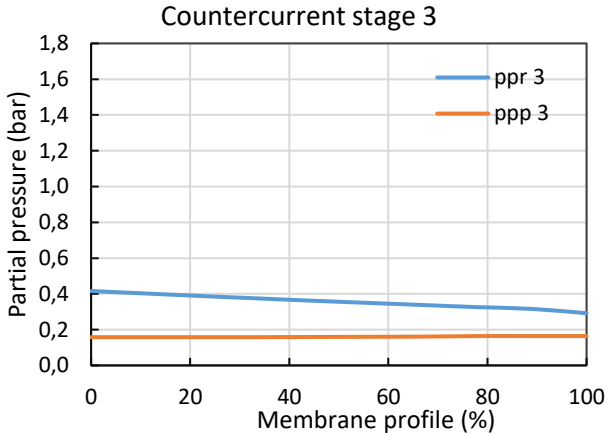

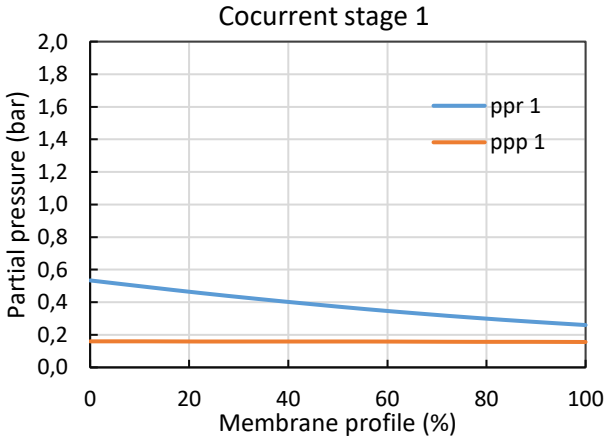

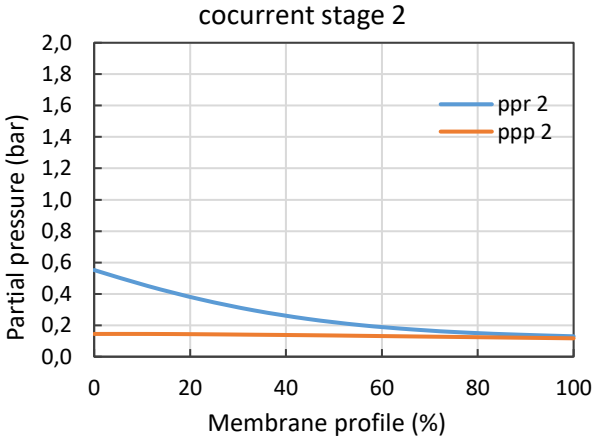

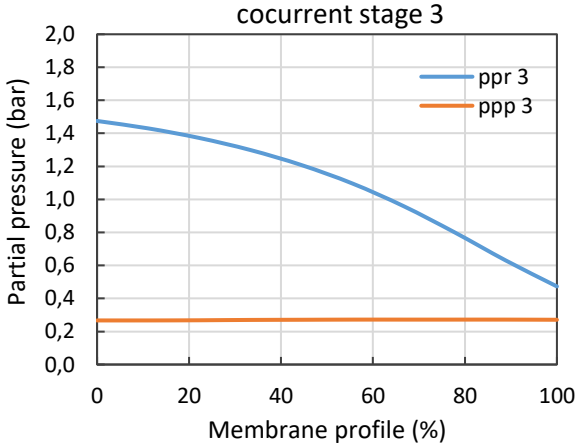

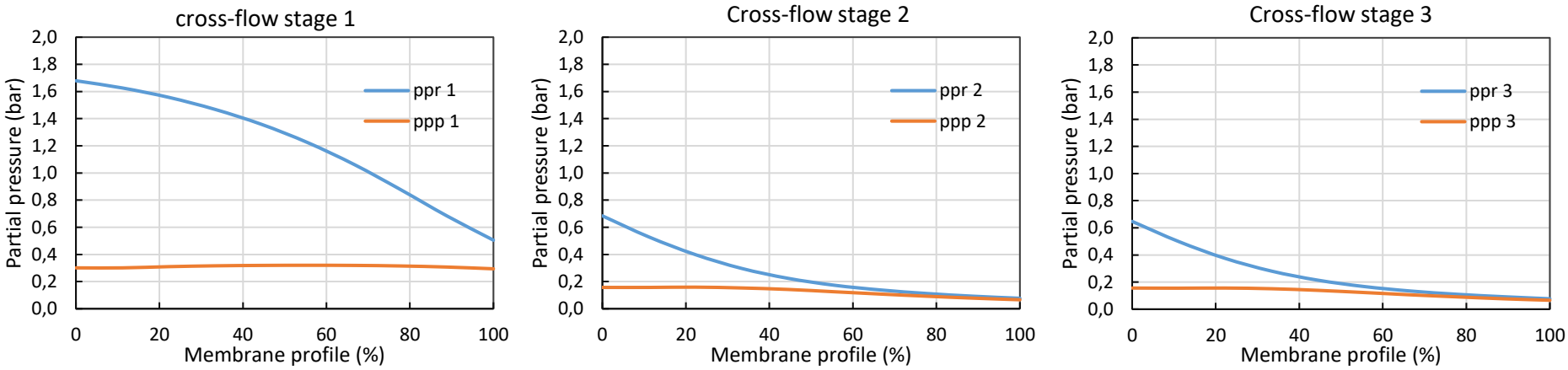

Figure A2. Partial pressure profiles along the membrane profiles

Appendix C. Copies of Journal articles published

1. Chapter 3

International Journal of Greenhouse Gas Control 104 (2021) 103182

Contents lists available at ScienceDirect

International Journal of Greenhouse Gas Control

journal homepage: www.elsevier.com/locate/ijggc

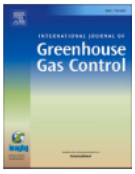

Optimisation of post-combustion carbon dioxide capture by use of a fixed site carrier membrane

Natsayi Chiwaye [a], Thokozani Majozi [a,*], Michael O. Daramola [a,b,*]

2. Chapter 5

Journal Pre-proof

On optimisation of N_2 and CO_2-selective hybrid membrane process systems for post-combustion CO_2 capture from coal-fired power plants

Natsayi Chiwaye, Thokozani Majozi, Michael O. Daramola

PII: S0376-7388(21)00637-2

DOI: https://doi.org/10.1016/j.memsci.2021.119691

Reference: MEMSCI 119691

To appear in: *Journal of Membrane Science*

Appendix D. Turnitin plagiarism report

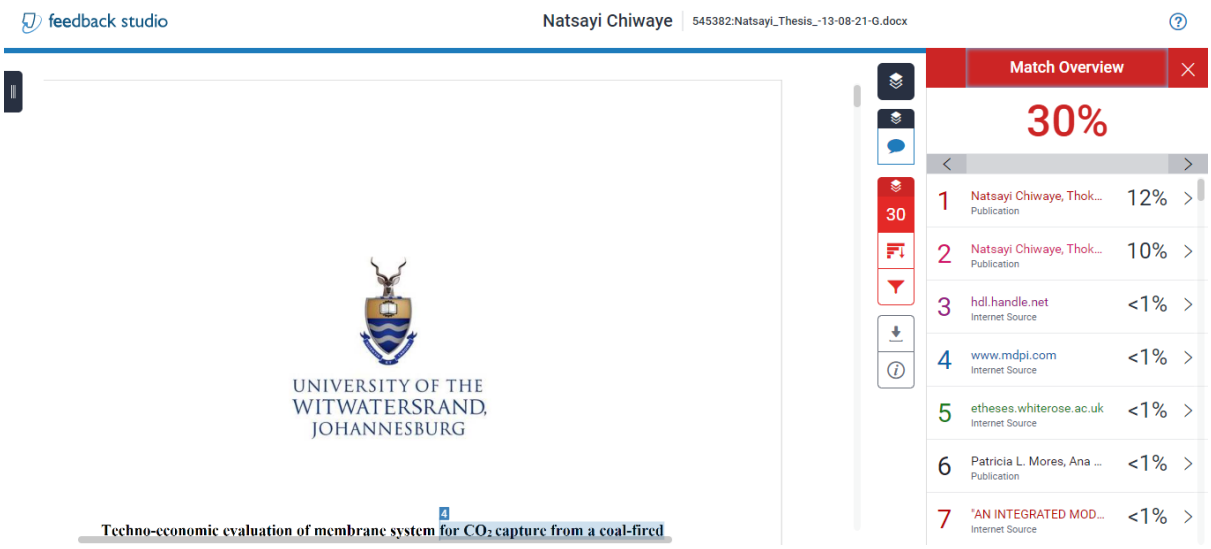

ORIGINALITY REPORT

30%	8%	26%	1%
SIMILARITY INDEX	INTERNET SOURCES	PUBLICATIONS	STUDENT PAPERS

PRIMARY SOURCES

1	Natsayi Chiwaye, Thokozani Majozi, Michael O. Daramola. "On optimisation of N2 and CO2-selective hybrid membrane process systems for post-combustion CO2 capture from coal-fired power plants", Journal of Membrane Science, 2021 Publication	12%
2	Natsayi Chiwaye, Thokozani Majozi, Michael O. Daramola. "Optimisation of post-combustion carbon dioxide capture by use of a fixed site carrier membrane", International Journal of Greenhouse Gas Control, 2020 Publication	10%
3	hdl.handle.net Internet Source	<1%
4	www.mdpi.com Internet Source	<1%
5	etheses.whiterose.ac.uk Internet Source	<1%

The high similarities to sources of 12% and 10% matches with the published work which has been reproduced with permission from the publishers Elsevier. The rest of the sources therefore sum up to 8% similarity. The permissions are shown in Appendix E.

Appendix E. Copyright permission for use of own published work in this thesis

Rights to Journal content published (Chapter 3)

6. Rights to Journal content published (Chapter 5)

Appendix F. Copyright Permission for Figures reproduced (Table and certificates)

Table of Permissions

Figure in thesis	**Figure Table**	**Authors**	**Original Source**	**DOI & website**	**Original Rightsholder**	**License**
Figure 2.2	**Figure 8 Page 6 -395**	Robeson, L.M.,	The upper bound revisited. J. Memb. Sci. 320, 390–400. https://doi.org/10.1016/j.memsci.2008.04.030	https://www.sciencedirect.com/science/article/pii/S0376738808003347	**Elsevier**	**5123190971787**
Figure 2.6	**Figure 1 Page 6 Page 562**	Harlacher and Matthias Wessling	Gas–Gas Separation by Membranes Thomashttps://doi.org/10.1016/B978-0-12-384746-1.00013-6	https://www.sciencedirect.com/science/article/pii/B9780123847461000136?via%3Dihub	**Elsevier**	**5123651166764**

Figure 2.7	**Figure 2** **Page 7 562**	Harlacher and Matthias Wessling	Gas–Gas Separation by Membranes Thomashttps://doi.org/10.1016/B978-0-12-384746-1.00013-6	https://www.sciencedirect.com/science/article/pii/B9780123847461000136?via%3Dihub	**Elsevier**	**5123651166764**
Figure 2.10	**Fig 12** **Page10** **-135**	Merkel, T.C., Lin, H., Wei, X., Baker, R., 2010.	Power plant post-combustion carbon dioxide capture: An opportunity for membranes. J. Memb. Sci., 359, 126–139. https://doi.org/10.1016/j.memsci.2009.10.041	https://www.sciencedirect.com/science/article/pii/S0376738809007832 reused	**Elsevier**	**5123650129327**
Figure 2.11	**Figure1** **Page 5** **-75**	Qi, Runhong, Henson, M.A.,	Optimal design of spiral-wound membrane networks for gas separations. J. Memb. Sci., 148, 71–89	https://www.sciencedirect.com/science/article/pii/S0376738898001434	**Elsevier**	**5123640031164**

			https://doi.org/10.1016/S0376-7388(98)00143-4			
Figure 2.12	**Figure 3** **Page 3** **-1990**	Aliaga-vicente, A., Caballero, J.A., Fernandez-Torres, M.,	Synthesis and Optimization of Membrane Cascade for Gas Separation via Mixed-Integer Nonlinear Programming DOI 10.1002/aic.15631 Published	https://aiche.onlinelibrary.wiley.com/doi/10.1002/aic.15631	**Wiley**	**5123661292502**

1. Permission Licence for Figure 2.2

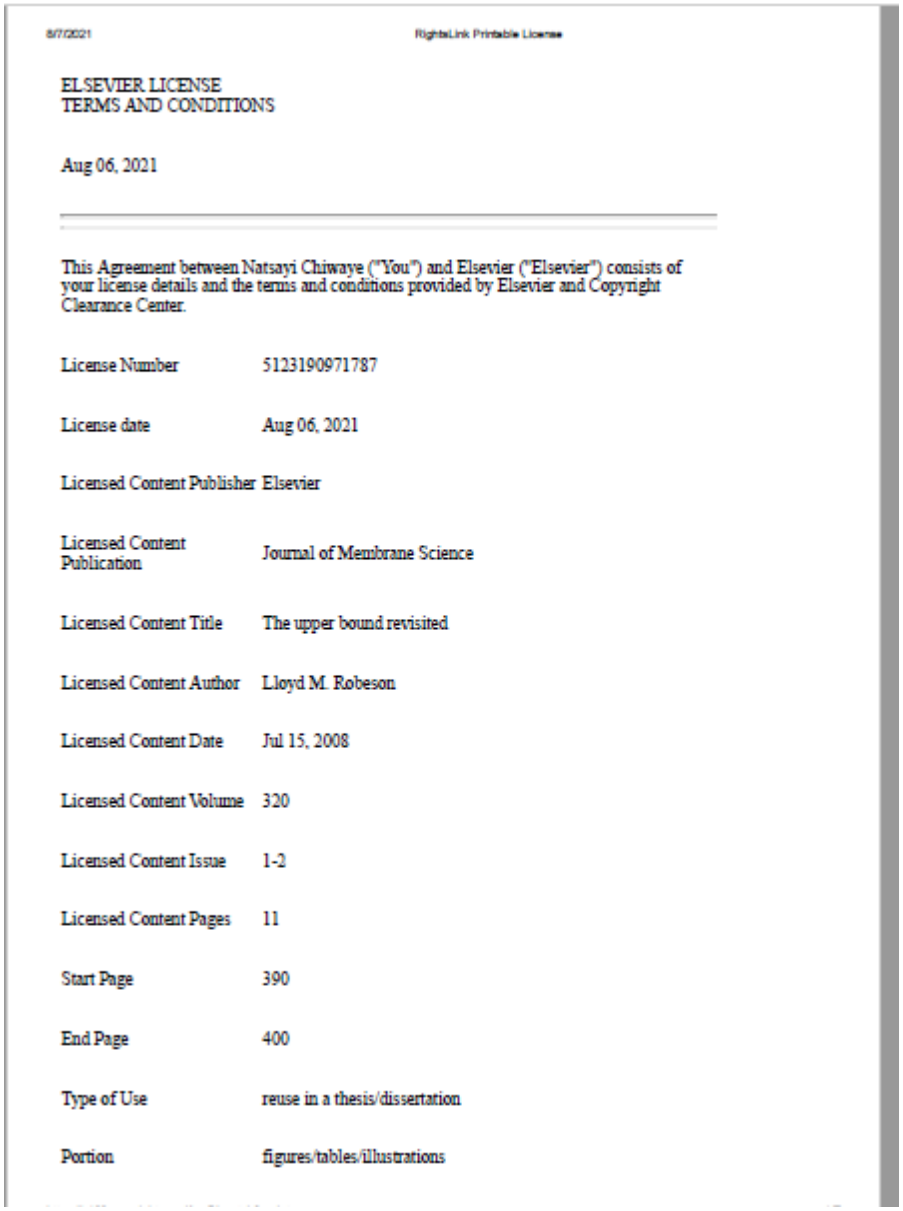

8/7/2021 RightsLink Printable License

ELSEVIER LICENSE
TERMS AND CONDITIONS

Aug 06, 2021

This Agreement between Natsayi Chiwaye ("You") and Elsevier ("Elsevier") consists of your license details and the terms and conditions provided by Elsevier and Copyright Clearance Center.

License Number	5123190971787
License date	Aug 06, 2021
Licensed Content Publisher	Elsevier
Licensed Content Publication	Journal of Membrane Science
Licensed Content Title	The upper bound revisited
Licensed Content Author	Lloyd M. Robeson
Licensed Content Date	Jul 15, 2008
Licensed Content Volume	320
Licensed Content Issue	1-2
Licensed Content Pages	11
Start Page	390
End Page	400
Type of Use	reuse in a thesis/dissertation
Portion	figures/tables/illustrations

2. Permission for Figure 2.6 and 2.7

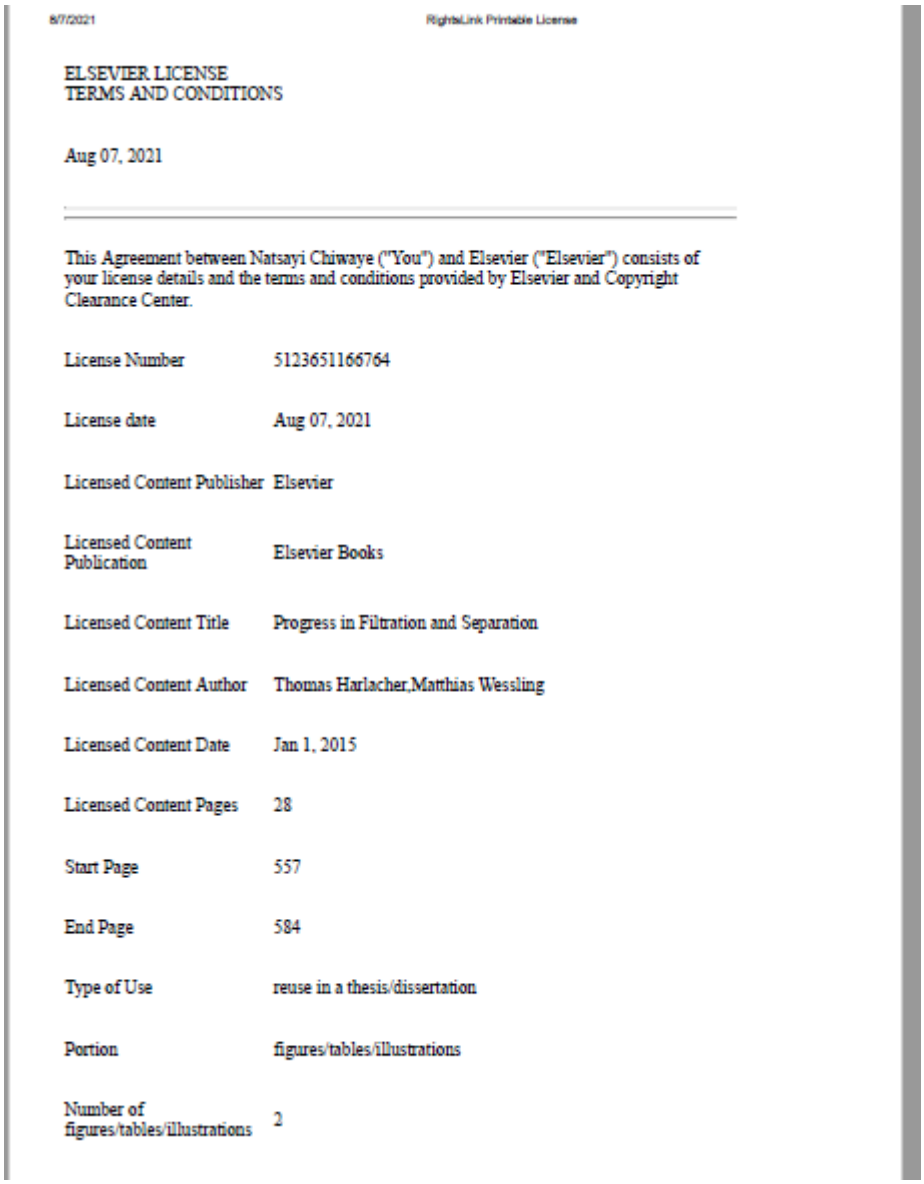

8/7/2021 RightsLink Printable License

ELSEVIER LICENSE
TERMS AND CONDITIONS

Aug 07, 2021

This Agreement between Natsayi Chiwaye ("You") and Elsevier ("Elsevier") consists of your license details and the terms and conditions provided by Elsevier and Copyright Clearance Center.

License Number	5123651166764
License date	Aug 07, 2021
Licensed Content Publisher	Elsevier
Licensed Content Publication	Elsevier Books
Licensed Content Title	Progress in Filtration and Separation
Licensed Content Author	Thomas Harlacher,Matthias Wessling
Licensed Content Date	Jan 1, 2015
Licensed Content Pages	28
Start Page	557
End Page	584
Type of Use	reuse in a thesis/dissertation
Portion	figures/tables/illustrations
Number of figures/tables/illustrations	2

3. Permission for Figures 2.11

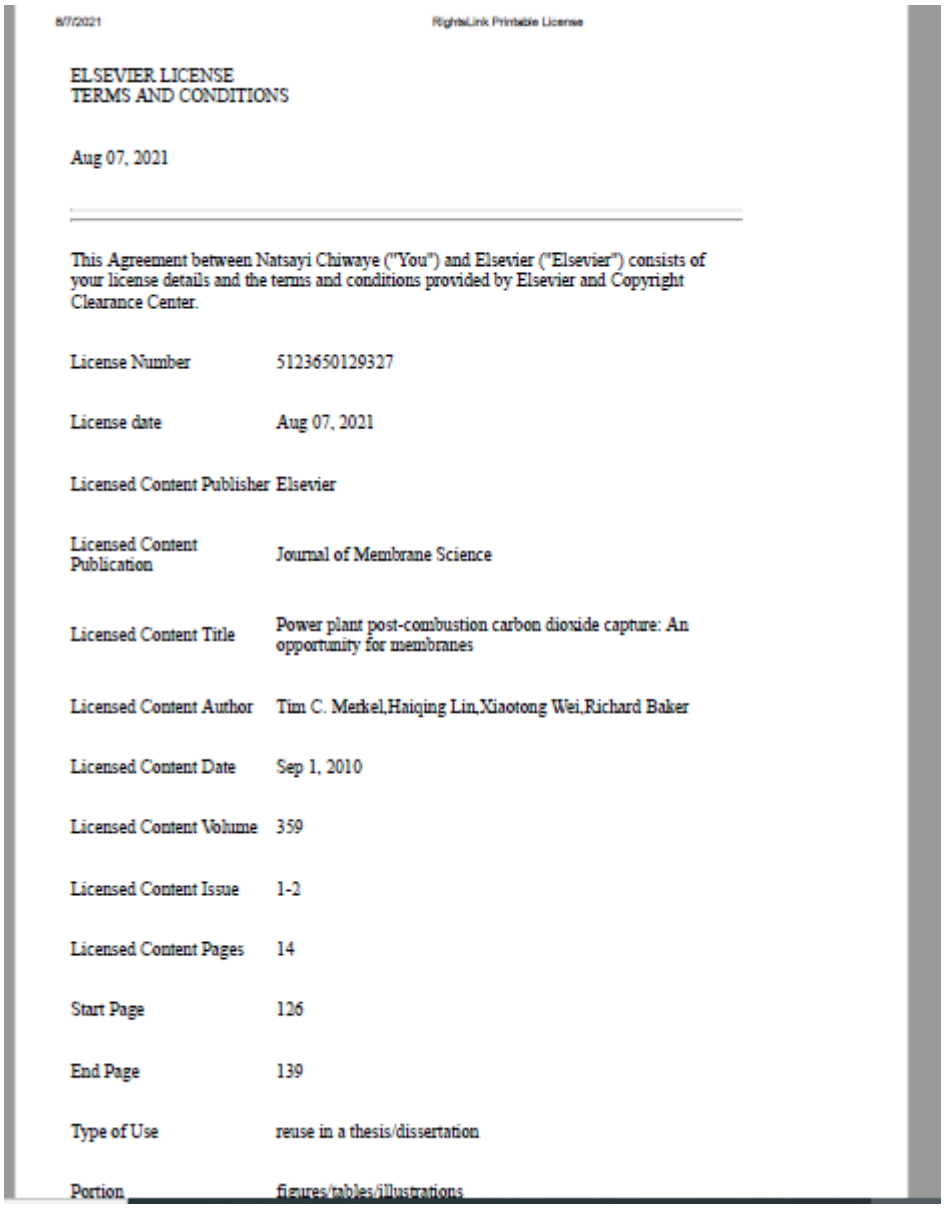

8/7/2021 RightsLink Printable License

ELSEVIER LICENSE
TERMS AND CONDITIONS

Aug 07, 2021

This Agreement between Natsayi Chiwaye ("You") and Elsevier ("Elsevier") consists of your license details and the terms and conditions provided by Elsevier and Copyright Clearance Center.

License Number	5123650129327
License date	Aug 07, 2021
Licensed Content Publisher	Elsevier
Licensed Content Publication	Journal of Membrane Science
Licensed Content Title	Power plant post-combustion carbon dioxide capture: An opportunity for membranes
Licensed Content Author	Tim C. Merkel,Haiqing Lin,Xiaotong Wei,Richard Baker
Licensed Content Date	Sep 1, 2010
Licensed Content Volume	359
Licensed Content Issue	1-2
Licensed Content Pages	14
Start Page	126
End Page	139
Type of Use	reuse in a thesis/dissertation
Portion	figures/tables/illustrations

4. Permission for Figure 2.12

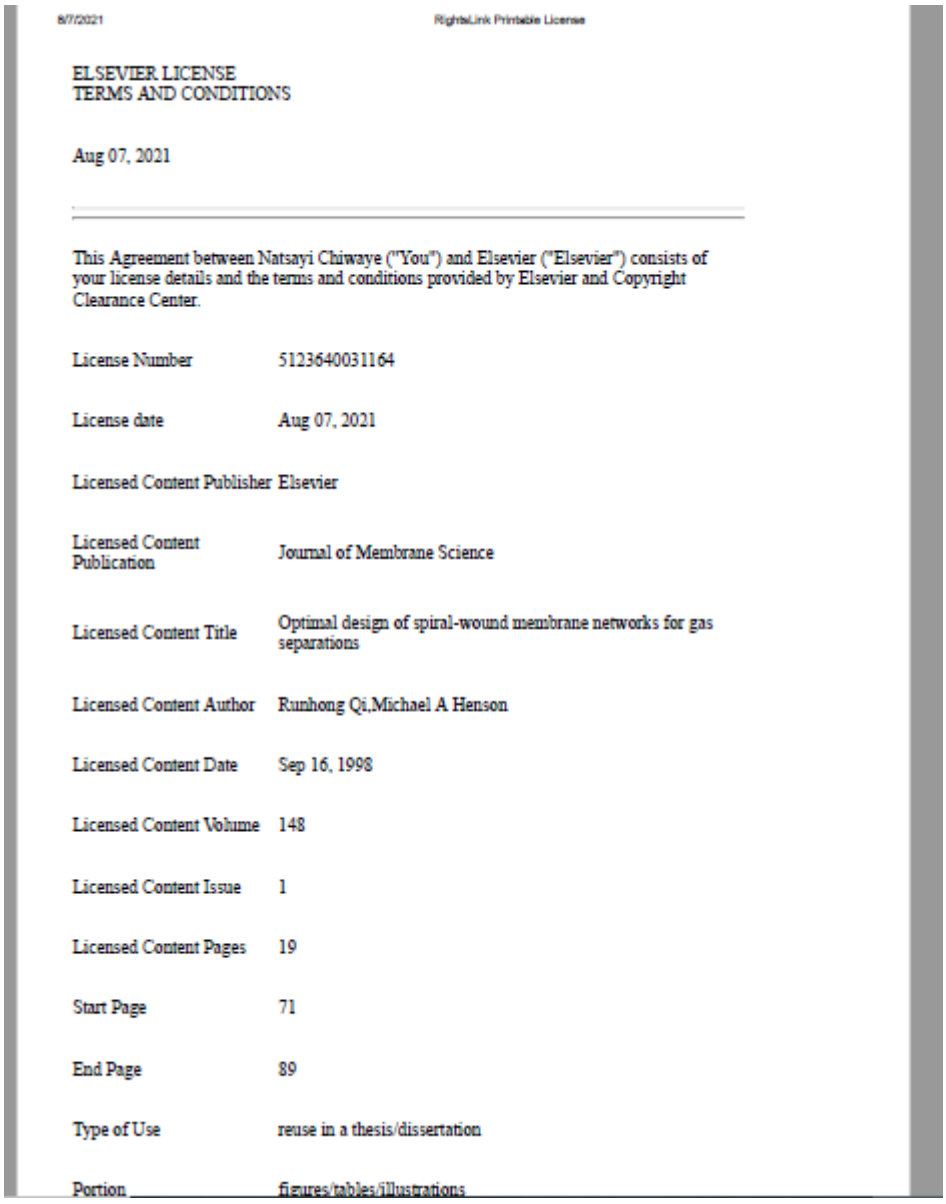

8/7/2021 RightsLink Printable License

ELSEVIER LICENSE
TERMS AND CONDITIONS

Aug 07, 2021

This Agreement between Natsayi Chiwaye ("You") and Elsevier ("Elsevier") consists of your license details and the terms and conditions provided by Elsevier and Copyright Clearance Center.

License Number	5123640031164
License date	Aug 07, 2021
Licensed Content Publisher	Elsevier
Licensed Content Publication	Journal of Membrane Science
Licensed Content Title	Optimal design of spiral-wound membrane networks for gas separations
Licensed Content Author	Runhong Qi,Michael A Henson
Licensed Content Date	Sep 16, 1998
Licensed Content Volume	148
Licensed Content Issue	1
Licensed Content Pages	19
Start Page	71
End Page	89
Type of Use	reuse in a thesis/dissertation
Portion	figures/tables/illustrations

5. Permission for Figure 2.13

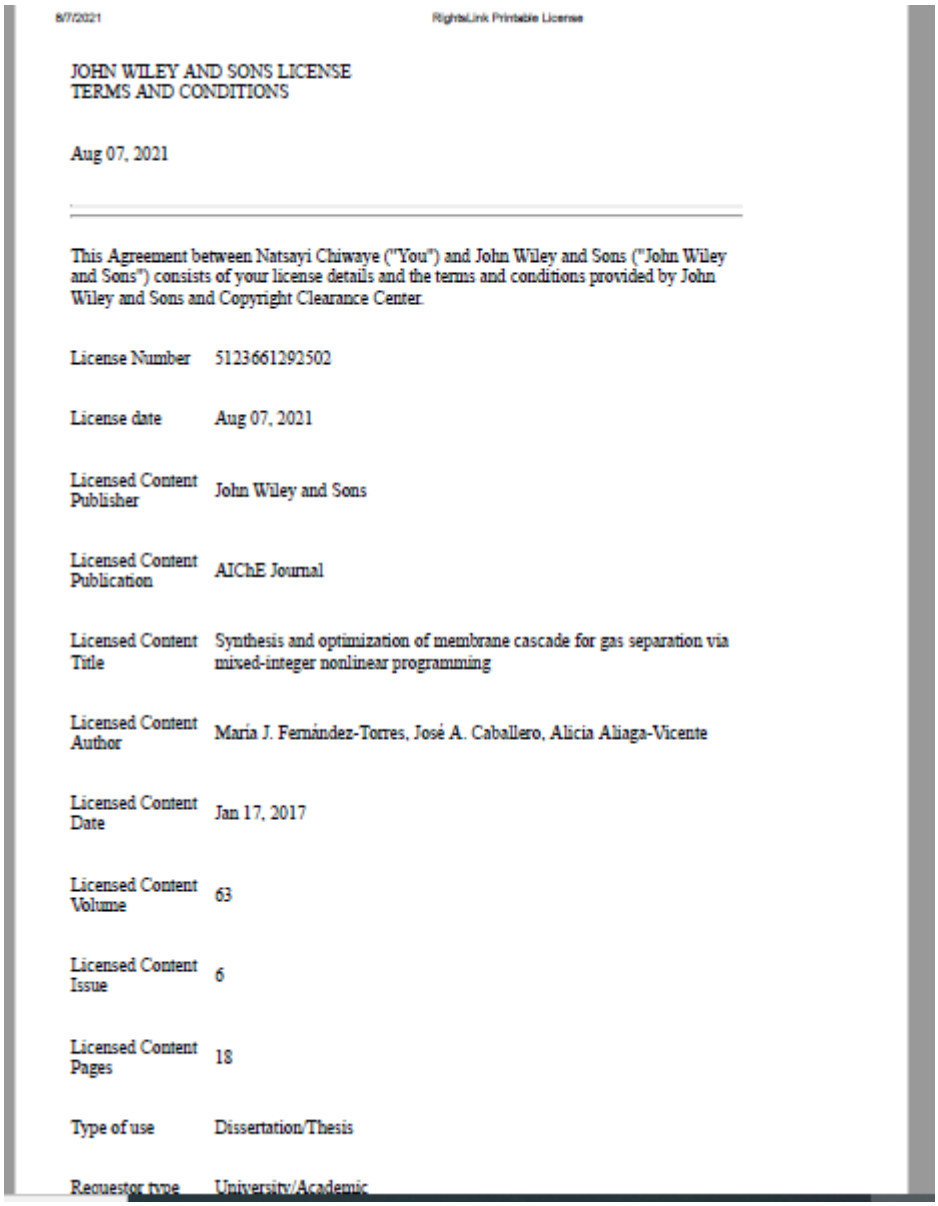

8/7/2021 RightsLink Printable License

JOHN WILEY AND SONS LICENSE
TERMS AND CONDITIONS

Aug 07, 2021

This Agreement between Natsayi Chiwaye ("You") and John Wiley and Sons ("John Wiley and Sons") consists of your license details and the terms and conditions provided by John Wiley and Sons and Copyright Clearance Center.

License Number	5123661292502
License date	Aug 07, 2021
Licensed Content Publisher	John Wiley and Sons
Licensed Content Publication	AIChE Journal
Licensed Content Title	Synthesis and optimization of membrane cascade for gas separation via mixed-integer nonlinear programming
Licensed Content Author	María J. Fernández-Torres, José A. Caballero, Alicia Aliaga-Vicente
Licensed Content Date	Jan 17, 2017
Licensed Content Volume	63
Licensed Content Issue	6
Licensed Content Pages	18
Type of use	Dissertation/Thesis
Requestor type	University/Academic

Appendix G. GAMS Files

Chapter 3. File

```
*FSC chapter 3, Scenario 3
$title Membrane
*MINLP
Sets
n membrane stages /n1*n3/
i components /i1*i4/
k subcompartments in a membrane /k1*k10/
* rrr retentate recycle streams /rrr1*rrr3/ npp
* pmr permeate recycle /pmr1*pmr3/ npppp ;
* i1= CO2 ; i2= N2 ; i3=h20 ,i4=O2
Alias (i, ip);
Alias (n, np,nppp,npppp);
* Alias (rrr, rrrp);
* Alias (pmr, pmrp);
Scalar

Cel dollarpMW 85.50 high usage tarriff 1.38889E-05 /0.04e-3/
Cmem dollarpm2 /35e-6/
Crep dollarpm2 to confirm /35e-6/
Cus dollarpkg(mol) to confirm dollar perkmol /0.357615894e-6/
Eff Efficiency of compressor vacuum expander /0.85/
Effc efficiency of interstage compressor /0.85/
RFT total mol flow rate of flue gas supplied to pcc kmolpmin /1596.667/
Pini final storage pressure lqd CO2 /1.013/
Patme bar /1/
Patm bar /1/
Tmem1 temperature of water exit condenser /353/
Tatm atmospheric temperature 25 deg C /298/
Tmem temperature of membranes (45 deg C) 313 is 40 /308/
Uclf cooler feed compressor KWpm2K 0.200 /0.110e-3/
Uclr cooler recycle KWpm2K 0.200 /0.110e-3/
CRF Capital recovery factor peryear /0.2/
Ccomp cost of compression $pW /850e-3/
Cco2comp co2 cost for storage /1350e-3/
Cco2pump co2 pumping cost for storage /1800e-3/
Cexp cost of expanding $pKW /630e-3/
Chexc cost of heat exchange from reference $pm2 /300e-6/
Cvac cost of vacuuming $pKW /1300e-3/
Pcut /75/
Pfin /110/
Uclco co2 compressor heat transfer coeffient 0.200 /0.100e-3/
Ucon heat transfer coefficient of feed condenser /0.100e-3/
Uclcop2 /0.900e-3/
Uclms warming of recycle stream of recycle Mw /0.3e-3/
Phxs Phxs bar /2/
Dac diffusivity of carrier solute complex m2ps m2pmin /2.6E-11 /
Da diffusivityof CO2 m2pmin /5.643E-9/
Keq equilibrium constant [complex]p[co2][carrier] all at feed m3pkmol /1.22e2/
Ct total concentration of effective carriers kmolpm3 /2.72e1/
Ha Henry s constant barm3pmol /37.957/
L membrane thickness m /0.8e-6/
* L membrane thickness thickest m /1.2e-6/
Parameters
yFTG(i) flue gas Feed concentration mole fraction
/i1 0.1374
i2 0.7288
i3 0.0973
i4 0.0365/
```

Mr(i) relative molecular weight g per mol or kjpkmol
/i1 44
i2 28
i3 18
i4 16/
FTG(i) ;
*FTG(i) = yFTG(i)*RFT ;*
**===*
Free Variables
TAC total cost ;
Binary Variables
Zrwo(n)
Zrwms(n)
**===*
Positive Variables
Amem membrane area for n (m2)
Qcfr power of recycle compressor cfr
Qexr power produced by the expander
Qcft power used by feed compressor KJps
Qvac
Qcopw
Qpum power of product pump
Qcomp power of the final product compresssor
Ppw
Qexs(n)
TNQ total net power consumed by compressors less recovered by expanders
Qhx(n)
Qclf
**Qclsg(n)*
Qclr(n)
xF(n) Split fraction of component i from flue gas Splitter SPFn flowing toward membrane stage n
xPOS(n) Fraction of component i from splitter SPPn towards product mixer MOP
xRRO(n) Fraction of component i from splitter SPRn supplied to mixer MOA
xRPR(n,np) Fraction of component i in RP from permeate splitter SPPn towards mixer MPn
** xRRR(n,rrr) Fraction of component i in stream RR from retentate splitter SPRn entering mixer MFn*
F(i,n)
FS(i,n) stream delivered to membrane module
yFS(i,n) mole fract feed steam to membrane
FSn(i,n)
yFSn(i,n)
FSnt(n)
**ppFS*
RRO(i,n) flow rate of i from (from SPR) in retentate to mixer MOA
RR(i,n) flow rate of retentate stream from membrane stage n towards splitter SPRn
RP(i,n) rate of component i in permeate stream from n to splitter SPPn
RPR(i,n) rate of i from permeate splitter towards permeate mixer n MPn
** Retrcy*
POS(i,n) residue stream from retentate splitter SPR(n) kmolpmin
MS
MSw
RWms
yMS
yMSw
OAt total residu
OPt total product
FT
RPS(i,n) flow rate of i from membrane stage n
yRPS(i,n) mol fraction of rps
RPSt(n) total flowrate of permeate from membrane stage n
RWOt(n) total removed from permeate stream
RWO(i,n) removed by condensors from permeate
yRWO(i,n) mol fraction of i in rwo
RWf

RWcon(i) flow rate removed by flue gas condenser- water only
RWcont total flow rate removed by condenser
yRWcon(i) mol fraction of i in rwcon
yFT (i) mole fracton i in ft flue gas after condenser
FTGt total flue gas flow to the membrane
FTt total flow of fue after condenser -water only
RWp(i) flow rate i removed by product condenser -water only
RWpt total removed
yRWp(i) mol faction
OPwt total flow of i opw
yRR(i,n) more fraction of i in retantate in stage n
OPw(i) flow rate i in product stream before eater remova in condenser
yOP(i) more fraction of i in product stream
yOA(i) more fraction of i in residue to atmosphere
R(i) recovery of gas component i
OA(i) flow rate of residue kmolpmin
OP(i) flow rate of product kmolps
RH(n) relative humidity
**SP(n) separation factor*
**299*
Aclf heat transfer area of the cooler
Aclsg(n)
Ahx(n)
DP(i) desired purity of CO2 enriched stream
lmTclf
lmTclr(n)
Perm(i,n,k)
RRk (i,n,k) flow rate i from compartment k on the retentate sideof stage n
RPk(i,n,k) flow rate i from compartment k on the permeate side of stage n
RRkt (n,k) total flow in k stage n retantate
RPkt (n,k) total flow in k stage n permeate side
ppP(i,n,k) partial pressure permeate side
ppR(i,n,k) partial pressure retantate side
Tcft temperate of gas exit feed compressor cft
Tcfr(n) temperature of gas exiting compressor recycle cfr
yRPk(i,n,k) Mole fraction of component i in the permeate side in the small area k in membrane stage n
yRRk(i,n,k) Mole fraction of component i in the retentate side in the small area k
yRRO(i,n) mole fraction of i in stream RRO of stage n send to residue
RRt(n) retantate from membrane n before splitter
RPt(n) permeate from membrane before splitter
FSt(n) fotal feed stream to membrane
yRP(i,n) mole fraction i in permeate
g(n) fraction to indicate sweep vapor flow
lmThx mean temp difference k
** Pini initial pressure for Co2 compressure equals PP*
Qco duty of co2 compressor
TC
**Qcsg(n) power of the sweep compressor*
**CCcsg(n) purchase cost of sweep compressor*
**Tcsg(n) temp of gas exiting sweep compressor*
**lmTclsg(n) logarithmn mean of the sweep cooler condenser*
yRR(i,n) more fraction of i in retantate in stage n
yOP(i) more fraction of i in product stream
yOA(i) more fraction of i in residue to atmosphere
TNQ total net power consumed br compressors less recovered by expanders
SG(i,n) sweep gas flow rate
Qhx(n) power of heat exchanger
Cpclf
*KqppP(i,n,k) multiplication Keq * partial pressure permeate side*
*KqppR(i,n,k) multiplication Keq * partial pressure retantate side*
ppP(i,n,k) partial pressure permeate side
ppR(i,n,k) partial pressure retantate side
perm permeance
*HKpp Ha+keq*partial p on permeate*
*HKpr Ha+keq*partial p on retantate*

*====Cost
Variables==========
TMA total membrane area
EC
TCCmem total capital cost of membrane
TCCU total capital cost of units
OPEX
CAPEX
CCco
CCclco
CCopw
Ppwe
ACmem(n) annual cost of membrane
Aclf heat transfer area of the cooler
Aclr area of cooler clr
*Capital annualised costs
CCclr(n) annual capital cost of cooler clr
CCcfr capital cost of cfr
CCcft capital cost of recycle compressor cfr
CCexr annual capital cost of expander on product retentate
CCclf annual cost of clf
CCvac
CCexs(n) annual capital cost of expander on sweeping gas
CChx(n) annual capital cost of heat exchanger
CCclsg(n)
*Operating costs
*OCbc(n)
*Var
CCco2comp purchace for the product compressor
CCco2pump purchase base cost for the product pum
CR compression ratio for the product compressor
Qexrn
Qexrrrn
Qexrrn ;
Binary variables
Zcrr(n,np)
Zexrr(n,np)
Zret(n,np)
Zro(n,np);
variables
*----------relavant positive variable ----------
*dPR(n,np)
CCcrrr capital cost of recycle compressor
CCexrr capital cost of recycle expander
PPe(n) PP**0.286 trying to simplify equations for fast solving
PRe(n) PR**0.286
PP(n) permeate pressure
PR(n) retentate pressure
*dPRc(np,n)
*dPRx(n,np)
Qcrrr power consumed by the recycle compressor compressing recycle stream Retrcy n-p
Qexrr power produced by the recycle expander expansion on recycle stream Retrcy n-p
xF(n) Split fraction of component i from flue gas Splitter SPFn flowing toward membrane stage n
xPOS(n) Fraction of component i from splitter SPPn towards product mixer MOP
xRRO(n) Fraction of component i from splitter SPRn supplied to mixer MOA
xRPR(n,np) Fraction of component i in RP from permeate splitter SPPn towards mixer MPn
* xRRR(n,rrr) Fraction of component i in st
xRRR Fraction of from retentate splitter recycled to stage rrr which correspond to Retrcy
Retrcy rate of stream from membrane stage (n) recycled to stage (rrr)
;
*----------retentate recycle design--------This is the manual notation I would like to automate more----------

*The following equations are based on the assumptions previously made that PR(3) is>= PR(2) >= PR (1) PRe(n)=PR**0.286

```
Equations
s76,s77 ;
*Calculation of power consumption of compressor Qcrrr

s76(n,np).. Qcrrr(n,np)*(PRe(n)) =e=( (1/Eff)*( (sum(ip, (Retrcy(ip,n,np)/60)))*8.3145e-3*Tmem*3.5*
((PRe(np))-(PRe(n)) ))) *Zcrr(n,np); ;
s77(n,np).. Qexrr(n,np)*(PRe(n))=e=( (Eff)*( ( (sum(ip, (Retrcy(ip,n,np)/60)))*8.3145e-3*Tmem*3.5*
((PRe(np))-(PRe(n)) ))))*Zexrr(n,np);

Equations
q46,q47,q48;
* this one plus 47+48
q46(n,np).. ( (PR(n)-PR(np))*Zcrr(n,np) ) -( (PR(n)-PR(np))*Zexrr(n,np) ) =l= PR(n)-PR(np) ;
*q47(n,np).. (PR(n)-PR(np))*Zcrr(n,np) =l=(-0.001)*Zcrr(n,np) ;
*q48(n,np).. (PR(n)-PR(np))*Zexrr(n,np) =g=0.001*Zexrr(n,np) ;
q47(n,np).. (PR(n)-PR(np))*Zcrr(n,np) - (-0.001)*Zcrr(n,np) =l= 0;
q48(n,np).. (PR(n)-PR(np))*Zexrr(n,np) - (0.001*Zexrr(n,np)) =g= 0 ;
Equations
s78,t54,t52;
*Capital cost of recycle expander
s78(n,np).. CCcrrr(n,np) =e= Ccomp*Qcrrr(n,np)*Zcrr(n,np) ;
t54(n,np).. Qexrrn(n,np) =e= (1/Eff)* Qexrr(n,np)*Zexrr(n,np) ;
t52(n,np).. CCexrr(n,np) =e= (Cexp*Qexrrn(n,np))*Zexrr(n,np) ;

*--------membrane model----------------------------------------------------------------------------------------------------------------------------
---------------------------------
Equations
e2,e3,e4,e5,e84b, e84a;
e2(i,n,k)$ (ord (k) = 2 ).. ( 4.5 * ( ( -RRk(i,n,k-1)+ RRk(i,n,k+1)) ))
+( (Amem(n)*Perm(i,n,k))*( ( ppR(i,n,k)- ppP(i,n,k)) ) )=e=0 ;
e3(i,n,k)$ (ord (k) > 2).. ( 4.5 *( (RRk(i,n,k-2) -(4*RRk(i,n,k-1)) +(3*RRk(i,n,k)) ))
+( (Amem(n)* Perm (i,n,k))* ( (ppR(i,n,k)- ppP(i,n,k)) ) )) =e= 0;
e4(i,n,k).. (RRk(i,n,k)-RRk(i,n,'k10')- RPk(i,n,k)) =e= 0 ;
e5(n,k).. (RRkt(n,k)-RRkt(n,'k10')-RPkt(n,k)) =e= 0;
e84b(i,n,k).. RRk(i,n,k)=g= RRk(i,n,k+1) ;
e84a(i,n,k).. RPk(i,n,k)=g= RPk(i,n,k+1) ;
equations
p1,p4,p5,p6,p7,p8,p9,p10;
p1(n,k).. perm ('i1',n,k)*(L*Ha)* (HKpr('i1',n,k)*HKpp('i1',n,k)) =e= ( Da*(HKpr('i1',n,k)*HKpp('i1',n,k) )) + (Ha*
Dac*Keq*Ct*Ha ) ;
p4(n,k).. KqppR('i1',n,k) =e= Keq*ppR ('i1',n,k) ;
p5(n,k).. KqppP('i1',n,k) =e= Keq*ppP ('i1',n,k) ;
p6(n,k).. HKpr('i1',n,k) =e= Ha +KqppR('i1',n,k) ;
p7(n,k).. HKpp('i1',n,k) =e= Ha+ KqppP ('i1',n,k) ;
p8(n,k).. Perm ('i2',n,k)=e= 1.10229E-05;
p9(n,k).. perm ('i3',n,k) =e= 0.001488095 ;
p10(n,k).. perm ('i4',n,k) =e= 4.96032E-05 ;
*L.lo=0.8e-6;
equations
p2,p3 ;
*e84c, e84d;
p2(i,n,k).. ppR(i,n,k) =e= PR(n)*yRRk(i,n,k) ;
p3(i,n,k).. ppP(i,n,k) =e= PP(n)*yRPk(i,n,k) ;
Equations
*ee26,e19, e20,
e25,
e1000, e1001, e708,e707,e710,e743,
e901, e903,e905, e724a,e709,e730,
*e715,e716,
e17, e904,e902,e906,
*e721a,e722a,
e710,e724 ;

e1000(i,n,k).. yRPk(i,n,k)*(sum(ip, (RPk(ip,n,k))))=e= RPk(i,n,k) ;
e1001(i,n,k).. yRRk(i,n,k)*(sum(ip, (RRk(ip,n,k))))=e= RRk(i,n,k) ;
```

```
* flow in k1
e707(n).. RRkt(n,'k1') =e=sum (ip, FS(ip,n)) ;
e708(n).. RPkt(n, 'k1')=e=sum (ip,RPS(ip,n)) ;
e17(i,n).. RPk(i,n,'k1') =e= RPS(i,n);
e709(i,n).. yRPk(i,n,'k1')=e= yRPS(i,n) ;
e710(i,n).. yRRk(i,n,'k1')=e= yFS(i,n);
*Flow k10
e743(i,n,k)$(ord(k)=card(k)).. RR(i,n) =e= RRk(i,n,k);
e730(i,n,k)$(ord(k)=card(k)).. yRR(i,n)=e= yRRk(i,n,k) ;
*e724(n,k)$(ord(k)=card(k)).. RRt(n)=e= RRkt(n,k) ;
e724(n,k).. (sum(ip, (RPk(ip,n,k)))) =e= RPkt(n,k) ;
e724a(n,k).. (sum(ip, (RRk(ip,n,k)))) =e= RRkt(n,k) ;
e905(i,n).. yRR(i,n)*(sum(ip, RR(ip,n))) =e= RR(i,n) ;
e901(i,n).. yFS(i,n)* (sum(ip, FS(ip,n)))=e= FS(i,n) ;
e903(i,n).. yRPS(i,n)*(sum(ip, RPS(ip,n))) =e= RPS(i,n) ;
e904(n).. sum(ip, yRPS(ip,n))=e= 1;
e902(n).. sum(ip, yFS(ip,n))=e= 1;
e906(n).. sum(ip, yRR(ip,n))=e= 1;
*e25(n).. FSt(n)+sum (ip, SG(ip,n)) =e= RRt(n)+RPSt(n) ;
*e25(n).. FSt(n)=e= RRt(n)+RPSt(n) ;
e25(i,n).. FS(i,n)=e= RR(i,n)+RPS(i,n) ;
Equation
e23,
*e760ee
*e760e,
e24 ;
e23(n,k).. sum (ip, yRRk(ip,n,k)) =e= 1 ;
e24(n,k).. sum (ip, yRPk(ip,n,k)) =e= 1 ;
*=====================================================================
equations
ec4,ec5,ec6,ec7, e27,e28 , ec11a,
ec10,ec11,ec12;
*balance on feed condenser
ec7(i).. FTG(i)=e= FT(i)+RWcon(i) ;
*to ensure only water is removed by the condenser
ec4.. RWcon('i1')=e= 0 ;
ec5.. RWcon('i2')=e= 0 ;
ec6.. RWcon('i4')=e= 0 ;
ec10(i).. yFT(i)* sum(ip, FT(ip))=e= FT(i);
ec11.. yFT('i3')*Patm=l=0.032;
ec11a.. yFT('i3')*Patm=g=0.03169;
ec12(n,k).. sum (ip, yFT(ip)) =e= 1 ;

* balance around flue gas splitter, split fraction sum, and the streams
e27.. sum (n, xF(n))=e= 1 ;
e28(i,n).. F(i,n) =e= xF(n)*FT(i) ;
xF.lo(n) = 0.0 ; xF.up(n) = 1 ;
*=================e68d,=================================================--------
-------------------------------------------------------------------------
Equations
e62, e68c,e67,e68a,e67a
e64,e65,e66,e69,e70,e68;
*ec25;
*balance on the permeate condenser
*e62b(i,n).. ( rps(i,n)) *(1-Zrwo(n)) =e= rp(i,n)*(1-Zrwo(n)) ;
*e62(i,n).. ( rps(i,n))*Zrwo(n) =e= (rp(i,n)+rwo(i,n))* Zrwo(n) ;
e62(i,n).. rps(i,n) =e= rp(i,n)+ (rwo(i,n)) ;
*to ensure only water is removed by the condenser
e64(n).. RWO('i1',n)=e= 0 ;
e65(n).. RWO('i2',n)=e= 0 ;
e66(n).. RWO('i4',n)=e= 0 ;
e67(n).. RWO('i3',n)=g= 0.0001*(Zrwo(n));
e67a(n).. RWO('i3',n)=l= 1500*(Zrwo(n));
e68(n).. ((yrps('i3',n)*Patm)* Zrwo(n)) - (0.031699* Zrwo(n)) =g= 0 ;
e68a(n).. ((yrps('i3',n)*Patm)*(1-Zrwo(n))) - (0.0316*(1-Zrwo(n))) =l= 0 ;
```

```
e69(i,n).. yrp(i,n)*(sum(ip, rp(ip,n)))=e= rp(i,n) ;
e70(n).. sum(ip, yrp(ip,n))=e= 1;
yRP.up(i,n) = 1;
e68c(n).. ((yrp('i3',n)*Patm)* Zrwo(n)) - (0.031699* Zrwo(n)) =e= 0 ;
*e68d(n).. (yrp('i3',n)*Patm)*(1-Zrwo(n))=l=(0.031284)*(1-Zrwo(n));
*-----------------------------------------------------------------------------------------------------------------------------------------------
---------------
Equations
epc1, epc5,epc9, epc10,epc12;
*balance on the final product condenser
epc1(i).. OPw(i) =e= RWp(i) +OP(i) ;
*to ensure all water is removed by the condenser
*epc5(i).. OPw('i3')=e= RWp('i3') ;
epc5.. yOP('i3')*Ppw=e= 0.031699 ;
*to ensure only water is removed by the condenser
epc10(n).. RWp('i1')=e= 0 ;
epc9(n).. RWp('i2')=e= 0 ;
epc12(n).. RWp('i4')=e= 0 ;
Ppw.lo=Patm ;
*epc2.. sum(ip, RWp(ip)) =e= RWpt ;
*-------------------------------------------------------------------------------------
Equation
n1, e45, e48,n4,n6,n7,n20;

xPOS.lo(n) = 0.0; xPOS.up(n) = 1;
xRRO.lo(n) = 0.0; xRRO.up(n) = 1;
xRPR.lo(n,np) = 0; xRPR.up(n,np) = 1;
xRRR.lo(n, np) = 0; xRRR.up(n,np) = 1;
e45(i).. OPw(i) =e= POS(i,'n1')+ POS(i,'n2') + POS(i,'n3') ;
e48(i).. OA(i)=e= RRO(i,'n1')+RRO(i,'n2') +RRO(i,'n3');
n1(n).. xRRO(n)+ sum (np, (xRRR(n,np))) =e=1;
n4(n).. xPOS(n)+ sum (np, (xRPR(n,np))) =e=1;
n6(i,n).. POS(i,n) =e= xPOS(n)*RP(i,n);
n7(i,n).. RRO(i,n) =e= xRRO(n)*RR(i,n);
n20(i,n,np).. RR(i,n)*xRRR(n,np) =e= Retrcy(i,n,np) ;
Equations
e90,e91,e92,e93,e94,e95;
**balance around permeate mixer (MPn)
e90(i).. MS(i,'n1')=e= sum (np, (RP(i,np)*xRPR(np,'n1') )) + f(i,'n1');
e91(i).. MS(i,'n2')=e= sum (np, (RP(i,np)*xRPR(np,'n2') )) + f(i,'n2');
e92(i).. MS(i,'n3')=e= sum (np, (RP(i,np)*xRPR(np,'n3') )) + f(i,'n3');
e93(i).. FS(i,'n1')=e= MSw(i,'n1')+ sum (np, (Retrcy(i,np,'n1'))) ;
e94(i).. FS(i,'n2')=e= MSw(i,'n2')+ sum (np, (Retrcy(i,np,'n2'))) ;
e95(i).. FS(i,'n3')=e= MSw(i,'n3')+ sum (np, (Retrcy(i,np,'n3'))) ;

Equation
n30,n31,n32;
n30.. xrrr('n1','n1')+xrpr('n1','n1')=l=1 ;
n31.. xrrr('n2','n2')+xrpr('n2','n2')=l=1 ;
n32.. xrrr('n3','n3')+xrpr('n3','n3')=l=1 ;
*-----------------------------------------------------------------------------------------------------------------------
equations
eb6;
*to ensure relative humity is 90% as related to saturation pressure 0.0562 bar and water partial pressure
eb6(n).. RH(n)*0.0562=e= yFS('i3',n)*PR(n) ;
*eb6(n).. 0.9*0.0562=e= yFS('i3',n)*PR(n) ;
RH.lo(n)=0.9 ; RH.up(n)=1;
*-----------------------------------------------------------------------------------------------------------------------------------------------
----------
Equations
e60, e69, e72,e71 ,e73,e74,e57a
e53,e54,e55,e56,e60a,e57,e58;
*balance on the feed condenser
*e52(i,n).. MS(i,n)*(1-Zrwms(n)) =e=MSw(i,n)*(1-Zrwms(n));
*e53(i,n).. MS(i,n)*Zrwms(n) =e= (MSw(i,n) +RWms(i,n))*Zrwms(n) ;
```

```
e53(i,n).. MS(i,n) =e= (MSw(i,n) +RWms(i,n));

*to ensure only water is removed by the condenser
e54(n).. RWms('i1',n)=e= 0 ;
e55(n).. RWms('i2',n)=e= 0 ;
e56(n).. RWms('i4',n)=e= 0 ;
e57(n).. RWms('i3',n)=g= 0.0001*Zrwms(n);
e57a(n).. RWms('i3',n)=l= 1500*Zrwms(n);
e58(i,n).. yMS(i,n)* sum(ip, MS(ip,n))=e= MS(i,n);
e71(i,n).. yMSw(i,n)* sum(ip, MSw(ip,n))=e= MSw(i,n);
e73(n).. sum(ip, yMS(ip,n))=e= 1;
e74(n).. sum(ip, yMSw(ip,n))=e= 1;
e60(n).. ((yms('i3',n)*PR(n))*Zrwms(n)) - ((0.0562)*Zrwms(n)) =g= 0;
e60a(n).. (yms('i3',n)*PR(n))*(1-Zrwms(n)) - ((0.056)*(1-Zrwms(n))) =l= 0;
yms.lo(i,n)= 0; yms.up(i,n)= 1;
yMsw.lo(i,n)= 0; ymsw.up(i,n)= 1;
e72(n).. ( yMSw('i3',n)*PR(n)*Zrwms(n)) - (0.05602*Zrwms(n)) =e= 0;
*-----------------------------------MS-----------------------------------------------------------------------------------------------------
------------------

PR.lo(n)=Patm; PR.up(n)=100;
PP.lo(n)=0.2; PP.up(n)= Patm;
Amem.lo(n) = 10000 ;
Amem.up(n) = 1000000 ;
Equations
e46,e161,e49,e50,ee52;
*desired product Co2 recovery capture ratio
e49(i).. R(i)*FTG(i)=e= OP(i) ;
e50.. R('i1')=g=0.9;
R.lo(i) = 0; R.up(i) = 1 ;
*final product mixer - compression for storage yOP is CO2 target purity
e46.. OPt =e= sum(ip, OP(ip)) ;
*e161(i,n).. yOP(i)* (sum(ip, OP(ip))) =e= OP(i) ;
e161(i,n).. yOP(i)*OPt=e= Op(i) ;
ee52.. yOP('i1') =e=0.95;
*e46a.. sum (ip, yOP(ip))=e=1;
yOP.up(i) = 1;
Equations

e160,e47;
*balance around the final residue mixer to - to atmosphere
e47.. OAt =e= sum (ip, OA(ip));
e160(i,n).. yOA(i)*OAt=e= OA(i) ;
*e160(i,n).. yOA(i)*(sum (ip, OA(ip)))=e= OA(i) ;
* yOA.up(i) = 1;
*-------------------------------------------------------------------------------------------------------------------------------
Equations
* s103
s102,s105,s106,s108,s109,s110,
obj;
*tnq net power, tma membrane area, ec electricity cost, 7500h per year, 15$phr labour
*s103.. TMA =e= sum (np, (Amem(np))) ;
s102.. TNQ =e= sum (np, Qcft(np))+sum (np, (Qvac(np)))+ Sum ((n,np),(Qcrrr(n,np)*Zcrr(n,np)))
-Sum ((n,np), (Qexrr(n,np)*Zexrr(n,np)))- sum(np, Qexr(np)) +Qcopw +Qpum+Qcomp;
s105.. OPEX =e= ((15e-6)*7500)+ EC ;
s106.. EC =e= (0.04e-3)*(TNQ)*7500;
s108.. CAPEX =e= TCCU*1.18*0.2 ;
s110.. TCCmem =e= (Cmem* sum (np, Amem(np))) +((Cmem*sum (np, Amem(np))) *0.8);
s109.. TCCU =e= (603.1/584.6)* (TCCmem+ CCopw+sum (np, CCcft(np)) + CCco2comp+CCco2pump
+sum(np,(CCvac(np)))+ sum (np, CCexr(np)) +sum(np,CCclf (np))
+ Sum ((n,np),(CCcrrr(n,np)*Zcrr(n,np)))+ Sum ((n,np),(CCexrr(n,np)*Zexrr(n,np))))
;
* (603.1/584.6)* ) (
Equations
s132, s133,s11;
```

```
*,s12,s13,s14,s15;
s132(n).. PPe(n) =e= (PP(n))**0.286 ;
S133(n).. PRe(n) =e= (PR(n))**0.286;
s11.. Ppwe =e= Ppw**0.286;
*-----------------------------------------------------------------------------------------------------------------------------
Equations
s1,s2,s9,s10 ,s14a,s15a;
s1(n).. Qcft(n)*Patme =e=(( (1/Eff)*( ( (sum(ip, (MS(ip,n)))/60)*8.3145e-3*Tatm*3.5* (PRe(n)-Patme) )))) ;
s2(n).. CCcft(n) =e= (Ccomp*Qcft(n)) ;
s9(n).. Qvac(n)*PPe(n)=e=( (1/Eff)* ( ( (sum(ip, RPS(ip,n)))/60)*8.3145*Tmem*3.5*(Patme -PPe(n))))*1e-3;
s10(n).. CCvac(n) =e= (Cvac*Qvac(n)) ;
s14a.. Qcopw*Patme =e=(( (1/Eff)*( ( (sum(ip, OPw(ip)))/60)*8.3145e-3*298*3.5* ((Ppwe)-Patme) ))) ;
s15a.. CCopw =e= Ccomp*Qcopw ;
*-----------------------------------------------------------------------------------------------------------------------------
---------
*$ontext
Equations
s18,s19,s20,s21,s22 ;
*feed compressor cooler from compressor temp Tcft to membrane temp (35 deg 308;)
*cw in= 20dec = 298k cw out = 25 deg =298
s18(n).. Tcft(n)*(Patm**0.286)=e= (Tatm*(PR(n)**0.286)) ;
s19(n).. Qclf(n)=e=( ( (sum (ip, (MS(ip,n)*Cpclf(ip,n)/60)))*(Tcft(n)-Tatm) )*1e-3) ;

s20(n).. lmTclf(n) * (log ( (Tcft(n)-298)/(15))) =e= (Tcft(n)-298)-(15) ;
s21(n).. Aclf(n) * (Uclf*lmTclf(n))=e= (Qclf (n)) ;
s22(n).. CCclf (n)=e= (Chexc*Aclf(n));
lmTclf.lo(n) = 0.01;
Tcft.lo(n) = 308.15;
equations
s60,s61,s62,s63 ;
s60(n).. Cpclf('i1',n)=e=( 10.34+(0.00274*Tcft(n))-(195500/(Tcft(n)**2)))*4.184 ;
s61(n).. Cpclf('i2',n)=e= (6.50+( 0.001*Tcft(n)))*4.184 ;
s62(n).. Cpclf('i3',n)=e= (8.22+( 0.00015*Tcft(n))+( 0.0000013*(Tcft(n)**2)))*4.184 ;
s63(n).. Cpclf('i4',n)=e= (8.27+(0.000258*Tcft(n))-(187700/(Tcft(n)**2)))*4.184 ;
*$offtext
*-----------------------------------------------------------------------------------------------------------------------------
Equations
s61a,s62a,s63a,s56, s57,s48,s49,s48a ;
*residue expander
s48(n).. Qexr(n)*PRe(n)=e=( (Eff)* (((sum(ip, RRO(ip,n)))/60) *8.314*3.5*Tmem* (PRe(n)-Patme) ) )*1e-3 ;
s48a(n).. Qexrn(n)*PRe(n)=e= (1/Eff)*Qexr(n) ;
s49(n).. CCexr(n) =e= Cexp*Qexrn(n) ;
*compression for storage
s61a.. Qpum=e= ((((sum (ip, OP(ip))/60)*22.4)/(Effc))*((Pfin-Pcut)))*1e-3 ;
s62a.. Qcomp =e=( (1/Effc)*(5*((sum(ip, OP(ip)))/60)*3.5*8.314*Tatm*(CR**0.286-1)))*1e-3 ;
s63a.. CR*(Ppw**0.20) =e= Pcut**0.20 ;
S56.. CCco2comp =e= Cco2comp*Qcomp ;
S57.. CCco2pump =e= Cco2pump*Qpum ;
obj.. TAC =e= OPEX + CAPEX ;
*-----------------------------------------------------------------------------------------------------------------------------
*finite boundaries
yRRk.lo(i,n,k)= 0; yRRk.up(i,n,k)= 1;
yRRk.lo(i,n,k)= 0; yRPk.up(i,n,k)= 1;
yFS.lo(i,n) = 0; yFS.up(i,n) = 1;
yRPS.lo(i,n)= 0 ; yRPS.up(i,n) = 1;
yRR.lo(i,n)= 0; yRR.up(i,n) = 1;
yFSn.up(i,n) = 1;
yFT.up(i) = 1;
*g.up(n)= 0.25;
FS.lo('i1',n) =1e-4;

RR.up(i,n) = 1800 ;
FS.up(i,n) = 1800 ;
RRO.up(i,n) = 1800 ;
RPS.up(i,n) = 1000 ;
```

```
OPw.up(i)=1000;
model membrane /all/;
*Model membrane/all, Qcrrr(freelinkcomp),Qexrr(freelinkexp)/ ;
$onecho > baron.opt
CompIIS 1
$offecho
membrane.optfile = 1;
OPTION SYSOUT=ON ;
option limrow = 5;
*option limcol=100;
*OPTION PROFILE = 2;
*OPTION PROFILETOL = 1.5;
*option work = 1258291 ;
option optcr=1e-9;
option reslim =3600;

option minlp = baron;
option decimals =8 ;
solve membrane using MINLP minimising TAC ;
```

Chapter 4. File

```
*Chapter 4, Optimisation of membrane based CO2 capture by FSC SA techno evaluation
$title    Membrane

*MINLP
Sets
      n membrane stages  /n1*n4/
      i components   /i1*i4/
      k subcompartments in a membrane   /k1*k10/
      rrr retentate recycle streams /rrr1*rrr4/
      pmr permeate recycle      /pmr1*pmr4/   ;
*     i1= CO2 ; i2= N2 ; i3=h20 ,i4=O2
      Alias (i, ip);
      Alias (n, np);
      Alias (rrr, rrrp);
      Alias (pmr, pmrp);

Scalar

      Cel     dollarpMW 85.50 high usage tarriff 1.38889E-05  /0.024088e-3/
      Cmem    dollarpm2                          /50e-6/
      Crep    dollarpm2     to confirm           /7.40e-6/
      Cus     dollarpkg(mol)  to confirm    dollar perkmol    /0.357615894e-6/
      Eff     Efficiency of compressor vacuum expander       /0.85/
      Effc    efficiency of interstage compressor            /0.80/
      RFT     total mol flow rate of flue gas supplied to pcc kmolpmin   /2040.00/
*     EY      effective year time ass 48 week online seconds  48 weeks   /7446/
      Pini    final storage pressure lqd CO2                 /0.81/
      Patme   bar                                /0.941513855/
      Patm    bar                                /0.81/
      Tmem1   temperature of water exit condenser   55deg C       /328/
      Tatm    atmospheric temperature     32.2 deg C           /305.35/
      Tmem    temperature of membranes (45 deg C)  313 is 35    /308/
      Tuwo    temperature at which cooling water leaves the heat exchanger 55deg C /328/
      Uclf    cooler feed compressor KWpm2K   0.200          /0.110e-3/
      Uclr    cooler recycle        KWpm2K    0.200         /0.110e-3/
      CRF     Capital recovery factor peryear               /0.103/
      Ccomp   cost of compression   $pW                     /850e-3/
      Cco2comp co2 cost for storage                         /1350e-3/
```

```
        Cco2pump co2 pumping cost for storage                /1800e-3/
        Cexp    cost of expanding       $pKW                 /630e-3/
        Efh     equipment cost factor for housing            /1.80/
        Chexc   cost of heat exchange from reference $pm2    /300e-6/
        Cmf     cost reference frame cost $                  /0.238e-6/
        Cvac    cost of vacuuming $pKW                       /1300e-3/
        Pcut                                                 /75/
        Pfin                                                 /150/
        Uclco   co2 compressor heat transfer coeffient 0.200    /0.100e-3/
         Ucon    heat transfer coefficient of feed condenser /0.50e-3/
        dHcon   enlthapty of condensation  Mjpkmol       /40700e-3/
        dHvap   enthalpy of evaporation   Mjpkmol       /40700e-3/

        Uclsg   cooler sweeping gas    Mw                 / 1.200e-3/
        Uclcop2                                           /0.900e-3/
        Uhx     heat exchanger        MW                  /1.000e-3/
        Uclms   warming of recycle stream of recycle    Mw      /0.3e-3/
        MSIN    marshal swift index                       / 1593.7 /
        Phxs    Phxs          bar                   /2/
        Dac     diffusivity    of carrier solute complex  m2ps m2pmin   /2.6E-11  /
        Da      diffusivityof CO2            m2pmin          /5.643E-9/
        Keq     equilibrium constant [complex]p[co2][carrier] all at feed  m3pkmol    /1.22e2/
        Ct      total  concentration of effective carriers   kmolpm3              /2.72e1/
        Ha      Henry s constant barm3pmol                                    /37.957/
        L       membrane thickness    m                   /0.8e-6/
*       L       membrane thickness   thickest m                    /1.2e-6/
Parameters
        yFTG(i)    flue gas Feed concentration  mole fraction
        /i1 0.1289
        i2  0.6778
        i3  0.1436
        i4  0.0414/

        Cp(i)   heat capacity KJpkmol.K  also J pmol
        / i1 37.172
        i2 29.070
        i3 33.650
        i4 26.000/

        Mr(i)  relative molecular weight  g per mol  or kjpkmol
        /i1 44
        i2 28
        i3 18
        i4 16/

        FTG(i)  ;
        FTG(i) = yFTG(i)*RFT ;

scalar
        cf              plant availabilty plant capacity         /0.85/
        MWnetwocc       net power without CC MW              /727.3/
        FOMwocc         fixed operating and mantainance  for plant w no CC= /45.04/
        TCRwocc         total related charge w no CC millions   /1926/
        VOMwocc         variable operating and mantainance fuel removed  /111.1/
        HR              net heating rate MJperMWh  /9863/
        FC              fuel cost $perMJ /1.712e-9/
        Cstrg           cost of storage $per ton /12.90e-6/
        Ctrans          cost of transport $per ton per metre      / 9.689E-09/

Positive Variables
        TCRcc
        FOMcc
        VOMcc
        fcf
        COEwocc
```

```
        VOMccpmw
        VOMwoccpmw
        hrspy
        mtaewocc
        mtaecc
        rt
        T
        rt
        Clb
        MWnetcc
        Ecca
        Ewocca
        MWhpywocc
        MWhpycc
        LCOEwocc
        Ewocc
         mtacoc
        ccastg
        ccatrans
        CTrStg
*=========================================================================
=====
Free Variables
        TAC       total cost
          COEcc      ;

*=========================================================================
====
Positive Variables
        Amem(n)         membrane area for n (m2)
        PP
        PR
        xF(n)            Split fraction of component i from flue gas Splitter SPFn flowing toward membrane stage n
        xPOS(n)           Fraction of component i from splitter SPPn towards product mixer MOP
        xRRO(n)           Fraction of component i from splitter SPRn supplied to mixer MOA
        xRPR(n,pmr)           Fraction of component i in RP from permeate splitter SPPn towards mixer  MPn
        xRRR(n,rrr)          Fraction of component i in stream RR from retentate splitter SPRn entering mixer MFn
        TNQ          total net power consumed br compressors less recovered by expanders
        Qcft              power used by feed compressor KJps
        Qvac
        Qexr              power produced by the expander
        R(i)              recovery of gas component i
        Ahx(n)
        Perm(i,n,k)
        Aclf          heat transfer area of the cooler
        DP(i)          desired purity of CO2 enriched stream
        F(i,n)
        FS(i,n)          stream delivered to membrane module
        FSn(i,n)
        RWf
        yFSn(i,n)
        FSnt(n)
         yFSnw
        FSnw
       Retrcy
        POS(i,n)          residue stream from retentate splitter SPR(n) kmolpmin
        MS
        MSw
        RWms
        yMS
        yMSw

        lmTclf
        lmTclr(n)
        OA(i)             flow rate of residue  kmolpmin
```

OP(i) *flow rate of product kmolps*
POS(i,n) *residue stream from retentate splitter SPR(n) kmolpmin*
Qclr(n) *heat removed in recyclecooler clr*
Qcfr *power of recycle compressor cfr*
Qhx(n)
Qclf
Qclr(n)
RRO(i,n) *flow rate of i from (from SPR) in retentate to mixer MOA*
RRWO
RRS
yRRS
yRR
RR(i,n)
RPS(i,n)
yRPS
yRP
RP
RRk (i,n,k) *flow rate i from compartment k on the retentate sideof stage n*
RPk(i,n,k) *flow rate i from compartment k on the permeate side of stage n*
RRkt (n,k) *total flow in k stage n retantate*
RPkt (n,k) *total flow in k stage n permeate side*
ppP(i,n,k) *partial pressure permeate side*
ppR(i,n,k) *partial pressure retantate side*
Tcft *temperate of gas exit feed compressor cft*
Tcfr(n) *temperature of gas exiting compressor recycle cfr*
yRPk(i,n,k) *Mole fraction of component i in the permeate side in the small area k in membrane stage n*
yRRk(i,n,k) *Mole fraction of component i in the retentate side in the small area k*
yRRO(i,n) *mole fraction of i in stream RRO of stage n send to residue*
RRt(n) *retantate from membrane n before splitter*
RPt(n) *permeate from membrane before splitter*
FSt(n) *fotal feed stream to membrane*
yRP(i,n) *mole fraction i in permeate*
OAt *total residu*
OPt *total product*
yFS(i,n) *mole fract feed steam to membrane*
lmThx *mean temp difference k*
Qco *duty of co2 compressor*
TC
RH(n) *relative humidity*
SP(n) *separation factor*
yRR(i,n) *more fraction of i in retantate in stage n*
yOP(i) *more fraction of i in product stream*
yOA(i) *more fraction of i in residue to atmosphere*
Qhx(n) *power of heat exchanger*
RPSt(n) *total flowrate of permeate from membrane stage n*
RPS(i,n) *flow rate of i from membrane stage n*
yRPS(i,n) *mol fraction of rps*
RWOt(n) *total removed from permeate stream*
RWO(i,n) *removed by condensors from permeate*
yRWO(i,n) *mol fraction of i in rwo*
FT
RWcon(i) *flow rate removed by flue gas condenser- water only*
RWcont *total flow rate removed by condenser*
yRWcon(i) *mol fraction of i in rwcon*
yFT (i) *mole fracton i in ft flue gas after condenser*
FTGt *total flue gas flow to the membrane*
FTt *total flow of fue after condenser -water only*
RWp(i) *flow rate i removed by product condenser -water only*
RWpt *total removed*
yRWp(i) *mol faction*
OPw(i) *flow rate i in product stream before eater remova in condenser*
OPwt *total flow of i opw*
RWpc
ROPCt
yROPC

yOPw
cpclsg(i) heat capacity of i at T
cpclr (i) heat capacity of i at the cooler
lmTclfms(n)
Aclfms(n)
CCclfms (n)
Qclfms(n)
dr(i,n,k) permeate across k kmolpmin
*KqppP(i,n,k) multiplication Keq * partial pressure permeate side*
*KqppR(i,n,k) multiplication Keq * partial pressure retantate side*
ppP(i,n,k) partial pressure permeate side
ppR(i,n,k) partial pressure retantate side
perm permeance
*HKpp Ha+keq*partial p on permeate*
*HKpr Ha+keq*partial p on retantate*

*====Cost Variables==========

* TAC
TMA tola membrane area
EC
TCCmem total capital cost of membrane
TCCU total capital cost of units
OPEX
COM
CAPEX
CCco
CCclco

ACmem(n) annual cost of membrane
Aclf heat transfer area of the cooler
Aclr area of cooler clr

**Capital annualised costs*
CCclr(n) annual capital cost of cooler clr
CCcfr capital cost of cfr
CCcft capital cost of recycle compressor cfr
CCexr annual capital cost of expander on product retentate
CCclf annual cost of clf
CCvac
CCexs(n) annual capital cost of expander on sweeping gas
CChx(n) annual capital cost of heat exchanger
CCclsg(n)
CCbc(n)
**Operating costs*
OCbc(n)
Var
Ppw
Qcopw
CCopw
Ppwe
Qpum power of product pump
Qcomp power of the final product compresssor
CCco2comp purchace for the product compressor
CCco2pump purchase base cost for the product pum
CR compression ratio for the product compressor
TcftD(n)
UlmTclf(n)
FSnCp(n)
PPe(n)
PRe(n)
Qexrn
CCcootal

TPpw
Qclrwp
Rwpc
Qclrwpc
Rwpc
lmclTrwpc
CCclrwpc
Aclrwpc
Rwo
Tvac
CCclrwo
Qclrwo
lmclTrwo
Aclrwo
CCclrwcon
Rwcon
lmclTrwcon
Uclcon
Qclrwcon
Aclrwcon
Aclrwp
lmclTrwp
CCclrwp
Qclfcon
lmclTfcon
Aclfcon
CCclfcon
Qclfdcon
lmclTfdcon
Aclfdcon
CCclfdcon
Qclpcon
Aclpcon
lmclTpcon
CCclpcon
Cpclrwcon
Cpclrwo
Cpclrwp
Qclrwocon(n)
lmclTrwocon(n)
Aclrwocon(n)
CCclrwocon(n)
Cpclf
TCcomp
CAPEXtrsg
OPEXtrsg
ECtrsg
TCCUtrsg
COMtrsg
TNQtrsg
Qexrn
Qexrrrn
Qexrrn ;

Binary variables
Zcrr(n,np)
Zrwms
Zexrr(n,np)
Zret(n,rrr)
Zrwf
Zrwo
Zrwpc;

variables
*----------*relavant positive variable*----------

```
      CCcrrr          capital cost of recycle compressor
      CCexrr          capital cost of recycle expander
      PPe(n)          PP**0.286    trying to simplify equations for fast solving
      PRe(n)          PR**0.286
      PP(n)           permeate pressure
      PR(n)           retentate pressure
      Qcrrr           power consumed by the recycle compressor  compressing recycle stream Retrcy n-p
      Qexrr           power produced by the recycle expander    expansion on recycle stream Retrcy n-p
      xF(n)           Split fraction of component i from flue gas Splitter SPFn flowing toward membrane stage n
      xPOS(n)         Fraction of component i from splitter SPPn towards product mixer MOP
      xRRO(n)         Fraction of component i from splitter SPRn supplied to mixer MOA
      xRRR            Fraction of  from retentate splitter recycled to stage rrr which correspond to Retrcy
      Retrcy          rate of stream from membrane stage (n) recycled to stage (rrr)

      Qcrrr
      Qexrr
;

*-------------------------------------------------------------------------------------------------
Equation
s76,s77;

s76..       Qcrrr('n1','rrr2')*PRe('n1') =e=( (1/Eff)*(( (sum(ip, Retrcy(ip,'n1','rrr2')/60)))*8.3145e-3*Tmem*3.5* (PRe('n2')-
PRe('n1') ))) ;
s77(n,rrr)..        CCcrrr(n,rrr) =e= (Ccomp*Qcrrr(n,rrr))  ;

Equations
 t76,t77
t81,t82,t84;

t76..       Qcrrr('n1','rrr3')*PRe('n1') =e=( (1/Eff)*(( (sum(ip, Retrcy(ip,'n1','rrr3')/60)))*8.3145e-3*Tmem*3.5* (PRe('n3')-
PRe('n1') ))) ;
t77..       Qcrrr('n2','rrr3')*PRe('n2') =e=( (1/Eff)*(( (sum(ip, Retrcy(ip,'n2','rrr3')/60)))*8.3145e-3*Tmem*3.5* (PRe('n3')-
PRe('n2') )))  ;

t81..       Qcrrr('n1','rrr4')*PRe('n1') =e=( (1/Eff)*(( (sum(ip, Retrcy(ip,'n1','rrr4')/60)))*8.3145e-3*Tmem*3.5* (PRe('n4')-
PRe('n1') )))  ;
t82..       Qcrrr('n2','rrr4')*PRe('n2') =e=( (1/Eff)*(( (sum(ip, Retrcy(ip,'n2','rrr4')/60)))*8.3145e-3*Tmem*3.5* (PRe('n4')-
PRe('n2') )))  ;
t84..       Qcrrr('n3','rrr4')*PRe('n3') =e=( (1/Eff)*(( (sum(ip, Retrcy(ip,'n3','rrr4')/60)))*8.3145e-3*Tmem*3.5* (PRe('n4')-
PRe('n3') )))  ;


Equations
t76,t78,t75,t77,t79,t80 ;
t78..       Qcrrr('n1','rrr1')*PRe('n1') =e=( (1/Eff)*(( (sum(ip, Retrcy(ip,'n1','rrr1')/60)))*8.3145e-3*Tmem*3.5* (PRe('n1')-
PRe('n1') )))  ;
t79..       Qcrrr('n2','rrr2')*PRe('n2') =e=( (1/Eff)*(( (sum(ip, Retrcy(ip,'n2','rrr2')/60)))*8.3145e-3*Tmem*3.5* (PRe('n2')-
PRe('n2') )))  ;
t75..       Qcrrr('n3','rrr3')*PRe('n3') =e=( (1/Eff)*(( (sum(ip, Retrcy(ip,'n3','rrr3')/60)))*8.3145e-3*Tmem*3.5* (PRe('n3')-
PRe('n3') )))  ;

t80..       Qcrrr('n4','rrr4')*PRe('n4') =e=( (1/Eff)*(( (sum(ip, Retrcy(ip,'n4','rrr4')/60)))*8.3145e-3*Tmem*3.5* (PRe('n4')-
PRe('n4') )))  ;


Equations
s50,s52,t50,t53,t54,t90,t92,t93;

*recycle expander
s50..           Qexrr('n3','rrr1')*PRe('n3')=e=(( (Eff)* ((sum(ip, Retrcy(ip,'n3','rrr1')/60)) *8.314*3.5*Tmem* (PRe('n3')-
PRe('n1') ) ))*1e-3);
*s51..          Qexrrn('n3','rrr1')=e= (1/Eff)*   Qexrr('n3','rrr1');
s52(n,rrr)..        CCexrr(n,rrr) =e= (Cexp*Qexrrn(n,rrr)) ;
```

```
* expander
t50..          Qexrr('n3','rrr2')*PRe('n3')=e=(( (Eff)* ((sum(ip, Retrcy(ip,'n3','rrr2')/60)) *8.314*3.5*Tmem* (PRe('n3')-
PRe('n2') ) ))*1e-3);

*expander
t53..          Qexrr('n2','rrr1')*PRe('n2')=e=( (Eff)* ((sum(ip, Retrcy(ip,'n2','rrr1')/60)) *8.314*3.5*Tmem* (PRe('n2')-
PRe('n1') ) ))*1e-3;
t90..          Qexrr('n4','rrr1')*PRe('n4')=e=( (Eff)* ((sum(ip, Retrcy(ip,'n4','rrr1')/60)) *8.314*3.5*Tmem* (PRe('n4')-
PRe('n1') ) ))*1e-3;
t92..          Qexrr('n4','rrr2')*PRe('n4')=e=( (Eff)* ((sum(ip, Retrcy(ip,'n4','rrr2')/60)) *8.314*3.5*Tmem* (PRe('n4')-
PRe('n3') ) ))*1e-3;

t93..          Qexrr('n4','rrr3')*PRe('n4')=e=( (Eff)* ((sum(ip, Retrcy(ip,'n4','rrr3')/60)) *8.314*3.5*Tmem* (PRe('n4')-
PRe('n3') ) ))*1e-3;



t54(n,rrr)..       Qexrrn(n,rrr)=e= (1/Eff)*   Qexrr(n,rrr)    ;

Equations

t56,t57,t58,t60;
t56..       Qexrr('n1','rrr1')*PRe('n1')=e=(( (Eff)* ((sum(ip, Retrcy(ip,'n1','rrr1')/60)) *8.314*3.5*Tmem*
                (PRe('n1')-PRe('n1') ) ))*1e-3);

t57..       Qexrr('n2','rrr2')*PRe('n2')=e=(( (Eff)* ((sum(ip, Retrcy(ip,'n2','rrr2')/60)) *8.314*3.5*Tmem*
                (PRe('n2')-PRe('n2') ) ))*1e-3);
t58..       Qexrr('n3','rrr3')*PRe('n3')=e=(( (Eff)* ((sum(ip, Retrcy(ip,'n3','rrr3')/60)) *8.314*3.5*Tmem*
                (PRe('n3')-PRe('n3') ) ))*1e-3);
t60..       Qexrr('n4','rrr4')*PRe('n4')=e=(( (Eff)* ((sum(ip, Retrcy(ip,'n4','rrr4')/60)) *8.314*3.5*Tmem*
                (PRe('n4')-PRe('n4') ) ))*1e-3);

Equations
s93,s94,s95,t10,t11,t12
t10,t17,t16 ;

t10..        PR('n4')-PR('n3')=g=0    ;
t11..        PR('n4')-PR('n2')=g=0    ;
t12..        PR('n4')-PR('n1')=g=0    ;
s93..        PR('n3')-PR('n1')=g=0    ;
s94..        PR('n3')-PR('n2')=g=0    ;
s95..        PR('n2')-PR('n1')=g=0    ;


t16..      Qcrrr('n2','rrr1') + Qcrrr('n3','rrr1') + Qcrrr('n3','rrr2')+ Qcrrr('n4','rrr1')+ Qcrrr('n4','rrr2')+ Qcrrr('n4','rrr3')
=e= 0;



t17..              Qexrr('n2','rrr3')+  Qexrr('n1','rrr3')+  Qexrr('n1','rrr2')+  Qexrr('n1','rrr4') +  Qexrr('n2','rrr4') +
Qexrr('n3','rrr4')=e=0;


*-------------------------------------------------------------------------------------------------------------------------------------------------------
----------
Equations
e2,e3,e4,e5,e84b, e84a;


e2(i,n,k)$ (ord (k) = 2 )..      ( 4.5 * ( ( -RRk(i,n,k-1)+ RRk(i,n,k+1)) ))
    +( (Amem(n)*Perm(i,n,k))*(  ( ppR(i,n,k)- ppP(i,n,k)) ) )=e=0  ;
```

```
e3(i,n,k)$ (ord (k) > 2)..      (  4.5 *(  (RRk(i,n,k-2) -(4*RRk(i,n,k-1)) +(3*RRk(i,n,k)) ))
              +(  (Amem(n)* Perm (i,n,k))* (  (ppR(i,n,k)- ppP(i,n,k))  ) )) =e= 0;



e4(i,n,k)..      (RRk(i,n,k)-RRk(i,n,'k10')-  RPk(i,n,k)) =e= 0 ;
e5(n,k)..        (RRkt(n,k)-RRkt(n,'k10')-RPkt(n,k)) =e= 0;


e84b(i,n,k).. RRk(i,n,k)=g= RRk(i,n,k+1) ;
e84a(i,n,k).. RPk(i,n,k)=g= RPk(i,n,k+1) ;



equations
p1,
p4,p5,p6,p7,
p8,p9,p10;


p1(n,k)..        perm ('i1',n,k)*(L*Ha)* (HKpr('i1',n,k)*HKpp('i1',n,k)) =e= ( Da*(HKpr('i1',n,k)*HKpp('i1',n,k) )) + (Ha*
Dac*Keq*Ct*Ha )  ;


p4(n,k)..      KqppR('i1',n,k)    =e= Keq*ppR ('i1',n,k)       ;
p5(n,k)..      KqppP('i1',n,k)    =e= Keq*ppP ('i1',n,k)       ;
p6(n,k)..      HKpr('i1',n,k)     =e= Ha +KqppR('i1',n,k)      ;
p7(n,k)..      HKpp('i1',n,k)     =e= Ha+ KqppP ('i1',n,k)     ;


p8(n,k)..       Perm ('i2',n,k)=e= 1.10229E-05;
p9(n,k)..       perm ('i3',n,k) =e=    0.001488095     ;
p10(n,k)..      perm ('i4',n,k) =e=   4.96032E-05       ;
*L.lo=0.8e-6;
equations
p2,p3 ;
*e84c, e84d;

p2(i,n,k)..      ppR(i,n,k)    =e= PR(n)*yRRk(i,n,k)           ;
p3(i,n,k)..      ppP(i,n,k)    =e= PP(n)*yRPk(i,n,k)           ;



Equations
e25,e1000, e1001, e708,e707,e710,e743,e901, e903,e905, e724a,e709,e730,
e17, e904,e902,e906,e710,e724  ;

e1000(i,n,k)..      yRPk(i,n,k)*(sum(ip,  (RPk(ip,n,k))))=e= RPk(i,n,k) ;
e1001(i,n,k)..      yRRk(i,n,k)*(sum(ip,  (RRk(ip,n,k))))=e= RRk(i,n,k) ;

* flow in k1

e707(n)..         RRkt(n,'k1') =e=sum (ip, FS(ip,n)) ;
e708(n)..         RPkt(n, 'k1')=e=sum (ip,RPS(ip,n)) ;
e17(i,n)..       RPk(i,n,'k1') =e= RPS(i,n);
e709(i,n)..       yRPk(i,n,'k1')=e= yRPS(i,n) ;
e710(i,n)..       yRRk(i,n,'k1')=e= yFS(i,n);

*Flow k10
e743(i,n,k)$(ord(k)=card(k))..       RR(i,n) =e= RRk(i,n,k);
e730(i,n,k)$(ord(k)=card(k))..       yRR(i,n)=e= yRRk(i,n,k) ;
*e724(n,k)$(ord(k)=card(k))..         RRt(n)=e= RRkt(n,k)  ;
```

```
e724(n,k)..            (sum(ip,  (RPk(ip,n,k)))) =e= RPkt(n,k)     ;
e724a(n,k)..           (sum(ip,  (RRk(ip,n,k)))) =e= RRkt(n,k)     ;


e905(i,n)..     yRR(i,n)*(sum(ip, RR(ip,n))) =e= RR(i,n) ;
e901(i,n)..     yFS(i,n)* (sum(ip, FS(ip,n)))=e= FS(i,n) ;
e903(i,n)..     yRPS(i,n)*(sum(ip, RPS(ip,n))) =e= RPS(i,n) ;


e904(n)..       sum(ip, yRPS(ip,n))=e= 1;
e902(n)..       sum(ip, yFS(ip,n))=e= 1;
e906(n)..       sum(ip, yRR(ip,n))=e= 1;


*e25(n)..        FSt(n)+sum (ip, SG(ip,n)) =e= RRt(n)+RPSt(n) ;
*e25(n)..        FSt(n)=e= RRt(n)+RPSt(n) ;
e25(i,n)..      FS(i,n)=e= RR(i,n)+RPS(i,n) ;


Equation
e23,
*e760ee
*e760e,
 e24    ;

e23(n,k)..      sum (ip, yRRk(ip,n,k)) =e= 1 ;
e24(n,k)..       sum (ip, yRPk(ip,n,k)) =e= 1 ;


*=====================================================================
equations
ec4,ec5,ec6,ec7, e27,e28 ,  ec11a,
ec10,ec11,ec12;


*balance on feed condenser
ec7(i)..   FTG(i)=e= FT(i)+RWcon(i)  ;

*to ensure only water is removed by the condenser
ec4..             RWcon('i1')=e= 0 ;
ec5..             RWcon('i2')=e= 0 ;
ec6..             RWcon('i4')=e= 0 ;

ec10(i)..      yFT(i)* sum(ip,  FT(ip))=e=  FT(i);
ec11..         yFT('i3')*Patm=l=0.0562;
ec11a..         yFT('i3')*Patm=g=0.05619;
ec12(n,k)..      sum (ip, yFT(ip)) =e= 1 ;

* balance around flue gas splitter, split fraction sum, and the streams
e27..             sum (n, xF(n))=e= 1   ;
e28(i,n)..         F(i,n) =e= xF(n)*FT(i)    ;
 xF.lo(n)    = 0.0 ;             xF.up(n)   = 1      ;


*=================e68d,=================================================---------
-------------------------------------------------------------------------------

Equations
e62, e68c,e62b,e67,e68a
e64,e65,e66,e69,e70,e68;
*ec25;
*balance on the permeate condenser
```

```
e62b(i,n)..      ( rps(i,n)) *(1-Zrwo(n)) =e= rp(i,n)*(1-Zrwo(n))    ;
e62(i,n)..       ( rps(i,n))*Zrwo(n)  =e= (rp(i,n)+rwo(i,n))* Zrwo(n)   ;

*e62(i,n)..      ( rpm(i,n))  =e= (rp(i,n)+rwo(i,n))  ;

*to ensure only water is removed by the condenser
e64(n)..         RWO('i1',n)=e= 0 ;
e65(n)..         RWO('i2',n)=e= 0 ;
e66(n)..         RWO('i4',n)=e= 0 ;
e67(n)..         RWO('i3',n)*(1-Zrwo(n))=e= 0*(1-Zrwo(n)) ;

e68(n)..         (yrps('i3',n)*Patm)* Zrwo(n)=g=(0.0562)* Zrwo(n);
e68a(n)..         (yrps('i3',n)*Patm)*(1-Zrwo(n))=l=(0.056)*(1-Zrwo(n));


e69(i,n)..       yrp(i,n)*(sum(ip, rp(ip,n)))=e= rp(i,n) ;
e70(n)..         sum(ip, yrp(ip,n))=e= 1;
yRP.up(i,n) = 1;

e68c(n)..         (yrp('i3',n)*Patm)* Zrwo(n)=e=(0.0562)* Zrwo(n);


*-------------------------------------------------------------------------------------------------------------------------------------------------------
---------------
Equations
epc1,  epc5,epc9, epc10,epc12;

*balance on the final product condenser
epc1(i)..        OPw(i) =e= RWp(i) +OP(i) ;

*to ensure all water is removed by the condenser

epc5..       yOP('i3')*Ppw=e=0.0562   ;

*to ensure only water is removed by the condenser
epc10(n)..       RWp('i1')=e= 0 ;
epc9(n)..        RWp('i2')=e= 0 ;
epc12(n)..       RWp('i4')=e= 0 ;
Ppw.lo=Patm    ;
*epc2..          sum(ip, RWp(ip)) =e= RWpt  ;

*-----------------------------------------------------------------------------------
Equation
n1, e45, e48,n4,n6,n7,n20;
xPOS.lo(n) = 0.0;            xPOS.up(n) = 1;
xRRO.lo(n) = 0.0;            xRRO.up(n) = 1;
xRPR.lo(n,pmr) = 0;          xRPR.up(n,pmr) = 1;
xRRR.lo(n, rrr) = 0;         xRRR.up(n,rrr) = 1;

e45(i)..        OPw(i) =e=  POS(i,'n1')+ POS(i,'n2') + POS(i,'n3') +POS(i,'n4');
e48(i)..        OA(i)=e=   RRO(i,'n1')+RRO(i,'n2') +RRO(i,'n3') +RRO(i,'n4');

n1(n)..          xRRO(n)+ sum (rrrp, (xRRR(n,rrrp))) =e=1;
n4(n)..          xPOS(n)+ sum (pmrp, (xRPR(n,pmrp))) =e=1;
n6(i,n)..        POS(i,n) =e= xPOS(n)*RP(i,n);
n7(i,n)..        RRO(i,n) =e= xRRO(n)*RR(i,n);

n20(i,n,rrr)..                RR(i,n)*xRRR(n,rrr) =e= Retrcy(i,n,rrr) ;

Equations
e90,e91,e92,e93,e94,e95,e92a,e95a;
**balance around permeate mixer (MPn)
e90(i)..         MS(i,'n1')=e= sum (np, (RP(i,np)*xRPR(np,'pmr1') )) + f(i,'n1');
e91(i)..         MS(i,'n2')=e= sum (np, (RP(i,np)*xRPR(np,'pmr2') )) + f(i,'n2');
```

```
e92(i)..          MS(i,'n3')=e= sum (np, (RP(i,np)*xRPR(np,'pmr3') )) + f(i,'n3');
e92a(i)..          MS(i,'n4')=e= sum (np, (RP(i,np)*xRPR(np,'pmr4') )) + f(i,'n4');


e93(i)..           FS(i,'n1')=e= MSw(i,'n1')+ sum (np, (Retrcy(i,np,'rrr1')))    ;
e94(i)..           FS(i,'n2')=e= MSw(i,'n2')+ sum (np, (Retrcy(i,np,'rrr2')))    ;
e95(i)..           FS(i,'n3')=e= MSw(i,'n3')+ sum (np, (Retrcy(i,np,'rrr3')))    ;
e95a(i)..          FS(i,'n4')=e= MSw(i,'n4')+ sum (np, (Retrcy(i,np,'rrr4')))    ;


Equation
n30,n31,n32,n33;
n30..              xrrr('n1','rrr1')+xrpr('n1','pmr1')=l=1 ;
n31..              xrrr('n2','rrr2')+xrpr('n2','pmr2')=l=1 ;
n32..              xrrr('n3','rrr3')+xrpr('n3','pmr3')=l=1  ;
n33..              xrrr('n4','rrr4')+xrpr('n4','pmr4')=l=1 ;

equations
eb6;
*to ensure relative humity is  90% as related to saturation pressure  0.0562 bar and water partial pressure
eb6(n)..       RH(n)*0.0562=e= yFS('i3',n)*PR(n) ;
*eb6(n)..      0.9*0.0562=e= yFS('i3',n)*PR(n) ;
RH.lo(n)=0.9 ; RH.up(n)=1;

*-------------------------------------------------------------------------------------------------------------------------------------------------------------
---------
Equations
e52, e60, e69, e72,e71 ,e73,e74
e53,e54,e55,e56,e60a,e57,e58;

*balance on the feed condenser
e52(i,n)..         MS(i,n)*(1-Zrwms(n)) =e=MSw(i,n)*(1-Zrwms(n));
e53(i,n)..         MS(i,n)*Zrwms(n) =e= (MSw(i,n) +RWms(i,n))*Zrwms(n) ;


*to ensure only water is removed by the condenser
e54(n)..        RWms('i1',n)=e= 0 ;
e55(n)..        RWms('i2',n)=e= 0 ;
e56(n)..        RWms('i4',n)=e= 0 ;
e57(n)..        RWms('i3',n)*(1-Zrwms(n))=e= 0* (1-Zrwms(n));


e58(i,n)..      yMS(i,n)* sum(ip, MS(ip,n))=e= MS(i,n);

e71(i,n)..      yMSw(i,n)* sum(ip, MSw(ip,n))=e= MSw(i,n);

e73(n)..           sum(ip, yMS(ip,n))=e= 1;
e74(n)..           sum(ip, yMSw(ip,n))=e= 1;

e60(n)..       (yms('i3',n)*PR(n))*Zrwms(n)=g=(0.0562)*Zrwms(n);
e60a(n)..      (yms('i3',n)*PR(n))*(1-Zrwms(n))=l=(0.056)*(1-Zrwms(n));


yms.lo(i,n)= 0;    yms.up(i,n)= 1;
yMsw.lo(i,n)= 0;    ymsw.up(i,n)= 1;

e72(n)..           yMSw('i3',n)*PR(n)*Zrwms(n)=e=0.05602*Zrwms(n);


*-----------------------------------MS-----------------------------------------------------------------------------------------------------------------

PR.lo(n)=1; PR.up(n)=5;
PP.lo(n)=0.2; PP.up(n)= Patm;

Amem.lo(n)  = 1000 ;
```

```
*Amem.up(n)  = 1500000 ;

Equations
e46,e161,e49,e50,ee52;

*desired  product Co2 recovery capture ratio
e49(i)..          R(i)*FTG(i)=e= OP(i)   ;
e50..             R('i1')=g=0.9;
R.lo(i) = 0; R.up(i) = 1   ;

*final product mixer - compression for storage yOP is CO2 target purity

e46..             OPt   =e= sum(ip, OP(ip)) ;
*e161(i,n)..       yOP(i)* (sum(ip, OP(ip))) =e= OP(i) ;
e161(i,n)..       yOP(i)*OPt=e= Op(i) ;
ee52..            yOP('i1') =g=0.95;
*e46a..             sum (ip, yOP(ip))=e=1;
yOP.up(i) = 1;

Equations
e160,e47;
*balance around the final residue mixer to - to atmosphere
e47..             OAt    =e= sum (ip, OA(ip));
e160(i,n)..       yOA(i)*OAt=e= OA(i) ;
*e160(i,n)..       yOA(i)*(sum (ip, OA(ip)))=e= OA(i) ;
* yOA.up(i) = 1;

*-------------------------------------------------------------------------------------------------------------------------

Equations
s1,s2,s3,s4,s5,s6,s7,s8;          ;

*tnq net power, tma membrane area, ec electricity cost, 7500h per year, 15$phr labour ,  hrspy hours per year online
*s103..         TMA =e=  sum (np, (Amem(np))) ;
s1..         TNQ =e=  sum (np, Qcft(np))+sum (np, (Qvac(np)))- sum(np, Qexr(np))+Qcopw
                  + Sum ((n,rrr),(Qcrrr(n,rrr)))
                  -Sum ((n,rrr),(Qexrr(n,rrr)))  ;

s2..         OPEX  =e=   COM + EC ;
s3..         EC    =e=   Cel *(TNQ)*hrspy;
s4..         CAPEX =e=   0.1059*(1+0.37)*TCCU  ;
s5..         TCCmem =e= Cmem*sum(np, Amem(np))+(Cmf*( (sum(np, Amem(np))/2000)**0.7));
*s110..         TCCmem =e= Cmem*TMA+(Cmf*((TMA/2000)**0.7));

s6..        COM =e=    (0.01*TCCmem)+ (  ((567.5/584.5) * 0.036) *(  sum (np, CCcft(np)) +CCopw +
                    sum(np,CCvac(np)) + sum (np, CCexr(np))  ))   ;


s7..         TCCU  =e=   TCCmem+ (   (567.5/584.5)  *   (    sum (np, CCcft(np)) +CCopw +
                       sum(np, CCvac(np)) + sum (np, CCexr(np))
                     +   Sum ((n,rrr),(CCcrrr(n,rrr)))
                        + Sum ((n,rrr),(CCexrr(n,rrr))) ))    ;


s8..        hrspy     =e=       cf*365.25*24  ;

*(603.1/584.6)*  (567.5/584.5)* ((567.5/584.5)*
Equations

s9,s10,s11 ;
s9(n)..           PPe(n) =e=   (PP(n))**0.286  ;
S10(n)..          PRe(n) =e=   (PR(n))**0.286;
s11..             Ppwe  =e=     Ppw**0.286;

Equations
```

```
s12,s13,s14,s15,s16,s17 ;

s12(n)..        Qcft(n)*Patme =e=(( (1/Eff)*( ( (sum(ip, MS(ip,n)))/60)*8.3145e-3*Tmem*3.5* (PRe(n)-Patme) )))  ;
s13(n)..        CCcft(n) =e= Ccomp*Qcft(n)      ;

s16(n)..        Qvac(n)*PPe(n)=e=( (1/Eff)* ( ( (sum(ip, RPS(ip,n)))/60)*8.3145*Tmem*3.5*(Patme -PPe(n))))*1e-3;
s17(n)..        CCvac(n) =e= (Cvac*Qvac(n)) ;


s14(n)..        Qcopw*Patme =e=(( (1/Eff)*( ( (sum(ip, OPw(ip)))/60)*8.3145e-3*Tatm*3.5* ((Ppwe)-Patme) ))) ;
s15(n)..        CCopw =e= Ccomp*Qcopw     ;


*
Equations
s23,s24,s25;

*residue expander
s23(n)..        Qexr(n)*PRe(n)=e=( (Eff)* (((sum(ip, RRO(ip,n)))/60) *8.314*3.5*Tmem* (PRe(n)-Patme) ) )*1e-3  ;
s24(n)..        Qexrn(n)*PRe(n)=e= (((sum(ip, RRO(ip,n)))/60) *8.314*3.5*Tmem* (PRe(n)-Patme) ) *1e-3;
s25(n)..        CCexr(n) =e= Cexp*Qexrn(n) ;



*---------------------------------------------------------------------------------------------------------------------------
Equation
s40;
s40..        TAC   =e=   OPEX + CAPEX  ;

*---------------------------------------------------------------------------------------------------------------------------
*compression for storage
*$ontext



Equation
s26,s27,s28,s29,s30 ;
*compression for storage
s26..     Qpum=e= ((((sum (ip, OP(ip)))/60)*22.4)/(Effc))*((Pfin-Pcut)))*1e-3   ;
s27..     Qcomp =e=( (1/Effc)*(5*((sum(ip, OP(ip)))/60)*3.5*8.314*Tmem*(CR**0.286-1)))*1e-3  ;
s28..     CR*(Ppw**0.20) =e= Pcut**0.20      ;

S29..     CCco2comp =e= Cco2comp*Qcomp ;
S30..     CCco2pump =e= Cco2pump*Qpum ;

equation
s60,s61,s62,s63,s64,s65,s66     ;
s60..          TNQtrsg =e= Qpum+Qcomp     ;
s61..          COMtrsg =e=   0.036*(  CCco2comp+CCco2pump);
s62..          TCCUtrsg  =e=  CCco2comp+CCco2pump  ;
s63..          ECtrsg    =e=  Cel *(TNQtrsg)*hrspy;
s64..          OPEXtrsg  =e=   COMtrsg + ECtrsg ;
s65..          CAPEXtrsg =e=   0.1059*(1+0.37)*TCCUtrsg  ;

s66..          TCcomp =e=  CAPEXtrsg +  OPEXtrsg    ;

Equations
s35,s36,s37,s38,s39 ,s58;

s58..        MWnetcc  =e=       727.3-TNQ-TNQtrsg;
*cost of storage   per year
s35..        mtacoc =e=( OP('i1')*Mr('i1') *60*hrspy)/1000 ;
s36..        ccastg =e= mtacoc* Cstrg  ;

*cost of transport   medupi to zululand basin 794km  per year, 1$/(km.ton) , storage $13/ton
```

```
s37..        ccatrans  =e= mtacoc * Ctrans *794  ;

s38..        CTrStg    =e= ccatrans + ccastg     ;

s39..        COEcc *(hrspy*MWnetcc)  =e= ( 360 + TAC + TCcomp +CTrStg     ) *1e6 ;

 MWnetcc.lo= 5;


*$offtext
*---------------------------------------------------------------------------------------------------------------

*$ontext
yFSn.up(i,n)  = 1;      yROPC.up(i)  = 1;      yFT.up(i)  = 1;        yRRk.up(i,n,k)= 1;
yRPk.up(i,n,k)= 1;      yFS.up(i,n)  = 1;      yRP.lo(i,n)= 0 ;       yRP.up(i,n) = 1;
yRR.lo(i,n)= 0;         yRR.up(i,n) = 1;       FS.lo('i1',n) =1e-3;
perm.up(i,n,k)= 1;      yRPS.up(i,n)=  1;      yRRS.up(i,n)=  1;
*FSnt.lo(n) = 0.1;
Amem.up(n)=1.5e6;


MS.up(i,n)=3000;
RR.up(i,n) =  2500 ;    FS.up(i,n) = 2500 ;    RRO.up(i,n) = 2500 ;
RPS.up(i,n) = 1000 ;    OPw.up(i)=800;         FT.up(i)  = 3500;

*$ontext
FS.up(i,n) =3000 ;
F.up(i,n)  = 2000;      OA.up(i)   =2500 ;
OP.up(i)   =  1000 ;    POS.up(i,n)   = 1000;

RRO.up(i,n) = 2500 ;    RR.up(i,n) =  2500 ;   RP.up(i,n) =  1500;    RRk.up(i,n,k) =  3500;
RPk.up(i,n,k)=2500;     RRkt.up(n,k) = 2500;   RPkt.up(n,k)= 2500;


Ppw.up=Pcut;

RPS.up(i,n) =2000 ;


model membrane /all/  ;

$onecho > baron.opt
compIIS 1
$offecho

membrane.optfile = 1;


option optcr  = 0 ;
*option minlp=antigone ;
option sysout= on ;
option work  =  1258291  ;
option reslim = 27000 ;
option minlp = baron;
solve membrane using MINLP minimising COEcc   ;

*display
*F.l,FSn.l,FS.l,RR.l, RPS.l,POS.l,RRO.l, RP.l;

*option minlp = baron;
*solve membrane using MINLP minimising COEcc   ;

*option minlp = antigone;
*option optcr  = 0 ;
*solve membrane using MINLP minimising COEcc   ;
```

Chapter 5 GAMS file

```
*1206 Hybrid system chapter5
$title    Membrane

*MINLP
Sets
      n membrane stages  /n1*n4/
      i components   /i1*i4/
      k subcompartments in a membrane   /k1*k10/
*       rrr retentate recycle streams /rrr1*rrr4/
*       pmr permeate recycle       /pmr1*pmr4/   ;
*      i1= CO2 ; i2= N2 ; i3=h20 ,i4=O2
      Alias (i, ip);
      Alias (n, np);
*       Alias (rrr, rrrp);
*       Alias (pmr, pmrp);

Scalar

      Cel     dollarpMW 85.50 high usage tarriff 1.38889E-05 /0.05e-3/
      Cmem    dollarpm2                          /50e-6/
      Crep    dollarpm2     to confirm           /50e-6/
      Cus     dollarpkg(mol)  to confirm    dollar perkmol    /0.357615894e-6/
      Eff     Efficiency of compressor vacuum expander       /0.85/
      Effc    efficiency of interstage compressor          /0.85/
      RFT     total mol flow rate of flue gas supplied to pcc kmolpm       /1339.2858/
      EY      effective year time ass 48 week online seconds  48 weeks       /27000000/
      E       flowrate upper bound  kmolpmin               /1300/
      IL      flowrate lowerbound kmopmin                  /0.1/
      Pini    final storage pressure lqd CO2               /1.0/
      Patme   bar                                  /1.00/
      Patm    bar                                  /1.0/
      Tmem1   temperature of water exit condenser          /353/
      Tatm    atmospheric temperature     25 deg C         /298/
      Tmem    temperature of membranes (45 deg C)  313 is 40  /313/
      Tuwo    temperature at which cooling water leaves the heat exchanger 55deg C /328/
      Uclf    cooler feed compressor KWpm2K   0.200        /0.110e-3     /
      Uclr    cooler recycle        KWpm2K    0.200       /0.110e-3     /
      CRF     Capital recovery factor peryear              /0.113/
      Ccomp   cost of compression   $pW                    /670e-3/
      Cco2comp co2 cost for storage                        /902e-3/
      Cco2pump co2 pumping cost for storage                /902e-3/
      Cexp    cost of expanding      $pKW                  /500e-3/
      Efh     equipment cost factor for housing            /1.80/
      Chexc   cost of heat exchange from reference $pm2     /300e-6/
      Cmf     cost reference frame cost $                  /0.238/
      Cvac    cost of vacuuming $pKW                       /1341e-3/
      Pcut                                         /75/
      Pfin                                         /150/
      tau       Liquid (water) hold up in the knockout drum  seconds 10      min  /600/
      Uclco   co2 compressor heat transfer coeffient 0.200    /0.100e-3     /
      Ucon     heat transfer coefficient of feed condenser /0.100e-3/
      Uclsg   cooler sweeping gas    Mw                    / 1.200e-3     /
      Uclcop2                                      /0.900e-3/
      Uhx     heat exchanger        MW                   /1.000e-3/
      Uclms    warming of recycle stream of recycle    Mw       /0.3e-3     /
      MSIN    marshal swift index                    / 1593.7 /
```

```
         Phxs    Phxs            bar                     /2/
         Dac     diffusivity    of carrier solute complex  m2ps m2pmin   / 2.6E-11  /
         Da      diffusivityof CO2              m2pmin           /5.643E-9/
         Keq     equilibrium constant [complex]p[co2][carrier] all at feed       m3pkmol    /1.22e2/
         Ct      total  concentration of effective carriers   kmolpm3               /2.72e1/
         Ha      Henry s constant barm3pmol                  /37.957/
         L       membrane thickness    m                   /0.8e-6/       ;
*        L       membrane thickness   thickest m                   /1.2e-6/        ;
;
  Parameters
*$ontext
         yFTG(i)    flue gas Feed concentration  mole fraction
         /i1 0.135
         i2  0.689
         i3  0.152
         i4  0.024/


        FTG(i)  ;
        FTG(i) = yFTG(i)*RFT ;

*=============================================================================
=====
Free Variables
       TAC       total cost       ;


Binary Variables
      Zco2
      zn2
      Zrwms(n)
      Zrwf
      Zrwo
      Zrrwo
      Zrpos                  ;
*=============================================================================
====
Positive Variables
       Ahx(n)
       Amem(n)        membrane area for n (m2)
       Perm(i,n,k)
       Aclf           heat transfer area of the cooler
       Aclsg(n)
       DP(i)          desired purity of CO2 enriched stream
       F(i,n)
       FS(i,n)         stream delivered to membrane module
       FSn
       yFSn
       FSnt
       lmTclf
       lmTclr(n)
       OA(i)           flow rate of residue  kmolpmin
       OP(i)           flow rate of product  kmolps
       POS(i,n)          residue stream from retentate splitter SPR(n) kmolpmin
       PP
       PR
       Qclr(n)          heat removed in  recyclecooler clr
       Qcfr            power of recycle compressor cfr
       Qexr            power produced by the expander
       Qcft            power used by feed compressor KJps
       Qclf
       Qvac
       Qexrpos(n)
       Qhx(n)
       Qclr(n)
```

R(i) recovery of gas component i
RRO(i,n) flow rate of i from (from SPR) in retentate to mixer MOA
RR(i,n) flow rate of retentate stream from membrane stage n towards splitter SPRn
RP(i,n) rate of component i in permeate stream from n to splitter SPPn
RPR(i,n) rate of i from permeate splitter towards permeate mixer n MPn
RPOS,
PRRO
yROPC
ROPC ,
ROAC
MS
MSw
RWms
yMS
yMSw
rwrrp
orrp
opp
rwrrp
yorrp
yopp
yrpos

*$ontext

RRk (i,n,k) flow rate i from compartment k on the retentate sideof stage n
RPk(i,n,k) flow rate i from compartment k on the permeate side of stage n
RRkt (n,k) total flow in k stage n retantate
RPkt (n,k) total flow in k stage n permeate side
ppP(i,n,k) partial pressure permeate side
ppR(i,n,k) partial pressure retantate side

*$offtext

* scut

Tcft temperate of gas exit feed compressor cft
Tcfr(n) temperature of gas exiting compressor recycle cfr
yRPk(i,n,k) Mole fraction of component i in the permeate side in the small area k in membrane stage n
yRRk(i,n,k) Mole fraction of component i in the retentate side in the small area k
yRRO(i,n) mole fraction of i in stream RRO of stage n send to residue
xF(n) Split fraction of component i from flue gas Splitter SPFn flowing toward membrane stage n
xRRO(n) Fraction of component i from splitter SPRn supplied to mixer MOA
xRRR Fraction of component i in stream RR from retentate splitter SPRn entering mixer MFn
xRPOS,
xPOS(n) Fraction of component i from splitter SPPn towards product mixer MOP
xRPR Fraction of component i in RP from permeate splitter SPPn towards mixer MPn
xPRRO
xOPR, xOAR
xOP , xOA
RRt(n) retantate from membrane n before splitter
RPt(n) permeate from membrane before splitter
FSt(n) fotal feed stream to membrane
yRP(i,n) mole fraction i in permeate
OAt total residu
OPt total product
yFS(i,n) mole fract feed steam to membrane
g(n) fraction to indicate sweep vapor flow
lmThx mean temp difference k
Qco duty of co2 compressor
TC
RH(n) relative humidity
SP(n) separation factor
yRR(i,n) more fraction of i in retantate in stage n
yOP(i) more fraction of i in product stream
yOA(i) more fraction of i in residue to atmosphere
TNQ total net power consumed br compressors less recovered by expanders
SG(i,n) sweep gas flow rate
Qhx(n) power of heat exchanger
RRS

```
    yRRS
    RPSt      total flowrate of permeate from membrane stage n
    RPS      flow rate of i from membrane stage n
    yRPS     mol fraction of rps
    RWOt      total removed from permeate stream
    RWO      removed by condensors from permeate
    yRWO     mol fraction of i in rwo
    RRWO      removed by condensors from permeate
    yRRWO     mol fraction of i in rwo
    FT
     yROPC
    ROPC ,
    ROAC
    RWf
   RWcon      flow rate removed by flue gas condenser- water only
   RWcont        total flow rate removed by condenser
   yRWcon      mol fraction of i in rwcon
   yFT          mole fracton i in ft flue gas after condenser
   RWp         flow rate i removed by product condenser -water only
   RWpt           total removed
   yRWp        mol faction
   RWpc
   yROPC
   OPw         flow rate i in product stream before eater remova in condenser
   OPwt           total flow of i opw
   yOPw
    Cpclf
    ppP(i,n,k)      partial pressure permeate side
    ppR(i,n,k)      partial pressure retantate side
    *HKpp            Ha+keq*partial p on permeate
    *HKpr            Ha+keq*partial p on retantate
    CCexrpos(n)
    Qexrposn(n)

*====Cost
Variables=========================================================================
===========
    TMA    tola membrane area
    EC
    TCCmem total capital cost of membrane
    TCCU   total capital cost of units
    OPEX
    CAPEX
    COM
    CCco
    CCclco
    Ppw
    Qcopw
    CCopw
    Ppwe
    ACmem(n)       annual cost of membrane
    Aclf          heat transfer area of the cooler
    Aclr           area of cooler clr

*Capital annualised costs
    CCclr(n)       annual capital cost of cooler clr
    CCcfr       capital cost of cfr
    CCcft          capital cost of recycle compressor cfr
    CCexr           annual capital cost of expander on product retentate
    CCclf          annual cost of clf
    CCvac
    CCexs(n)       annual capital cost of expander on sweeping gas
    CChx(n)        annual capital cost of heat exchanger
    yRetrcy
    Var
```

```
        Qpum              power of product pump
        Qcomp             power of the final product compresssor
        CCco2comp           purchace for the product compressor
        CCco2pump           purchase base cost for the product pum
        CR              compression ratio for the product compressor
        Qexrn
        Qexrn
        Qexrrrn
        Qexrrn     ;

         Binary variables
        Zcrr(n,np)
        Zexrr(n,np)
        Zret(n,np)
        Zro(n,np)
        Zrro
        Zexr(n)
        Zcfr(n);

        variables
*-------------------------------------------------relavant positive variable ----------------------------------------------
*         dPR(n,np)
        CCcrrr            capital cost of recycle compressor
        CCexrr            capital cost of recycle expander
         Qcfrn
        PPe(n)           PP**0.286    trying to simplify equations for fast solving
        PRe(n)           PR**0.286
        PP(n)           permeate pressure
        PR(n)          retentate pressure
*         dPRc(np,n)
*         dPRx(n,np)
        Qcrrr    power consumed by the recycle compressor  compressing recycle stream Retrcy n-p
        Qexrr    power produced by the recycle expander    expansion on recycle stream Retrcy n-p
         xF(n)          Split fraction of component i from flue gas Splitter SPFn flowing toward membrane stage n
        xPOS(n)         Fraction of component i from splitter SPPn towards product mixer MOP
        xRRO(n)         Fraction of component i from splitter SPRn supplied to mixer MOA
        xRPR(n,np)     Fraction of component i in RP from permeate splitter SPPn towards mixer  MPn
*         xRRR(n,rrr)     Fraction of component i in st
        xRRR      Fraction of  from retentate splitter recycled to stage rrr which correspond to Retrcy
        Retrcy rate of stream from membrane stage (n) recycled to stage (rrr)
;
*-------------------------------------------------------------------------------------------------------------------------------------------------------
----------------------

Equations
s76,s77 ;


s76(n,np)..          Qcrrr(n,np)*(PRe(n))   =e=( (1/Eff)*( (sum(ip, (Retrcy(ip,n,np)/60)))*8.3145e-3*Tmem*3.5* ((PRe(np))-
(PRe(n)) ))) *Zcrr(n,np); ;

s77(n,np)..              Qexrr(n,np)*(PRe(n))=e=( (Eff)*( (  (sum(ip, (Retrcy(ip,n,np)/60)))*8.3145e-3*Tmem*3.5*((PRe(n))-
(PRe(np)) ))))*Zexrr(n,np);


Equations
q46,q47,q48;
* this one plus 47+48
q46(n,np)..              ( (PR(n)-PR(np))*Zcrr(n,np) )  -( (PR(n)-PR(np))*Zexrr(n,np) )    =l= PR(n)-PR(np) ;

*q47(n,np)..               (PR(n)-PR(np))*Zcrr(n,np)  =l=(-0.001)*Zcrr(n,np)  ;
*q48(n,np)..               (PR(n)-PR(np))*Zexrr(n,np) =g=0.001*Zexrr(n,np) ;
```

```
q47(n,np)..              (PR(n)-PR(np))*Zcrr(n,np) - (-0.001)*Zcrr(n,np)    =l= 0;
q48(n,np)..              (PR(n)-PR(np))*Zexrr(n,np) - (0.001*Zexrr(n,np)) =g= 0 ;

Equations
s78,t54,t52;
*Capital cost of recycle expander
s78(n,np)..    CCcrrr(n,np) =e= Ccomp*Qcrrr(n,np)*Zcrr(n,np)  ;
t54(n,np)..    Qexrrn(n,np)=e= (1/Eff)*   Qexrr(n,np)*Zexrr(n,np)    ;
t52(n,np)..    CCexrr(n,np) =e= (Cexp*Qexrrn(n,np))*Zexrr(n,np) ;


*-------------------------------------------------------------------------------------------------------------------------------------------------------
---------------------------------------


ppw.lo= 0; Ppw.up=10 ;

Equations
epc1,  epc5,epc9, epc10,epc12,ec2,p30 ;

*balance on the final product condenser
epc1(i)..          OPw(i) =e= RWp(i) +Opp(i) ;

*to ensure all water is removed by the condenser
*epc5(i)..          OPw('i3')=e= RWp('i3') ;

epc5..         yOPP('i3')*Ppw=e=  0.031699   ;

*to ensure only water is removed by the condenser
epc10(n)..         RWp('i1')=e= 0 ;
epc9(n)..          RWp('i2')=e= 0 ;
epc12(n)..         RWp('i4')=e= 0 ;
Ppw.lo=Patm     ;
* Ppw.up=15     ;

ec2(i).. sum(n,pos(i,n))=e= Opw(i)      ;


p30(i)..     yOPP(i)*(sum(ip, OPP(ip))) =e= OPP(i) ;

Equation
f40;
f40(i)..           sum (np, orrp(i,np))+ opp(i) =e= OP(i) ;


*-------------------------------------------------------------------------------------------------------------------------------------------------------
-----------------------------------------------
$ontext
Equations
f20,f32,f31,f40,f27;

*balance on the final product condenser
f20(i,n) $ (ord(i)<> (3))..          rpos(i,n) =e= orrp(i,n) ;

f31(i,n)$ (ord(i)=(3))..          rpos(i,n) =e= rwrrp(i,n) +orrp(i,n) ;

f32(n)..         ((yorrp('i3',n)*Ppw))  =e= 0.031699;

f27(i,n)..     yorrp(i,n)*(sum(ip, orrp(ip,n))) =e= orrp(i,n) ;
$offtext

*$ontext
```

```
Equations
f20,f32,f31,f40,f27,f30,f26,f33;

*balance on the final product condenser ,f33
f20(i,n) $ (ord(i)<> (3)).. rpos(i,n) =e= orrp(i,n) ;

f31(i,n)$ (ord(i)=(3)).. rpos(i,n) =e= rwrrp(i,n) +orrp(i,n) ;

f26(i,n).. yrpos(i,n)*(sum(ip, rpos(ip,n))) =e= rpos(i,n) ;
f27(i,n).. yorrp(i,n)*(sum(ip, orrp(ip,n))) =e= orrp(i,n) ;


f30(n).. ((yrpos('i3',n)*Ppw)*Zrpos(n)) - (0.032*Zrpos(n)) =g= 0;
*f34(n).. ((yrpos('i3',n)*Ppw)*(1-Zrpos(n))) - (0.03169*(1-Zrpos(n))) =l= 0;


f32(n).. ((yorrp('i3',n)*Ppw)*Zrpos(n))- (0.032*Zrpos(n)) =e= 0;
f33(i,n).. ((yorrp('i3',n)))*(1-Zrpos(n)) - yrpos('i3',n)*(1-Zrpos(n)) =e= 0 ;

*$offtext

*=====================================================================
=====================================================================
=====================================

Equations
e2,e3,e4,e5,e84b, e84a;


e2(i,n,k)$ (ord (k) = 2 ).. ( 4.5 * ( ( -RRk(i,n,k-1)+ RRk(i,n,k+1)) ))
+( (Amem(n)*Perm(i,n,k))*( ppR(i,n,k)- ppP(i,n,k)) ) )=e=0 ;


e3(i,n,k)$ (ord (k) > 2).. ( 4.5 *( (RRk(i,n,k-2) -(4*RRk(i,n,k-1)) +(3*RRk(i,n,k)) ))
+( (Amem(n)* Perm (i,n,k))* ( (ppR(i,n,k)- ppP(i,n,k)) ) )) =e= 0;


e4(i,n,k).. (RRk(i,n,k)-RRk(i,n,'k10')- RPk(i,n,k)) =e= 0 ;
e5(n,k).. (RRkt(n,k)-RRkt(n,'k10')-RPkt(n,k)) =e= 0;


e84b(i,n,k).. RRk(i,n,k)=g= RRk(i,n,k+1) ;
e84a(i,n,k).. RPk(i,n,k)=g= RPk(i,n,k+1) ;


equations
p2,p3 ;

p2(i,n,k).. ppR(i,n,k) =e= PR(n)*yRRk(i,n,k) ;
p3(i,n,k).. ppP(i,n,k) =e= PP(n)*yRPk(i,n,k) ;


*-------------------------------------------------------------------------------------------------------------------------------------------------------
----------------------------

*equations
*p1,p8,p9,p10;


*p1(n,k).. perm ('i1',n,k) =e= 0.0020357 ;
*p8(n,k).. Perm ('i2',n,k) =e= 0.0000407 ;
```

```
*p9(n,k)..      perm ('i3',n,k)      =e=    0.0040714   ;
*p10(n,k)..     perm ('i4',n,k)      =e=    0.0000814   ;

*L.lo=0.8e-6;



*equations
*p40,p41,p43,p42 ;

*p40(n,k)..     (Perm ('i2',n,k)*Zn2(n))+ (Perm ('i2',n,k)* Zco2(n))   =e=   (3.92E-03*Zn2(n)) +  (0.0000407* Zco2(n)) ;
*p41(n,k)..     (Perm ('i1',n,k)*Zn2(n)) +(perm ('i1',n,k)* Zco2(n))   =e=   (1.67E-04*Zn2(n)) +  (0.0020357 * Zco2(n) ) ;
*p42(n,k)..     (Perm ('i3',n,k)*Zn2(n))+ (perm ('i3',n,k)* Zco2(n))   =e=   (3.92E-06*Zn2(n)) +  (0.0040714 * Zco2(n))  ;
*p43(n,k)..     (Perm ('i4',n,k)*Zn2(n))+ (perm ('i4',n,k)* Zco2(n))   =e=   (3.92E-06*Zn2(n)) +   ( 0.0000814 * Zco2(n)) ;


equations
p40,p41,p43,p42 ;

p40(n,k)..      Perm ('i2',n,k)*(Zn2(n) + Zco2(n))   =e=   (3.92E-03*Zn2(n)) +  (0.0000407* Zco2(n)) ;
p41(n,k)..      Perm ('i1',n,k)* (Zn2(n) + Zco2(n))  =e=   (1.67E-04*Zn2(n)) +  (0.0020357 * Zco2(n) ) ;
p42(n,k)..      Perm ('i3',n,k)* (Zn2(n) + Zco2(n))  =e=   (3.92E-06*Zn2(n)) +  (0.0040714 * Zco2(n))  ;
p43(n,k)..      Perm ('i4',n,k)* (Zn2(n) + Zco2(n))  =e=   (3.92E-06*Zn2(n)) +   ( 0.0000814 * Zco2(n)) ;
*-------------------------------------------------------------------------------------------------------------------------------------------------------------
--------------

Equations

e25,
e1000, e1001, e708,e707,e710,e743,
e901, e903,e905, e724a,e709,e730,

e17, e904,e902,e906,

e710,e724  ;


e1000(i,n,k)..     yRPk(i,n,k)*(sum(ip,  (RPk(ip,n,k))))=e= RPk(i,n,k) ;
e1001(i,n,k)..     yRRk(i,n,k)*(sum(ip,  (RRk(ip,n,k))))=e= RRk(i,n,k) ;


e707(n)..       RRkt(n,'k1') =e=sum (ip, FS(ip,n)) ;
e708(n)..       RPkt(n, 'k1')=e=sum (ip,RPS(ip,n)) ;
e17(i,n)..      RPk(i,n,'k1') =e= RPS(i,n);
e709(i,n)..     yRPk(i,n,'k1')=e= yRPS(i,n) ;
e710(i,n)..     yRRk(i,n,'k1')=e= yFS(i,n);

*Flow k10
e743(i,n,k)$(ord(k)=card(k))..      RRS(i,n) =e= RRk(i,n,k);
e730(i,n,k)$(ord(k)=card(k))..      yRRS(i,n)=e= yRRk(i,n,k) ;
*e724(n,k)$(ord(k)=card(k))..       RRt(n)=e= RRkt(n,k)  ;
e724(n,k)..           (sum(ip,  (RPk(ip,n,k)))) =e= RPkt(n,k)     ;
e724a(n,k)..           (sum(ip,  (RRk(ip,n,k)))) =e= RRkt(n,k)     ;



e905(i,n)..     yRRS(i,n)*(sum(ip, RRS(ip,n))) =e= RRS(i,n) ;
e901(i,n)..     yFS(i,n)* (sum(ip, FS(ip,n)))=e= FS(i,n) ;
e903(i,n)..     yRPS(i,n)*(sum(ip, RPS(ip,n))) =e= RPS(i,n) ;



e904(n)..       sum(ip, yRPS(ip,n))=e= 1;
e902(n)..       sum(ip, yFS(ip,n))=e= 1;
e906(n)..       sum(ip, yRRS(ip,n))=e= 1;
```

```
e25(i,n)..      FS(i,n)=e= RRS(i,n)+RPS(i,n) ;


Equation
e23, e24    ;

e23(n,k)..      sum (ip, yRRk(ip,n,k)) =e= 1 ;
e24(n,k)..      sum (ip, yRPk(ip,n,k)) =e= 1 ;

*-------------------------------------------------------------------------------------------------------------------------------------------------------
-----------------------------
equations
ec4,ec5,ec6,ec7, e27,e28 ,  ec11a,
ec10,ec11,ec12;


*balance on feed condenser
ec7(i)..   FTG(i)=e= FT(i)+RWcon(i)  ;

*to ensure only water is removed by the condenser
ec4..           RWcon('i1')=e= 0 ;
ec5..           RWcon('i2')=e= 0 ;
ec6..           RWcon('i4')=e= 0 ;

ec10(i)..      yFT(i)* sum(ip,  FT(ip))=e=  FT(i);
ec11..         yFT('i3')*Patm=l=0.032;
ec11a..         yFT('i3')*Patm=g=0.03169;
ec12(n,k)..      sum (ip, yFT(ip)) =e= 1 ;

* balance around flue gas splitter, split fraction sum, and the streams
e27..           sum (n, xF(n))=e= 1   ;
e28(i,n)..       F(i,n) =e= xF(n)*FT(i)    ;
 xF.lo(n)    = 0.0 ;            xF.up(n)   = 1      ;


*------------------condenser on permeate condenser  ----------------------------------------------------------------------------------------------
---------------------------------------
Equations
e62, e68c,e67,e68a,e67a
e64,e65,e66,e69,e70,e68;


e62(i,n)..              rps(i,n)  =e= rp(i,n)+ (rwo(i,n))  ;

*to ensure only water is removed by the condenser
e64(n)..          RWO('i1',n)=e= 0 ;
e65(n)..          RWO('i2',n)=e= 0 ;
e66(n)..          RWO('i4',n)=e= 0 ;

e67(n)..          RWO('i3',n)=g= 0.0001*(Zrwo(n));
e67a(n)..          RWO('i3',n)=l= 1500*(Zrwo(n));


e68(n)..          ((yrps('i3',n)*Patm)* Zrwo(n))      -     (0.031699* Zrwo(n))  =g=     0  ;
e68a(n)..          ((yrps('i3',n)*Patm)*(1-Zrwo(n)))  - (0.0316*(1-Zrwo(n)))      =l=     0   ;



e69(i,n)..          yrp(i,n)*(sum(ip, rp(ip,n)))=e= rp(i,n) ;
e70(n)..            sum(ip, yrp(ip,n))=e= 1;
yRP.up(i,n) = 1;
```

```
e68c(n)..          ((yrp('i3',n)*Patm)* Zrwo(n))  -  (0.031699* Zrwo(n))  =e=  0 ;


*-----------------------------------------------condenser on ----------------------------------------------------------------------------------------
-------------------------------
Equations
d21,d20, d6, d12,d10
*d1, d6, ,d10
d8,d3,d4,d5,d7,d2;
*ec25;
*balance on the retentate condenser

*d1(i,n)..          RRS(i,n)*(1-Zrrwo(n))=e= RR(i,n)*(1-Zrrwo(n)) ;
d2(i,n)..          RRS(i,n)=e= RR(i,n)+RRWO(i,n)  ;

*to ensure only water is removed by the condenser
d3(n)..            RRWO('i1',n)=e= 0 ;
d4(n)..            RRWO('i2',n)=e= 0 ;
d5(n)..            RRWO('i4',n)=e= 0 ;


d6(n)..            RRWO('i3',n)=g= 0.0001*Zrrwo(n);
d10(n)..           RRWO('i3',n)=l= 1500*Zrrwo(n);

d20(n)..           ((yrrs('i3',n)*PR(n))* Zrrwo(n)) - (0.07385* Zrrwo(n)) =g= 0 ;
d21(n)..           ((yrrs('i3',n)*PR(n))*(1-Zrrwo(n))) -(0.073849*(1-Zrrwo(n))) =l= 0;



d7(i,n)..          yRR(i,n)*(sum(ip, RR(ip,n)))=e= RR(i,n) ;
d8(n)..            sum(ip, yRR(ip,n))=e= 1;
yrrs.lo(i,n)= 0 ;      yrrs.up(i,n)= 1 ;



d12(n)..           ((yrr('i3',n)*PR(n))* Zrrwo(n)) -  (0.07385* Zrrwo(n))      =e= 0  ;

 yRR.up(i,n) = 1;



*-----------------------------------------------------------------------------------------------------------------------------------------------
Equation
n1,n4,n6,n7,n20,n17,n18;


n1(n)..            xRRO(n)+ sum (np, xRRR(n,np))  +xRPOS(n) =e=1;
n4(n)..            xPOS(n)+ sum (np, xRPR(n,np))  +xPRRO(n) =e=1;
n6(i,n)..          POS(i,n) =e= xPOS(n)*RP(i,n);
n7(i,n)..          RRO(i,n) =e= xRRO(n)*RR(i,n);
n17(i,n)..          RPOS(i,n) =e= xRPOS(n)*RR(i,n);
n18(i,n)..          PRRO(i,n) =e= xPRRO(n)*RP(i,n);

n20(i,n,np)..                  RR(i,n)*xRRR(n,np) =e= Retrcy(i,n,np);
*n21 (i,n,np)..                  RRS(i,n)=e=RR(i,n);

*-----------------------------------------------------------------------------------------------------------------------------------------------
-------------------
Equation
e40,e140,e141,e142;

*e40(i)..              MS(i,'n1')  =e=      sum (np, (RP(i,np)*xRPR(np,'n1') )) +     (ROAC(i)*xOAR('n1'))  +   f(i,'n1');
*e140(i)..             MS(i,'n2')  =e=      sum (np, (RP(i,np)*xRPR(np,'n2') )) +     (ROAC(i)*xOAR('n2'))  +   f(i,'n2');
*e141(i)..             MS(i,'n3')  =e=      sum (np, (RP(i,np)*xRPR(np,'n3') )) +     (ROAC(i)*xOAR('n3'))  +   f(i,'n3');
```

```
*e142(i)..          MS(i,'n4')  =e=      sum (np, (RP(i,np)*xRPR(np,'n4') )) +     (ROAC(i)*xOAR('n4'))  +   f(i,'n4');

e40(i)..           MS(i,'n1')  =e=      sum (np, (RP(i,np)*xRPR(np,'n1') ))  +   f(i,'n1');
e140(i)..          MS(i,'n2')  =e=      sum (np, (RP(i,np)*xRPR(np,'n2') ))  +   f(i,'n2');
e141(i)..          MS(i,'n3')  =e=      sum (np, (RP(i,np)*xRPR(np,'n3') ))  +   f(i,'n3');
e142(i)..          MS(i,'n4')  =e=      sum (np, (RP(i,np)*xRPR(np,'n4') )) +      f(i,'n4');


Equation
n10,n11,n12,n13;
*e110,



n10(i)..           FS(i,'n1')=e=  sum (np, (FSn(i,np,'n1')))  +  MSw(i,'n1')  ;
n11(i)..           FS(i,'n2')=e=  sum (np, (FSn(i,np,'n2')))  +  MSw(i,'n2') ;
n12(i)..           FS(i,'n3')=e=  sum (np, (FSn(i,np,'n3'))) +   MSw(i,'n3')  ;
n13(i)..           FS(i,'n4')=e=  sum (np, (FSn(i,np,'n4'))) +   MSw(i,'n4')  ;



xPOS.lo(n) = 0.0;          xPOS.up(n)    =  1;
xRRO.lo(n) = 0.0;          xRRO.up(n)    =  1;
xRPR.lo(n,np) = 0;         xRPR.up(n,np) =  1;
xRRR.lo(n, np) = 0;        xRRR.up(n,np) =  1;
*xPRRO.lo(n) =  0;         xPRRO.up(n)   =  1;
*xRPOS.lo(n) = 0;          xRPOS.up(n)   =  1;


*-------------------------------------------------------------------------------------------------------------------------------------------------------
--------

Equation
n30,n31,n32,n33;

n30..              xrrr('n1','n1')+xrpr('n1','n1')=l=1 ;
n31..              xrrr('n2','n2')+xrpr('n2','n2')=l=1 ;
n32..              xrrr('n3','n3')+xrpr('n3','n3')=l=1  ;
n33..              xrrr('n4','n4')+xrpr('n4','n4')=l=1  ;

*-------------------------------------------------------------------------------------------

Equations
e48a;

*e45a(i)..        OPw(i,n)       =e=    xOP * ROPC(i) ;
e48a(i)..         OA(i)          =e=   sum(n, RRO(i,n))+ sum(n, PRRO(i,n)) ;
*-------------------------------------------------------------------------------------------------------------------------------------------------------
-----------------

Equation
n53;
n53(i,n,np)..          Retrcy(i,n,np)   =e=  FSn(i,n,np)  ;


*-------------------------------------------------------------------------------------------------------------------------------------------------------
-----------------------------------

Equations
e60,  e72,e71 ,e57, e57a
e53,e54,e55,e56,e60a,e58;
*balance on the feed condenser  e69,   e57a,  ,e73,e74,
```

```
e53(i,n)..          MS(i,n) =e= MSw(i,n) +RWms(i,n);

*to ensure only water is removed by the condenser
e54(n)..            RWms('i1',n)=e= 0 ;
e55(n)..            RWms('i2',n)=e= 0 ;
e56(n)..            RWms('i4',n)=e= 0 ;

e57(n)..            RWms('i3',n)=g= 0.0001*Zrwms(n);
e57a(n)..           RWms('i3',n)=l= 1500*Zrwms(n);
*e57(n)..           RWms('i3',n)*(1-Zrwms(n))=e= 0* (1-Zrwms(n));

e58(i,n)..       yMS(i,n)* sum(ip, MS(ip,n))=e= MS(i,n);
e71(i,n)..       yMSw(i,n)* sum(ip, MSw(ip,n))=e= MSw(i,n);


*e73(n)..           sum(ip, yMS(ip,n))=e= 1;
*e74(n)..           sum(ip, yMSw(ip,n))=e= 1;


e60(n)..        ((yms('i3',n)*PR(n))*Zrwms(n))   -  (0.07385*Zrwms(n))     =g=   0;
e60a(n)..       (yms('i3',n)*PR(n))*(1-Zrwms(n)) -  ( 0.073849*(1-Zrwms(n)))  =l=   0;


yms.lo(i,n)= 0;     yms.up(i,n)= 1;
yMsw.lo(i,n)= 0;    ymsw.up(i,n)= 1;


e72(n)..            ( yMSw('i3',n)*PR(n)*Zrwms(n))  - ( 0.07385*Zrwms(n)) =e= 0;

*----------------------------------------------------------------------------------------------------nnnnn----------------------------------
----------
Equation
c1;

*c1(i)..              FTG(i)=e== OA(i)+Op(i)+Rwcon(i)+rwo(i)+rrwo(i)+rwms(i)+rwf(i)+rwp(i);

c1(i)$(ord (i)<>3)..          FTG(i)=e= OA(i)+Op(i);


*----------------------------------------------------------------------------------------------------------------------------------------
nnnnn-----------------------------------------------

equations
eb6;
*to ensure relative humity is less than saturation
eb6(n)..       yFS('i3',n)*PR(n) =l= 0.07385 ;
*---------------------------------------------------------------------------------------------------------------------


Equations
*p20,p21,p22,p23,
p44;

p44(n)..        Zco2(n)+ Zn2(n) =e= 1  ;
*P20..           Zn2('n1') =e= 1   ;
*P21..           Zn2('n2') =e= 1   ;
*P22..           Zn2('n3') =e= 1   ;
*P23..           Zco2('n4') =e= 1   ;


Amem.lo(n)  = 1000;
Amem.up(n)  = 1000000 ;
```

```
PR.lo(n)=Patm;       PR.up(n)= 250;
*PR 250
PP.lo(n)=0.2;          PP.up(n)= Patm;
*-------------------------------------------------------------------------------------------------------------------------
Equations
e46,e161,e49,e50,ee52,e160,e47
;


*desired  product Co2 recovery capture ratio
e49(i)..            R(i)*FTG(i)=e= OP(i)   ;
e50..               R('i1')=g=0.9;
R.lo(i) = 0; R.up(i) = 1   ;

*final product mixer - compression for storage yOP is CO2 target purity

e46..               OPt   =e= sum(ip, OP(ip)) ;
*e161(i,n)..         yOP(i)* (sum(ip, OP(ip))) =e= OP(i) ;
e161(i,n)..          yOP(i)*OPt=e= Op(i) ;
ee52..              yOP('i1') =g=0.95    ;
 yOP.up(i) = 1;


*balance around the final residue mixer to - to atmosphere
e47..               OAt    =e= sum (ip, OA(ip));
e160(i,n)..          yOA(i)*OAt=e= OA(i) ;
*e160(i,n)..         yOA(i)*(sum (ip, OA(ip)))=e= OA(i) ;
 yOA.up(i) = 1;

*-------------------------------------------------------------------------------------------------------------------------
------------------------


Equations
*       s103    COM
       s102,s105,s106,s108,s109,s110, s107,

       obj;

*tnq net power, tma membrane area, ec electricity cost, 7500h per year, 15$phr labour
*s103..          TMA =e=  sum (np, (Amem(np))) ;
s102..          TNQ =e=  sum (np, Qcft(np))+sum (np, (Qvac(np))) +Qpum+Qcomp + Sum ((n,np),(Qcrrr(n,np)*Zcrr(n,np)))
                         -Sum ((n,np), (Qexrr(n,np)*Zexrr(n,np)))
                        - sum(np, Qexr(np)) +Qcopw +sum (np, (Qcfr(np)) )        ;

s105..          OPEX  =e=   COM + EC ;
s106..          EC    =e=   Cel *(TNQ)*6570;
s108..          CAPEX =e=   CRF*(1+0.37)*TCCU  ;
s110..          TCCmem =e= Cmem*sum(np, Amem(np))+(Cmf*((sum(np, Amem(np))/2000)**0.7));

s107..          COM   =e=   (0.01*(TCCmem))+ ( 0.036*(   +CCco2comp+CCco2pump + CCopw
                  +sum(np,CCvac(np)) + sum (np, CCcft(np))+  sum(np, CCexr(np))
                +   Sum ((n,np),(CCcrrr(n,np)*Zcrr(n,np)))+ Sum ((n,np),(CCexrr(n,np)*Zexrr(n,np)))
                +  sum (np, (CCcfr(np)))    ))  ;


s109..          TCCU  =e=   (603.1/567.3)*(TCCmem +  CCco2comp+CCco2pump +   CCopw
                + sum(np,CCvac(np)) + sum (np, CCcft(np)) +  sum(np, CCexr(np))
                 +   Sum ((n,np),(CCcrrr(n,np)*Zcrr(n,np)))+ Sum ((n,np),(CCexrr(n,np)*Zexrr(n,np)))
                 +   sum (np, (CCcfr(np)))   ) ;

* (603.1/584.6)*  ) (     CCexr(n) +  CCcfr(n)  + Qexr(n)*Zexr(n) + Qcfr(n)*Zcfr(n)
```

```
Equations
s132, s133,s11;

s132(n)..  PPe(n) =e=   (PP(n))**0.286  ;
S133(n)..  PRe(n) =e=   (PR(n))**0.286;
s11..      Ppwe  =e=     Ppw**0.286;


Equations
s1,s2,s9,s10  ;
*,s14,s15;


s1(n)..              Qcft(n)*Patme =e=(( (1/Eff)*( ( (sum(ip, MS(ip,n)))/60)*8.3145e-3*Tatm*3.5* (PRe(n)-Patme) )))   ;
s2(n)..              CCcft(n) =e= (Ccomp*Qcft(n))      ;


s9(n)..              Qvac(n)*PPe(n)=e=( (1/Eff)* ( ( (sum(ip, RPS(ip,n)))/60)*8.3145*Tmem*3.5*(Patme -PPe(n))))*1e-3;
s10(n)..              CCvac(n) =e= (Cvac*Qvac(n)) ;

Equations
f4,f6 ;

*residue expander

*f4(n)..             Qcfr(n)*(PR(n)**0.286)=e= ( (1/Eff)* (((sum(ip, RRO(ip,n)))/60) *8.314e-3*3.5*Tmem* ((Ppw**0.286) -
(PR(n)**0.286))  ))  ;
f4(n)..          Qcopw*(Patme)=e= ( (1/Eff)* (((sum(ip, opw (ip)))/60) *8.314e-3*3.5*Tatm* ((Ppwe) -(Patme))  )) ;
f6(n)..          CCopw =e= Ccomp*Qcopw   ;  ;


*feed compressor cooler clf


*-------------------------------------------------------------------------------------------------------------------------------------------------------
-------
*Equations
*s80,s81,s82;
*s80(n)..          Qexrpos(n)*PRe(n)=e=( (Eff)* (((sum(ip, RPOS(ip,n)))/60) *8.314*3.5*Tmem* (PRe(n)-Patme) ) )*1e-3  ;
*s81(n)..          Qexrposn(n)*PRe(n)=e=(  (((sum(ip, RPOS(ip,n)))/60) *8.314*3.5*Tmem* (PRe(n)-Patme) ) )*1e-3  ;
*s82(n)..          CCexrpos(n) =e= Cexp*Qexrpos(n) ;

Equations
f7,f8 ;

*residue expander

*f4(n)..             Qcfr(n)*(PR(n)**0.286)=e= ( (1/Eff)* (((sum(ip, RRO(ip,n)))/60) *8.314e-3*3.5*Tmem* ((Ppw**0.286) -
(PR(n)**0.286))  ))  ;
f7(n)..          Qcfr(n)*(PRe(n))=e= ( (1/Eff)* (((sum(ip, RPOS(ip,n)))/60) *8.314e-3*3.5*Tmem* ((Ppwe) -(PRe(n)))  ))  ;
f8(n)..          CCcfr(n) =e= Ccomp*Qcfr(n) ;

ppw.lo= 0; Ppw.up=10 ;


*-------------------------------------------------------------------------------------------------------------------------------------------------------
-----------------------------------
Equations
s48,s49,s48a ;

*residue expander
s48(n)..          Qexr(n)*PRe(n)=e=( (Eff)* (((sum(ip, RRO(ip,n)))/60) *8.314*3.5*Tmem* (PRe(n)-Patme) ) )*1e-3  ;
s48a(n)..          Qexrn(n)=e=(1/Eff)* Qexr(n) ;
s49(n)..          CCexr(n) =e= Cexp*Qexrn(n) ;
```

```
Equations
s61a,s62a,s63a,s56, s57;


*compression for storage
s61a..      Qpum=e= ((((sum (ip, OP(ip))/60)*22.4)/(Effc))*((Pfin-Pcut)))*1e-3   ;
s62a..      Qcomp =e=( (1/Effc)*(5*((sum(ip, OP(ip)))/60)*3.5*8.314*Tatm*(CR**0.286-1)))*1e-3  ;
s63a..      CR*(Ppw**0.20) =e= Pcut**0.20      ;

S56..      CCco2comp =e= Cco2comp*Qcomp ;
S57..      CCco2pump =e= Cco2pump*Qpum ;


obj..            TAC   =e=   OPEX + CAPEX  ;


*-------------------------------------------------------------------------------------------------------------------------------------------------------
-------------------------
*finite boundaries
yRRk.lo(i,n,k)= 0;              yRRk.up(i,n,k)= 1;
yRRk.lo(i,n,k)= 0;              yRPk.up(i,n,k)= 1;
yFS.lo(i,n) = 0;               yFS.up(i,n)  = 1;
yRPS.lo(i,n)= 0 ;               yRPS.up(i,n) = 1;
yRR.lo(i,n)= 0;                yRR.up(i,n) = 1;
yFSn.up(i,n,np) = 1;
yFT.up(i) = 1;

FS.lo('i1',n) =1e-4;
ppw.lo= 0; Ppw.up=15 ;
RPS.up('i1',n) =  400 ;
RPS.up('i2',n) =  1900 ;
RPS.up('i3',n) =  450 ;
RPS.up('i4',n) =  130 ;

RR.up('i1',n) =  400 ;
RR.up('i2',n) =  1900 ;
RR.up('i3',n) =  450 ;
RR.up('i4',n) =  130 ;

RP.up('i1',n) =  400 ;
RP.up('i2',n) =  1900 ;
RP.up('i3',n) =  450 ;
RP.up('i4',n) =  130 ;

MS.up('i1',n) =  400 ;
MS.up('i2',n) =  1900 ;
MS.up('i3',n) =  450 ;
MS.up('i4',n) =  130 ;

RRS.up('i1',n) =  400 ;
RRS.up('i2',n) =  1900 ;
RRS.up('i3',n) =  450 ;
RRS.up('i4',n) =  130 ;

PRRO.up('i1',n) =  400 ;
PRRO.up('i2',n) =  1900 ;
PRRO.up('i3',n) =  450 ;
PRRO.up('i4',n) =  130 ;

RPOS.up('i1',n) =  400 ;
RPOS.up('i2',n) =  1900 ;
RPOS.up('i3',n) =  450 ;
RPOS.up('i4',n) =  130 ;
```

```
Qpum.up    = 50;
Qcomp.up   = 1000 ;
Qvac.up(n) = 1000;
Qcft.up(n) = 1000;
Qcfr.up(n) = 1000;
Qcopw.up   = 1000 ;


*-------------------------------------------------------------------------------------------------------------------------------------------------------
-------------------

model  membrane /all/;

$onecho > baron.opt
CompIIS 1
$offecho

membrane.optfile = 1;

OPTION SYSOUT=ON ;
option limrow=0;
option limcol=0;
*OPTION PROFILE = 2;
*OPTION PROFILETOL = 1.5;
option work  =  1258291  ;
option optcr=1e-6 ;
option reslim =25000;

option rminlp =baron;
option decimals =4 ;

solve membrane using rMINLP minimising TAC    ;
*solve membrane using NLP minimising TAC    ;



*display
*F.l,FSn.l,FS.l,RR.l, RPS.l,POS.l,RRO.l, RP.l; stop 1


$onecho > dicopt.opt
maxcycles  4000
relaxfixedinfeas 1
$offecho

OPTION SYSOUT=ON ;
option reslim =27600;

option nlp=conopt3;
option mip = cplex;
option minlp = dicopt ;

solve membrane using MINLP minimising TAC    ;
```